INFN

Annual Report 2009

Laboratori Nazionali del Gran Sasso
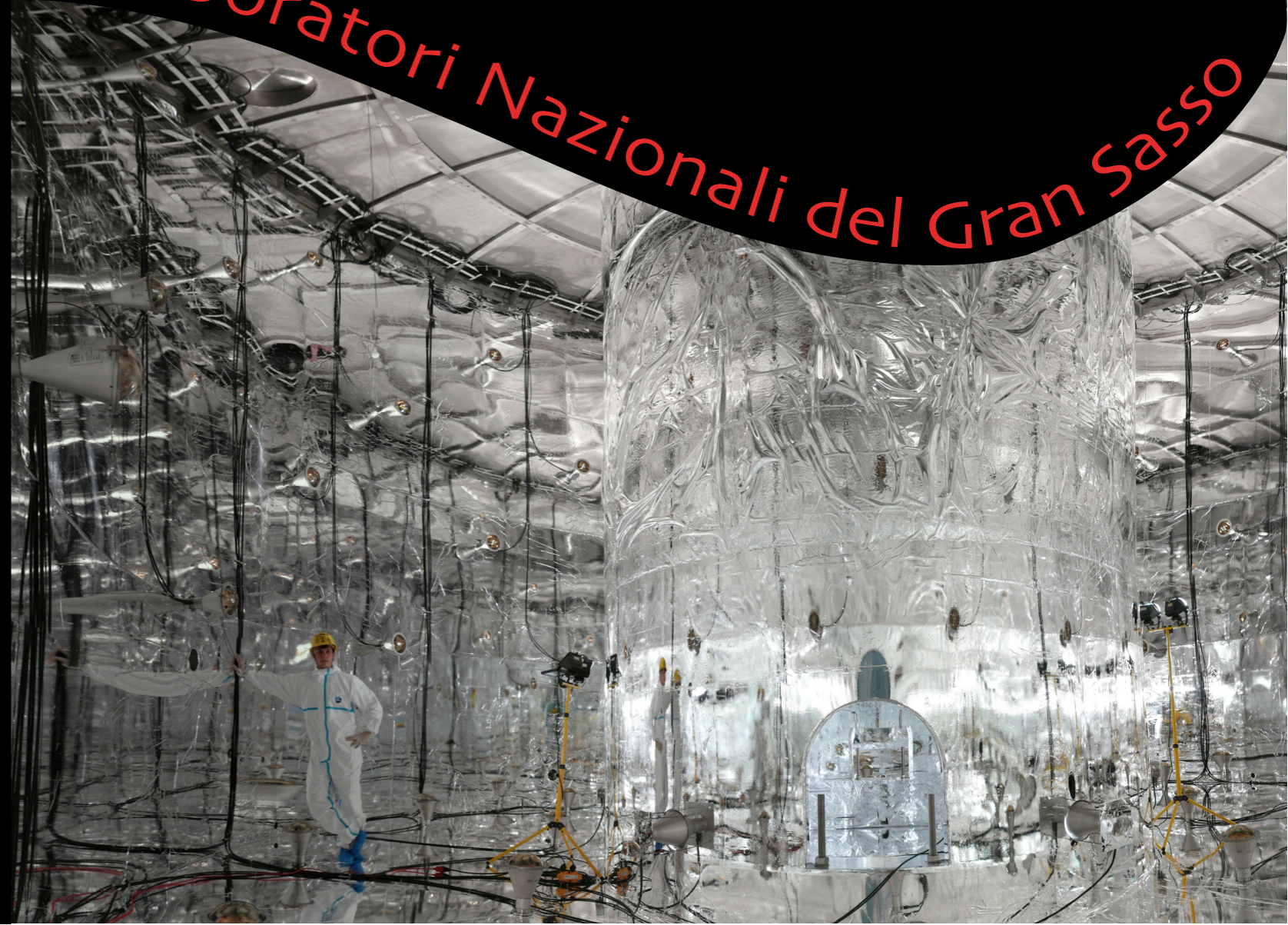
ANNUAL REPORT 2009

Annual Report 2009

The Gran Sasso National Laboratory

My mandate as Director at LNGS took effect from September 2009 and it would be unthinkable to start this introduction to the 2009 LNGS annual report without mentioning the earthquake of last April which left 370 people dead, 15,000 injured and devastated the surrounding area together with the social and economic life of L'Aquila.

Most of the lab personnel as well as the 70,000 inhabitants in L'Aquila were rendered homeless. Fortunately the Laboratory survived the devastating earthquake and escaped damage. This was possible thanks to two factors: the acceleration experienced deep underground, (0.03g), as expected, was lower than that of the external laboratory (0.15 g) and much lower than in L'Aquila (0.64 g).; the anti-seismic design of the apparatus protected the underground installations.

In April Eugenio Coccia was still on duty as Director of the Lab, and I think it is proper to mention how effective his dedication and actions were, in providing support to the laboratory personnel and assuring the immediate restarting of the activities in the Laboratory.

From April 6th access to the laboratory was limited, a series of inspections by LNGS staff, Engineers from the Department of Civil Protection, experts on structures, geology and hydro-geology resulted on April 24th in the Laboratory being granted certification of safe use and occupancy.

Thanks to the dedication of the Lab staff who, despite their quite serious personal difficulties, immediately after the earthquake worked toward the safe operation of the laboratory, on May 4th access and the normal operation of all the experiments resumed. The INFN management has also strongly contributed to the setting up of a plan of support: hosting the homeless people in hotels, guest houses and trailers inside the lab area; making donations for immediate needs; refunding travel expenses to and from the new accommodation (mainly on the Adriatic coast) and the Lab.

The general situation is now slowly improving and the new challenge is more ambitious, that of contributing to the rebirth of the L'Aquila community. The Laboratory has a significant role in the life of the town: if we preserve this feature of excellence, our international research activities will offer hope of renewal of the cultural, social and economic life of L'Aquila. We are also trying to stimulate new initiatives such as allowing the Municipality to set up a school in our external area, hosting meetings, and intensifying relationships with the local Institutions. For example we are involved in setting up a new interactive science museum in a park in the heart of the ruined medieval center of L'Aquila.

Despite the troubles and discomfort connected to the earthquake, from a scientific point of view, 2009 was an auspicious year. It marked the thirtieth anniversary of the official birth of the Gran Sasso Laboratory project and the twentieth anniversary of the first experimental data published by the MACRO experiment. The scientific legacy I inherited is definitely impressive and my first duty is to ensure the laboratories maintain their worldwide leadership in astroparticle physics.

The Gran Sasso National Laboratory of INFN is a research infrastructure devoted to astroparticle physics It has no equal elsewhere and offers the most advanced underground Laboratory in terms of dimensions, complexity and completeness of the infrastructure.

Located between L'Aquila and Teramo, about 120 km from Rome, the underground structures are on one side of the highway tunnel (10 km long) which crosses the Gran Sasso massif, towards Rome, and consist of three huge experimental halls, (each one 100 m long, 20 m large and 18 m high) and a bypass tunnel, for a total volume of about 180.000 m^3 and a surface of 18.000 m^2. The halls are equipped with all the technical and safety equipment and apparatus necessary for the experimental activities at the same time as ensuring proper working conditions for the people involved.

The 1400 m. of rock overhead provide a cover which is able to reduce the cosmic rays flux by a million times; moreover, the flux of neutrons in the underground halls is about thousand

times less than on the surface due to the very small amount of Uranium and Thorium of the Dolomite calcareous rock of the mountain.

The permeability of cosmic radiation provided by the rock coverage, the huge dimensions and the impressive basic infrastructure, make the Laboratory absolutely unique for the detection of weak or rare signals, relevant for astroparticle, sub nuclear and nuclear physics.

On the outside, near the Assergi tollgate on the highway A24, an area of more than 23 acres belonging to a National Park of exceptional environmental and naturalistic interest on the slopes of Gran Sasso, hosts the laboratories of chemistry, electronic, mechanical, design and workshops, the Computing Centre, the Directorate and the various Offices. The high international status enjoyed by the LNGS is reflected in the large number of publications to come out of its work , and in the fact that about 950 scientists take part in its research. Half of them come from 29 different countries. At present we have fifteen experiments in different phases of realization.

The study of the intrinsic properties of neutrino is of prime interest in particle physics and one of the main research topics of the present scientific program of the Laboratory. In order to properly comprehend the mechanism of neutrino oscillation, it is necessary to measure the elements of the mixing matrix by means of various neutrino sources, both natural (the Sun or other Stars) and artificial (particle accelerators). Besides, the study of the phenomenon of neutrinoless double beta decay could allow us to find out if the neutrino overlaps with its antiparticle, thus providing a very significant answer towards the comprehension of the evolution of the Universe. Neutrino physics therefore offers a window to a new theory of elementary particles and to the comprehension of the evolution of the Universe.

Finally, neutrinos from the cosmos are very important messengers which transport information fundamental to our understanding of the functioning of the stars as energy sources, their evolution and what happens when they "turn off".

LNGS activities range among various aspects of the neutrino physics' study.

The measurement of neutrino oscillations in appearance mode is the main goal of OPERA experiment, which aims to the detection of tau neutrinos in the artificial neutrino beam from CERN to Gran Sasso (CNGS), originally constituted by muon neutrinos only. Throughout 2009 Opera has collected 3700 events on target in addition to the 1689 events collected in 2008. By now 19 charmed events have been identified in 2008 data, showing that the experiment is capable of detecting events with topologies very similar to τ production. The expected number of ν_τ for the entire statistics collected up to now is about 2.

Another experiment able to detect CNGS beam will be ICARUS, an innovative apparatus consisting of a big mass (about 600 tons) of liquid Argon, allowing a 3D imaging of any interactions of charged particles inside its volume. ICARUS is in the phase of commissioning and expected to be filled with argon in spring 2010.

Borexino measures in real-time the interactions of solar neutrinos flux by means of a 300 ton sphere of scintillating liquid. This allows us to study the functioning of the Sun and at the same time neutrino properties. Throughout 2009 a calibration campaign has led to a strong reduction of the systematic errors of the ^{7}Be neutrino flux measurement. The contemporary measurement of the ^{7}Be and the ^{8}B neutrino flux will grant a determination in the same experiment of the ratio vacuum/matter of the oscillation parameters. The search for terrestrial antineutrino interactions has become a hot point of the data analysis.

The LVD experiment is continuously monitoring the Galaxy with its 1000 tons of liquid scintillator, looking for collapsing stars and it also offers an original monitoring of the CNGS neutrino beam. LVD participates in the SuperNovae Early Warning System of detectors.

The study of neutrino properties through the research into a rare process called 'neutrinoless double beta decay' may give a direct indication as to the value of its mass ascertaining its nature of Majorana particles (that is particle and antiparticle coinciding). At present LNGS is host to several experiments devoted to research neutrinoless double beta decay events.

The experiment GERDA will use the same enriched Germanium crystals of the Heidelberg-Moscow experiment, but they will be directly immersed in 60 m^3 of liquid Argon, which is a first protection from cosmic radiation. A 10 m diameter tank built all around the cryostat is a further protection and acts as a veto Cerenkov for muons. Once the installation of the apparatus had been completed in 2009 the cryostat was successfully filled with Argon and, after final checks currently ongoing, the external shield will be filled with water.

The experiment CUORE, after the success of CUORICINO, is the most recent and ambitious development of the 'TeO2 bolometers' technique, in which INFN has more than 20 years experience. CUORE will use about a thousand TeO$_2$ crystals, with a total mass of about 740 Kg cooled at a temperature next to absolute zero. Significant improvements have been made in 2009 in the preparation of CUORE0, the first of the 19 towers to be installed and operated.

Finally COBRA completes the outline of research activities on neutrinoless double beta decay. The basic idea of the experiment is to use CdZnTe (CZT) semiconductors as detectors as they have a low radioactive background level, good energy resolution and operated at room temperature. The collaboration has been reinforced in 2009 and an ultimate design of the experiment should be ready in the near future.

The Dark Matter search represents another main topics of the scientific program of the Laboratory. As well known, experimental evidence indicates the existence in the Universe of an amount of mass larger than the one observable by means of telescopes, called dark matter because it neither emits nor absorbs radiation. It is supposed to be five times bigger than ordinary matter, which constitutes only 5% of our Universe.

At LNGS four experiments are devoted to the hunt for dark matter candidates and their direct detection, each one by means of a different technology. These experiments keep Gran Sasso Laboratory in the forefront of such studies.

The experiment DAMA/LIBRA, made up of 250kg of NaI(Tl) extremely radio-pure crystals, has been recording data since 2003. Results so far published have confirmed the annual modulation of very low energy signals induced in the detector. Such modulation is identical to the one expected from the dark Matter particle flux, if we consider the composition of the Earth revolution velocity with the Sun velocity around the Galaxy. The interesting result has produced a lively debate inside the scientific community as well as the production of theoretical models able to conciliate such results with the absence of positive signals by other experiments. In the months to come new photomultipliers will allow the experiment to start a new and more sensitive data-collecting campaign.

WARP100 lt is a cryogenic detector that uses double phase argon and it is based on a double detection technique, the scintillation in liquid argon and the ionization in the gaseous state. A technical run of the detector started in May after the April earthquake and ended in August in order to fix a problem in the high voltage system supply and to optimize the scintillation light collection. The restart of the experiment is scheduled for the beginning of 2010.

Xenon100 is also a two-phase liquid cryogenic detector and the apparatus contains 170 kg of Xenon, 65 kg of which constitute the active part while the remaining ones act as a shield.

In 2009 the detector has been fully commissioned and the detector calibration has been accomplished. The experiment started the data-taking just at the end of 2009.

The experiment CRESST is based on the bolometer technique with CaWO$_4$ crystals cooled at 10 mK as well as on the simultaneous detection of scintillation light and the heat resulting by the interaction of a particle with the crystals. The detector started the data-taking with 10 crystals. Further R&D activities should allow to finalize an experiment proposal of higher/larger mass.

Using the 400 kV accelerator, LUNA continued its successful activity for the measurements of the cross section of nuclear reactions of astrophysical interest. Throughout 2009 activities have been focused mainly on tests meant to measure the $D(\alpha,\gamma)^6Li$, whose great interest is due to the possibility to determine the percentage of primordial Li from the BIG BANG.
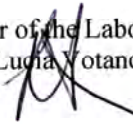
The Laboratory hosts experiments aimed to study cosmogenic and primordial radionuclides in solid and fluid matrix inside LNGS, and experiments of geophysical interest as well.

The activity of the theory group and of the staff and visitor scientists covers various aspects of astroparticle and particle physics, including Supernova neutrinos, ultra high energy cosmic rays, high energy neutrinos and cosmology, large scale structures and dark matter, phenomenology of Planck scale physics. An important activity took place also for computer simulations on Lattice Field Theories.

Despite the seismic event occurred in April we have carried out several initiatives meant to promote science and didactics activities dedicated to students and general public as the "Gran Sasso – South Dakota – Princeton Summer School, the competition "Anch'io Scienziato", the "Incontri con la Scienza" and the European Astroparticle Week.

Assergi, May 12 2010

The Director of the Laboratory
Dr. Lucia Votano

Contents

THE BOREXINO EXPERIMENT

Borexino collaboration

G. Bellini[a], J. Benziger[c], S. Bonetti[a], M. Buizza Avanzini[a], B. Caccianiga[a], L. Cadonati[t],
F.P. Calaprice[d], C. Carraro[i], A. Chavarria[d], F. Dalnoki-Veress[d], D. D'Angelo[h], S. Davini[i],
H. de Kerret[o], A. Derbin[u], A. Etenko[s], K. Fomenko[m], D. Franco[a], C. Galbiati[d],
S. Gazzana[b], C. Ghiano[b], M.G. Giammarchi[a], M. Goeger-Neff[h], A. Goretti[d], C. Grieb[n],
S. Hardy[n], A. Ianni,[b], A.M. Ianni[d], M. Joyce[n], V. Kobychev[v], G. Korga[b], D. Kryn[o],
M. Laubenstein[b], M. Leung[d], T. Lewke[h], E. Litvinovich[s], B. Loer[d], P. Lombardi[a],
L. Ludhova[a], A. Lund[t], I. Machulin[s], S. Manecki[m], W. Maneschg[j], G. Manuzio[i], F. Masetti[g],
K. McCarty[d], Q. Meindl[h], E. Meroni[a], L. Miramonti[a], M. Misiaszek[q], D. Montanari[b],
V. Muratova[u], L. Oberauer[h], M. Obolensky[o], F. Ortica[g], M. Pallavicini[i], L. Papp[b],
L. Perasso[a], S. Perasso[i], A. Pocar[d], R.S. Raghavan[n], G. Ranucci[a], A. Razeto[b], A. Re[a],
P. Risso[i], A. Romani[g], D. Rountree[n], A. Sabelnikov[s], R. Saldanha[d], C. Salvo[i], S. Schönert[j],
H. Simgen[j], M. Skorokhvatov[s], O. Smirnov[m], A. Sotnikov[m], S. Sukhotin[s], Y. Suvorov[s],
R. Tartaglia,[b], G. Testera[i], D. Vignaud[o], B. Vogelaar[n], F. von Feilitzsch[h], M. Wojcik[q],
M. Wurm[h], O. Zaimidoroga[m], S. Zavatarelli[i], G. Zuzel[j]

[a]Dip. di Fisica dell'Università and Infn Milano - Italy
[b]Laboratori Nazionali del Gras Sasso, Assergi (Aq) - Italy
[c]Dept. of Chemical Engineering, Princeton University - NJ USA
[d]Dept. of Physics, Princeton University - NJ USA
[g]Dip. di Chimica dell'Università and Infn Perugia - Italy
[h]Dept. of Physics, Technische Universität München - Germany
[i]Dip. di Fisica dell'Università and Infn Genova - Italy
[j]Max Planck Inst. für Kernphysik, Heidelberg - Germany
[m]Joint Institute for Nuclear Research Dubna - Russia
[n]Dept. of Physics, Virginia Polytechnic Institute - VA USA
[o]Laboratoire de AstroParticule et Cosmologie, Paris - France
[q]Institute of Physics, Jagellonian University, Kracow - Poland
[s]RRC Kurchatov Institute, Moscow - Russia
[t]Dept. of Physics, University of Massachusetts, Amherst - MA USA
[u]St. Petersburg Nuclear Physics Institute, Gatchina, Russia
[v]Kiev Institute for Nuclear Research, Kiev, Ukraine

Abstract

Borexino is a solar neutrino detector located in the Hall C of LNGS to study solar neutrino physics and other rare physical phenomena. The data taking started in May 2007 and led to the first real time measurement of ^{7}Be solar neutrinos and the first experimental evidence of the matter/vacuum transition in solar neutrino oscillations. We summarize here the status of the project and briefly discuss the perspectives for future measurements.

1 Introduction

Solar neutrino physics is a topic that originally started from the perspective of studying the basic working principle of the core of the Sun, nuclear fusion reactions producing energy and emitting neutrinos.

The pioneer Davis experiment [1] was the first one to measure (with radiochemical methods) solar neutrinos as predicted by theoretical models and to detect a significant deficit in the predicted flux. New experiments were performed starting from the end of the 80's, both in radiochemical mode [2, 3, 4] and in real-time mode [5, 6] while the most widely accepted model of the Sun evolved into what is now known as the Standard Solar Model [7].

As a general statement, real-time experiments have been performed with large water Cerenkov detectors with an energy threshold of about 5 MeV, mainly due to natural radioactivity. This implies that only ∼0.001% of the total neutrino flux has been observed in real time prior to 2007.

The issue of directly measuring low energy solar neutrinos has been the subject of an intensive research study carried out in the frame of the Borexino development and starting from the very beginning of the 90's. Borexino [10] is a real time experiment to study sub-MeV solar neutrinos having as the main experimental goal the detection of the 0.862 MeV ^{7}Be solar neutrino line through the neutrino-electron elastic scattering reaction $\nu e \to \nu e$. The maximum energy of the recoiling electron is 664 KeV and the experimental design threshold is of 50 keV while the analysis threshold is 200 keV. The detection reaction is observed in a large mass (100 tons fiducial volume) of well shielded liquid scintillator.

The prediction of the ^{7}Be solar flux depends both on the Standard Solar Model and the value of the parameters of the LMA solution of neutrino oscillations [8] [9]. The Borexino experimental program makes it possible to specifically test this prediction in a direct way as well as opening up the unexplored territory of real time sub-MeV solar neutrino spectroscopy.

The main problem of an experiment with such a low energy threshold is the background coming from natural sources such as cosmic rays or radioactivity. This problem has been addressed by means of an intense R&D program focused on low radioactivity materials and purification techniques. This effort was complemented by a comparably thorough research in the field of detection and measurement of very low radioactivity levels [11]. As a part of this program, a prototype of the Borexino detector, called Counting Test Facility [12], was built and operated at LNGS to demonstrate very low radioactive contamination levels (10^{-16} g/g of U-238 equivalent or less [13]) in a ton scale scintillator detector. The CTF is currently now being used as a low background facility for quality tests of the Borexino scintillator and possible future physics programs.

This research and development culminated into the construction, filling and operation of the full-scale Borexino detector. The experimental data taking in the final configuration began in May 2007.

2 The Borexino Detector

Borexino [10] is an unsegmented scintillation detector featuring 300 tonnes of well shielded liquid ultrapure scintillator viewed by 2200 photomultipliers (fig. 1). The detector core is a transparent spherical vessel (Nylon Sphere, $100\mu m$ thick), 8.5 m of diameter, filled with 300 tonnes of liquid scintillator and surrounded by 1000 tonnes of high-purity buffer liquid. The scintillator mixture is PC and PPO (1.5 g/l) as a fluor, while the buffer liquid consists of PC alone (with the addition of DMP as light quencher). The photomultipliers are supported by a Stainless Steel Sphere, which also separates the inner part of the detector from the external shielding, provided by 2400 tonnes of pure water (water buffer).An additional containment vessel (Nylon film Radon barrier) is interposed between the Scintillator Nylon Sphere and the photomultipliers, with the goal of reducing Radon diffusion towards the internal part of the detector.

The outer water shield is instrumented with 200 outward-pointing photomultipliers serving as a veto for penetrating muons, the only significant remaining cosmic ray background at the Gran Sasso depth (about 3500 meters of water equivalent). The innermost 2200 photomultipliers are divided into a set of 1800 photomultipliers equipped with light cones (so that they see light only from the Nylon Sphere region) and a set of 400 PMT's without light cones, sensitive to light originated in the whole Stainless Steel Sphere volume. This design greatly increases the capability of the system to identify muons crossing the PC buffer (and not the scintillator).

The Borexino design is based on the concept of a graded shield of progressively lower intrinsic radioactivity as one approaches the sensitive volume of the detector; this culminates in the use of 200 tonnes of the low background scintillator to shield the 100 tonnes innermost Fiducial Volume. In these conditions, the ultimate background will be dominated by the intrinsic contamination of the scintillator, while all backgrounds from the construction materials and external shieldings will be negligible.

Borexino also features several external systems conceived to purify the experimental fluids (water, nitrogen and scintillator) used by the experiment.

3 Status of the project

The Borexino filling started in January 2007, with scintillator displacing the purified water from inside the detector volumes. The detector was completed and the data taking started in May 2007.

The radiopurity of the detector has been found in general to be better than the specifications. In particular, among the best radioactivity levels found during the data taking:

1. C-14 contamination of the scintillator was found to be at $\sim 2 \times 10^{-18}$ ^{14}C/^{12}C.

2. The general level of Th-232 contamination - as measured by means of $^{212}Bi/^{212}Po$ delayed coincidences was found to be at $\sim 6.8 \times 10^{-18}$ g/g.

3. The U-238 family contamination - assessed by studying the $^{214}Bi/^{214}Po$ delayed coincidence rate, was measured to be 1.6×10^{-17} g/g.

4. Kr-85 contamination, of considerable importance due to the spectral shape similar to the one of the signal searched for was found (by means of the ^{85m}Rb decay and the related β/γ tagging) to be at the level of less than 35 count/day in the 100 tons fiducial volume.

This level of radiopurity, together with the use of mild cuts and the α/β discrimination technique has allowed the first real-time detection of the Be-7 solar signal [14] and the first observation of the B-8 spectrum below 5 MeV [16].

While we refer the interested reader to the published papers for the detailed description of the analysis [15], fig. 2 shows a spectrum of the singles rate obtained after analysis cuts (including veto of external muons, Radon-related activity and Po-210 subtraction) in the Borexino fiducial volume. The Be-7 flux was determined by fitting the experimental distribution to the light yield, to the Be-7 interaction rate and to the other contributions shown in the figure. Neutrinos from Be-7 are visible in the electron recoil spectrum by means of the Compton-like shoulder generated by $\nu e^- \to \nu e^-$ scattering (fig. 2).

The systematic error was dominated by the knowledge of the fiducial mass and the detector response function, since the detector calibration was not yet carried out at that time. The published measurement of $49 \pm 3_{stat} \pm 4_{syst}$ counts/(day·100 ton) has to be compared to the expected (high-metallicity) Standard Solar Model without oscillations of 74 ± 4 or to the expected number of 48 ± 4 when LMA oscillations of solar neutrinos are taken into account [9].

This analysis was made during the first 192 live days of the detector and prior to the calibration.

Further accumulation of data prior to the calibration (246 days) allowed to observe the more rare B-8 solar neutrino component [16], which is important because the solar model with MSW-LMA solution predicts that electron neutrino survival probability is dominated by vacuum oscillations at low energies and by resonant matter-enhanced oscillations (taking place in the Sun) at higher (E>5 MeV) energies. In Borexino this component can be studied down to 2.8 MeV electron energy, lower than the previously considered 5 MeV.

The combination of the Be-7 and B-8 measurements constitutes the first evidence of matter/vacuum transition of neutrino oscillations obtained in the same experiment.

Following these measurements, an intensive calibration campaign was carried out by deploying radioactive sources in the scintillator volume. In particular, a Rn-222 source was deployed in more than 100 points throughout the Inner Vessel volume to study the performance of the position reconstruction alghoritm and the uniformity of light collection. Several gamma sources with energy spanning between 100 keV and 1.5 MeV were also inserted to calibrate the energy scale (Mn54, Sr-85, Hg-203, Zn-65, Co-57, Ce-139 and Co-60). An AmBe neutron source was deployed in several (20) points mapping the Fiducial Volume, to investigate the energy and position response at high energies (above 2 MeV); this in particular is crucial for the analysis concerning high energies neutrinos, like B-8 neutrinos and geoneutrinos. This calibration campaign allowed to check and improve the position and energy reconstruction capability. In particular it lead to the significant reduction of the systematic error on the determination of the Fiducial Mass. These studies were also fundamental to tune several parameters (light yield, quenching factor KB and
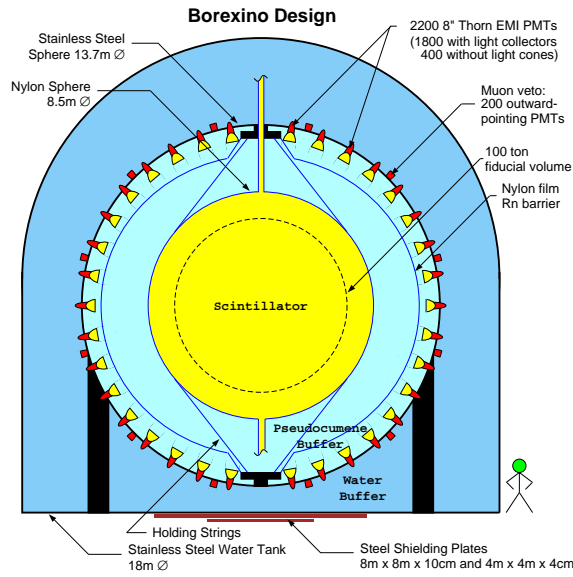
4

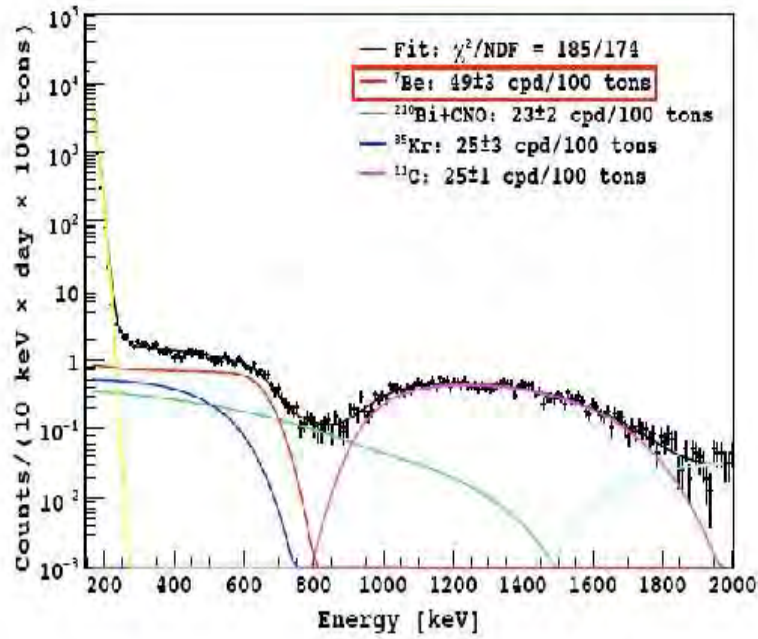Figure 1: Schematic view of the Borexino detector.

Figure 2: The observed Borexino spectrum after cuts, showing the shoulder due to solar Be-7 neutrino events (red line) and the Po-210 subtraction. The other main fit components in this energy region are also shown.

so on) in input to the Montecarlo code to improve the agreement between data and simulations.

During the year 2009, science data taking has resumed and one of the first analyses that came to completion was a high-sensitivity study of the Pauli exclusion principle [**?**] that made use of 485 days of data.

4   Future perspectives

A purification champaign is being planned for year 2010 in order to reduce Kr-85 and other backgrounds. This will improve the understanding of the detector and reduce the experimental error on the Be-7 measurement.

In addition, the following additional physics topics are under study or being considered for future investigation, depending on the background conditions and on the refinement of the ongoing analysis:

1. Measuring (or putting upper limits) on CNO and possibly pep solar neutrinos.

2. Search for terrestrial antineutrino interactions (geoneutrinos).

3. Study the very low energy part of the spectrum to the goal of looking for pp neutrinos.

4. Watch for neutrino bursts from Supernovae events.

In addition, neutrino source calibrations (with a ^{51}Cr source) are being considered, both to the goal of a final calibration and to the study of neutrino magnetic moment.

5   List of articles published in year 2009

1. G. Alimonti et al., *The Borexino detector at the Laboratori Nazionali del Gran Sasso.* Nucl. Instr. & Methods, A600 (2009) 568.

2. G. Alimonti et al., *The liquid handling systems for the Borexino solar neutrino detector.* Nucl. Instr. & Methods, A609 (2009) 58.

3. G. Bellini et al., *New experimental limits on the Pauli forbidden transitions in ^{12}C nuclei obtained with 485 days Borexino data.* arXiv:0911.0548v1, submitted to Phys. Rev. C.

References

[1] R. Davis, Nobel Prize Lecture 2002.

[2] W. Hampel et al., Phys. Lett. B 447 (1999) 127.

[3] J.N. Abdurashitov et al., Phys. Rev. Lett. 83 (1999) 4686.

[4] M. Altmann et al., Phys. Lett. B 616 (2005) 174.

[5] S. Fukuda et al., Phys. Rev. Lett. 86 (2001) 5651; Phys. Lett. B 539 (2002) 179.

[6] Q.R. Ahmad et al., Phys. Rev. Lett. 87 (2001) 071301.

[7] J.N. Bahcall and M.H. Pinsonneault, Phys. Rev. Lett. 92 (2004) 121301.

[8] J.N. Bahcall et al., JHEP 0408 (2004) 016.

[9] G.L. Fogli et al., Progr. Nucl. Phys., 57 (2006) 742.

[10] G. Alimonti et al., Astroparticle Physics 16 (2002) 205.

[11] C. Arpesella et al., Astroparticle Physics 18 (2002) 1.

[12] G. Alimonti et al., Nucl. Instr. & Methods A406 (1998) 411.

[13] G. Alimonti et al., Astroparticle Physics 8 (1998) 141.

[14] C. Arpesella et al., Phys. Lett. B 658 (2008) 101.

[15] C. Arpesella et al., Phys. Rev. Lett. 101 (2008) 091302.

[16] G. Bellini et al.,arXiv:0808.2868.

COBRA

G. Anton[a], V. Bocarov[b], P. Cermak[b], O. Civitarese[c], J. Durst[a], A. Fauler[d]. M. Fiederle[d],
A. Garson[e], D. Gehre[f], C. Gößling[g], H. Gastrich[g], C. Hagner[h], M. Heine[f], N. Heidrich[h],
B. Janutta[f], M. Junker[i], T. Köttig[g], S. Kietzmann[h], H. Krawczynski[e], V.K. Lee[e], Q. Li[e],
F. Lück[a], J. Martin[e], T. Michel[a], D. Münstermann[g], T. Neddermann[g], C. Oldorf[h],
S. Rajek[g], O. Reinecke[f], W. Schmidt-Parzefall[h], O. Schulz[g], M. Schwenke[f], F. Simkovic[j],
J. Suhonen[k], I. Stekl[b], J. Timm[h], W. Thurow[f], B. Wonsak[h], Y. Yin[e], R. Zimmermann[h],
K. Zuber[f,*]

[a] Universität Erlangen–Nürnberg – Germany
[b] Technical University of Prague – Czech Republic
[c] University of La Plata – Argentina
[d] Freiburg Materials Research Center – Germany
[e] Washington University in St. Louis – USA
[f] Technische Universität Dresden – Germany
[g] Technische Universität Dortmund – Germany
[h] Universität Hamburg – Germany
[i] Laboratori Nazionali del Gran Sasso – Italy
[j] University of Bratislava – Slovakia
[k] University of Jyvaskyla – Finnland
(* Spokesperson)

Abstract

The COBRA collaboration searches for the neutrinoless double beta decay with
a large array of Cadmium Zinc Telluride (CZT) semiconductor detectors. CZT
offers the low radioactivity levels and the energy resolution needed for a rare decay
search, with the advantage of operation at room temperature. It contains a number
of double beta decay candidates, among which ^{116}Cd is the most promising one.
Its Q-value of 2.8 MeV is well above many of the possible background contributions
from natural radioactivity. Besides a prototype apparatus consisting of 64 detectors
is being established at LNGS, the first CZT pixel detector system was installed to
investigate the major experimental issues of operating tracking CZT detectors in low
background mode. Additional studies into the detector technology are proceeding
in surface laboratories.

1 Introduction

Over the last decade the fact that neutrinos oscillate between flavour states was well established. The oscillation is explained by assigning a non-vanishing rest mass to the neutrinos. The absolute mass scale can not be probed with oscillation experiments. Additionally to the unknown absolute mass scale of the neutrino, the fundamental nature of neutrinos, i.e. if the neutrino is a Majorana or Dirac particle, is still unknown. Both of these questions can be answered in neutrinoless double beta decay experiments. The COBRA experiment looks for the neutrinoless double beta decay of ^{116}Cd isotope in a large array of Cadmium Zinc Telluride (CZT) semiconductor detectors.

1.1 Neutrinoless Double Beta Decay

Considering the binding energies of nuclei, one will find that for 35 known nuclides the single beta decay is energetically forbidden, but the double beta decay is not. This process is a second order process in the Standard Model of particle physics which will read:

$$(Z, A) \rightarrow (Z + 2, A) + 2e^- + 2\bar{\nu}_e \quad (2\nu\beta\beta\text{--decay}). \tag{1}$$

A neutrinoless decay would also occur, if the neutrino was its own antiparticle. In that case, all the energy of the decay would be carried away by the two emitted electrons:

$$(Z, A) \rightarrow (Z + 2, A) + 2e^- \quad (0\nu\beta\beta\text{--decay}). \tag{2}$$

Based on the rate of this process the calculation of the effective Majorana neutrino mass is possible.

   The results from oscillation experiments suggest an absolute mass scale of the order of $\sim 50\,$meV in the inverted mass scheme. Searches for the $0\nu\beta\beta$ did not yet observe the predicted signals, yielding an upper limit on the neutrino mass of the order of 0.2-0.5 eV. The observational evidence for $0\nu\beta\beta$ of ^{76}Ge[1], published in 2002, has resulted in a lot of discussion in the field. To verify this result, further large scale experiments are planned. In addition, any Ge-specific backgrounds and the uncertainties deriving from the calculations of the nuclear matrix elements have to be ruled out, thus exploration of other nuclei is vital in this field.

2 COBRA

The idea of COBRA is to use a large quantity of CZT semiconductor material, which contains a number of nuclides that are able to undergo double beta decay[2]. The main focus will be on ^{116}Cd, which is well suited for a double beta search due to its high Q-value of 2809 keV. Calculations show that the theoretical rates of $0\nu\beta\beta$--decay for ^{116}Cd is favourably high. First shell model calculations for nuclei heavier than ^{48}Ca make ^{116}Cd the most sensitive isotope from the theoretical point of view [3].

   COBRA follows the strategy that source and detector are identical, a method proven to be successful in various other double beta decay approaches. As a semiconductor, CZT crystals can be produced with good energy resolution and low levels of intrinsic

radioactivity. Due to a large bandgap, the detectors can be operated at room temperature avoiding extensive cooling operations.

The COBRA experiment is still in the R&D phase and there are two competing concepts for the layout of the experiment. One would be an array of $40 \times 40 \times 40$ $1\,\text{cm}^3$ coplanar grid (CPG) CZT detectors, the other would be a huge solid state time projection chamber (TPC) consisting of CZT pixel detectors. Both concepts add up to about $400\,\text{kg}$ of CZT, enriched to 90% in ^{116}Cd, to achieve a neutrino mass sensivity of $50\,\text{meV}$ and below. The modular design of the COBRA experiment in both cases would lead to a significant background reduction, as for example high energetic gamma rays are likely to interact in multiple detectors, while the energy deposited in a double beta decay is most probably contained in a single crystal. In a fine grained pixelated detector, it would be possible to reconstruct tracks of throughgoing particles. Two electrons emerging from a pixel would result in a line shaped track, while for example alpha particles of comparable energy would only hit very few pixels arranged within a circle, thus a pixelated solution would reduce the background even further.

3   R&D Activities

Since there are two different approaches for a COBRA experiment, namely an array of CPG CZT detectors or a solid state TPC consisting of pixelated CZT detector systems, the R&D activities have to be divided into a couple of subcategories. First of all, there are activities concerning the CPG detector option, which concern handling and operation of the CPG detectors as well as operating a CPG test setup at the LNGS laboratory. Second we have a number of institutes working on the pixel detector option. There are a number of different pixelated CZT detector systems available to the collaboration, which have to be characterized to figure out which best fits our needs. So far CZT pixel systems have not been operated underground and for the first time we managed to install and operate a pixel detector system underground at LNGS in 2009. Common to both approaches and all low background experiments is the issue of shielding. There are a variety of different choices concerning the shielding of the COBRA experiment. These vary from a purely passive shielding to an active shielding realized by a big tank of liquid scintillator. To optimize the shield geometry we have to run detailed Monte Carlo studies as well as experimental cross checks. Another part of the R&D activities is the growing of CZT crystals, in particular to be independent from commercial suppliers. Furthermore, a lot of effort has been put into building a material screening facility at TU Dortmund.

The details on the general purpose and the progress made in the different fields in 2009 are given in the following.

3.1   CPG activities

The COBRA collaboration has been operating a prototype setup for CPG detectors at the LNGS laboratory for a couple of years. This setup has been used to provide information on the background levels of the various setup components and thereby helped to reduce the background level step by step. Furthermore the setup will provide valuable information

about methods of instrumentation, long term stability and construction applicable to a larger array.

The setup in its current status can house up to 64 1 cm^3 detectors in the innermost volume, the nest. These are arranged in 4 layers, each housing 4×4 detectors. The nest, measuring $10 \times 10 \times 10$ cm^3, is surrounded by 10 cm of pure copper, again surrounded by 20 cm of low radioactivity lead. These metal layers, called castle, are a passive shield against exterior gamma radiation. This castle is embedded in a copper faraday cage which is located within a neutron shield, consisting of 7 cm thick slabs of borated polyethylen. Low diameter coaxial cables and copper traces on Kapton foils are used to supply the bias voltage and read out the signals. These are feed through the shielding.

In 2008 the first layer was installed into the prototype setup and with the data taken we were able to identify two of the major contributions to the background, namely the red color in the passivation lacquer of the crystals and the air within the setup. This was affirmed by operating colorless passivated detectors provided by the manufacturer and installing a liquid nitrogen flushing system. The spectrum can be seen in Figure 1. With
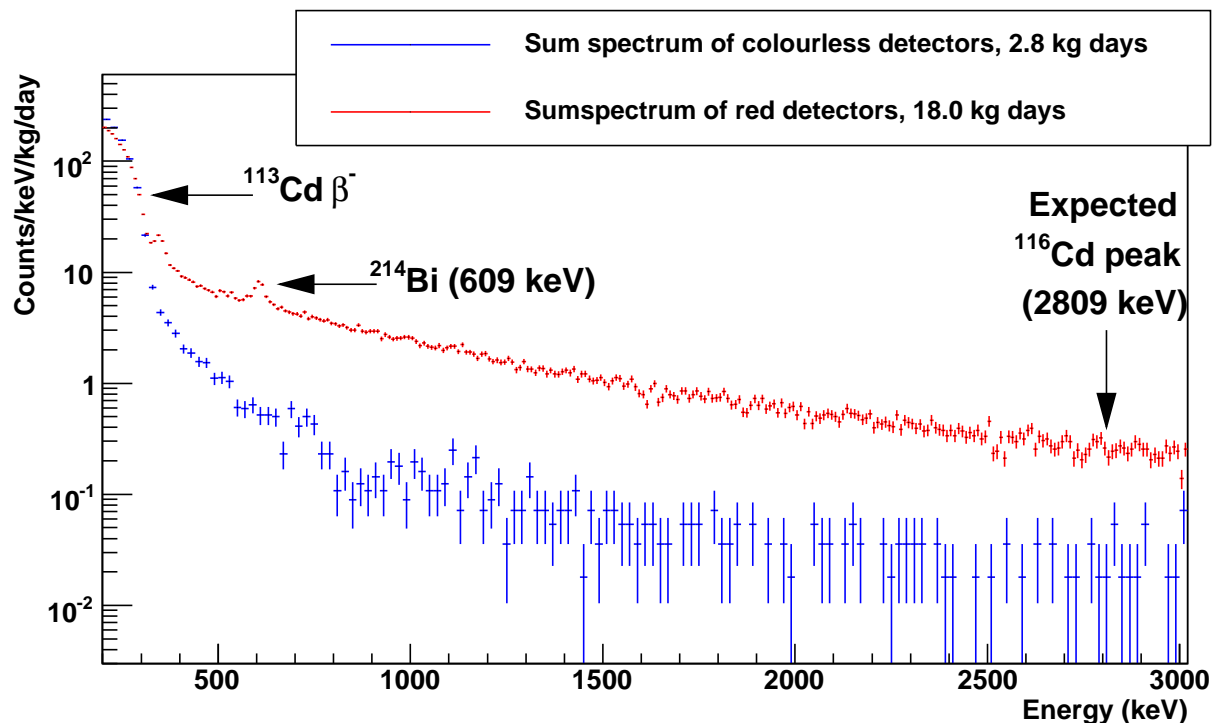

Figure 1: Sum spectrum of the first layer with an exposure of 18.0 kg·days and a layer with colourless passivation and nitrogen flushing with an exposure of 2.8 kg·days. The background level could be decreaded by an order of magnitude.

this significant reduction of the background level, the $2\nu\beta\beta$ decay of ^{116}Cd is nearly in reach to be measured. It contributes approximately 10 % to the spectrum in the region from 1 MeV to 2 MeV.

Since the lacquer contributed to the background so significantly, it did not make sense to install the remaining 48 detectors with red passivation and the collaboration decided to remove the red passivation from the crystals and look for cleaner passivations

to replace the red lacquer. For test purposes four detectors were stripped of the red passivation and re-coated with a commercial alternative, Cyclotene. These operations were executed at TU Dortmund. First investigations showed a good performance and stability of the recoated detectors, they even offered a better energy resolution than before the repassivation. Furthermore no degradation was measurable. Thus the detectors were installed at LNGS in december 2008.

3.2   Pixel detectors

Currently there is a variety of pixel systems available to the COBRA collaboration. A number of custom made systems are under investigation at the Washington University in St. Louis, a system developed by the Timepix collaboration used at Erlangen and Prague, and a large volume pixel detector, called Polaris provided by a group at University of Michigan.

One major drawback with pixelated detectors is, the usually very compact format with the electronics sitting directly on the detector, which are expected to be quite dirty from the low background point of view. Furthermore, there is practically no experience with operating such devices underground, i.e. it is not known whether the background suppression that one gets from the pixelation can compensate for the dirty environment. The high potential of pixelated systems is obvious, looking at a $0\nu\beta\beta$ decay within these systems. Propagating through the detector it is possible to distinguish one electron events from two electron events both depositing the same energy in the detector. Because electrons lose more energy at the end of their track. Thus, one would clearly observe high energy depositions at both ends of the two electron track, while for a one electron track, one would only get high energy depositions at one end of the track.

In september 2009 a Polaris system was installed within the COBRA setup at LNGS, running till end of 2009. Furthermore we have been continuing the investigations on the Timepix systems and measurements at the Laboratoire Souterrain de Modane (LSM) and at the Dresden Felsenkeller have been performed.

3.2.1   Polaris at LNGS

As for the CPG setup we provided a neutron shield, a lead shield and nitrogen flushing for the Polaris system. This was the first time to operate such a device under low background condition. The system installed consists of a large volume CZT crystal, $2 \times 2 \times 1.5\,\mathrm{cm}^3$, with 11×11 pixels, with custom made readout electronics. With a pixel pitch of $2\,\mathrm{mm}$ this detector cannot resolve tracks, but from pulse shapes one could distinguish electrons from alpha and gamma particles. With a mass of 36 grams this is the worlds largest CZT detector. The readout electronics provide not only 2D information coming from the pixels, but also reads out drift times to provide depth information.

Compared to a germanium or silicon crystal, CZT crystals are quiet inhomogeneous, causing a worse energy resolution. With the depth sensing provided by the detector systems from University of Michigan it is possible to divide the detector into $40 \times 11 \times 11$ volumes, so called voxels, and calibrate each of the voxels separately. This yields an overall resolution of better than $2\,\%$. A preliminary spectrum is shown in Figure 2. To obtain
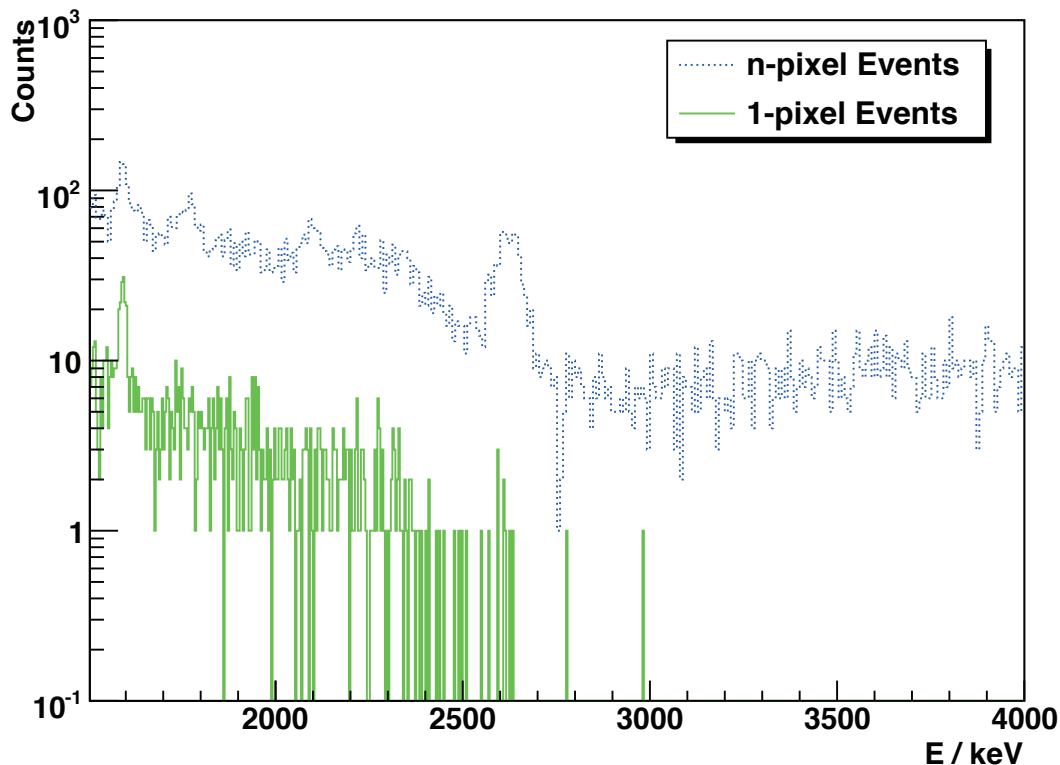
Figure 2: Spectrum obtained with the Polaris detector system. It shows that by only taking into account non surface voxels and single crystal hits, the background can be reduced significantly.

this spectrum some cuts were applied to the data. First of all, hits coming from boundary voxels were rejected. Furthermore events with more than one voxel hit were rejected, since a double beta event would always be a single site event. From the spectrum one can clearly see that these kind of devices have a big potential of background reduction. A detailed analysis on the data taken is ongoing.

3.2.2 Timepix detectors at LSM and Dresden Felsenkeller

The Timepix is a CMOS pixel detector readout chip designed by the Medipix Collaboration. It is designed to be connected to a semiconductor sensor. To investigate the radioactive contamination a system with a $300\,\mu$m thick silicon sensor (65536 readout channels with a pixel pitch of $55\,\mu$m) was installed at the Dresden Felsenkeller laboratory. Another silicon timepix system was operated at the LSM. Recently two CdTe systems became available.

The installation at Dresden Felsenkeller (about 11n m.w.e.) was done in september 2009 and the system is still running. From the events seen in Figure 3 and Figure 4 one easily understands the power of background reduction achieved by pixelated detector systems. The data taken so far will be used to develop algorithms for α, β, γ and μ identification in small pitch pixel devices.

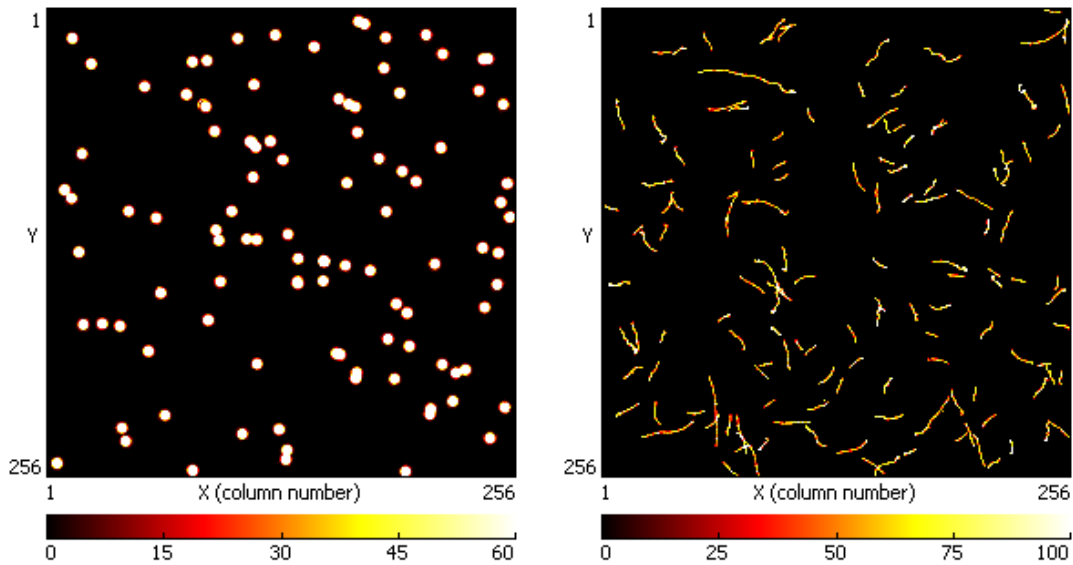Furthermore, we had the chance to operate another Timepix silicon system at the LSM

Figure 3: The left side shows a collection of α events recorded by a silicon pixel detector at LSM, on the right is a collection of β tracks.
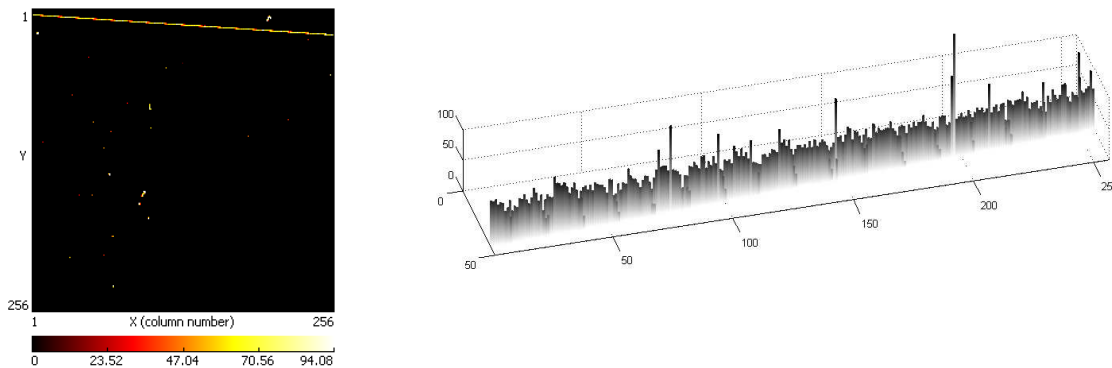

Figure 4: Example of a muon track crossing the whole detector (left) and the per-pixel energy (not calibrated) deposition (right).

and we also had the opportunity to measure the internal contamination of the readout electronics with an ultra–low background setup located in LSM. It consists of a planar type HPGe detector with a volume of $150\,\mathrm{cm}^3$. The next step will be to use the low background HPGe to measure samples of readout electronics components, to identify and replace the parts with the highest contamination.

3.2.3   Custom made pixel system

At Washington University in St. Louis there are a variety of readout electronics available. The energy resolution of pixelated detector system decreases with smaller pixel sizes, be-

cause the charge is shared among neighboring pixels. The group at Washington University St. Louis has $2 \times 2 \times 0.5\,\text{cm}^3$ crystals with different pixel sizes ranging from $350\,\mu\text{m}$ to $600\,\mu\text{m}$, to study this effect. They used a collimated ^{57}Co source of $250 \times 270\,\mu\text{m}^2$ cross–section. For the smallest pixel sizes the energy resolution of less than $10\,\%$ could not be achieved.
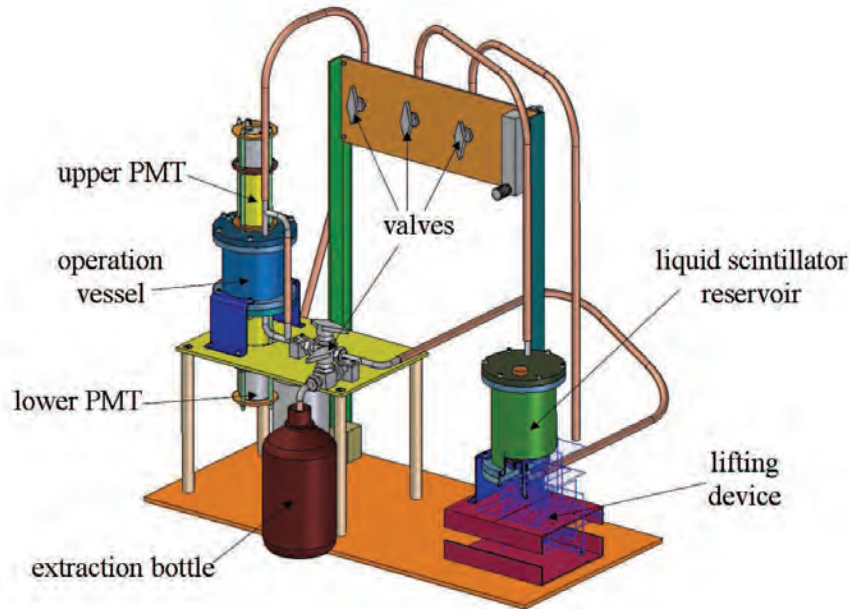
3.3   Shielding

Figure 5: Schematics of the vessel construction.

Besides the traditional shield concepts containing passive neutron shield and passive gamma shield materials like lead and copper, another concept is followed within the collaboration. This would dump bare crystals into liquid scintillator (LS), which would act as an active veto and shield. A sophisticated approach also considering statistics (several detectors) and long term stability is on its way. The design of the test setup built and operated at Hamburg is shown in Figure 5. Since studies concerning the operations of CZT detectors in LS are still at their very beginning, the setup should yield a maximum of flexbility concerning the scintillators used. The setup is ready for operation now and it is also implemented into the COBRA Monte Carlo framework.

3.4   Crystal growing

A crucial part of the COBRA experiment is the availability of big quantities of CZT crystals and their preparation for a large scale experiment. To be independent of commercial suppliers, the COBRA collaboration wants to grow its own crystals and does all necessary tasks in preparation self-dependently. During 2009 significant improvements were made

on the crystal growing apparatus, especially on the temperature stability. We managed to grow 75 mm CZT wafers for the first time now. These show good homogeneity and high resistivity. A picture of the wafer grown in Freiburg is shown in Figure 6. The CPG
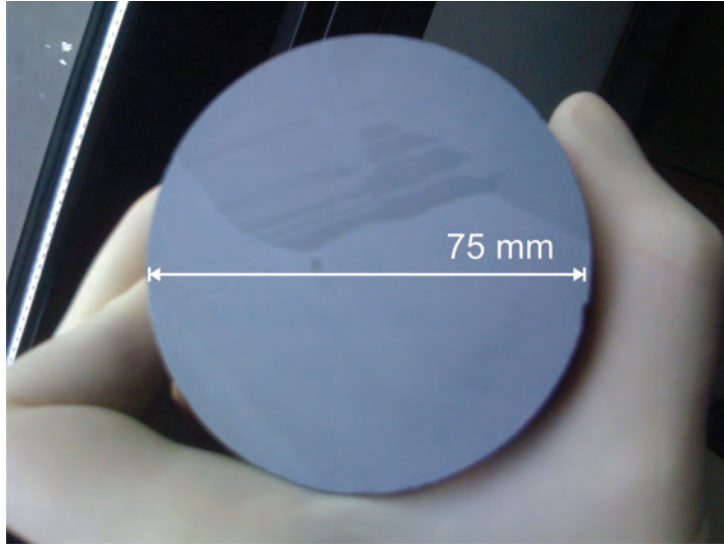

Figure 6: CdZnTe wafer with 75 mm diameter grown in Freiburg.

detectors grown and prepared in Freiburg reach an energy resolution of 3.1 % FWHM at 662 keV.

3.5 Dortmund Low Background Facility

During the last year a material screening facility, equipped with a 60 % relative efficiency ultra low background germanium detector, was set up at TU Dortmund. Although it is located at the surface, it has an overburden of more than 10 m.w.e. This overburden consists of 325 t of concrete and 43 t of iron and it reduces the flux of cosmic rays already considerably. The Ge-detector is shielded by lead, electrolytic copper and a neutron shield of boron loaded polyethylene. This shield suppresses the natural γ-background very efficiently. The remaining background is dominated by cosmic ray induced processes. This can be further reduced by nearly an order of magnitude with an active veto. In total background reduction of three orders of magnitude was achieved (Figure 7) at the Dortmund Low Background facility. In the current status of completion of the veto an upper limit of integral background counting rate of 0.07 counts/kg/s (40-2700 keV) is achieved, with potential for further improvement.

4 Conclusions

The COBRA experiment searches for the neutrinoless double beta decay of ^{116}Cd. We are to reach sensitivities up to 10^{26} years. The year 2009 was successful for the COBRA collaboration. After identifying two of the major contributions to the background in our CPG low background setup at LNGS in 2008, found circumventions proved to be clean
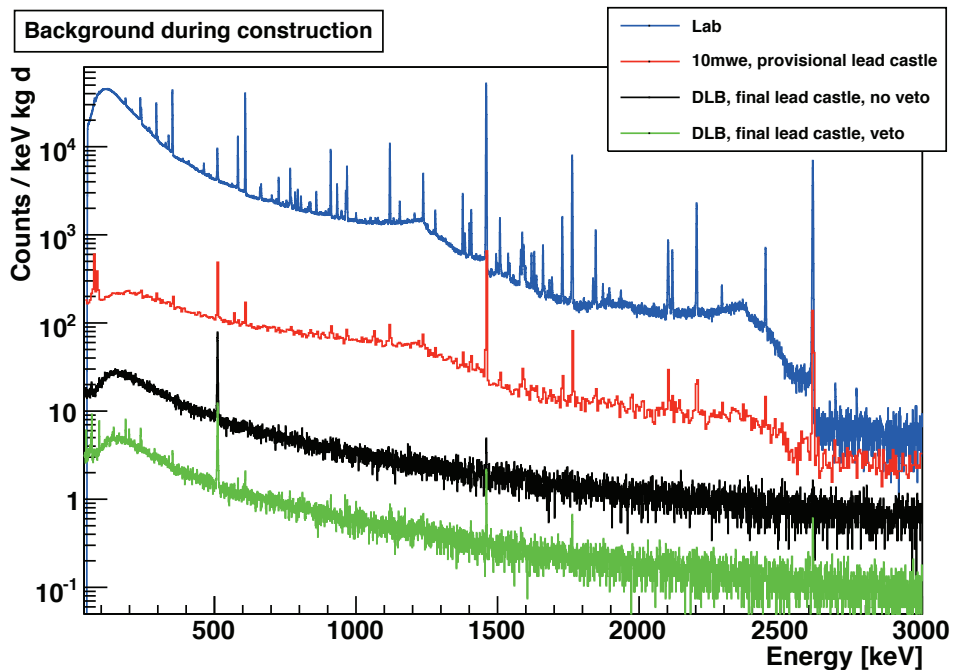
Figure 7: Reduction of background during construction

and reliable. The spectra from the newly handled detectors look very promising and with an installation of 64 CPG detectors sheduled for mid 2010 and a general upgrade of the setup, we might be able to study the $2\nu\beta\beta$ of ^{116}Cd.

The progress made on the pixelated detector option look very promising as well. Preliminart results of the first installation and operation of a pixel system in a low background environment look very promising. The collaboration will increase its commitment in 2010 and the analysis of the data already in hand promise a fruitful 2010.

5   List of Publications

1. *Experimental study of double-beta decay modes using a CdZnTe detector array*, J. V. Dawson et al, Phys. Rev. C 80, 025502 (2009)

2. *An Investigation into the 113-Cd Beta Decay Spectrum using a CdZnTe Array* , J. V. Dawson et al, Nucl. Phys. A 818, 264 (2009)

3. *First Results on Double Beta Decay Modes of Cd, Te and Zn Isotopes with the COBRA Experiment*, T. Bloxham et al, Phys. Rev. C. 76, 025501 (2007)

4. *Radiation Shielding for Underground Low-background Experiments*, D.Y. Stewart et al, Nucl. Inst. Meth. A 571,651 (2007)

5. *Evaluation of Pixellated CZT Detectors for Neutrinoless Double Beta-decay Measurements*, T.R. Bloxham, M. Freer, Nucl. Inst. Meth. A 572,722 (2007)

6. *Energy resolution improvement in room temperature CZT detectors*, Y. Ramachers, D. Y. Stewart, JINST 2:P12003 (2007)

7. *Updates on activities since the Durham meeting and status of COBRA*, K. Zuber, AIP Conf.Proc.942:96 (2007)

References

[1] H. V. Klapdor-Kleingrothaus et al., Mod. Phys. Lett. A **16** (2001) 2409

[2] K. Zuber, Physics Letters B **519** (2001) 1

[3] E. Caurier et al., Phys. Rev. Lett.**100** (2008) 052503

The CRESST Dark Matter Search

G. Angloher [a], M. Bauer [e], I. Bavykina [a], C. Bucci [d], A. Brown [b], C. Ciemniak [c],
R. Falkenstein [e], F. von Feilitzsch [c], D. Hauff [a], P. Huff [a], S. Henry [b], S. Ingleby [b], C. Isaila
[c], J. Jochum [e], M. Kiefer [a], M. Kimmerle [e], R. Kleindienst [a], H. Kraus [b], Q. Kronseder [a],
J.C. Lanfranchi [c], F. Petricca [a], S. Pfister [c], W. Potzel [c], F. Pröbst [a], S. Roth [c], K. Rottler
[e], S. Scholl [e], J. Schmaler [a], W. Seidel [a, +], C. Strandhagen [e], L. Stodolsky [a], A. J.
B. Tolhurst [b]

[a] MPI für Physik, Föhringer Ring 6, 80805 Munich, Germany
[b] University of Oxford, Department of Physics, Oxford OX1 3RH, U.K.
[c] Technische Universität München, Physik Department, D-85747 Garching, Germany
[d] Laboratori Nazionali del Gran Sasso, I-67010 Assergi, Italy
[e] Eberhard-Karls-Universität Tübingen, D-72076 Tübingen, Germany
[+] Spokesperson E-mail address: seidel@mppmu.mpg.de
[*] present address: University of Warwick, Coventry CV4 7AL, U.K.

Abstract

The aim of CRESST (**C**ryogenic **R**are **E**vent **S**earch with **S**uperconducting
Thermometers) is to search for particle Dark Matter and to contribute to the elu-
cidation of its nature. The experiment is located at the 'Laboratori Nazionali del
Gran Sasso' (LNGS), Italy, and it uses low background cryogenic detectors with
superconducting phase transition thermometers for the direct detection of WIMP-
nucleus scattering events.

1 Dark Matter

There is strong evidence for the existence of dark matter on all astronomical scales, ranging
from dwarf galaxies, through spiral galaxies like our own, to large-scale structures. The
history of the universe is difficult to reconstruct without dark matter, be it Big Bang
Nucleosynthesis or structure formation.

Despite this persuasive indirect evidence for its existence, the direct detection of dark
matter remains one of the outstanding experimental challenges of present-day physics and
cosmology.

A plausible candidate for the dark matter is the Weakly Interacting Massive Particle
(WIMP) and it is possible that it can be detected by laboratory experiments, particularly
using cryogenic methods, which are well adapted to the small energy deposit anticipated.
Supersymmetry provides a well-motivated WIMP candidate in the form of the Lightest
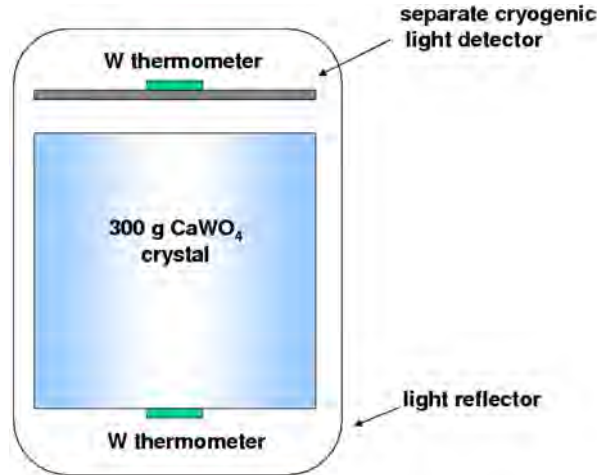
Figure 1: Schematic representation of the detector for simultaneous phonon and light measurement. It consists of two separate cryogenic detectors enclosed in a highly reflective housing, read out by tungsten superconducting phase-transition thermometers. This concept, developed by scientists of the institute, is used in CRESST-II. It allows a very efficient discrimination of the searched nuclear recoil signals from the dominant radioactive β- and γ-backgrounds.

Supersymmetric Particle. WIMPs are expected to be gravitationally bound in a roughly isothermal halo around the visible part of our galaxy with a density of about $0.3\,\mathrm{GeV/cm^3}$ at the position of the Earth.

Interaction with ordinary matter is expected via elastic scattering on nuclei. This elastic scattering can occur via coherent ("spin-independent") and spin-dependent interactions. For the coherent case, a factor A^2 is expected in the cross-section, favouring heavy nuclei.

Conventional methods for direct detection rely on the ionisation or scintillation caused by the recoiling nucleus. This leads to certain limitations connected with the low ionisation or scintillation efficiency of the slow recoil nuclei. The cryogenic detectors developed for CRESST measure the deposited energy calorimetrically, independent of the type of interaction, and allow for the detection of much smaller recoil energies. When such a calorimetric measurement of the deposited energy is combined with a measurement of scintillation light, an extremely efficient discrimination of the nuclear recoil signals from radioactive background signals can be obtained. These type of detectors are being used in the present phase CRESST-II.

2   Detection Principle

The low-temperature calorimeters consist of a target crystal with an extremely sensitive superconducting phase transition thermometer on its surface. A weak thermal coupling to a heat bath restores again the equilibrium temperature after an interaction. The thermometer is made of a tungsten film evaporated onto the target crystal. Its temperature is stabilised within the transition from the superconducting to the normal conducting
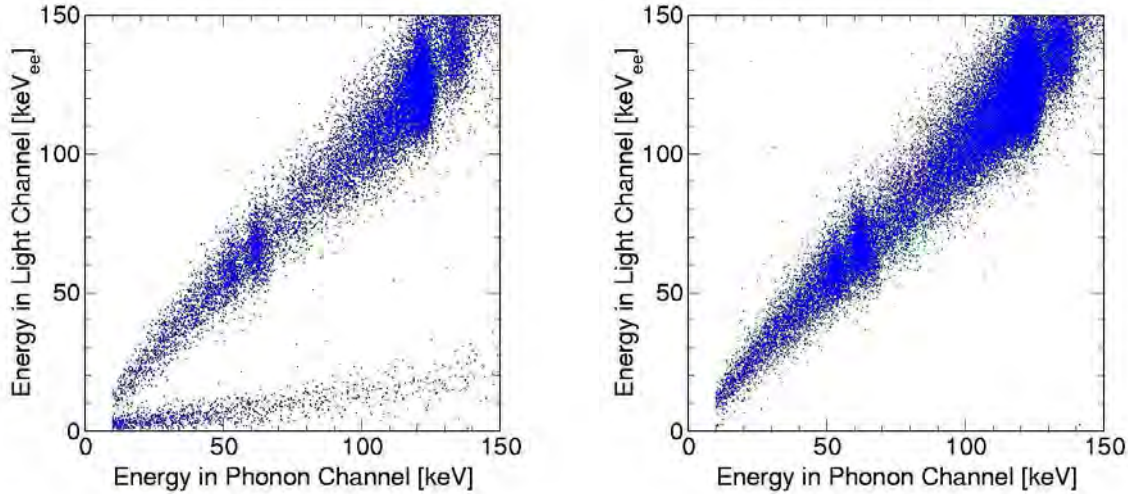
Figure 2: Coincident detection of phonons and scintillation light with a CaWO$_4$ detector. Left: The upper band of events is due to irradiation of the CaWO$_4$ crystal with electrons and gammas, whereas the lower band with lower light yield, is from nuclear recoils caused by a neutron source. Right: Removing the neutron source confirms that there is no leakage of ionising events into the nuclear recoil region.

state, which occurs at temperatures of about 10 mK. A typical width of the transition is about 1 mK. A small temperature rise e.g. from a WIMP–nucleus scattering event (typically some μK), leads to an increase of resistance, which is measured with a SQUID (**S**uperconducting **Qu**antum **I**nterference **D**evice). For the first phase of CRESST, which ended in 2001, 262 g sapphire detectors had been developed at MPI. These detectors provided an excellent energy resolution of 133 eV at 6 keV and a very low energy threshold of 600 eV.

In the second phase, CRESST-II, we are using 300 g scintillating CaWO$_4$ target crystals. The scintillating crystal is equipped with a superconducting tungsten phase-transition thermometer for the detection of the phonons created by a particle interaction in the scintillating crystal. A small fraction of $\sim 1\%$ of the deposited energy is emitted as scintillation light, which is measured with a separate cryogenic detector, optimised for light detection. Fig. 1 shows a scheme of this composite detector.

Starting with a proof-of-principle experiment in 1998, the technique of simultaneous measurement of phonons and scintillation light has been developed at the Max-Planck-Institute. The important advantage of this technique is that it offers an extremely efficient suppression of the radioactive background down to very low recoil energies of about 10 keV. While the phonon signal measures the deposited energy, the amplitude of the corresponding light signal depends on the type of interaction. Nuclear recoils, such as WIMP or neutron scattering events, emit substantially less scintillation light than fully ionising interactions, e.g. γ or β interactions, do. As the overwhelming part of the background consists of β and γ interactions, this phonon/light technique provides a very effective

method of background suppression. Fig. 2 illustrates this detection method.

Compared with the alternative approach of simultaneous measurement of phonons and charge in a semiconductor crystal, which is applied in the experiments CDMS-II and Edelweiss-II, the method developed for CRESST-II has the important advantage that it does not suffer from dead layers at the surface. A reduced charge collection for ionising events occurring close to the surface in semiconducting crystals may lead to a false identification of low energetic γ's and β's as nuclear recoils. The result in Fig. 2, which was obtained with a gamma and beta source, confirms that the suppression also works for low-energy electrons impinging onto the crystal surface.

3   The CRESST Setup in Gran Sasso

The central part of the CRESST installation at Gran Sasso is the cryostat, sketched in Fig. 3. The low temperature which is generated in the mixing chamber of the dilution refrigerator is transferred into the radio-pure cold box, via a 1.5 m long cold finger. The cold finger is protected by thermal radiation shields, all fabricated of low-background copper. The detectors are mounted inside the cold box at the end of the cold finger. Two internal cold shields consisting of low-level lead are attached to the mixing chamber and to a thermal radiation shield at liquid N_2 temperature, respectively, in order to block any line-of-sight from the non-radio-pure parts of the dilution refrigerator to the detectors inside the cold box. The design completely avoids potentially contaminated cryogenic liquids inside the cold box.

An extensive passive shielding of low-background copper and lead surrounds the cold box and serves to shield radioactivity from the surrounding rock. The entire shielding is enclosed inside a gas-tight radon box that is flushed with boil of N_2 gas and maintained at a small overpressure. Special care was taken to minimise above-ground exposure of the construction materials of the cold box and the shielding to cosmic rays, in order to avoid activation.

This setup has been upgraded for the experimental program of CRESST-II, to allow the operation of 33 phonon/light detector modules. The upgrade included the installation of a 66-channel SQUID readout in the existing cryostat, a system for the integration of the 33 detectors in the cold box, the installation of a passive neutron shield, a muon veto, and a new multichannel electronics and DAQ. The cryostat with the upgraded shielding is shown schematically in Fig. 4. In this upgrade the institute was responsible for the neutron shield, the wiring of the cryostat from the mixing chamber down to the detectors, the detector integration system and the DAQ. The upgrade began in 2004 after a 52-day run with two 300 g prototype phonon/light detector modules in the old setup. With this short run a competitive sensitivity of 1.6×10^{-6} pb for the WIMP nucleon scattering cross section was reached despite the absence of any neutron shield.
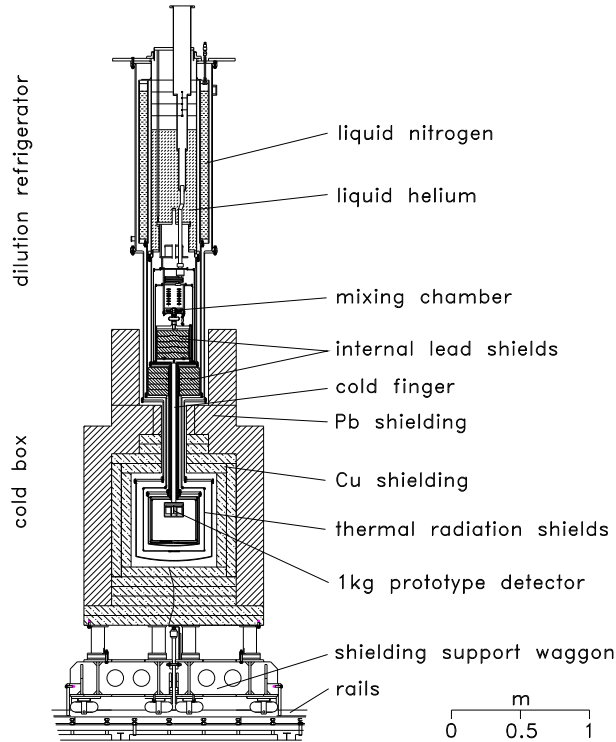
Figure 3: Layout of the CRESST ^{3}He/^{4}He dilution refrigerator and low-background cold box with its shielding.

4 Situation After Previous Runs

4.1 Commissioning Run

CRESST has shown the success of the combined phonon-light technique for the first time in a commissioning run in the year 2007. Although this was mainly for optimization purposes, two detector modules could be reliably operated and collected data with a total exposure of about 48 kg days. In this data, a total of three candidate events were found in the acceptance region of the tungsten recoils (between 10 and 40 keV of recoil energy). From this, using standard assumptions for the dark matter distribution in our galaxy, we derived an upper limit on the coherent WIMP-mucleon scattering cross section which is as low as 4.8×10^{-7} pb for an assumed WIMP mass of $50 \, \mathrm{GeV/c^2}$ [1].

While the above analysis is based on the conventionally made assumption of an elastic WIMP scattering, also other theories have been proposed. In particular, Smith and Wiener suggested a model named *inelastic Dark Matter*, which assumes that the WIMP undergoes a transition to an excited state (order of 100 keV above the ground state) during the scattering process [2]. The different kinematics of such an interaction changes the sensitivities of experiments such that the DAMA annual modulation signal can be reconciled with the absence of a positive signal in the other experiments, rendering this model particularly interesting. Due to its heavy target nucleus (tungsten), CRESST is able to give the tightest limits of the current experiments on this inelastic Dark Matter, and already from the data of the commissioning run large areas of the parameter space
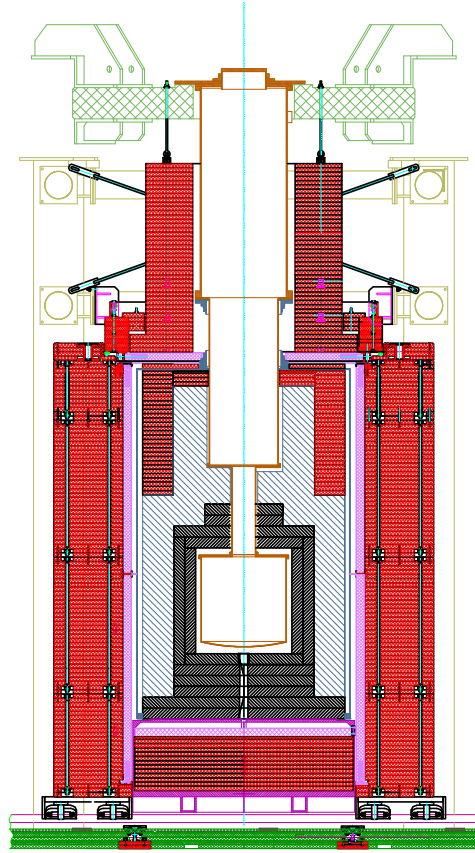
25

Figure 4: Dilution refrigerator and low-background cold box with its shielding upgraded for CRESST-II. The gas-tight radon box enclosing the Cu (shown in gray) and Pb (blue) shielding is completely covered by a plastic scintillator μ-veto (pink) and 40 cm of polyethylene (red).
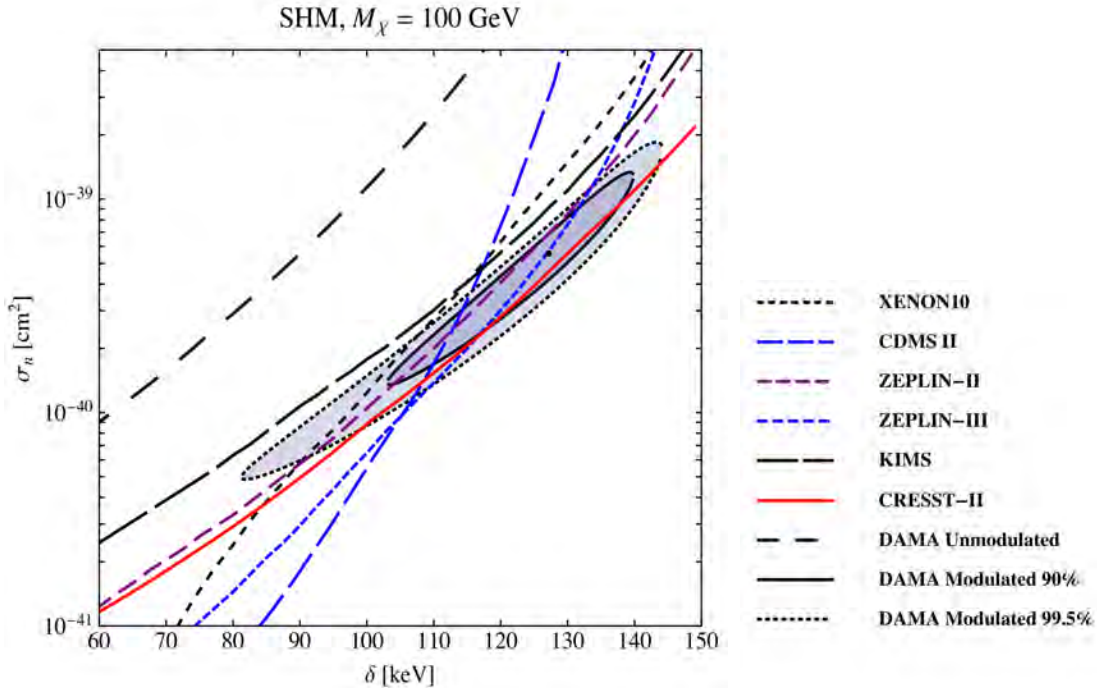
Figure 5: Exclusion plot for inelastic Dark Matter and an assumed WIMP mass of $100 \, \text{GeV/c}^2$. CRESST sets the tightest limits over most of the parameter range and already excludes most of the parameter space compatible with the DAMA signal. Plot taken from [3].

could be excluded [3]. Fig. 5 shows the excluded scattering cross section as a function of the mass splitting δ between the excited WIMP state and the ground state for the example of a $100 \, \text{GeV/c}^2$ WIMP. Also shown is the parameter space which is compatible with the DAMA signal. A small fraction of it could not yet be excluded by other experiments, thus leaving this model still a possible explanation.

4.2 2008 Data Taking

In order to improve on the limit obtained from the commissioning run, a subsequent run was performed between August and December 2008, with the goal to get a better understanding and suppression of the remaining events in the signal acceptance region. The target mass was increased to 9 operational detector modules. Apart from that, the main changes with respect to the commissioning run were the following:

1. New phonon detectors with a higher light output were developed. This was realized by not directly evaporating the tungsten film onto the large crystal but on a separate smaller crystal which was then glued to the actual target crystal. This avoids a degradation of the light output of the target crystal during the evaporation process. The higher amount of scintillation light then allows for a considerably better discrimination of nuclear recoils. In the 2008 run, one such crystal was operational.

2. New holding clamps for the crystals were manufactured which were completely covered with scintillating epoxy. This abolished the last non-scintillating areas in the vicinity of our detectors. Such a scintillating surrounding is important as a veto for surface α-decays. If an α-decay happens on a surface near one of the crystals, it can happen that the α-particle escapes detection but the recoiling daughter nucleus hits the crystal and mimics a WIMP event. However, if the α-particle hits a scintillating surface, this creates additional light in coincidence with the recoil event, moving the event out of the signal acceptance region.

During analysis, it turned out that almost all detector modules in this run had seen events where no scintillation light could be detected (and which therefore lie within the signal acceptance region), with the rate of such events varying considerably between the different detectors. Part of these events showed a slightly different pulse shape (longer decay time) from normal particle pulses and could thus be rejected by pulse shape cuts, but several events with particle-like pulses still remained. We attribute these no-light events to stress-relaxation processes which can happen at the contact surface between the crystals and their holding clamps due to the rather tight clamping. While one would expect a particle-like pulse shape if such a relaxation happens in the crystal (in the form of a microscopic crack), similar relaxations in the clamps might explain the no-light events with longer pulses. In particular, it seems that the epoxy layer on the clamps can be a major source of such events, since one module which had been mounted with pure metal clamps for comparison was almost background free (one event only).

As a consequence of the 2008 run, the holding clamps of all crystals were exchanged by redesigned, new ones. They are made from thinner bronze material to be as soft as possible (in order not to lead to cracks in the crystals) and any kind of scintillating coverage is avoided. This requires even more cleanliness during detector mounting and handling in order to avoid contamination of the surfaces.

5   2009 Data Taking

The 2009 run finally started in May after it had been delayed for several weeks by the earth quake in the L'Aquila region. 10 complete detector modules are operational and have been taking data since then. Included are three crystals with a glued thermometer as described above, one crystal made from the alternative material $ZnWO_4$ (which, compared to $CaWO_4$, has a considerably higher light output at low temperatures), as well as one detector module which is equipped with two light detectors (one on each side of the crystal) in order to collect as much scintillation light as possible. A gamma calibration of all modules was performed before starting the background run.

Generally, the detectors are running stably, with occasional disturbances due to the continuing seismic activity. The new, softer clamps have lead to an even higher sensitivity to external vibrations, even the ones coming from the cryostat itself (e.g. bubbling in the nitrogen or helium tank). In order to eliminate the influence of the nitrogen level in the tank, a cooling system has been installed which uses a continuous flow of cold nitrogen gas and thus avoids liquid in the tank.

A preliminary (but already blind) analysis of several modules has shown that the new clamps have lead to an improvement of the background situation. No-light events with different pulse shape are not observed anymore, which supports the hypothesis that the scintillating layer on the clamps was the source of these events.

A first look at the current data also showed that most detector modules have seen few no-light events within the acceptance region in an exposure similar to the one presented here. They have a particle-like pulse shape and look like potential signal events. We aim for a continuation of this run so that the nature of these events can be clarified. With respect to the inelastic Dark Matter scenario in particular, CRESST should have the potential to rule out this theory or to detect the corresponding annual modulation signal over large parts of the available parameter space. A total duration of at least one year (i.e. a full oscillation period) is therefore planned for this run.

6   R&D-Cryostat

Due to strong pile up effects CRESST detector modules cannot be operated in an overground or a shallow underground laboratory. Up to now, these modules could thus only be tested in the CRESST cryostat at the LNGS. In the past, this situation forced us to use "untested modules" (except for the transition temperature of the thermometers) in CRESST and to mix R&D and physics measurements in the Dark Matter experiment.

In order to decouple these two issues, we now have set up a small, simple, moderately shielded cryostat in the LNGS underground lab. This cryostat will be dedicated to R&D work and will enable us to test and develop detector modules before we use them in the CRESST low background cryostat. This will certainly optimize the outcome of the low background measuring runs and gives us the possibility to respond faster and more effectively to various detector issues. The turn-around time of this cryostat is extremely fast (cooldown in less than a day) and will also give our shifters the opportunity to perform interesting and important measurements during their stay at the LNGS.

The installation of the cryostat has been completed by now and a short commissioning phase will follow. Since the cryostat has been used at MPI Munich for many years before, we expect that it will be fully operational soon, probably in very early 2010.

References

[1] Godehard Angloher et al. Commissioning run of the CRESST-II dark matter search. *Astropart. Phys.*, 31(4):270 − 276, 2009.

[2] David Smith and Neal Weiner. Inelastic dark matter. *Phys.Rev.D*, 64:043502, 2001.

[3] John March-Russell, Christopher McCabe, and Matthew McCullough. Inelastic dark matter, non-standard halos and the DAMA/LIBRA results. arxiv:0812.1931, December 2008.

CUORE

F. Alessandria[8], E. Andreotti[6,10], R. Ardito[11], C. Arnaboldi[10], F. T. Avignone III[25],
T. I. Banks[19], G. Bari[15], M. Balata[5], I. Bandac[25], S. Banfi[9,10],
M. Barucci[1,2], A. Bau[9,10], J. W. Beeman[18], F. Bellini[12,13], E. Bissiato[7],
T. Bloxham[18], C. Brofferio[9,10], A. Bryant[18,19], C. Bucci[5], E. Buccheri[13],
X. Cai[27], L. Canonica[3,4], S. Capelli[9,10], M. Capodiferro[13], L. Carbone[10], M. Carrettoni[9,10],
G. Cerruti[10], M. Clemenza[9,10], C. Crescentini[15], D. Conventi[7], C. Cosmelli[12,13],
O. Cremonesi[10], R. J. Creswick[25], I. Dafinei[13], A. Debiasi[7], M. P. Decowski[18,19],
A. De Lucia[9,10], M. M. Deninno[14,15], A. de Waard[17], S. Di Domizio[3,4],
M. J. Dolinski[19,21], L. Ejzak[26], R. Faccini[12,13], D. Fang[27], H. A. Farach[25],
E. Ferri[9,10], F. Ferroni[12,13], S. Finelli[15], E. Fiorini[10],
L. Foggetta[6,10], S. J. Freedman[18,19], R. Gaigher[10], C. Gargiulo[13], A. Giachero[10], L. Gironi[9,10],
A. Giuliani[6,10], P. Gorla[5], C. Gotti[10], C. Guandalini[15], E. Guardincerri[4],
M. Guerzoni[15], T. D. Gutierrez[24], E. E. Haller[18,20], K. Han[18], K. M. Heeger[26], H. Z. Huang[23],
K. Ichimura[19], R. Kadel[18], K. Kazkaz[21], S. Kraft[9,10], G. Keppel[7],
L. Kogler[18,19], Yu. G. Kolomensky[18,19], M. Iannone[13], X. Liu[23], E. Longo[12,13], Y. Ma[27],
C. Maiano[9,10], G. Maier[11], R. H. Maruyama[26], C. Martinez[25], M. Martinez[10,16],
R. Mazza[10] R. Michinelli[15], N. Moggi[14,15], S. Morganti[13], S. Nisi[5],
S. Newman[25], C. Nones[6,10], E. B. Norman[21,22], A. Nucciotti[9,10], M. Olcese[4], F. Orio[12,13],
D. Orlandi[5], P. Ottonello[3,4], G. Pancaldi[15], M. Pallavicini[3,4], V. Palmieri[7],
A. Passerini[9,10], L. Pattavina[9,10], M. Pavan[9,10], M. Pedretti[21],
A. Pelosi[13], M. Perego[10], G. Pessina[10], V. Pettinacci[13],
S. Pirro[10], E. Previtali[10], V. Rampazzo[7], F. Rimondi[14,15], L. Risegari[1,2],
C. Rosenfeld[25], C. Rusconi[6,10], C. Salvioni[6,10], S. Sangiorgio[26], D. Schaeffer[9,10],
N. D. Scielzo[21], M. Sisti[9,10], A. R. Smith[18], E. Tatananni[5] W. Tian[27],
C. Tomei[13], l D. Torazza[3,4], S. Trentalange[23], G. Ventura[1,2], M. Vignati[12,13],
H. Wang[27], C. Whitten Jr[23], N. Xu[18], L. Zanotti[9,10], C. Zarra[5],
S. Zucchelli[14,15] and A. Zullo[13]

[1] Dip. di Fisica dell'Università di Firenze, Firenze I-50125 - Italy
[2] INFN - Sez. di Firenze, Firenze I-50125 - Italy
[3] Dip. di Fisica dell'Università di Genova, Genova I-16146 - Italy
[4] INFN - Sez. di Genova, Genova, I-16146 - Italy
[5] Laboratori Nazionali del Gran Sasso, Assergi (L'Aquila) I-67010 - Italy
[6] Dip. di Fisica e Matematica dell'Univ. dell'Insubria, Como I-22100 - Italy
[7] Laboratori Nazionali di Legnaro, I-35020 Legnaro (Padova) - Italy
[8] INFN - Sez. di Milano, Milano I-20133 - Italy
[9] Dip. di Fisica dell'Università di Milano-Bicocca, Milano I-20126 -Italy
[10] INFN - Sez. di Milano Bicocca, Milano I-20126 - Italy
[11] Dip. di Ingegneria Strutturale del Politecnico di Milano, Milano I-20133 - Italy
[12] Dip. di Fisica dell'Università di Roma La Sapienza, Roma I-00185 - Italy
[13] INFN - Sez. di Roma, Roma I-00185 - Italy
[14] Dip. di Fisica dell'Università di Bologna, Bologna I-40126 - Italy
[15] INFN - Sez. di Bologna, Bologna I-40126 - Italy
[16] Lab. de Fisica Nuclear y Altas Energias, Univ. de Zaragoza, Zaragoza E-50009 - Spain
[17] Kamerling Onnes Laboratory, Leiden University, 23000 RAQ, Leiden, The Netherland
[18] Lawrence Berkeley National Lab., Berkeley, CA 94720 - USA
[19] Dept. of Physics, Univ. of California, Berkeley, CA 94720 - USA
[20] Dept. of Materials Sc. and Engin., Univ. of California, Berkeley, CA 94720 - USA
[21] Lawrence Livermore National Laboratory, Livermore, California, 94550 - USA
[22] Dept. of Nuclear Engineering, Univ. of California, Berkeley, CA 94720 - USA
[23] Dep. of Physics and Astronomy, University of California, Los Angeles, CA 90095-1547 - USA
[24] California Polytechnic State Univ., San Luis Obispo, CA 93407 - USA
[25] Dept.of Phys. and Astron., Univ. of South Carolina, Columbia, South Carolina 29208 - USA
[26] Univ. of Wisconsin, Madison, Wisconsin 53706 - USA
[27] Shanghai Institute of Applied Physics (Chinese Academy of Science), Shanghai - China

Abstract

We present a report on the most relevant activities carried out during 2009 for the CUORE experiment.

1 Introduction

The nature of neutrino mass is one of the frontier problems of fundamental physics. Neutrinoless Double Beta Decay ($\beta\beta(0\nu)$) is a powerful tool to investigate the mass hierarchy and possible extensions of the Standard Model. The $\beta\beta(0\nu)$ is a rare spontaneous nuclear transition where a nucleus (A,Z) decays into an (A, Z+2) nucleus with the emission of two electrons and no neutrino, resulting in a peak at the sum energy spectrum of the electrons. The decay is possible only if the neutrino is a Majorana massive particle, its transition width is proportional to the square of $|\langle m_\nu \rangle|$. From the $\beta\beta(0\nu)$ half-life it is therefore possible to infer importat information concerning the mass hierarchy and the absolute mass scale of neutrinos.

CUORE (Cryogenic Underground Observatory for Rare Events) [1] aims at searching for $\beta\beta(0\nu)$ of ^{130}Te exploiting the high energy resolution of the bolometric technique.

The CUORE detector is a system of 988 cryogenic bolometers. The array is composed by 19 vertical towers cooled by means of a dilution (^{3}He/^{4}He) refrigerator to a temperature of $\sim$10 mK. A tower consists of 13 layers of 4 bolometers each. The bolometer is a TeO$_2$ cubic crystal, 5×5×5 cm^3 in size, with an NTD Ge thermistor and a heater (a Si resistor doped with As) glued onto the crystal surface and used respectively for the signal read-out and the detector gain control. The dielectric TeO$_2$ crystal has a very low heat capacity and a very large (27% in mass) natural isotopic abundance of the $\beta\beta(0\nu)$ candidate ^{130}Te. Each cube has a weight of 750 g, so the detector is a granular calorimeter with a total mass of $\sim$741 kg, corresponding to $\sim$200 kg of ^{130}Te. Each of the 19 towers is made of a copper skeleton where crystals are held in position through PTFE spacers. The towers are fasten to a thick copper plate that provides the thermal contact toward the low temperature heat sink.

The array is mounted inside a specially designed cryostat made of six nested vessels and its base temperature, without heat loads, is expected to be as low as 6 mK. Three lead shields are used to protect the detector from environmental radioactivity and from contaminations in the building materials. A 25 cm thick lead layer outside the OVC shields the detector from radiations coming from the bottom and from the sides. An equivalent shielding against radiation coming from the top is placed inside the cryostat, just above the detector. This is a 30 cm thick lead disk. An additional shielding of detector's sides and bottom is provided by a 6 cm lead layer just outside the Steel shield. Outside the external lead shield an 18 cm thick polyethylene layer will be added in order to thermalize environmental neutrons that will then be absorbed by a 2 cm layer of H$_3$BO$_3$ powder contained in the hollow space between the lead and the polyethylene itself. On the top and on the bottom of the setup, due to construction difficulties, the neutron shield will be made of a single 20 cm layer made of polyethylene with 5% in boron.

The experimental set-up was described in details in [3, 2]. Here we summarize the 2009 achievements with regards to the most important activities.

2 Crystals

The year 2009 was the year of consolidated large scale production of TeO$_2$ crystals for CUORE. The production and shipment process was performed in the conditions described in detail in [3]. The total number of crystals shipped in 2009 was 221, which makes a total of 314 crystals produced and sent to LNGS for CUORE. Fig. 1 gives the crystal shipment status at the end of 2009.

Currently, the TeO$_2$ crystal production facility at SICCAS Jiading has a nominal production capacity of 30 crystals/month. Fig. 2 gives the production status in 2009 and the production foreseen for the next year, 2010. As described in the previous report [3], the production of crystals is systematically controlled and each production phase is certified by INFN experts. In the case of radio-purity the certification is based on the results obtained in at least 2 of the three laboratories where samples are systematically sent for analysis (SINAP, LNGS and Berkeley). Fig. 3 gives the origin of ICP-MS measurements

shipment ID	shipment date	delivery date	quantity	barcode from	barcode to	current* location
INFN-01	March 24, 2009	May 12, 2009	26	080070	080097	CUORE-PSA, LNGS
INFN-02	April 9, 2009	June 4, 2009	36	080099	080136	CUORE-PSA, LNGS
INFN-03	May 12, 2009	June 22, 2009	32	080137	080170	CUORE-PSA, LNGS
INFN-04	August 21, 2009	September 29, 2009	60	080171	080236	CUORE-PSA, LNGS
INFN-05	September 20, 2009	October 27, 2009	34	080237	080274	CUORE-PSA, LNGS
INFN-06	October 25, 2009	November 25, 2009	33	080275	080311	CUORE-PSA, LNGS
INFN-07	November 19, 2009		34	080312	080348	Milano, Italy
INFN-08	December 11, 2009		32	080349	080381	on the sea
INFN-09	December 24, 2009		27	080382	080409	on the sea

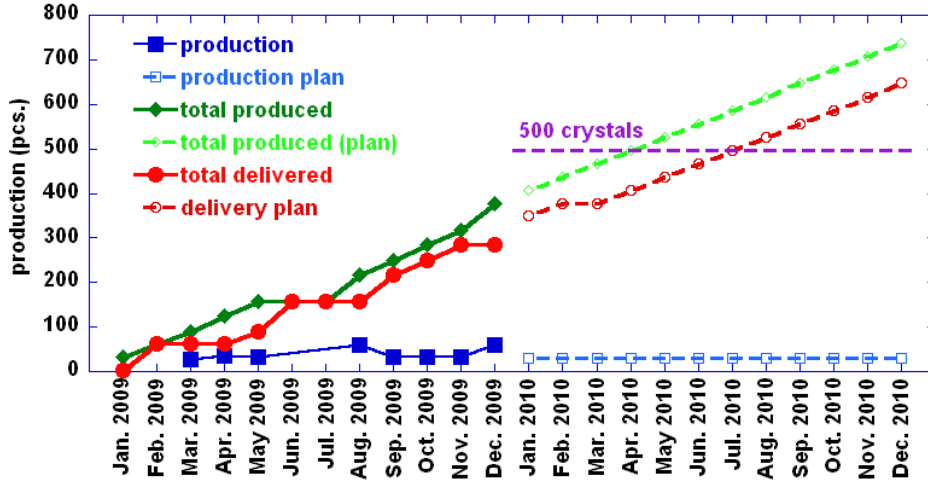Figure 1: Crystal shipments for CUORE.

Figure 2: CUORE crystals production status in 2009 and the production foreseen for 2010.

used for the certification of raw materials and intermediary products for the certification of CUORE crystals.

Very strict certification conditions were also applied for the dimensions of the crystals and for the quality of surface processing. The results of planarity measurements made on the 2 hard faces ($< 100 >$) and 4 soft faces ($< 110 >$) of the crystals produced in 2009 are given in Fig. 4 together with the dimensions of these crystals. The slightly larger mean value of crystals dimension on the hard $< 100 >$ direction is due to the difficult polishing of the corresponding (hard) faces.

The final mechanical processing also has the purpose of deep cleaning the crystal surfaces, which may have been contaminated during the rough mechanical processing (cutting, shaping, grinding and lapping). The cleaning process is made in two steps, first by chemical etching and second by polishing. The polishing also smooths the crystal faces, possibly damaged by chemical etching. The targeted number of atomic layers to be taken away by these two procedures is on the order of 104 in order to eliminate all impurity atoms that may have adsorbed on the crystal face and further diffused in its bulk. As Fig. 5 a) shows, the mean depth of the crystal layer washed away by chemical etching is 13.5 microns and the least value of this width is 10.2 microns which makes more than 105 atomic layers. Polishing is the next step in the surface cleaning procedure. As Fig. 5 b)
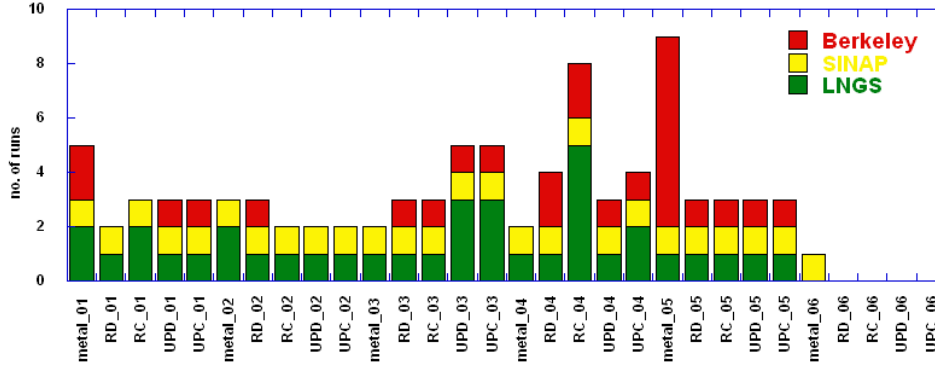
34

Figure 3: CUORE raw materials certification (ICP-MS measurements).

and c) show, approximately 105 atomic layers are taken away by polishing. The relatively large spread of the polishing depth is due to the fact that polishing is not only a surface cleaning process. Besides removing a surface layer possibly contaminated with radioactive isotopes, the polishing is also intended to bring the crystal dimensions as close as possible to the nominal values and to improve the surface quality by removing possible extended defects induced by chemical etching. As mentioned in the previous report [3] the direct measurement of planarity of crystal faces and crystal dimensions is made only once, at the beginning of the crystal surface processing. After that, planarities and dimensions are calculated based on crystal weight measurement and on the assumption that chemical etching has the same efficiency on all crystal faces. The algorithm applied is also based on the assumption that mechanical polishing maintains the parallelism of crystal faces unchanged. The validity of the algorithm was checked in 2009 by direct measurement of crystals which were subject to chemical etching and eventually polished on one or several faces after which were discarded due to bulk defects revealed by final visual inspection. Five crystals were subject to this test and the results are summarized in Fig. 6 and 8. As Fig. 6 shows, the chemical etching generally has a smoothing effect on crystal faces. Polishing also is supposed to have this effect but the results are biased especially in the case of soft faces by the difficult control of polishing parameters in the case of handmade processing. The validity of the algorithm is demonstrated by the fact that the dimensions measured directly after clean room processing are equal to those calculated (see Fig. 7). A dedicated cryogenic setup mounted and operated at LNGS is used to test TeO_2 crystals. The tests are performed on crystals randomly chosen from each production batch and is aimed at checking the radioactive contamination level of crystals and their bolometric performance, measured in conditions similar to those planned to be used for CUORE.

Three CUORE Crystals Validation Runs (CCVR) were performed till present. Fig. 8 gives the ID number of the crystals measured in each run. The crystals showed excellent bolometric characteristics, including a very good energy resolution (FWHM better than 5 keV in the spectral region of interest for CUORE). In the $\sim$52 days long CCVR-1 run it was possible to fix upper buonds (90% C.L.) of 1.8 10^{-14} g/g and 5.5 10^{-14} g/g respectively for ^{238}U and ^{232}Th contaminations. These values are well below the concentration limits requested for TeO_2 crystals to be used in CUORE experiment. The energy spectra of coincident events (simultaneous signals from neighboring crystals in the
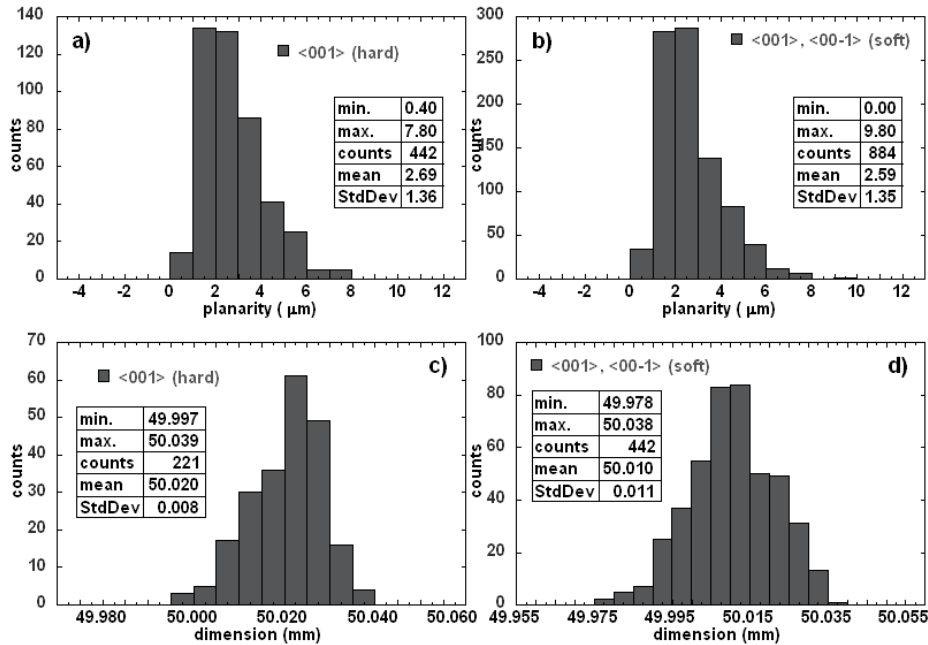
Figure 4: Planarity and dimension measurement results for the TeO$_2$ crystals for delivered in 2009.

array) were used to estimate the surface contamination of the crystals, resulting in an upper limit of $1.4 \ 10^{-8}$ Bq/cm^2 for both ^{238}U and ^{232}Th contaminations.

3 Cryostat

Cryogenics is one of the most complex items of the CUORE setup. Besides the challenge of developing an effective, low noise, cryogen-free, low radioactivity system for operating a massive detector at very low temperatures it involves in fact a number of separately designed parts (wiring, suspension, cold lead shields, calibration, cooling and damping system) which require a detailed integration job.

Progresses have been obtained on the various cryogenic systems whose integration is expected to start mid of 2010. First step will be the assembly of the 300K, 40K and 4K vessels with one detector calibration box, the suspension upper parts, one upper wire insert and two pulse tubes. The system will be cooled at 4K and the functionality of the various systems will be tested. The dilution unit integration will follow shortly.

- Cryostat. The Milano group is engaged with the cryostat construction and integration. The preliminary operations for the cryostat construction has started during 2009. Copper and stainless steel procurement and radioactive assay have been completed. Electron beam welding procedures have been defined and qualified. TIG welding has been checked for radioactivity and some tuning in the procedure has been necessary to minimize the welding contamination. The vessels bottoms have been formed and prepared for welding. The work on the vessel flanges has started.
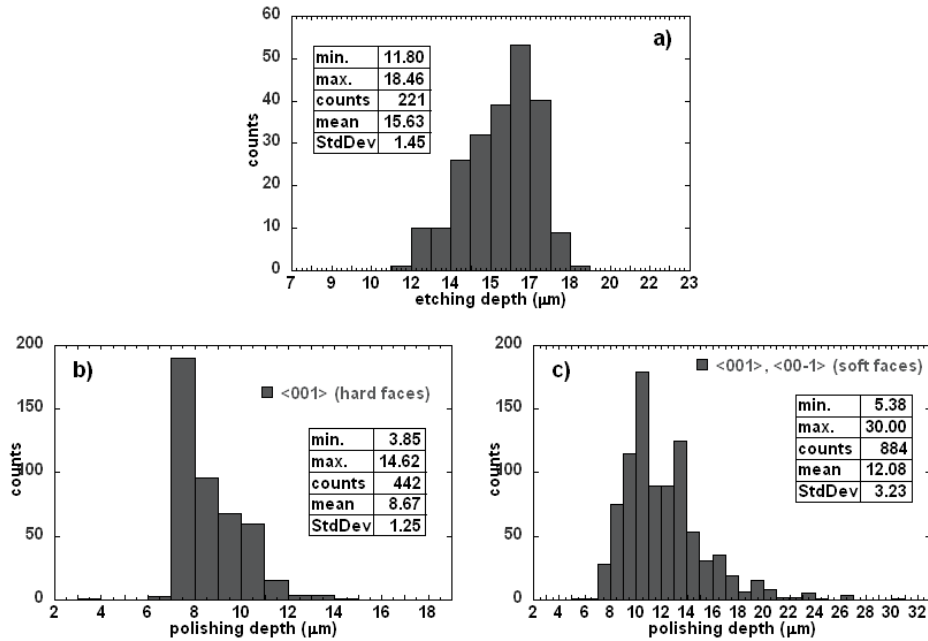
36

Figure 5: Width of the layers chemically etched (a) and mechanically polished (b and c) from the surface of the TeO_2 crystals delivered in 2009 for CUORE.

The design of many internal and external components (inner vacuum access tubes, thermal links, vacuum auxiliary systems, assembly tools...) has been completed and the procurement has started.

- Detector Calibration System (DCS). In 2009 the University of Wisconsin (UW) completed the detailed design of the DCS and prepared for constructing the first Motion Box. Following the 2008 DCS review, a new improved thermal sinking at 4K has been designed and tested. The calibration, cryostat, and integration groups are continuing to work together very closely for the detailed integration of the DCS into the CUORE experimental setup. An extensive cooldown and motion test of the full-size DCS is planned during the cryostat commissioning. For this purpose a temporary support structure has been designed and is being constructed. During the TTT run a test of the CUORE source string has been performed, aiming at evaluating both the fabrication procedures and the high-rate effects on the calibration.

- Detector and Lead Shield Suspensions. The Genova group is making progresses with the construction aiming at installing the suspensions during the first 4K commissioning for a vibration isolation test. The "Y" support structure has been installed on top of the Main Support Structure in the CUORE underground site together with the custom designed isolating "anti-springs". The TIG weldings for thermal coupling stages are being tested for the radioactivity and the vacuum feedthrough are being assembled. The Kevlar section of the suspension has been subject of further investigations: the design has been improved and the Kevlar creeping at low

crystal ID	Hard faces			Soft faces		
	before	after	processing	before	after	processing
080143	2.4	1.6	etched and polished	1.2	6.8	etched and polished
				1.8	7.6	etched and polished
	5.0	1.8	etched and polished	4.0	9.8	etched and polished
				4.4	11.2	etched and polished
080161	6.6	2.0	etched	4.4	1.2	etched
				4.4	3.2	etched
	5.4	1.2	etched	5.0	3.8	etched
				5.6	4.0	etched
080303	1.2	0.8	etched	2.8	4.0	etched
				3.0	4.4	etched
	1.8	4.6	etched	4.0	6.4	etched
				4.2	6.6	etched
080321	2.8	2.0	etched and polished	1.2	5.4	etched
				1.2	5.4	etched
	3.2	3.4	etched	1.8	6.0	etched
				1.8	7.4	etched
080324	3.8	1.8	etched and polished	2.6	4.4	etched
				3.6	5.6	etched
	3.0	2.0	etched	4.2	5.6	etched
				4.4	6.6	etched

Figure 6: Planarities (in microns) of crystal faces as measured before and after processing in the clean room.

temperature has been extensively characterized.

- Upper Wiring System (UWS). The Firenze group has placed the order for the wire insert assembly and is carrying on further studies to improve the wire thermal sinking between 300K and 4K.

- Dilution Unit (DU) and Fast Cooling System (FCS). Work is in progress at Leiden-cryogenics for the construction of the DU. The DU is being assembled for testing in a dedicated cryogen-free cryostat with two pulse tubes. Tests have been carried out to design a special variable flow impedance to achieve high He^3 circulation rates in a cryogen-free system.

- Movement Tools and Assembly Procedure. The Bologna group has completed the design of cryostat vessel lifting system and the order have been placed.

4   Radioactivity

The radioactivity working group takes care of selection and control of all the materials used for the experiment construction, as well as of the materials and procedures used to clean, store and handle detector and cryostat components. In the following we summarize the main activities undertaken during year 2009.

crystal ID	computed (mm)	measured (mm)	processed	type
080143	50.022±0.006	50.010±0.004	etched and polished	hard
	50.010±0.004	50.007±0.007	etched and polished	soft
	50.000±0.006	50.014±0.011	etched and polished	soft
080161	50.040±0.006	50.033±0.003	etched	hard
	50.029±0.005	50.024±0.004	etched	soft
	50.034±0.004	50.023±0.003	etched	soft
080303	50.034±0.002	50.033±0.004	etched and polished*	hard
	50.039±0.004	50.034±0.007	etched	soft
	50.038±0.004	50.038±0.006	etched	soft
080321	50.038±0.003	50.033±0.003	etched and polished*	hard
	50.025±0.002	50.028±0.007	etched	soft
	50.022±0.003	50.032±0.008	etched	soft
080324	50.028±0.004	50.033±0.003	etched and polished*	hard
	50.028±0.004	50.040±0.008	etched	soft
	50.028±0.005	50.030±0.007	etched	soft

Figure 7: Dimension and tolerances (in mm) of crystals as measured before and after processing in the clean room.

CCVR-1	CCVR-2	CCVR-3
080007	080076	0800190
080011	080096	0800236
080039	080007	0800180
080041	080011	0800229

Figure 8: Crystals measured in validation runs performed in 2009.

4.1 Radon

The radon diffusion and implantation on material surfaces directly facing the detector was investigated. The sealed box with a high concentration of radon (300 kBq/m^3 of ^{222}Rn) at Milano Bicocca Universtity was used to better understand the total induced background that can be produced by radon and its progeny. A similar development was performed at the Berkeley labs using a dedicated apparatus. It was observed that the contamination on copper and TeO$_2$ surfaces was mainly due to the Po isotopes that are present in the ^{222}Rn chain. In principle the high ^{222}Rn concentration in the atmosphere does not produce direct deposition or diffusion of the radon inside the materials. On the contrary it is clearly visible the effect due to Po concentration, that sticks on surfaces with a relatively high efficiency. It can be interpreted as a possible high chemical affinity of the Po atoms with respect to materials like copper or TeO$_2$. It is observed also a net diffusion of the deposited atoms on copper, the clear tail visible in the collected energy spectra can be accounted as alpha emission produced not directly from the surfaces. The same diffusion is not immediately visible in the case of the TeO$_2$ samples, probably due to the roughness of the TeO$_2$ surfaces. Using the collected information a better definition of the assembly condition and storage can be defined in order to reduce the possible radon influence on the final detector.

4.2 Cryostat preparation procedures

One of the main problem that was identified during the design of the cryostat was the soldering procedures that can be applied to the various copper parts. To perform the electron beam soldering of the thermal shield cylinders it is necessary to maintain the two parts of the copper edges in place. It was clearly visible that TIG electrodes contain normally an high concentration of ^{232}Th. Normally the TIG approach acts without material transfer, in reality it was observed that, depending to the soldering conditions, a relatively high concentration of ^{232}Th was found on the soldered copper surfaces. To avoid this contamination, that in the final cryostat will be directly facing the CUORE detector, many different approaches for surface cleaning was studied, also taking into account the final mechanical configuration in which such cleaning procedures will be applied. A combination of mechanical surface treatment and a chemical etching will be identified as the better approach.

The identification of a clean approach can be directly used also in all the other cases where, also with a less impact on the possible induced background, a TIG soldering will be necessary. This is the case also to the thermal link within the cryostat and the suspension where soft copper strips must be strictly connected with the two parts. A defined soldering procedure will be designed also to these parts that will be necessary at the level of the cryostat mixing chamber.

4.3 Internal lead shield: measurement and procurement

CUORE internal lead shield, placed inside the cryostat very close to the detector, will be made using ancient roman lead. Measurements were performed in order to qualify the internal contamination in ^{238}U and ^{232}Th. Using gamma rays spectroscopy with HPGe detectors and NAA, the limits for internal contaminations were fixed at value well below 10^{11} g/g for the two radioactive chain. The ^{210}Pb content in this kind of lead was previously measured [4] to be lower than 4 mBq/kg.

The final configuration of the internal lead is now well defined and it was necessary to obtain the total amount of roman lead. With the acquisition of other 3 tons of ancient roman lead there is now a sufficient amount of lead to realize all the shields with a low radioactivity material.

4.4 Permanent storage Area (PSA)

With the start of the production of the various CUORE components (crystals, copper, PTFE, etc.) there was the need to create a storage area. The PSA is placed in the underground laboratory in order to avoid radioactivity induced by cosmic rays, in particular it is well known that tellurium and copper will suffer an important activation if exposed to cosmic rays. At the same time the PSA must avoid possible ri-contamination of the components due to the influence created by the environment. To guaranty that the relative high concentration of radon in the underground laboratory air will influence the surface contamination of the detector parts the packages that contain the various part will be placed in a selected cabinets that are contiguously fluxed with nitrogen.

During the last year many tests were realized in order to define the correct procedure to maintain the radon concentration in the cabinets at a sufficient low level in each operational phase. At the same time the total nitrogen flux must be keep sufficiently low for safety reasons, we cannot saturate the rooms where the cabinets are installed, and for the limits imposed by the total nitrogen consumption, we cannot store underground a very large amount of nitrogen bottles. Using the cabinets in high contaminated radon atmosphere it was possible the definition of the correct operational condition that guaranties a radon concentration in the cabinet around few Bq/m^3. In this way there are the correct conditions to store in the PSA for a relatively long time all the CUORE detector components.

4.5 Radioactivity validation of various materials

Measurements dedicated to the specific material selection were done. In particular a new limit on ^{232}Th in selected copper was obtained with a dedicated measurements with Neutron Activation Analysis (NAA). In this measurement the new limit was fixed in 6 10^{-13} g/g that can be considered one of the best limits ever obtained on ^{232}Th on copper. This is an important data also to establish the possible background contribution that can be extrapolated for the final CUORE detector.

Other materials characterized were relevant for the cleaning components, the hut accessories, cryostat structures and for the assembly line. In particular for the last point a specific selection of PTFE, Aluminum and stainless steel was done in order to minimize the radioactivity of the gluing line. For the cryostat the selection of the stainless steel necessary to account the anti shock security of the thermal shields, it was in fact proposed to install specific designed stainless steel springs between the internal and the external vessels. This material will be separated by the detector only by a small amount of lead (around 6 cm) that cannot guaranties the necessary background reduction. The selection of material with the correct elastic and radioactivity characteristics is under study, a better definition of all the parameters must done in order to obtain a successful configuration.

4.6 Copper production and cleaning

All copper parts constituting the CUORE detector will be entirely - or partly, when the design does not allow it - machined by EDM (Electrical Discharge Machining) to minimize the use of tools and lubricants that may include undesired contaminants in the copper during manufacturing. Moreover the copper surface roughness must be reduced as much as possible in order to minimize the area of possible contaminant implantation and to give more effectiveness to the following surface cleaning procedure: also from this point of view EDM is advantageous with respect to other conventional tools. Two second-hand EDMs have been acquired by the INFN in 2009 and have been fully dedicated to CUORE detector copper part production: one installed in the INFN-LNL workshop, that is in charge of producing the copper frames which hold the CUORE crystals, and one installed in INFN-Milano Bicocca workshop, that is in charge of producing all other copper pieces that constitute CUORE towers. After a first period of trial stage with the

new EDMs, in late spring 2009 both workshops started the machining of copper pieces for CUORE-0 (completed within 2009) and CUORE, which should take a total of about two years. In order to facilitate the logistics - when not in use for machining or cleaning the copper must be stored underground to minimize cosmogenic activation - some room has been reserved to CUORE copper in the Baradello underground site, near Como. In early 2009 a fine tuning of the various steps (tumbling, electropolishing, chemical etching, plasma etching) of the CUORE surface cleaning procedure has been performed in order to remove an average of $100\,\mu$m from the surface of all copper pieces. The removal of this thickness should be enough to minimize surface contaminants while keeping the mechanical tolerances. Critical regions (mostly threads and holes) where the effect of electropolishing has shown to be more pronounced have been protected with PTFE during this cleaning step. The final cleaning of CUORE-0 copper parts started in summer 2009 and will be followed - starting from 2010 - by the cleaning of all CUORE copper pieces close to the TeO$_2$ crystals. The cleaning procedure adopted for these pieces - based on a complex recipe developed at LNL and consisting of a sequence of mechanical, electro-chemical, chemical and plasma treatment (TECM) - have been tested and compared with different technique in a dedicated measurement. Three independent arrays of 12 TeO$_2$ bolometers (Three Tower Detector) in which the crystals had all been processed with the CUORE recipe have been operated in Hall A. The only difference among the three towers was in the Cu supporting structures that have been processed with different methods: 1) TECM recipe, 2) Electro Chemical (EC) processing with ultrapure certified materials and 3) wrapping with Polyethylene films (PW). The comparison between the different towers showed that the three technique allow to reach comparable level of surface contaminations. Consequently the TECM method, already chosen as the baseline, was maintained.

5   Assembly

The CUORE Assembly Working group (CAWg) is responsible of the CUORE Detector Assembly that must be accomplished following very strict prescriptions, due to the extraordinary level of radio-purity required for a successful DBD experiment and to the challenges that a 1-ton detector working at 10 mK presents. The words summarizing the philosophy with which the CAWg is realizing the design of the complete assembly line are: "simple, fast, reproducible and recontamination-free". This translates into the need of an optimization and standardization of the processes in the different assembly steps (they are more than ten!), taking into account that they must be all realized inside glove-boxes flushed with nitrogen gas to avoid exposure of any part of the detector to air during assembly. Several servo-systems have been implemented to overcome this rigid constraint and some of them are shown in the pictures hereafter. Aside to this work, but thought as a real "demonstrator" of many of the procedures to be applied to CUORE, the CAWg is taking care also of CUORE-0 detector: a single CUORE-like tower to be assembled and put into operation in 2010. The main impact this work has had on CAWg schedule in 2009 has been the design and purchase of a special radiation shield for this tower, that will not be part of CUORE structure. It will be realized at the beginning of 2010 by a
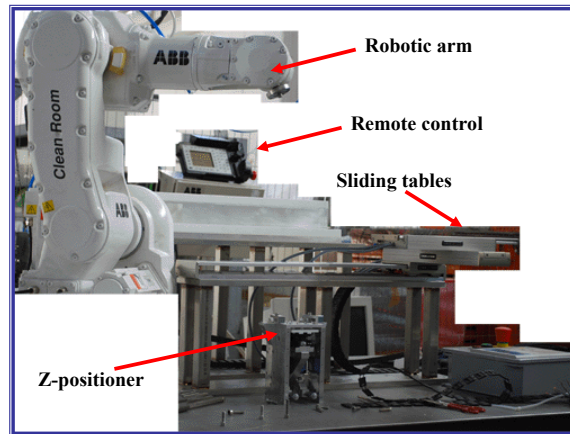
Figure 9: The gluing line. The robotic arm, the z-positioner and the sliding tables are shown.

Figure 10: The paper prototype of the garage (now ordered) containing the tower elevator with its servo system for rotation and z-movement (the remote control cabin is not shown).

specially selected company, with expertise for high vacuum and low radioactivity requests.

In the following a "state of the art" report on the different parts of the assembly line will be given.

- The gluing of a thermistor and a heater on each crystal will be accomplished in a glove-box by means of a robotic arm and motorized sliding tables, software controlled (see Fig. 9). The glue will be dropped using an automatic dispenser, to be as quick and reproducible as possible, and the fine-tuned positioning of chips with respect to crystal surface will be obtained with an extremely precise, specially designed z-positioner. All these parts have been realized or purchased during year 2009 and will be assembled and put into operation inside a special glove-box in 2010.

- During year 2009 the Tower Elevator, needed to move the single tower of CUORE inside the different glove boxes while assembled, was finally instrumented for a com-

plete remote control of the operator, using step motors, and tested for Rn emanation.

- The Garage, containing the elevator and the tower when in standby between two assembly steps, has been finalized and ordered. See Fig. 10.

- A complete mock-up of the Mechanical Glove-Box, that will be used during the assembly of the different planes of a single CUORE tower, has been realized and used to study ergonomics and needed tools for 2 operators to accomplish all the procedures needed (see Fig. 11). A draft protocol for this assembly step has been written and checked with real actors. Several tools and some parts of the box have already been purchased.

- Some conceptual studies for the Pre-Cabling and the Cabling Glove-boxes have been accomplished along with the work in progress on the wire tapes for the read-out of the bolometers and the wire trays that must contain them, both finalized only at the end of 2009 and now in production. These glove-boxes will be used also for the assembly of CUORE-0 shield and therefore their final design will come only when real samples of all the parts to be assembled will be available.

- Year 2009 has seen a very big effort towards the preparation of the Bonding system and Glove-box. To be able to bond the chips after the tower has been assembled, the bonding machine was modified to make it work in vertical. But it needs also to be integrated inside a glove box and many of the movements normally accomplished by the operator will have to be substituted by step motors, remotely controlled. This servo-system has been realized and partially tested for ergonomics optimization in 2009. All the system has also been equipped with special cameras, with a remotely controlled zoom, that will help the operator during bonding. See Fig. 12. The difficulties of bonding very small pads with 25 μm gold wires, having the tower and the machine inside a glove box, are huge and many tests have been performed to check the feasibility of such an approach and will continue in 2010 on the final wire tapes and trays, and with the motorized tower, to finalize the glove box design, the support tools and a final bonding protocol.

- Finally, since several towers, once completed, must wait before assembly in the cryostat several months, a nitrogen flushed Storage Box (Fig. 13) has been designed and the first prototype realized. It will also be used to move around the tower, once completed and was therefore equipped with hooks and slots for a fork-lift.

Since all detector parts need also to be stored after cleaning for very long periods, a relevant task of the CAWg is the realization of a Parts Storage Area (PSA). Special stocking cupboards for clean room environments were purchased in 2009. They were tested to optimize nitrogen gas fluxes and to study emergency situations. A dedicated trailer was bought and instrumented to become a reliable PSA, in safety conditions. A software database was implemented to govern the in/out fluxes during delivery and assembly, on a time schedule of several years, and was used in 2009 to keep track of the crystals delivery from China and of the stocking of the first copper parts for the CUORE-0 tower. In parallel, another database is now available to note down the "history" of every single

Figure 11: Ergonomic studies with mech-box paper mock-up.

copper part that will be used in the assembly, from its delivery after lamination, up to its storage in the PSA. Both will be embedded in the general Production Database, that will preserve all information about the detector assembly.

6 Electronics

The CUORE Electronic System consists of many parts, the design of most of which is based on the experience of the pilot experiment CUORICINO. Space occupation of the CUORE front-end will be smaller by about a factor close to 3 with respect to the CUORICINO set-up, thanks to the optimization of the electronic components. The part of the front-end that takes care the programming of all the necessary parameters, mastered by the acquisition system, will be implemented by microcontrollers based on the ARM core, featuring a great flexibility at a low cost. The present status of the front-end and the next progress of the development are given.

- The preamplifier has been designed and prototyped at Milano-Bicocca. A pre-production has been made at USC, in USA. It is a differential voltage sensitive preamplifier. The differential JFETs at its input has been selected based on a semi-custom process. The JFETs are already available for the full production, fully supported with INFN funds. The final production will take place during the first quart of 2010. In figure 14 a photograph of the prototype preamplifier is shown.

- The main very-front board will consist of 6 channels each including a preamplifier, a second stage, a detector biasing network, the detector load resistors, a number of secondary features, the glue logic and the remotely-programmable interface, ARM-microcontroller based. It has been fully designed in breadboard during 2009. In 2010 it will be prototyped and qualified.

- The antialiasing filter consist in a board that contain 12 6-poles Thomson, or Bessel, active filters having each 4 independent programmable frequencies. It was proto-typed by the group of Genova, following the design from Milano-Bicocca. This
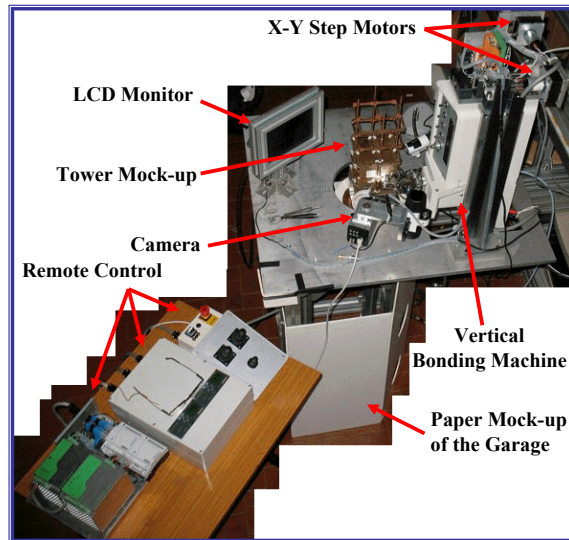
Figure 12: The vertical bonding machine with its servo systems and visual tools to help the operator once it will be closed in a glove box.

board has been validated during 2009. The antialiasing filter is shown in figure 15, while the back-plane for it is in figure 16.

- 2 switching power supplies for the remote (48 V) supply voltage of the Electronic System are already available, supported by INFN. Another pair of modules will be provided by USC within the first half of 2009.

- Switching low noise modules for the pre-regulated (48 V => +/-12 V and 48 V => +/- 5 V) supply voltage are in the prototype phase.

- A new generation of programmable voltage pulse are under the prototype phase. Its purpose is to deliver a very stable heating pulse for detector stabilization.

6.1   CUORE-0

CUORE-0 is essentially a single column of CUORE to be installed and operated in the existing dilution refrigerator placed in the hall A of the Gran Sasso Laboratory. CUORE-0 will adopt all the procedures for the assembly foreseen for CUORE itself, which will be totally different from the ones adopted for CUORICINO. The main point is that all the handling and assembly operations will be performed without any contact with ambient air. A set of proper glove boxes will allow to build the detectors in a controlled nitrogen atmosphere and according to a rigid protocol which will make the assembly procedure essentially operator independent. In particular, the very delicate operation of absorber-sensor coupling through bi-component epoxy will be almost automated and realized through programmable robots, aiming at a better detector reproducibility. We would like to add that CUORE-0 will represent by itself a powerful experiment to search

Figure 13: The Storage Box.

for neutrinoless double beta decay of ^{130}Te. The CUORE-0 motivations are manifold, and can be summarized as follows:

- test of the CUORE assembly chain and procedure.

- high statistics test of crucial components of the estimated CUORE background.

- test of the bolometric behavior of the detectors.

- test of the CUORE Data Acquisition.

- test of the CUORE analysis tools.

Being the first operating CUORE tower, prepared and assembled according to the same protocols and tools, CUORE-0 development and preparation strictly follows the evolution of the CUORE project. The time schedule of each item anticipates however the mass production of CUORE and serves as a general test of it. The following is a summary of its present status item by item:

Crystals. All the CUORE-0 crystals are ready, packaged in controlled atmosphere and stored in nitrogen fluxed cupboards underground since February 2009. Test samples of the pre-production have been operated as bolometers in hall C at LNGS. The specifications of the crystals are met, both from the radio-purity and bolometric point of views.

Heaters. All the CUORE-0 heaters have been produced and characterized. Their cleaning procedure is defined: organic solvent (ethanol or acetone) in PTFE container in ultrasound bath. Cleaning and packaging will be performed within May 31st, 2010.

Thermistors. All the CUORE-0 thermistors have been produced in Berkeley with some redundancy (120 samples) from existing neutron-irradiated Ge wafers. They have been cleaned and packed ready for the gluing procedure. A sample of five thermistors has been
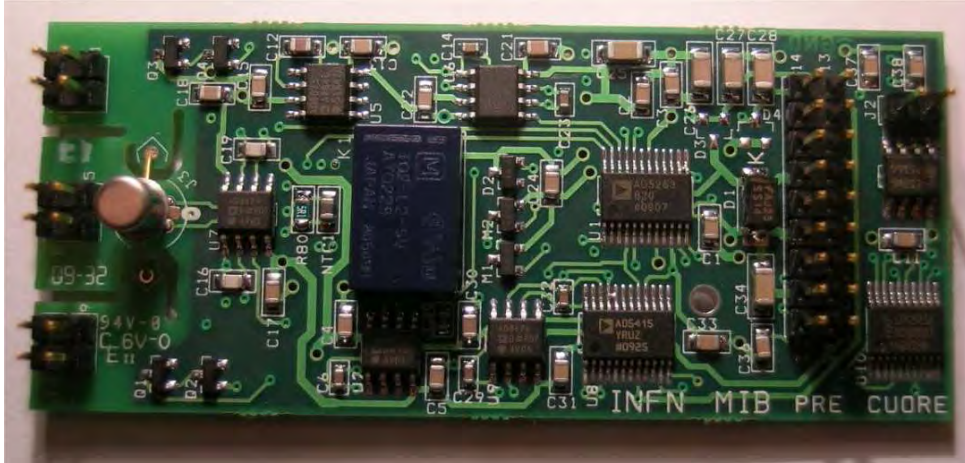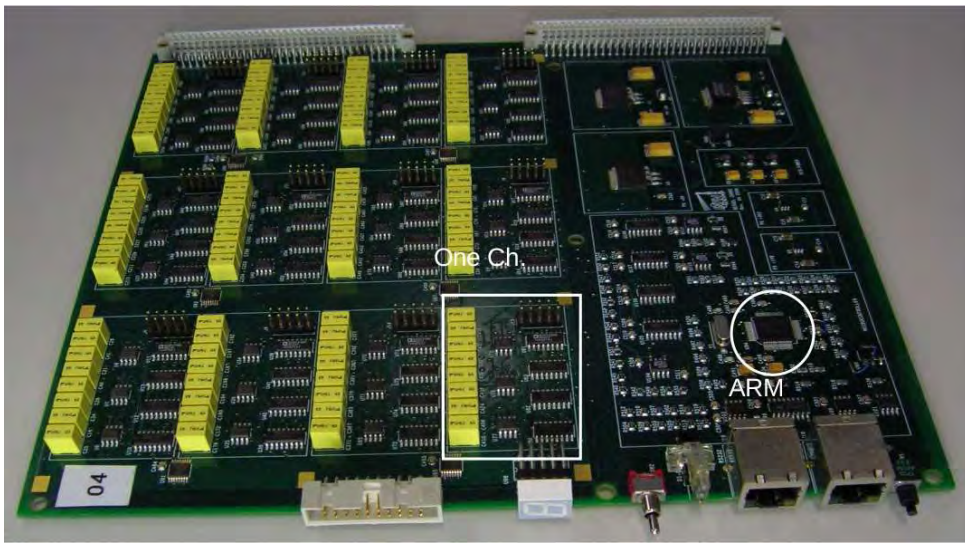
Figure 14: Preamplifier.

Figure 15: Thomson (Bessel) antialiasing filter.

characterized down to 20 mK in Como, showing the correct behavior in terms of R-T curves. The thermistors have a special contact structure that allows frontal bonding after thermistor gluing, a crucial element for the planned assembly procedure.

Cu part production. The main copper pieces for the CUORE-0 crystal holders are (i) frames which surround a set of four crystals and (ii) columns that connect vertically the frames. All the columns have been produced in the Milano-Bicocca workshop, while the frames have all been realized in the LNL workshop. The cable rails for the wiring in the CUORE-0 tower have been produced too. The most delicate point is represented by the very complex thermal shield of the tower, that, for cleaning purpose, needs to be sectioned in several parts and must be realized by an external company, which has been carefully selected to avoid danger of contamination during the machining process. The delivery of the shield is foreseen for March 31st, 2010.

Figure 16: Back-plane for the Thomson antialisaing filter.

PTFE blocks. These blocks are used to secure the crystals at the copper frame introducing a weak thermal link. The preparation of these blocks is a smooth operation managed by Milano-Bicocca and LNGS, and is proceeding according to the schedule. A recent manpower input from Genoa has allowed to solve a manpower issue connected to the cleaning operations.

Copper cleaning. This very delicate operation, tested in the three tower run recently stopped, is performed in LNL according to the CUORE-0 and CUORE baselines. There are still some not fully defined elements in the cleaning procedure, in particular in connection to the protection of the most delicate frame mechanical details to avoid erosion during the cleaning operation. However, these points will be clarified soon and the cleaning should be finished within April 30th, 2010.

Wiring. In spite of the large difference between the CUORE cryostat and the hall A cryostat, the wiring structure of CUORE-0 will be kept as similar as possible to that of CUORE. The wiring design has been completed long ago and a significant fraction of the elements have been procured. The tower section of the wiring is responsibility of Milano-Bicocca and is fully under control. The cryostat section is responsibility of Florence, where some delay should be possible for manpower problem. Anyway, the completion is foreseen for April 30th, 2010.

Assembly. From the preceding list of the CUORE-0 parts, it is clear that all the elements will be ready for assembly or for installation in the cryostat within May 2010. The assembly line (which is responsibility of Rome and Milano-Bicocca) and the gluing system (which is responsibility of Como, LNGS and Livermore) cannot be ready at the same time, but will suffer probably of 1-2 months delay, since their final definition requires the availability of a set of pieces sufficient for an assembly test of a fraction of the tower. This test is mandatory for a correct finalization of the set of glove boxes required for the detector construction in controlled atmosphere. Presumably, the assembly line will be ready in the Borexino clean room in June 2010, and the actual assembly will be performed within August 2010.

Tower-Cryostat interface. The same suspension used in CUORICINO and in the three-tower test will be used in CUORE-0, with small modifications.

Final operations. These consist first in two preliminary steps: the cryostat maintenance (performed by LNGS), and the installation of a special system developed in Genoa to keep the cryostat in a rigorously vertical alignment through a computer-controlled pneumatic method. This is crucial to avoid touches between the CUORE-0 tower and the 50 mK thermal shield. After this, CUORE-0 will be assembled, installed in the cryostat, cooled down and optimized for data taking, which is foreseen for November 2010.

7 List of 2009 Publications

1. S. Sangiorgio et al., *The low-temperature energy calibration system for the CUORE bolometer array*, AIP Conf. Proc, Vol 1185, pp. 677-680 (2009).

2. M. Martinez et al., *Progress on the CUORE Cryogenic System*, AIP Conf. Proc, Vol 1185, pp. 693-696 (2009).

3. V. Martinelli et al., *Low Temperature Thermal Conductivity of Candidate Materials for the Supports of CUORE*, AIP Conf. Proc, Vol 1185, pp. 685-688 (2009).

4. E.Andreotti et al., *The low radoactivity link of the CUORE experiment*, Journal of Instrumentation **4**, (2009) 1.

5. C.Arnaboldi et al., *A progammable multichannel antialiasing filter for the CUORE experiment*, NIM A, doi:10.1016/j.nima.2009.09.023, 2009

6. E. Andreotti et al., *Muon-induced backgrounds in the CUORICINO experiment*, Submitted to Astroparticle Physics, e-Print: arXiv:0912.3779.

7. F. Bellini et al., *Monte Carlo evaluation of the external gamma, neutron and muon induced background sources in the CUORE experiment*, Accepted for pubblication on Astroparticle Physics, e-Print: arXiv:0912.0452.

8. P. Gorla for the CUORE collaboration, *Search for neutrinoless double beta decay with the CUORE experiment*, AIP Conf.Proc.1182:116-119,2009.

9. F. Bellini for the CUORE collaboration, *Neutrinoless double beta decay search with CUORICINO and CUORE experiments*, Nucl.Phys.Proc.Suppl.188:65-67,2009.

10. S. Di Domizio and the CUORE collaboration, *Status of CUORE and results from CUORICINO*, Nuclear Physics B - Proceedings Supplements Volume 197, Issue 1, 15 December 2009, Pages 9-14

11. M. Sisti, *From CUORICINO to CUORE: investigating neutrino properties with double beta decay*, To be published in Journal of Physics, Conference Series (Editors: E. Coccia, L. Pandola, N. Fornengo, R. Aloisio).

12. M. Pedretti on behalf of the CUORE collaboration, *A ton-scale bolometric detector for the search for neutrinoless double beta decay*, AIP Conference Proceedings Volume 1185, pp. 562-564

References

[1] C. Arnaboldi et al.,NIM A 518 (2004) 775

[2] CUORE Collaboration, LNGS Annual Report 2007.

[3] CUORE Collaboration, LNGS Annual Report 2008.

[4] A. Alessandrello et al., NIM A **142**, (1998) 454.

[5] E.Andreotti et al., Journal of Instrumentation **4**, (2009) 1.

[6] C.Arnaboldi et al., NIM A in Press, doi:10.1016/j.nima.2009.09.023

DAMA

Collaboration:

P. Belli[a], R. Bernabei[a,@], A. Bussolotti[a,*], F. Montecchia[a], F. Nozzoli[a], A. d'Angelo[b], F. Cappella[b], A. Incicchitti[b], A. Mattei[b,*], D. Prosperi[b], R. Cerulli[c], C.J. Dai[d], H.L. He[d], H.H. Kuang[d], X.H. Ma[d], X.D. Sheng[d], Z.P. Ye[d,e], R.G. Wang[d], Y.J. Zhang[d]

in some detector developments, by-product results and small scale experiments:

O.P. Barinova[f], R.S. Boiko[g], V.B. Brudanin[h], N. Bukilic[i], D.M. Chernyak[g], F.A. Danevich[g], S. d'Angelo[a], V.Ya. Degoda[j], J.R. de Laeter[i], A.E. Dossovitskiy[k], A.M. Dubovik[n], B.V. Grinyov[n], E.N. Galashov[l], Yu.A. Hyzhnyi[j], S.V. Ildyakov[l], S.V. Kirsanova[f], V.V. Kobychev[g], O.S. Kolesnyk[j], G.P. Kovtun[m], V.M. Kudovbenko-Mokina[g], B.N. Kropivyansky[g], M. Laubenstein[c], A.L. Mikhlin[k], L.L. Nagornaya[n], P.G. Nagornyi[j], S.S. Nagorny[g], S.G. Nedilko[j], A.S. Nikolaiko[g], S. Nisi[c], D.V. Poda[g], R.B. Podvujanyuk[g], O.G. Polischuk-Shkulkova[g], A.P. Shcherban[m], V.P. Shcherbatskyi[j], V.N. Shlegel[l], D.A. Solopikhin[m], Yu.G. Stenin[l], V.I. Tretyak[g], Ya.V. Vasiliev[l], V.D. Virich[m], Yu.Ya. Vostretsov[n], S.S. Yurchenko[g], I.M. Vyshnevskyi[g]

in some studies on $\beta^+\beta^+$, EC/β^+, EC/EC decay modes (under the joint Indo-Italian DST-MAE project):

P.K. Raina[o], A.K. Singh[o], P.K. Rath[o], A. Shukla[o]

[a]Dip. Fisica, Univ. Roma "Tor Vergata" and INFN-Roma Tor Vergata, Roma, Italy.
[b]Dip. Fisica, Univ. Roma "La Sapienza" and INFN-Roma, 00185 Roma, Italy.
[c]Laboratorio Nazionale del Gran Sasso, INFN, 67010 Assergi (Aq), Italy.
[d]IHEP, Chinese Academy, P.O. Box 918/3, Beijing 100039, China.
[e]Physics Dept, Jing Gangshan University 343009, Jiangxi, China.
[f]Russian Chemistry-Technological University of D.I.Mendeleev, Moscow, Russia.
[g]Institute for Nuclear Research, MSP 03680, Kiev, Ukraine.
[h]Joint Institute for Nuclear Research, 141980 Dubna, Russia.
[i]Department of Applied Physics, Curtin University, GPO, Box U1987 Perth, Australia.
[j]Kiev National Taras Shevchenko University, MSP 01033 Kiev, Ukraine.
[k]Joint stock company NeoChem, 117647 Moscow, Russia.
[l]Nikolaev Institute of Inorganic Chemistry, 630090 Novosibirsk, Russia.

^{m}National Science Center Kharkiv Institute of Physics and Technology, Kharkiv, Ukraine.
^{n}Institute for Scintillation Materials, 61001 Kharkiv, Ukraine.
^{o}Indian Institute of Technology, Kharagpur, India.

@ Spokesperson
* technical staff

Abstract

DAMA is an observatory for rare processes located deep underground at the Gran Sasso National Laboratory of the I.N.F.N. (LNGS). It develops and uses low background scintillators. At present the main low background experimental set-ups in operation are: i) the second generation DAMA/LIBRA set-up (sensitive mass: $\simeq$ 250 kg highly radiopure NaI(Tl)); ii) the DAMA/LXe set-up (sensitive mass: $\simeq$ 6.5 kg liquid Kr-free Xenon enriched either in ^{129}Xe or in ^{136}Xe); iii) the DAMA/R&D set-up (a facility dedicated to test prototypes and to perform small scale experiments, mainly investigating double beta decay modes in various isotopes; iv) the DAMA/Ge set-up (mainly dedicated to sample measurements and to specific measurements on rare processes). A third generation R&D is also in progress towards a possible 1 ton set-up, DAMA proposed in 1996. In the following main arguments on the activity developed during 2009 are summarized.

1 DAMA/LIBRA

The highly radio-pure DAMA/NaI set-up ($\simeq$ 100 kg of highly radiopure NaI(Tl)) [1, 2, 3, 4, 5, 6, 7, 8, 9, 10, 11, 12, 13, 14] has been a pioneer Dark Matter (DM) experiment of suitable exposed mass, sensitivity and stability of the running conditions. It took data at LNGS over seven annual cycles up to July 2002.

The main aim of DAMA/NaI was the investigation of the presence of Dark Matter particles in the galactic halo by exploiting the DM annual modulation signature (see refs. [3, 4, 5, 6, 15, 16, 17, 18, 19, 20, 21, 7, 8, 22, 10, 11, 12] and the 2009 publication list). In addition, profiting from its low-background features and from the high collected exposure, several results were also achieved both on Dark Matter particle investigations with different approaches and on several other rare processes [13].

The DAMA/LIBRA set-up ($\simeq$ 250 kg highly radiopure NaI(Tl); see refs. [23, 24] and in the 2009 publication list) represents the second generation experiment.

Both DAMA/NaI and DAMA/LIBRA have the main aim to perform a direct detection of Dark Matter particles in the galactic halo by exploiting the model independent DM annual modulation signature, originally suggested by [25, 26] in the mid–80's. In fact, as a consequence of its annual revolution around the Sun, which is moving in the Galaxy travelling with respect to the Local Standard of Rest towards the star Vega near the constellation of Hercules, the Earth should be crossed by a larger flux of Dark Matter particles around $\sim$ 2 June (when the Earth orbital velocity is summed to the one of the solar system with respect to the Galaxy) and by a smaller one around $\sim$ 2 December

(when the two velocities are subtracted). Thus, this signature has a different origin and peculiarities than the seasons on the Earth and than effects correlated with seasons (consider e.g. the expected value of the phase as well as the other requirements listed below).

Thus, the contribution of the signal to the counting rate in the k–th energy interval can be written as: $S_k = S_{0,k} + S_{m,k} \cos \omega (t - t_0)$, where: i) $S_{0,k}$ is the constant part of the signal; ii) $S_{m,k}$ is the modulation amplitude; iii) $\omega = \frac{2\pi}{T}$ with period T; iv) t_0 is the phase.

The DM annual modulation signature is very distinctive since it requires the simultaneous satisfaction of all the following peculiarities: the rate must contain a component modulated according to a cosine function (1) with one year period (2) and a phase that peaks roughly around $\simeq 2^{nd}$ June (3); this modulation must only be found in a well-defined low energy range, where DM particle induced events can be present (4); it must apply only to those events in which just one detector of many actually "fires" (*single-hit events*), since the DM particle multi-interaction probability is negligible (5); the modulation amplitude in the region of maximal sensitivity must be $\lesssim 7\%$ for usually adopted halo distributions (6), but it can be larger in case of some possible scenarios such as e.g. those in refs. [27, 28]. Only systematic effects or side reactions able to fulfil these requirements and to account for the whole observed modulation amplitude could mimic this signature; thus, no other effect investigated so far in the field of rare processes offers a so stringent and unambiguous signature.

At present status of technology the DM annual modulation is the only model independent signature available in direct dark matter investigation that can be effectively exploited.

DAMA/LIBRA further investigates the presence of DM particles in the galactic halo, pointed out by the former DAMA/NaI [5, 6], by exploiting the DM annual modulation signature and has also the aim to get improved information on the corollary quests on the nature of the candidate particle(s) and on the related astrophysics, nuclear and particle physics models. Moreover, second order effects are planned to be investigated (see e.g. ref. [6, 8]), and future dedicated data takings will also allow the study of many other rare processes (as e.g. already performed with DAMA/NaI [13, 14]) thanks to the peculiarity of the experimental set-up.

During 2009 – after an upgrading occured on October 2008 – DAMA/LIBRA has continued its data taking uninterruptedly. In the following, we will just briefly recall the first results on the Dark Matter particle investigation obtained by DAMA/LIBRA over four annual cycles (exposure: 0.53 ton×yr) and the combined analysis with the previous data collected over 7 annual cycles by DAMA/NaI (0.29 ton×yr), corresponding to 11 annual cycles for a total exposure of 0.82 ton×yr, orders of magnitude larger than the exposures typically collected in the field.

The data collected in the period 2007-2009, corresponding to other two annual cycles, will be released in the first months of 2010.

1.1 The model-independent experimental result on DM

As already reported in the LNGS Annual report 2008 (see also [23, 24] and references therein), several analyses investigating the model-independent DM annual modulation

signature have been performed on the DAMA/LIBRA data collected over the first four annual cycles (exposure: 0.53 ton×yr). They have further confirmed the peculiar annual modulation of the *single-hit* events in the (2–6) keV [1] energy region satisfying all the many requests of the DM annual modulation signature. The cumulative exposure with the former DAMA/NaI is 0.82 ton×yr – corresponding to 11 annual cycles – which is orders of magnitude larger than the exposures typically collected in the field.

In fact, as required by the DM annual modulation signature: 1) the *single-hit* events show a clear cosine-like modulation as expected for the DM signal; 2) the measured period is equal to (0.998 ± 0.003) yr well compatible with the 1 yr period as expected for the DM signal; 3) the measured phase (144 ± 8) days is well compatible with the roughly $\simeq 152.5$ days expected for the DM signal; 4) the modulation is present only in the low energy (2–6) keV interval and not in other higher energy regions, consistently with expectation for the DM signal; 5) the modulation is present only in the *single-hit* events, while it is absent in the *multiple-hit* ones as expected for the DM signal; 6) the measured modulation amplitude in NaI(Tl) of the *single-hit* events in the (2–6) keV energy interval is: (0.0131 ± 0.0016) cpd/kg/keV (8.2 σ C.L.).

As previously done for DAMA/NaI [5, 6], careful investigations on absence of any significant systematics or side reaction effect in DAMA/LIBRA have been quantitatively carried out and reported in details in ref. [24]. No effect able to account for the measured modulation amplitude and simultaneously satisfy all the requirements of the signature has been found or suggested by anyone over more than a decade.

Just as an example we recall here the case of muons, whose flux has been reported by the MACRO experiment to have a 2% modulation with phase around mid–July [29]. In particular, it has been shown that not only this effect would give rise in the DAMA set-ups to a quantitatively negligible contribution [24, 5, 6], but several of the six requirements necessary to mimic the annual modulation signature – namely e.g. the conditions of presence of modulation just in the *single-hit* event rate at low energy and of the phase value – would also fail. Moreover, even the pessimistic assumption of whatever hypothetical (even exotic) cosmogenic product – whose decay or de-excitation or whatever else might produce: i) only events at low energy; ii) only *single-hit* events; iii) no sizeable effect in the *multiple-hits* counting rate – cannot give rise to any side process able to mimic the investigated DM signature. In fact, not only this latter hypothetical process would be quantitatively negligible [24], but in addition its phase – as it can be easily derived – would be (much) larger than July 15th, and therefore well different from the one measured by the DAMA experiments and expected by the DM annual modulation signature ($\simeq$ June 2nd). Recently, a LVD analysis [30] has been reported for the muon flux relatively to the period 2001–2008, which partially overlaps the DAMA/NaI running periods and completely those of DAMA/LIBRA. A value of $\simeq 185$ days has been measured by LVD in this period for the muon phase to be compared with (144 ± 8) days [24] which is the measured phase by the DAMA/NaI and DAMA/LIBRA for the low energy peculiar *single-hit* rate modulation. Thus, the latter one is $\geq 5\sigma$ far from the muon modulation phase measured at LNGS by the large surface apparata MACRO and LVD. Similar facts also hold for the results on muon flux variation by Borexino experiment released in early 2010 [31]. In conclusion, any

---

[1]Here and after, keV means keV electron equivalent.

possible effect from muons can be safely excluded on the basis of all the given quantitative facts.

Recently, it was claimed [32] that some role might be played by ^{40}K; this possibility is evidently discarded by the data, by the published analyses and also by simple considerations. A dedicated discussion can be found in the 2009 publication list.

In conclusion, DAMA/LIBRA has confirmed the presence of an annual modulation satisfying all the requirements of the DM annual modulation signature, as previously pointed out by DAMA/NaI; in particular, the evidence for the presence of DM particles in the galactic halo is cumulatively supported by the exposure of 0.82 ton × yr collected over 11 annual cycles at 8.2 σ C.L..

The obtained model-independent evidence is compatible with a wide set of scenarios regarding the nature of the DM candidate and related astrophysical, nuclear and particle Physics (see e.g. ref. [5, 6, 7, 9, 10, 11, 12], Appendix A of ref. [24] and in literature, for example see [27, 33, 34, 35]); and many other possibilities are open. Further future works are also foreseen.

It is worth noting that no other experiment exists, whose result can be directly compared in a model-independent way with those by DAMA/NaI and DAMA/LIBRA. In particular, let us also point out that results obtained with different target materials and/or different approaches cannot intrinsically be directly compared among them even when considering the same kind of candidate and of coupling, although apparently all the presentations generally refer to cross sections on nucleon. Therefore, claims for contradictions made by experiments insensitive to the DM annual modulation signature, using different target materials and approaches, having well different sensitivities to various DM candidate and interactions, etc. have by the fact no impact even in the single arbitrary scenario they usually consider without accounting for experimental and theoretical uncertainties, using often crude approximation in the calculation, etc. Moreover, (see for example [5, 36] and in the 2009 publication list), some critical points exist in those activities, claiming for some exclusion, on important experimental aspects (energy threshold, energy scale, multiple selection procedures, stabilities, etc.). A relevant argument is also the methodological robustness [37]. Finally, they generally quote the implications of the DAMA model independent result in incorrect, partial and unupdated way.

It is also worth noting that, whenever an experiment using the same identical target material and methodological approach would be available in future, as usual in whatever field of Physics a serious comparison would require – in every case – e.g. a deep investigation of the radiopurity of all the part of the different set-ups, of their specific performances in all the aspects, of the detailed procedures used by each one, of the used exposures, of the stability parameters, etc.

Finally, as regards the indirect detection searches, let us note that also no direct model-independent comparison can be performed between the results obtained in direct and indirect activities, since it does not exist a biunivocal correspondence between the observables in the two kinds of experiments. Anyhow, if possible excesses in the positron to electron flux ratio and in the γ rays flux with respect to an assumed simulation of the hypothesized contribution, which has to be expected from standard sources, might be interpreted in terms of Dark Matter (but huge and still unjustified boost factor and new interaction types are required), this would be not in conflict with the effect observed by

DAMA experiments, as also discussed in literature at some extent.

Finally, as aforementioned, the data of two other annual cycles (one before and one after the upgrade occurred in September 2008) are at hand. The set-up is continuously running waiting for the new upgrade foreseen in fall 2010 when all the low background PMTs will be replaced by new ones having higher quantum efficiency. Then, a long data taking is foreseen in the new running condition to achieve all the physical goals of the experiment.

1.2 New search for processes violating the Pauli-Exclusion-Principle (PEP) in Sodium and in Iodine with DAMA/LIBRA

Despite the foundation of PEP lies deep in the structure of the Quantum Field Theory, a simple explanation is still missing. Thus, the exact validity of the PEP is still an open question in spite of all its known successes. In fact, the general principles of the quantum theory allow to go beyond the Bose and Fermi statistics and to also consider generalized statistics [38, 39, 40]. Many experimental tests of the PEP validity following the first pioneering experiments [41, 42] have been carried out so far by various approaches searching for PEP forbidden states and transitions [43, 44, 45, 46, 47, 48, 49, 50, 51] and in the 2009 publication list. It is worth noting that in 1980 Amado and Primakoff [52] criticized – on the basis of the assumption that the total Hamiltonian, describing the atoms, is completely symmetric in the electrons – the possibility of testing the Pauli principle by searching for PEP-forbidden transitions. However, their arguments can be evaded as demonstrated in refs. [53, 54]. In particular, since the nucleus is a fermion system, the nuclear structure is stable in case of an exact PEP, unless channels for strong, weak or electromagnetic decays are open. Thus, the usually considered stable nucleus would not a priori be absolutely stable in case small violations of the PEP would exist and some exotic transitions (normally forbidden by PEP) in a stable nucleus may occur.

The value of the average mixing probability of non-fermion statistics δ^2 – which quantifies the possible PEP violations – can be derived considering the relation:

$$\tilde{\Gamma} = \tilde{\Gamma}(^{23}Na) + \tilde{\Gamma}(^{127}I) = \Gamma/\delta^2, \tag{1}$$

where: i) Γ is the total width of the PEP violating nucleon transition; ii) $\tilde{\Gamma}$ is the total width of the corresponding PEP allowed nucleon transition in case final states are empty, calculated for ^{23}Na and ^{127}I according to possible models for the momentum distribution functions of the nucleons in the bound state.

Following previous studies [45, 49, 46], the present best limit on the investigation of non-paulian nuclear processes in NaI(Tl) scintillators has been set in 2009 by means of DAMA/LIBRA (see the 2009 publication list); in particular, the non-paulian emissions of protons with $E_p \geq 10$ MeV in ^{23}Na and in ^{127}I have been studied by analysing the data collected in a devoted running period of 23.7 days, when the data taking was optimized for the very high energy region. The process has been investigated by analysing the events in the MeV energy region where just one detector fires (i.e. each detector has all the others as veto). The presence of identified alphas from residual U/Th contamination have also offered references for the energy scale [23].

The obtained results are discussed in details in paper in the 2009 publication list. Here Table 1 summarizes the experimental results, obtained with the DAMA/LIBRA detectors (24 in operation during the considered running period) by combining them in independent groups. The expected background events are also quoted; in this energy region the background is essentially due to very high energy muons possibly surviving the mountain. Generally the very high energy muons give rise in DAMA/LIBRA to events, in which several detectors fire, and thus they can be easily identified and are not competing background in the search for the PEP violating processes. Thus, only muons, impinging the sensitive volume of the set-up with a direction that forbids them to hit more than one detector, can play the role of background for the processes searched for and have to be considered. Therefore, a suitable MonteCarlo simulation has been realized on the basis of the features of the DAMA/LIBRA set-up [23], of the vertical muon intensity distribution and of the Gran Sasso rock overburden map of ref. [55].

Table 1: Comparison between the number of background events expected above 10 MeV from high energy muons surviving the mountain and the number of measured events, considering various groups (J) of detectors in the experimental set-up (5 rows by 5 columns detectors matrix, but an external detector out of operation [23, 24]). Upper limits on the rates (λ) of non-paulian processes leading to the emission of protons with $E_p \geq 10$ MeV are also reported for the various configurations; the final combined result is given. See text. For details see the paper in the 2009 publication list.

Group (J) of considered detectors	Corresponding exposure ($N_J t$) (nuclei $\times$ s)	Expected background events (b_J)	Measured events (n_J)	Upper Limit on λ (90% C.L.) (s^{-1})
Just the 4 detectors at corners (I)	3.2×10^{32}	12.1	11	1.99×10^{-32}
Just the remaining 6 detectors in the upper and lower rows (II)	4.8×10^{32}	8.7	6	9.33×10^{-33}
Just the 14 central detectors (III)	1.1×10^{33}	2.2	0	2.06×10^{-33}
Just the 9 core detectors (IV)	7.2×10^{32}	0.057	0	3.19×10^{-33}
Combined analysis (I+II+III):				1.63×10^{-33}

From the final combined result given in Table 1: $\lambda \leq 1.63 \times 10^{-33}$ s^{-1}, the limit on the non-paulian nuclear transition width has been derived to be: $\Gamma = \Gamma(^{23}Na) + \Gamma(^{127}I) = \hbar\lambda \leq 1.1 \times 10^{-54}$ MeV (90% C.L.). This is an improvement of about a factor 3 with respect to the limits previously available [48, 49]. From this value – considering the same nuclear Physics frameworks as in ref. [49] – a cautious estimate of the average probability, δ^2, which quantifies the possible PEP violations, has been derived to be: $\delta^2 \lesssim 3 - 4 \times 10^{-55}$, and a lower limit on the mean life for non-paulian proton emission has also be set: $\tau_{Na} \gtrsim 2 \times 10^{25}$ yr and $\tau_I \gtrsim 2.5 \times 10^{25}$ yr. These latter limits improve those previously available [48, 49]; moreover, it is worth noting that more stringent limit (down to $\delta^2 < 6.8 \times 10^{-56}$) can be derived depending on the model considered in evaluating $\tilde{\Gamma}$.

59

A much larger sensitivity can be obtained in future by suitably increasing the dedicated collected exposure, considering the high self-veto efficiency of the 9 inner core detectors (see Table 1). In particular, less than 1 background event is expected in the 9 NaI(Tl) detectors in the inner core of DAMA/LIBRA during ~ 1000 days exposure in the $10 - 35$ MeV energy interval; this can allow to explore (at 90% C.L.) probability of admixed symmetric component at level of $\delta^2 \lesssim 1 - 2 \times 10^{-56}$ or down to $\delta^2 \lesssim 2.5 \times 10^{-57}$ depending on the model considered in the evaluation of $\tilde{\Gamma}$. Thus, in ~ 3 years exposure – optimized for the MeV energy region – the sensitivity of DAMA/LIBRA to non-paulian nuclear transitions in ^{23}Na and ^{127}I can be improved of more than/about one order of magnitude without using any simulated muon background subtraction.

1.3 PEP violating electron transitions in Iodine atom with DAMA/LIBRA

The case of PEP violating electron transitions in atoms has also been investigated. For this purpose, the data collected by DAMA/LIBRA in the low energy range of interest during the first four annual cycles has been considered; the exposure is 0.53 ton $\times$ yr. It is worth noting that in this case the available exposure is very large since the set-up usually takes data in a condition optimized for the low energy region because of other kinds of investigations [24].

Since the electron atomic transitions of Sodium atoms are below the experimental energy threshold, we have analysed just the case of electron atomic transitions of Iodine atoms. Following a PEP violating electronic transition, X-rays and Auger electrons can be emitted due to both the transition itself and to the subsequent atomic shell rearrangements; at these energies large NaI(Tl) detectors – as those of DAMA/LIBRA – practically collect all the energies (detection efficiency ~ 1). The total energy release is expected to be at level of the ionization energy for the considered shell; however, it actually is slightly lower (by a term Δ), because of the presence of the other electrons in the already filled shells. In case of detectors with very sharp energy resolution, the precise knowledge of the small energy shift between the PEP violating transitions and the PEP allowed ones can be exploited in order to disentangle among them. In the present case, considering the shielding due to the extra electron filling the final shell, the energy of PEP violating transitions in Iodine (Z = 53) should be similar to the relative PEP allowed transitions in Tellurium (Z = 52) and, thus, in the case of K shell: $\Delta \lesssim 1.5$ keV. This value has to be compared with the energy resolution: $\sigma \sim 3$ keV at the energy of the Iodine K-shell [23], i.e. in the present case Δ is well below the energy resolution of the used detectors; therefore, precise estimations by Dirac-Fock method are unnecessary. Thus, the energy of 32 keV is considered for the K-shell PEP violating Transition in Iodine.

As shown in the dedicated paper in the 2009 publication list, no evidence for the expected peak is present there. Thus the number of events, which can be ascribed – at a give C.L. – to the process searched for, has been estimated to be: $S = (0.038 \pm 0.022)$ cpd/kg, which corresponds to an upper limit of: $S < 0.074$ cpd/kg (90%C.L.) following the Feldman and Cousins procedure [56]. It worth noting that slightly moving the gaussian peak position (± 1 keV) similar or more stringent values are obtained. Since 4.01×10^{24} Iodine atoms are present in one kg of NaI(Tl), the previous limit implies that lifetimes

(τ_{PV}) shorter than 4.7×10^{30} s can be excluded at 90%C.L.. It should be noted that the τ_{PV} is related to the lifetime (τ^0) of the PEP allowed transition of outer electrons into a free K-shell when an hole is present: $\tau^0 = \delta_e^2 \tau_{PV}$; δ_e^2 is the probability of the admixed symmetric component for the electron [45]. The normal electromagnetic dipole transition to Iodine K-shell is typically $\tau^0 \sim 6 \times 10^{-17}$ s [42]; therefore, the limit: $\delta_e^2 < 1.28 \times 10^{-47}$ (90% C.L.), holds. It is worth noting that the achieved limit is one order of magnitude more Stringent than the one by ELEGANTS V [45].

Finally, in ref. [53] superficial violations of the PEP due to the possible substructure of electrons has been discussed in composite models of quarks and leptons. In this theory the possible finite size of the electron, r_0, is related to δ_e^2 by the relation [53]:

$$\delta_e^2 = \left[\frac{4}{3} \left(\frac{3}{7} \right)^5 \left(\frac{Zr_0}{a_0} \right)^3 \right]^2 , \tag{2}$$

where a_0 is the Bohr radius ($= 0.53 \times 10^{-8}$ cm) and Z is The atomic number. Thus, the upper limit on δ_e^2 obtained above implies an upper limit on the electron size: $r_0 < 5.7 \times 10^{-18}$ cm; this value corresponds to an energy scale of $E \gtrsim 3.5$ TeV.

1.4   Upgrades and perspectives

A first upgrade of the DAMA/LIBRA set-up was performed in September 2008. One detector was recovered by replacing a broken PMT and a new optimization of some PMTs and HVs was done. The transient digitizers were replaced with new ones, the U1063A Acqiris 8-bit 1GS/s DC270 High-Speed cPCI Digitizers, having better performances, and a new DAQ with optical read-out was installed; since October 2008 DAMA/LIBRA is again in operation. The data of two further annual cycles are at hand. It is worth noting that – by the fact – DAMA has already realized a ton experiment over one year of running time.

Considering the relevance to lower the software energy threshold of the experiment, in order to improve the performance and the sensitivity of the experiment and to allow also deeper corollary information on the nature of the DM candidate particle(s) and on the various related astrophysical, nuclear and particle Physics scenarios, the replacement of all the PMTs with new ones with higher quantum efficiency has been planned and work is in progress.

DAMA/LIBRA will also study several other rare processes as already done by the former DAMA/NaI apparatus [13] and by itself so far (see 2009 publication list).

2   R&D-III towards DAMA/1ton

A third generation R&D effort towards a possible NaI(Tl) ton set-up (we already proposed in 1996 [14]) has been funded by I.N.F.N.. This new low background NaI(Tl) set-up would act as a "general purpose" experiment allowing the further investigation of Dark Matter particles, of other approaches for Dark Matter, and also of many other interesting topics in underground Physics. The main design of the mechanical assembling of the detectors, of the shield automated motions and of the calibration system has already been

defined in the framework of a POR-Abruzzo fellowship, considering a possible location deep underground.

Activities have been continued in the light of overcoming the present problems regarding the supplying of high quality NaI and, mainly, TlI powders. Possible purification test, whose achievements however strongly depend on the initial radiopurity of the powders, has been considered at some extent.

3   DAMA/LXe

We pointed out many years ago (see e.g. ref. [57]) the possible interest in using the liquid Xenon as target-detector material for particle dark matter investigations. Since the end of 80's (former Xelidon experiment of the INFN) we have realized several liquid Xenon (LXe) prototype detectors and, then, we have preliminarily put in measurement the set-up used in the data taking of ref. [58, 59] at LNGS in the framework of the DAMA project. This set-up (having a Cu inner vessel filled by $\simeq$ 6.5 kg - i.e. $\simeq$ 2 l - of liquid Xenon) was firstly upgraded at fall 1995 [60, 61, 62, 63, 64]. At that time it used Kr-free Xenon enriched in ^{129}Xe at 99.5%. Then, in 2000 the set-up was deeply modified reaching the configuration of ref. [65] in order to alternatively handle also Kr-free Xenon enriched in ^{136}Xe at 68.8%. The main features of the set-up, details on the data acquisition, on the cryogenic and vacuum systems and on the running parameters control can be found in refs. [63, 64, 65, 66, 67]. Some other upgrades have been carried out in recent years.

Investigations on several rare processes have been carried out with time passing in the various configurations, as well as measurements at low energies both with neutron source and with neutron beams by using a reference detector [58, 59, 60, 61, 62, 63, 64, 65, 68, 66, 69, 70, 71, 72]. In particular, first and/or competing results have been obtained on some approaches for Dark Matter investigations (including pulse shape analysis), on double beta decay modes in ^{136}Xe and ^{134}Xe, on possible charge non-conserving processes, on nucleon, di-nucleon and tri-nucleon decay into invisible channels both in ^{129}Xe and in ^{136}Xe.

On the contrary of the NaI(Tl) case, plans for enlarging the exposed mass have never been considered because of the technical reasons (specific of liquid noble gas detectors and, in particular, of liquid xenon detectors), we pointed out several times in the past (see e.g. [73]) and confirmed by the features of recent detectors (see in 2009 publication list); moreover, the extremely expensive cost of needed Kr-free (and possibly enriched) Xenon is an additional constraint.

After the forbiddeness of using cryogenic liquids in the LNGS underground laboratories, the set-up took data just few months until December 2004; then, it has been put in standby waiting for the restarting of the LNGS cooling water plant and of the local water refrigeration system. We profited from this period to perform several upgrades of the apparatus. Finally, thanks to a new chiller system and to the restoring of the use of water plants deep underground, the DAMA/LXe set-up restarted the data taking in December 2007, continuously during 2008 up to January 2009. Then, the Leybold periodical maintenance has occurred as well as an improvement of the remote computer control and setting of the cryogenic parameters. Then, the data taking has been restarted at fall

2009. During 2008 and 2009 DAMA/LXe was filled with Xenon enriched in ^{136}Xe and it has taken data focusing in this period the high energy region.

4 DAMA/R&D

DAMA/R&D is a low-background set-up dedicated to measurements on low background prototype scintillators and PMTs realized in various R&D works with industries. Moreover, it is regularly also used to perform relatively small scale experiments (often in collaboration with INR-Kiev as foreseen in the agreements). This set-up has been upgraded several times. The measurements mainly investigate 2β decay modes in various isotopes; both the active and the passive source techniques have been exploited as well as – sometimes – the coincidence technique.

In 2009 the activity of DAMA/R&D was mainly focused on:

1. Measurements using different $ZnWO_4$ crystals for a deeper investigation of the 2β decay modes in Zn and W and of the detectors performaces following different production strategies. Part of the data have been published; other developments are in progress.

2. Measurements with a $CeCl_3$ scintillator. First preliminary measurements suggest the $CeCl_3$ scintillator as an interesting detector for several possible applications in the search for rare processes. A data taking in DAMA/R&D has been completed and the data analysis is in progress.

3. Measurements with a commercial BaF_2 crystal to obtain accurate determinations of the decay times of some Po and Rn isotopes (in U/Th chain) and study of rare α processes. Data analysis is in progress.

4. Measurements started with a $CdWO_4$ crystal enriched with ^{106}Cd at 66% to study 2β processes in ^{106}Cd. The work on the detector creation procedures has been completed. The data taking has been started at fall 2009.

5. Design of new measurements at LNGS with low background $CdWO_4$ crystals with Cd enriched in ^{116}Cd as preliminary feasibility study for future measurements able to reach a sensitivity to the $2\beta0\nu$ decay of ^{116}Cd at level of 10^{24} yr.

6. Preliminary works for future measurements.

Some of the results obtained in 2009 are summarized in the following.

4.1 Search for 2β decay in Zinc and Tungsten with low-background $ZnWO_4$ crystal scintillators

A search for 2ε capture and $\varepsilon\beta^+$ decay of ^{64}Zn with the help of large low background $ZnWO_4$ crystal scintillators has been performed. In addition, the search for double beta decays of ^{70}Zn, ^{180}W, and ^{186}W has been realised as a by-product of the experiment.

Results for double positron decay ($2\beta^+$), electron capture with positron emission ($\varepsilon\beta^+$), and capture of two electrons from atomic shells (2ε) are much more modest respect to $2\beta^-$ studies. The most sensitive experiments give limits on the 2ε, $\varepsilon\beta^+$ and $2\beta^+$ processes on the level of $10^{17} - 10^{21}$ yr [74]. Reasons for this situation are: (1) lower energy releases in 2ε, $\varepsilon\beta^+$ and $2\beta^+$ processes in comparison with those in $2\beta^-$ decay, that result in lower probabilities of the processes, as well as making background suppression difficult; (2) usually lower natural abundances of $2\beta^+$ isotopes (which are typically lower than 1% with only few exceptions). Nevertheless, studies of neutrinoless 2ε and $\varepsilon\beta^+$ decays could help to explain the mechanism of neutrinoless $2\beta^-$ decay (is it due to non-zero neutrino mass or to the right-handed admixtures in weak interactions) [75].

The nucleus ^{64}Zn is one of the few exceptions among $2\beta^+$ nuclei having big natural isotopic abundance (see Table 2 where properties of potentially 2β active nuclides present in zinc tungstate ($ZnWO_4$) crystals are listed). With the mass difference between ^{64}Zn and ^{64}Ni nuclei being 1095.7 keV [76], double electron capture and electron capture with emission of positron are energetically allowed.

Table 2: Potentially 2β active nuclides present in $ZnWO_4$ crystals.

Transition	Energy release (keV) [76]	Isotopic abundance (%) [77]	Decay channels	Number of nuclei in 100 g of $ZnWO_4$ crystal
^{64}Zn→^{64}Ni	1095.7(0.7)	48.268(0.321)	2ε, $\varepsilon\beta^+$	9.28×10^{22}
^{70}Zn→^{70}Ge	998.5(2.2)	0.631(0.009)	$2\beta^-$	1.21×10^{21}
^{180}W→^{180}Hf	144(4)	0.12(0.01)	2ε	2.31×10^{20}
^{186}W→^{186}Os	489.9(1.4)	28.43(0.19)	$2\beta^-$	5.47×10^{22}

It should be noted that possible evidence for $\varepsilon\beta^+$ decay of ^{64}Zn, with $T_{1/2}^{(0\nu+2\nu)\varepsilon\beta^+} = (1.1 \pm 0.9) \times 10^{19}$ yr, was presented in Ref. [78]. Earlier experiments with CdZnTe semiconductor detectors [79] and $ZnWO_4$ crystal scintillator [80] were not sensitive enough to check this claim due to the small mass of detectors used (few grams). Experiment [81] with two detectors (HP Ge 456 cm^3 and CsI(Tl) $\simeq$400 cm^3) and a 460 g Zn sample only gave a limit on the $\varepsilon\beta^+$ decay of ^{64}Zn: $T_{1/2}^{(0\nu+2\nu)\varepsilon\beta^+} > 1.3 \times 10^{20}$ yr. Further improvements of sensitivity were reached at the first stage [82] of the experiment summarised here and have already been described in the 2008 LNGS report.

The $ZnWO_4$ crystal scintillators considered here were produced from two crystal boules; their masses are 117, 699, and 168 g, respectively. The crystal boules were grown by the Czochralski method from $ZnWO_4$ compounds prepared from two batches of zinc oxide provided by different producers, and from the same tungsten oxide. To estimate the presence of naturally occurring radioactive isotopes, as well as some other elements important for growing of the crystals, the $ZnWO_4$ samples were measured with the help of Inductively Coupled Plasma - Mass Spectrometry (ICP-MS, Agilent Technologies model 7500a).

The $ZnWO_4$ crystals were fixed inside a cavity of $\oslash 47 \times 59$ mm in the central part of a polystyrene light-guide 66 mm in diameter and 312 mm in length. The cavity was

filled up with high purity silicone oil. The light-guide was optically connected on opposite sides by optical couplant to two low radioactivity EMI9265–B53/FL 3" photomultipliers (PMT). The light-guide was wrapped by PTFE reflection tape.

The detector has been installed deep underground in the low background DAMA/R&D set-up. An event-by-event data acquisition system accumulates the amplitude and the arrival time of the events. The sum of the signals from the PMTs was recorded with the sampling frequency of 20 MS/s over a time window of 100 μs by a 8 bit transient digitizer (DC270 Acqiris).

The measurements were carried out in four runs (see Table 3 for details). First, the

Table 3: Description of low background measurements with $ZnWO_4$ crystal scintillators. Times of measurements (t), energy intervals of data taking (ΔE), energy resolutions at the 662 keV γ line of ^{137}Cs (FWHM), and background counting rates (BG) in different energy intervals are specified.

Run	Crystal scintillator	t (h)	ΔE (MeV)	FWHM (%)	BG (counts/(day×keV×kg)) in energy interval (MeV)			
					0.2–0.4	0.8–1.0	2.0–2.9	3.0–4.0
1	ZWO-1	1902	0.01–1	11.5	1.93(3)	0.27(1)		
2	ZWO-1	2906	0.05–4	12.6	1.71(2)	0.25(1)	0.0072(7)	0.0003(1)
3	ZWO-2	2130	0.05–4	14.6	1.07(1)	0.149(3)	0.0072(4)	0.00031(7)
4	ZWO-2a	3292	0.01–1	11.0	1.52(2)	0.211(7)		

energy interval of data taking was chosen as $0.01 - 1$ MeV with the aim to search for the neutrino accompanied double electron capture in ^{64}Zn. In particular, the data of the Run 1 has already been analyzed and published in [82]. Then the energy interval was changed to $0.05 - 4$ MeV in order to search for other possible double beta processes in ^{64}Zn (Run 2). After that, the large ZWO-2 crystal was installed and the experiment was carried out in the same energy range (Run 3). Finally the ZWO-2 crystal was cleaved in two parts; one (ZWO-2a) was used in the Run 4 with the energy interval of data taking $0.01 - 1$ MeV. The energy scale and resolution of the $ZnWO_4$ detectors have been measured with ^{22}Na, ^{133}Ba, ^{137}Cs, ^{228}Th and ^{241}Am γ sources at the beginning and end of each run. The energy resolutions of the $ZnWO_4$ detectors for 662 keV γ quanta of ^{137}Cs are presented in Table 3.

The energy spectra accumulated over Runs 2 and 3 with the $ZnWO_4$ detectors in the low background set-up are shown in Fig.1. The spectra are normalized to the mass of the crystals and to the time of the measurements.

The time-amplitude analysis, the pulse-shape discrimination, and the Monte Carlo simulation were applied to reconstruct the background spectra and to estimate the radioactive contamination of the $ZnWO_4$ detectors. We have found $ZnWO_4$ crystal scintillators extremely radiopure detectors with typical contamination at the level of μBq/kg (^{228}Th and ^{226}Ra), ≤ 0.06 mBq/kg (^{210}Po), total α activity (U/Th) 0.2–0.4 mBq/kg, ≤ 0.4 mBq/kg (^{40}K), ≤ 0.05 mBq/kg (^{137}Cs), ≤ 0.4 mBq/kg (^{90}Sr–^{90}Y), ≤ 0.01 mBq/kg
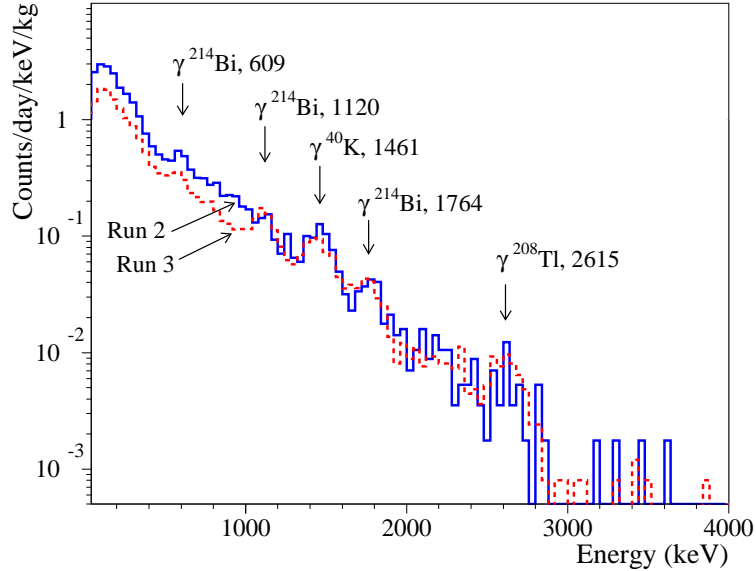
Figure 1: (Color online) Energy spectra of ZnWO$_4$ scintillators measured in the low background set-up during Run 2 (solid line) and Run 3 (dashed line). Energies of γ lines are in keV.

(^{147}Sm), and ≤ 3 mBq/kg (^{87}Rb).

There are no clear peculiarities in the measured energy spectra of the ZnWO$_4$ detectors, which can be interpreted as double beta decay of Zinc or Tungsten isotopes. Therefore only lower half-life limits can be set according to the formula:

$$\lim T_{1/2} = N \cdot \eta \cdot t \cdot \ln 2 / \lim S,$$

where N is the number of potentially 2β unstable nuclei, η is the detection efficiency, t is the measuring time, and $\lim S$ is the number of events of the effect searched for which can be excluded at a given confidence level (C.L.).

We have used different combinations of the accumulated data to reach maximal sensitivity to the sought double beta processes. The response functions of the ZnWO$_4$ detectors for the 2β processes were simulated with the help of the GEANT4 code [83]. The initial kinematics of the particles emitted in the decays was generated with the DECAY0 event generator [84]. All the half-life limits on 2β decay processes in Zinc and Tungsten obtained in the present experiment are summarized in Table 4 where results of the most sensitive previous experiments are given for comparison.

The obtained bounds are well below the existing theoretical predictions [86, 87]; nevertheless most of the limits are near one order of magnitude higher than those established in previous experiments. It should be stressed that in contrast to a level of sensitivity obtained for double β^- decay ($10^{23} - 10^{25}$ years in the best experiments), only two nuclei (^{40}Ca and ^{78}Kr) among potentially 2ε, $\varepsilon\beta^+$, $2\beta^+$ active isotopes were investigated at the level of $\sim 10^{21}$ yr.

Further improvements in sensitivity can be reached by increasing the mass of the

Table 4: Half-life limits on 2β processes in Zn and W isotopes.

Transition	Decay channel	Level of daughter nucleus	$T_{1/2}$ limit (yr)	
			Present work 90%(68%) C.L.	Previous results 90%(68%) C.L.
$^{64}Zn \rightarrow {}^{64}Ni$	$0\nu2\varepsilon$	g.s.	$\geq 1.1(2.8) \times 10^{20}$	$\geq 0.7(1.0) \times 10^{18}$ [80]
				$\geq 3.4(5.5) \times 10^{18}$ [82]
	$0\nu\varepsilon\beta^+$	g.s.	$\geq 4.3(5.7) \times 10^{20}$	$\geq 2.8 \times 10^{16}$ [79]
				$\geq 2.4(3.6) \times 10^{18}$ [80]
				$\geq 1.3 \times 10^{20}$ [81]
				$\geq 2.2(6.1) \times 10^{20}$ [82]
	$2\nu\varepsilon\beta^+$	g.s.	$\geq 0.70(2.1) \times 10^{21}$	$= (1.1 \pm 0.9) \times 10^{19}$ [78]
				$\geq 4.3(8.9) \times 10^{18}$ [80]
				$\geq 1.3 \times 10^{20}$ [81]
				$\geq 2.1(7.4) \times 10^{20}$ [82]
$^{70}Zn \rightarrow {}^{70}Ge$	$0\nu2\beta^-$	g.s.	$\geq 1.8(3.0) \times 10^{19}$	$\geq 0.7(1.4) \times 10^{18}$ [80]
	$2\nu2\beta^-$	g.s.	$\geq 2.3(4.0) \times 10^{17}$	$\geq 1.3(2.1) \times 10^{16}$ [80]
	$0\nu2\beta^-M1$	g.s.	$\geq 1.0(1.4) \times 10^{18}$	
$^{180}W \rightarrow {}^{180}Hf$	$0\nu2\varepsilon$	g.s.	$\geq 0.86(1.2) \times 10^{18}$	$\geq 0.9(1.3) \times 10^{17}$ [85]
	$2\nu2K$	g.s.	$\geq 6.6(9.4) \times 10^{17}$	$\geq 0.7(0.8) \times 10^{17}$ [85]
$^{186}W \rightarrow {}^{186}Os$	$0\nu2\beta^-$	g.s.	$\geq 2.1(4.2) \times 10^{20}$	$\geq 1.1(2.1) \times 10^{21}$ [85]
	$0\nu2\beta^-$	2^+ (137.2 keV)	$\geq 2.1(4.2) \times 10^{20}$	$\geq 1.1(2.0) \times 10^{21}$ [85]
	$0\nu2\beta^-M1$	g.s.	$\geq 5.8(8.6) \times 10^{19}$	$\geq 1.2(1.4) \times 10^{20}$ [85]
	$2\nu2\beta^-$	g.s.	$\geq 2.3(2.8) \times 10^{19}$	$\geq 3.7(5.3) \times 10^{18}$ [85]
	$2\nu2\beta^-$	2^+ (137.2 keV)	$\geq 1.8(3.6) \times 10^{20}$	$\geq 1.0(1.3) \times 10^{19}$ [85]

ZnWO$_4$ detector, suppression of external background and development of ZnWO$_4$ scintillators with lower level of radioactive contamination. High abundance of ^{64}Zn (48.3%) allows to build a large scale experiment without expensive isotopical enrichment. An experiment involving $\approx$10 tons of *non-enriched* crystals (9×10^{27} nuclei of ^{64}Zn) could reach the half-life sensitivity $\sim 3 \times 10^{28}$ yr (supposing zero background during ten years of measurements). Such a sensitivity could contribute to our understanding of the neutrino mass mechanism and right-handed currents in neutrinoless processes [75]. The two neutrino double electron capture should be surely observed: in accordance with theoretical expectations [86, 87], $T_{1/2}$ for the $2\nu2\varepsilon$ process is predicted on the level of $10^{25} - 10^{26}$ yr. Further R&D developments of high performances, high radiopurity, large mass ZnWO$_4$ scintillators are foreseen for this and other kinds of searches for rare processes.

4.2 Investigation of double β decay of ^{106}Cd

The ^{106}Cd isotope is one of the best candidates for the double β^+ decay because of: 1) its natural isotopic abundance and of the possibility to achieve samples enriched up to 100% with the present technology; 2) its rather large Q$_{\beta\beta}$ value (2771 keV) and of the possibility to study the various $2\beta^+$, $\varepsilon\beta^+$ e 2ε decay modes; 3) the favourable theoretical estimates of the half-lives. In particular, a low background CdWO$_4$ detector with Cd enriched in ^{106}Cd at 66% has been realised (a technical paper has been in preparation during 2009) and at the end of 2009 the detectors has been put in measurement in the low background DAMA/R&D set-up.

5 Measurements with DAMA/Ge and LNGS Ge facility

Various R&D developments to improve low background set-ups and scintillators as well as new developments for higher radiopure PMTs are regularly carried out. The related measurements on samples are usually performed by means of the DAMA low background Ge detector, specially realized with a low Z window. It is operative deep underground in the low background facility of the LNGS since many years. Some selected materials are in addition measured with high sensitivity ICP-MS and mass spectrometers.

In particular, main data taking/results during year 2009 are:

- regular measurements on samples.

- first limits on neutrinoless resonant 2ϵ captures in ^{136}Ce and new limits for other 2β processes in ^{136}Ce and ^{138}Ce isotopes with a CeCl$_3$ crystal.

- analysis of the measurements (named ARMONIA) with a Molybdenum sample (mass $\simeq$ 1 kg enriched in ^{100}Mo at 99.5%) installed in the 4π low-background HP Ge detectors facility completed and scientific paper in preparation in order to investigate the $2\nu2\beta$ decay of ^{100}Mo to the first excited 0_1^+ level of ^{100}Ru.

- new measurements with LiF(W) aiming mainly to investigate ^{7}Li solar axion and new efforts for future measurements.

- measurements with about Ru samples to investigate the radiopurity of this material and to preliminariyly investigate the 2β processes of ^{96}Ru and ^{104}Ru.

- the properties of a lithium molybdate (Li$_2$MoO$_4$) single crystal – a potential detector in searches for rare nuclear events – have been studied.

- new measurements on various subjects for next years are in preparation.

In the following just some of the results achieved in 2009 are summarized.

5.1 Properties of a Li$_2$MoO$_4$ single crystal: a potential detector in searches for rare events

Properties of a lithium molybdate (Li$_2$MoO$_4$) single crystal have been studied. Its radiopurity has been measured deep underground with a HP Ge detector. The crystal is not polluted by usual radioactive contaminants (activities were found to be <20 mBq/kg for ^{238}U chain, <30 mBq/kg for ^{232}Th chain, <4 mBq/kg for ^{137}Cs and <8 mBq/kg for ^{60}Co), excluding ^{40}K with (170 ± 80) mBq/kg.

The perspectives of this crystal scintillator as a possible detector for search for some rare nuclear processes has been estimated; in particular: double beta decay of ^{100}Mo, and resonant capture of possible solar axions on ^{7}Li.

The data collected with the Li$_2$MoO$_4$ during 1240 h has allowed to set limit on the ^{7}Li solar axion mass of 22 keV at 90% C.L. While this value is worse than the most stringent

limit known to-date $m_a < 13.9$ keV, obtained with samples of LiF powder and LiF(W) crystal by our collaboration [88], nevertheless it is better than that obtained in the first search for the ^{7}Li solar axions $m_a < 32$ keV [89], giving space for possible good future perspectives. In fact, the m_a limit value obtained in the present work was restricted, in particular, by the low value of efficiency (4.4%) and this could, clearly, be improved if Li_2MoO_4 crystals will be used as detectors in a "source = detector" approach.

5.2 First limits on neutrinoless resonant 2ϵ captures in ^{136}Ce and new limits for other 2β processes in ^{136}Ce and ^{138}Ce isotopes

The preliminary measurements performed with a small new CeCl$_3$ crystal and a low-background HP Ge detector (244 cm^3) has been used to determine the internal radioactive contamination of this crystal. Only limits (90% C.L.) were set for activity of radioactive nuclides in the ^{232}Th chain (<0.2 Bq/kg), of ^{40}K (<1.7 Bq/kg), of ^{60}Co (<0.04 Bq/kg), of ^{137}Cs (<0.06 Bq/kg), and for some radioactive isotopes in the lanthanide series: ^{152}Eu (<0.13 Bq/kg), ^{154}Eu (<0.06 Bq/kg), ^{176}Lu (<0.05 Bq/kg). However, activity was observed for ^{235}U as 0.36(19) Bq/kg, ^{238}U as 0.70(7) Bq/kg, ^{138}La as 0.68(5) Bq/kg (U
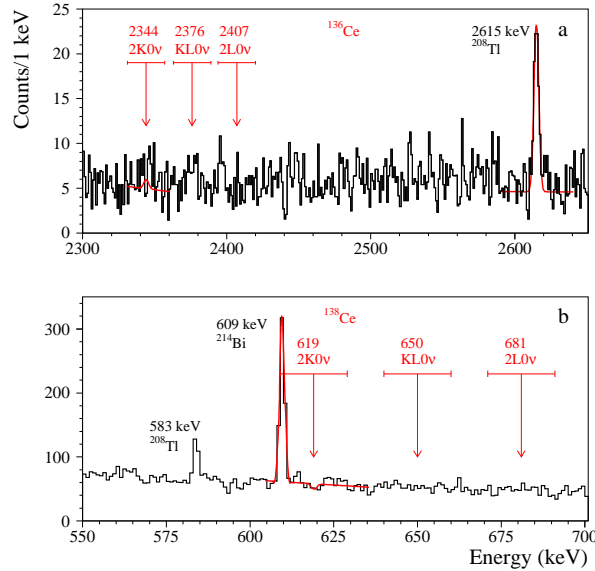
Figure 2: (Color online) Part of the CeCl$_3$ experimental spectrum in the energy region of the $2\varepsilon 0\nu$ captures in ^{136}Ce (a) and ^{138}Ce (b). The arrows show the expected energies for the $2K0\nu$, $KL0\nu$ and $2L0\nu$ decays; their error bars reflect the uncertainty in the knowledge of the atomic mass differences: 13 keV for ^{136}Ce–^{136}Ba and 10 keV for ^{138}Ce–^{138}Ba. The results of the fit of some peaks are also shown as examples: (a) the 2615 keV peak of ^{208}Tl and the expected peak at 2344 keV (^{136}Ce $2K0\nu$); (b) the 609 keV peak of ^{214}Bi and the expected peak at 619 keV (^{138}Ce $2K0\nu$).

69

activities could be related with the plastic and copper container of the $CeCl_3$ crystal). These results are important for further developments and applications of this new kind of scintillator.

The search for the characteristic radiation in the energy spectrum (see Fig. 2) has allowed to set, for the first time, half life limits for different double electron captures in ^{136}Ce to the excited levels of ^{136}Ba; the obtained results are in the range of $(1-6)\times10^{15}$ yr. Several other decay modes in ^{136}Ce and ^{138}Ce isotopes have been investigated; see in the 2009 publication list. In particular, the resonant $2\varepsilon0\nu$ captures to the levels of 2392.1 keV and 2399.9 keV of ^{136}Ba are limited as $T_{1/2} > 2.4\times10^{15}$ yr and $T_{1/2} > 4.1\times10^{15}$ yr at 90% C.L., respectively. The sensitivity is limited by the small mass of the $CeCl_3$ sample (6.9 g) and by the low natural abundance of ^{136}Ce isotope (0.185%); these can be improved in future experiments. In the simplest approach, a Ce sample with mass of $\simeq1$ kg can be measured underground with a HP Ge detector. More sophisticated scheme with use of big $CeCl_3$ (or CeF_3, or $CeBr_3$) scintillator working in coincidence with a HPGe detector is under consideration too (also in relation with possibility to investigate 2β processes in other scintillators). Expected sensitivity with use of natural Ce is at least around 10^{18} yr, and would be better with Ce enriched in ^{136}Ce isotope.

5.3 Search for double β decays of ^{96}Ru and ^{104}Ru by ultra-low background HPGe spectrometry

A search for double β processes in ^{96}Ru and ^{104}Ru was realized with the help of ultra–low background HPGe γ spectrometr (468 cm^3). The measurements performed over 158 h with a 473 g sample of ruthenium were used to set new limits on double β processes in ^{96}Ru in the range of $T_{1/2} \sim 10^{18-19}$ yr, which are two–three orders of magnitude higher than those obtained in the previous experiment [90]. Search for 2β transition of ^{104}Ru to the 556 keV excited level of ^{104}Pd was carried out at the first time giving the limit $T_{1/2} > 3.5 \times 10^{19}$ yr. In particular, Fig. 3 shows part of the energy spectrum considered for the $\varepsilon\beta^+$ transition of ^{96}Ru to the excited 2^+ 778 keV level of ^{96}Mo; the peak expected with the half-life 5.8×10^{18} yr is shown there.

These preliminary measurements demonstrate availability of ^{96}Ru as a favourable nuclide to search for 2ε, $\varepsilon\beta^+$ and $2\beta^+$ processes thanks to the large energy of the decay and the comparatively high isotopic abundance. The search for the resonant $0\nu KL$ capture to the 2700 keV level, and the $0\nu2L$ capture to the 2713 keV level is of a particular interest. From this point of view more accurate determination of the difference in atomic masses of ^{96}Ru and ^{96}Mo isotopes is strongly required. Precise study of the characteristics of the 2700 and 2713 keV levels of ^{96}Mo (spin, parity, decay scheme) is important too.

The experiment is in progress. Preliminary results after 158 h of measurements are reported in 2009 publication list; obtained half-life limits are $2-3$ orders of magnitude higher than those in literature; at present the data collected during 2164 h are under analysis. However, the sensitivity is mainly limited by contamination of the ruthenium by potassium on the level of 10^{-4} g g^{-1}. R&D to purify the material is under way in collaboration with the Kharkiv Institute of Physics and Technology (National Academy of Sciences of Ukraine). When reducing the potassium contamination in the presently available 1 kg of Ru by at least one order of magnitude and increasing the exposure up
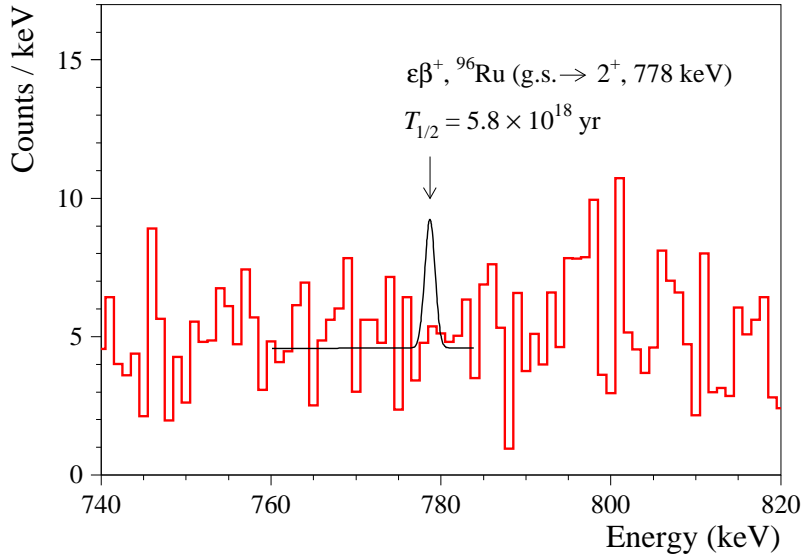
Figure 3: (Color online) Part of energy spectra accumulated with the ruthenium sample over 158 h in the energy region of peak expected for $\varepsilon\beta^+$ transition of ^{96}Ru to the excited 2^+ 778 keV level of ^{96}Mo. Area of the peak corresponds to the half–life 5.8×10^{18} yr excluded at 90% C.L.

to one–two years×kg, the sensitivity of the experiment would be improved of at least one–two orders of magnitude in terms of half–life.

Further improvement of sensitivity can be achieved by using enriched ^{96}Ru isotope, and by increasing the detection efficiency and the exposition. Specially developed multi–crystal HPGe detectors could be applied to reach a sensitivity to double β processes in ^{96}Ru on the level of 10^{22-24} yr. It corresponds to the theoretical predictions for the two neutrino mode of 2ε and $\varepsilon\beta^+$ processes.

5.4   ARMONIA

The measurements, named ARMONIA, with a Molybdenum sample (mass $\simeq 1$ kg enriched in ^{100}Mo at 99.5%) installed in the 4π low-background HP Ge detectors facility was already completed. The aim was to investigate the $2\beta2\nu$ decay of ^{100}Mo to the first excited 0_1^+ level of ^{100}Ru by investigating the spectrum of coincidence between two HP Ge detectors when the energy window of one of the detectors is set to the expected energy of the gamma quanta emitted in the $2\beta2\nu$ decay to ^{100}Ru* (540 or 591 keV; width of window 2 keV is in accordance with the energy resolution of the HP Ge at these energies). After some very preliminary analysis on partial statistics [91]; new results, based on a statistics of about 17000 h, have preliminarily been released in ref. [92]. The final paper with complete data analysis is in preparation.

Moreover, taking into account the previous results of the joint research with the group

from INR-Kiev, and the works presently in progress, a program of research has been developed that can profit of DAMA/R&D and/or DAMA/Ge. In particular we just list main present and future activities in the following.

Research to be completed (continued):

- **Search for 2β decay of zinc and tungsten with ZnWO$_4$ crystal scintillators.** Further developments and measurements of/with ZnWO$_4$ crystal scintillators with aim to improve the search for 2β decay of zinc and tungsten, measurements of half-life of ^{180}W relatively to α decay, estimation of radioactive contamination of ZnWO$_4$ crystal scintillators.

- **Search for ^{7}Li solar axions.** Completion of the data analysis of the mesurement to search for solar axions by using new LiF samples and ultra-low-background γ spectrometers of the LNGS. Completion of the data analysis of the measurements of radioactive contamination of LiI(Eu) and LiF(W) crystal scintillators by the low-background γ spectrometers of the LNGS. R&D to develop new LiI(Eu) or/and LiF crystal scintillators to be used in DAMA/R&D or DAMA/Ge.

- **Search for 2β processes in ^{96}Ru and ^{104}Ru.** Continuation of the measurement to search for 2β decay of ^{96}Ru and ^{104}Ru by using samples of ruthenium installed in ultra-low background HP Ge γ spectrometers at the LNGS. Radio-purification of the samples.

- **Search for the 2β decay of ^{106}Cd with the help of cadmium tungstate crystal scintillators enriched in ^{106}Cd.** Search for 2β decay of ^{106}Cd with the help of cadmium tungstate crystal scintillators enriched in stable isotope ^{106}Cd (^{106}CdWO$_4$) at the level of sensitivity of theoretical predictions (T$_{1/2} \sim 10^{21} - 10^{22}$ yr for $2\epsilon 2\nu$ process) with the final goal to observe the neutrino accompanied mode of 2ϵ, $\epsilon\beta^+$, and $\beta^+\beta^+$ processes in ^{106}Cd. Further R&D developments for future measurements are foreseen.

Main measurements in preparation with INR-Kiev:

- **Search for double β decay of ^{116}Cd with enriched ^{116}CdWO$_4$ crystal scintillators.** Advanced preparation with INR-Kiev of a measurement in DAMA/R&D to search for 2β decay of ^{116}Cd with enriched ^{116}CdWO$_4$ crystal scintillators at the level of sensitivity T$_{1/2} \sim 10^{24}$ yr, comparable to the best current and planned experiments.

- **Investigation of 2β decay of ^{150}Nd to excited levels of ^{150}Sm.** Investigation of the feasibility to test the previous report on observation of $2\nu 2\beta$ decay of ^{150}Nd to the first excited 0_1^+ level of ^{150}Sm by using neodymium sample of a few kg mass installed in an ultra-low background HP Ge γ spectrometers of LNGS and improvements.

- **Search for 2ϵ and $\epsilon\beta^+$ decay of ^{190}Pt.** First search for 2ϵ (including the resonant process) and $\epsilon\beta^+$ decay of ^{190}Pt by using $\simeq 0.1$ kg sample of platinum installed in an ultra-low background HP Ge γ spectrometer of the LNGS.

- **Search for 2ϵ and $\epsilon\beta^+$ decay of ^{184}Os.** First search for 2ϵ (including the resonant process) and $\epsilon\beta^+$ decay of ^{184}Os by using about 0.3 kg sample of ultra-pure osmium installed in an ultra-low background HPGe γ spectrometer of LNGS.

- **R&D of radiopure BaF$_2$ crystal scintillators to search for 2β decay of ^{130}Ba and ^{132}Ba.** R&D of radiopure BaF$_2$ crystal scintillators to search for 2β decay of ^{130}Ba and ^{132}Ba on the level of sensitivity $\sim 10^{21} - 10^{22}$ yr with aim to confirm or disprove the result of a geochemical experiment.

Subsequent improvements of all these measurements are foreseen depending on the achieved results.

6   Conclusions

In conclusion, the main activities during year 2009 can be summarized as in the following:

I. The DAMA/LIBRA set-up is regularly in data taking and other two annual cycles are at hand. We remind that the analysis of an exposure of 0.53 tons×year collected during the first four annual cycles has already confirmed the presence of DM particles in the galactic halo (8.2σ C.L. cumulatively with the former DAMA/NaI) by exploiting the model independent DM annual modulation signature. Further corollary model-dependent investigations have been regularly pursued. Moreover, new limits on possible PEP violating processes in Sodium and Iodine have been published.

II. The development of new low background PMTs with higher quantum efficiency has been started. It is planned to install them in DAMA/LIBRA at fall 2010.

III. The RD-III towards the possible DAMA/1ton has been carried out on various aspects.

IV. The DAMA/LXe set-up has been in maintenance and, then, again in data taking with Kr-free Xenon enriched in ^{136}Xe.

V. The DAMA/R&D set-up has been used to perform various kinds of measurements; several data analyses have been completed and other ones are in progress. Various other relatively small scale experiments are in preparation.

VI. The DAMA/Ge is regularly in operation and various small scale experiments have been performed, are in progress and in preparation.

7   List of Publications during 2009

1. R. Bernabei, P. Belli, F. Montecchia, F. Nozzoli, F. Cappella, A. d'Angelo, A. Incicchitti, D. Prosperi, R. Cerulli, C. J. Dai, H. L. He, H. H. Kuang, J. M. Ma, X. D. Sheng, Z. P. Ye, "Dark Matter particles in the galactic halo", SIF Atti di Conferenze 98 (2009), 131.

2. R. Bernabei, P. Belli, F. Montecchia, F. Nozzoli, F. Cappella, A. d'Angelo, A. Incicchitti, D. Prosperi, R. Cerulli, C. J. Dai, H. L. He, H. H. Kuang, J. M. Ma, X. D. Sheng, Z. P. Ye, "Dark Matter particles in the galactic halo", Phys. of Atom. Nucl. 72 (2009), 2076.

3. O.P. Barinova, F. Cappella, R. Cerulli, F. A. Danevich, S.V. Kirsanova, V.V. Kobychev, M. Laubenstein, S.S. Nagorny, F. Nozzoli, V.I. Tretyak, "Intrinsic radiopurity of a Li_2MoO_4 crystal", Nucl. Instr. & Meth. A 607 (2009) 573.

4. R. Bernabei, P. Belli, F. Montecchia, F. Nozzoli, F. Cappella, A. d'Angelo, A. Incicchitti, D. Prosperi, R. Cerulli, C. J. Dai, H. L. He, H. H. Kuang, J. M. Ma, X. D. Sheng, Z. P. Ye, "First DAMA/LIBRA Results and Beyond", in the volume "Progress in High energy Physics and Nuclear Safety", ISBN 978-90-481-2285-1, pages 31-45 (2009) Springer ed.

5. P. Belli, R. Bernabei, S. d'Angelo, F. Cappella, R. Cerulli, A. Incicchitti, M. Laubenstein, D. Prosperi, V.I. Tretyak, "First limits on neutrinoless resonant 2ϵ captures in ^{136}Ce and new limits for other 2β processes in ^{136}Ce and ^{138}Ce isotopes", Nucl. Phys. A 824 (2009) 101.

6. R. Bernabei, P. Belli, F. Cappella, R. Cerulli, C. J. Dai, A. d'Angelo, H. L. He, A. Incicchitti, H. H. Kuang, X. M. Ma, F. Montecchia, F. Nozzoli, D. Prosperi, X. D. Sheng, Z. P. Ye, "New search for processes violating the Pauli-Exclusion-Principle in Sodium and in Iodine", Eur. Phys. J. C 62 (2009) 327.

7. R. Bernabei, P. Belli, F. Cappella, R. Cerulli, C. J. Dai, A. d'Angelo, H. L. He, A. Incicchitti, H. H. Kuang, X. M. Ma, F. Montecchia, F. Nozzoli, D. Prosperi, X. D. Sheng, Z. P. Ye, "Non-paulian nuclear processes in highly radiopure NaI(Tl): status and perspectives", in press on Foundation of Physics, DOI:10.1007/s10701-009-9362-1 (2009).

8. R. Bernabei, P. Belli, F. Cappella, R. Cerulli, C. J. Dai, A. d'Angelo, H. L. He, A. Incicchitti, H. H. Kuang, X. M. Ma, F. Montecchia, F. Nozzoli, D. Prosperi, X. D. Sheng, Z. P. Ye, "Results from DAMA/LIBRA at Gran Sasso", in press on Foundation of Physics, DOI:10.1007/s10701-009-9368-8 (2009).

9. R. Bernabei, P. Belli, A. Incicchitti and D. Prosperi, "Liquid Noble gases for Dark Matter searches: a synoptic survey", Exorma Ed., Roma, ISBN 978-88-95688-12-1, 2009, pages 1–53 (arXiv:0806.0011v2).

10. R. Bernabei, P. Belli, F. Cappella, R. Cerulli, C. J. Dai, A. d'Angelo, H. L. He, A. Incicchitti, H. H. Kuang, J. M. Ma, F. Montecchia, F. Nozzoli, D. Prosperi, X. D. Sheng, Z. P. Ye, "Particle Dark Matter in the galactic halo: results from DAMA/LIBRA" , Il Nuovo Cimento C32 (2009), 313.

11. P. Belli, R. Bernabei, F. Cappella, R. Cerulli, F.A. Danevich, B.V. Grinyov, A. Incicchitti, V.V. Kobychev, V.M.Mokina, S.S. Nagorny, L.L. Nagornaya, S. Nisi, F. Nozzoli, D.V. Poda, D. Prosperi, V.I. Tretyak, S.S. Yurchenko, "Search for double

beta decay of zinc and tungsten with low background ZnWO4 crystal scintillators", Nucl. Phys. A 826 (2009) 256.

12. P. Belli, R. Bernabei, F. Cappella, R. Cerulli, F.A. Danevich, S. d'Angelo, A. Incicchitti, M. Laubenstein, O.G. Polischuk, D. Prosperi, V.I. Tretyak, "Search for double beta decays of ^{96}Ru and ^{104}Ru by ultra-low background HPGe gamma spectrometry", Eur. Phys. J. A, 42 (2009) 171.

13. P. Belli, R. Bernabei, F. Cappella, R. Cerulli, F.A. Danevich, B.V. Grinyov, A. Incicchitti, V.V. Kobychev, V.M.Mokina, L.L. Nagornaya, S.S. Nagorny, S. Nisi, F. Nozzoli, D.V. Poda, D. Prosperi, V.I. Tretyak, S.S. Yurchenko, "Preliminary results of search for 2β processes in zinc and tungsten with the help of zinc tungstate crystal scintillator", in the volume of the Proceed. of the Int. conf. NPAE 2008, ed. INR-Kiev (2009), 433.

14. P. Belli, R. Bernabei, R. S. Boiko, F. Cappella, R. Cerulli, F.A. Danevich, S. d'Angelo, A. Incicchitti, V.V. Kobychev, B.N. Kropivyansky, M. Laubenstein, P.G. Nagornyi, S.S. Nagorny, S. Nisi, F. Nozzoli, D.V. Poda, D. Prosperi, O.G. Shkulkova, V.I. Tretyak, I.M. Vyshnevskyi, S.S. Yurchenko, "Preliminary results on the search for ^{100}Mo 2β decay to the first excited 0_1^+ level of ^{100}Ru", in the volume of the Proceed. of the Int. conf. NPAE 2008, ed. INR-Kiev (2009),473.

15. R. Bernabei, P. Belli, F. Montecchia, F. Nozzoli, F. Cappella, A. d'Angelo, A. Incicchitti, D. Prosperi, R. Cerulli, C.J. Dai, H.L. He, H.H. Kuang, J.M. Ma, X.D. Sheng, Z.P. Ye, "First results from DAMA/LIBRA", in the volume of the Proceed. of the Int. conf. NPAE 2008, ed. INR-Kiev (2009), 72.

16. R. Bernabei, P. Belli, F. Montecchia, F. Nozzoli, F. Cappella, A. Incicchitti, D. Prosperi, R. Cerulli, C.J. Dai, H.L. He, H.H. Kuang, J.M. Ma, X.D. Sheng, Z.P. Ye, "Investigating the dark halo", in the Procced. of the 13 Lomonosov Conf. on Elementary Particle Physics, World Scie. (2009), 214.

17. P. Belli, R. Bernabei, R.S. Boiko, F. Cappella, R. Cerulli, C.J. Dai, F.A. Danevich, A. d'Angelo, S. d'Angelo, B.V. Grinyov, A. Incicchitti, V.V. Kobychev, B.N. Kropivyansky, M. Laubenstein, P.G. Nagornyi, S.S. Nagorny, S.Nisi, F.Nozzoli, D.V.Poda, D.Prosperi, A.V. Tolmachev, V.I. Tretyak, I.M. Vyshnevskyi, R.P. Yavetskiy, S.S. Yurchenko, "Search for rare processes at Gran Sasso", in the Procced. of the 13 Lomonosov Conf. on Elementary Particle Physics, World Scie. (2009), 225.

18. P. Belli, R. Bernabei, R. S. Boiko, V.B. Brudanin, R. Cerulli, F.A. Danevich, S. d'Angelo, A.E. Dossovitskiy, B.V. Grinyov, A. Incicchitti, V.V. Kobychev, G.P. Kovtun, A.L. Mikhlin, V.M.Mokina, L.L. Nagornaya, S.S. Nagorny, F. Nisi, R.B. Podvujanyuk, D. Prosperi, D.A. Solopikhin, V.I. Tretyak, I.A. Tupitsyna, A. P. Shcherban, V. D. Virich, "Development of enriched Cadmium tungstate Crystal scintillators to search for double beta decay processes in ^{106}Cd", in the volume of the Proceed. of the Int. Conf. NPAE 2008, ed. INR-Kiev (2009) 477 (preprint ROM2F/2008/17)

19. R. Bernabei, P. Belli, F. Cappella, R. Cerulli, C. J. Dai, A. d'Angelo, H. L. He, A. Incicchitti, H. H. Kuang, J. M. Ma, F. Montecchia, F. Nozzoli, D. Prosperi, X. D. Sheng, Z. P. Ye, "Direct detection of Dark Matter particles", to appear in Nucl. Phys. B (RICAP-2009).

20. R. Bernabei, P. Belli, F. Montecchia, F. Nozzoli, F. Cappella, A. d'Angelo, A. Incicchitti, D. Prosperi, R. Cerulli, C. J. Dai, H. L. He, H. H. Kuang, X. H. Ma, X. D. Sheng, Z. P. Ye, "Particle Dark Matter in the galactic halo: results from DAMA/LIBRA", to appear on the Proceed. of the Rencontres de Moriond EW 2009 Conference, La Thuile (Aosta), Italy.

21. R. Bernabei, P. Belli, F. Montecchia, F. Nozzoli, F. Cappella, A. d'Angelo, A. Incicchitti, D. Prosperi, R. Cerulli, C. J. Dai, H. L. He, H. H. Kuang, X. H. Ma, X. D. Sheng, Z. P. Ye, "Signal from the Dark Universe: where we are, where we are going", to appear on the Proceed. of the DARK 2009 Conference, Christchurch, New Zealand.

22. R. Bernabei, P. Belli, F. Cappella, R. Cerulli, C. J. Dai, A. d'Angelo, H. L. He, A. Incicchitti, H. H. Kuang, J. M. Ma, F. Montecchia, F. Nozzoli, D. Prosperi, X. D. Sheng, Z. P. Ye, "Signals from the Dark Universe", in publication on the Proceed. of the XLV^o International Meeting on Nuclear Physics, January 2009, Bormio (It).

23. R. Bernabei, P. Belli, F. Cappella, R. Cerulli, C. J. Dai, A. d'Angelo, H. L. He, A. Incicchitti, H. H. Kuang, J. M. Ma, F. Montecchia, F. Nozzoli, D. Prosperi, X. D. Sheng, Z. P. Ye, "Searches for processes violating the Pauli Exclusion Principle In Sodium and Iodine", to appear in the Proceed. of NPA4 (Nuclear Physics in Astrophysics IV), June 2009, LNF (It).

24. R. Bernabei, P. Belli, F. Cappella, R. Cerulli, F.A. Danevich, B.V. Grinyov, A. Incicchitti, V.V. Kobychev, V.M. Mokina, S.S. Nagorny, L.L. Nagornaya, S. Nisi, F. Nozzoli, D.V. Poda, D. Prosperi, V.I. Tretyak, S.S. Yurchenko, "Search for double beta decay of zinc and tungsten with low background ZnWO4 crystal scintillators", to appear in the Proceed. of NPA4 (Nuclear Physics in Astrophysics IV), June 2009, LNF (It).

25. R. Bernabei, P. Belli, F. Cappella, R. Cerulli, C. J. Dai, A. d'Angelo, H. L. He, A. Incicchitti, H. H. Kuang, J. M. Ma, F. Montecchia, F. Nozzoli, D. Prosperi, X. D. Sheng, Z. P. Ye, "Particle Dark Matter in the galactic halo: results from DAMA/LIBRA", to appear in the Proceed. of SUSY09, June 2009, Boston (USA).

26. R. Bernabei, P. Belli, F. Cappella, R. Cerulli, C. J. Dai, A. d'Angelo, H. L. He, A. Incicchitti, H. H. Kuang, J. M. Ma, F. Montecchia, F. Nozzoli, D. Prosperi, X. D. Sheng, Z. P. Ye, "Direct detection of Dark Matter particles", to appear in the Proceed. of ICATP09, October 2009, Como (It).

27. R. Bernabei, P. Belli, F. Cappella, R. Cerulli, C. J. Dai, A. d'Angelo, H. L. He, A. Incicchitti, X. H. Ma, F. Montecchia, F. Nozzoli, D. Prosperi, X. D. Sheng, R. G.

Wang, Z. P. Ye, "Results from the DAMA/LIBRA experiment", to appear in the Proceed. of TAUP2009, July 2009, Roma (It).

28. R. Bernabei, P. Belli, F. Cappella, R. Cerulli, C. J. Dai, A. d'Angelo, H. L. He, A. Incicchitti, X. H. Ma, F. Montecchia, F. Nozzoli, D. Prosperi, X. D. Sheng, R. G. Wang, Z. P. Ye, "Technical aspects and dark matter searches", arXiv:0912.4200 and to appear in the Proceed. of TAUP2009, July 2009, Roma (It).

29. R. Bernabei, P. Belli, F. Cappella, R. Cerulli, C. J. Dai, A. d'Angelo, H. L. He, A. Incicchitti, X. H. Ma, F. Montecchia, F. Nozzoli, D. Prosperi, X. D. Sheng, R. G. Wang, Z. P. Ye, "Particle Dark Matter and DAMA/LIBRA", arXiv:0912.0660[astro-ph.GA] and to appear in the Proceed. of scineghe09, October 2009, Assisi (It).

References

[1] P. Belli, R. Bernabei, C. Bacci, A. Incicchitti, R. Marcovaldi, D. Prosperi, DAMA proposal to INFN Scientific Committee II, April 24th 1990.

[2] R. Bernabei et al., Phys. Lett. B 389 (1996) 757; R. Bernabei et al., Phys. Lett. B 424 (1998) 195; R. Bernabei et al., Phys. Lett. B 450 (1999) 448; P. Belli et al., Phys. Rev. D 61 (2000) 023512; R. Bernabei et al., Phys. Lett. B 480 (2000) 23; R. Bernabei et al., Phys. Lett. B 509 (2001) 197; R. Bernabei et al., Eur. Phys. J. C 23 (2002) 61; P. Belli et al., Phys. Rev. D 66 (2002) 043503.

[3] R. Bernabei et al., Il Nuovo Cim. A 112 (1999) 545.

[4] R. Bernabei et al., Eur. Phys. J. C18 (2000) 283.

[5] R. Bernabei el al., La Rivista del Nuovo Cimento 26 n.1 (2003) 1-73.

[6] R. Bernabei et al., Int. J. Mod. Phys. D 13 (2004) 2127.

[7] R. Bernabei et al., Int. J. Mod. Phys. A 21 (2006) 1445.

[8] R. Bernabei et al., Eur. Phys. J. C. 47 (2006) 263.

[9] R. Bernabei et al., Int. J. Mod. Phys. A 22 (2007) 3155.

[10] R. Bernabei et al., Eur. Phys. J. C 53 (2008) 205.

[11] R. Bernabei et al., Phys. Rev. D 77 (2008) 023506.

[12] R. Bernabei et al., Mod. Phys. Lett. A 23 (2008) 2125.

[13] R. Bernabei et al., Phys. Lett. B408 (1997) 439; P. Belli et al., Phys. Lett. B460 (1999) 236; R. Bernabei et al., Phys. Rev. Lett. 83 (1999) 4918; P. Belli et al., Phys. Rev. C60 (1999) 065501; R. Bernabei et al., Il Nuovo Cimento A112 (1999) 1541; R. Bernabei et al., Phys. Lett. B 515 (2001) 6; F. Cappella et al., Eur. Phys. J.-direct C14 (2002) 1; R. Bernabei et al., Eur. Phys. J. A 23 (2005) 7; R. Bernabei et al., Eur. Phys. J. A 24 (2005) 51; R. Bernabei et al., Astrop. Phys. 4 (1995) 45.

[14] R. Bernabei, in the volume *The identification of Dark Matter*, World Sc. Pub. (1997) 574.

[15] R. Bernabei et al., Phys. Lett. B 424 (1998) 195.

[16] R. Bernabei et al., Phys. Lett. B 450 (1999) 448.

[17] P. Belli et al., Phys. Rev. D 61 (2000) 023512.

[18] R. Bernabei et al., Eur. Phys. J. C 18 (2000) 283.

[19] R. Bernabei et al., Phys. Lett. B 509 (2001) 197.

[20] R. Bernabei et al., Eur. Phys. J. C 23 (2002) 61.

[21] P. Belli et al., Phys. Rev. D 66 (2002) 043503.

[22] R. Bernabei et al., Int. J. Mod. Phys. A 22 (2007) 3155-3168.

[23] R. Bernabei et al., *Nucl. Instr. & Meth.* **A592**, 297–315 (2008).

[24] R. Bernabei et al., *Eur. Phys. J.* **C56**, 333–355 (2008).

[25] K.A. Drukier et al., Phys. Rev. D 33 (1986) 3495.

[26] K. Freese et al., Phys. Rev. D 37 (1988) 3388.

[27] D. Smith and N. Weiner, Phys. Rev. D 64 (2001) 043502.

[28] K. Freese et al., Phys. Rev. **D71**, 043516–15 (2005); *Phys. Rev. Lett.* **92**, 111301–4 (2004).

[29] M. Ambrosio et al., *Astropart. Phys.* **7**, 109-124 (1997).

[30] M. Selvi on behalf of the LVD coll., Proceedings of The 31st International Cosmic Ray Conference (ICRC2009) Lodz, Poland, 2009, in press.

[31] Borexino coll., talk given at the Int. Conf. Beyond 2010, Cape Town, February 2010.

[32] see e.g. B. Sadoulet, talk at TeV Particle Astrophysics; C. Galbiati talk at WIN09.

[33] A. Bottino, N. Fornengo, and S. Scopel, Phys. Rev. D 67 (2003) 063519; A. Bottino, F. Donato, N. Fornengo, and S. Scopel, Phys. Rev. D 69 (2003) 037302; Phys. Rev. D 78 (2008) 083520; A. Bottino, F. Donato, N. Fornengo, S. Scopel, arXiv:0912.4025.

[34] R. Foot, Phys. Rev. D 78 (2008) 043529.

[35] Y. Bai and P.J. Fox, arXiv:0909.2900

[36] A. Benoit et al., *Phys. Lett.* **B637**, 156–160 (2006).

[37] R. Hudson, Found. Phys. 39 (2009) 174-193.

[38] A. M. Messiah and O. W. Greenberg, Phys. Rev. 136 (1964) B248.

[39] O. W. Greenberg, Phys. Rev. Lett. 64 (1990) 705; R. N. Mohapatra, Phys. Lett. B 242 (1990) 407; O. W. Greenberg and R. C. Hilborn, Fund. Phys. 29 (1999) 397.

[40] G. Gentile, Nuovo Cimento 17 (1940) 493; H. S. Green, Phys. Rev. 90 (1953) 270; A.Yu. Ignatiev and V.A. Kuzmin, Sov. J. Nucl. Phys. 461 (1987) 786; V. N. Gavrin, A. Yu. Ignatiev and V. A. Kuzmin, Phys. Lett. B 206 (1988) 343; O. W. Greenberg and R. N. Mohapatra, Phys. Rev. Lett. 59 (1987) 2507.

[41] M. Goldhaber and G. Goldhaber, Phys. Rev. 73 (1948) 1472; E. Fischbach, T. Kirsten, and O. A. Schaeffer, Phys. Rev. Lett. 20 (1968) 1012; B. A. Logan and A. Ljubicic, Phys. Rev. C 20 (1979) 1957.

[42] F. Reines and H. W. Sobel, Phys. Rev. Lett. 23 (1974) 954.

[43] see e.g.: V. M. Novikov et al., Phys. Lett. B 240 (1990) 227; K. Deilamian et al., Phys. Rev. Lett. 74 (1995) 4787; A. S. Barabash, et al., JETP Lett. 68 (1998) 112; D. Javorsek II et al., Phys. Rev. Lett. 85 (2000) 2701.

[44] E. Nolte et al., J. Phys. G 17 (1991) S355.

[45] H. Ejiri et al., Nucl. Phys. B (Proc. Suppl.) 28A (1992) 219.

[46] P. Belli et al., Phys. Lett. B 460 (1999) 236.

[47] S. Bartalucci et al., Phys. Lett. B 641 (2006) 18; E. Milotti et al., Int. J. Mod. Phys. A 22 (2007) 242.

[48] H. Ejiri and H. Toki, Phys. Lett. B 306 (1993) 218.

[49] R. Bernabei et al., Phys. Lett. B 408 (1997) 439.

[50] R. Arnold et al., Eur. Phys. J. A 6 (1999) 361; Nucl. Phys. B (Proc. Suppl.) 87 (2000) 510.

[51] H. O. Back et al., Eur. Phys. J. C 37 (2004) 421.

[52] R. D. Amado and H. Primakoff, Phys. Rev. C 22 (1980) 1338.

[53] K. Akama et al., Phys. Rev. Lett. 68 (1992) 1826.

[54] see e.g. O. W. Greenberg and R. N. Mohapatra, Phys. Rev. D 39 (1989) 2032.

[55] M. Ambrosio et al, Phys. Rev. D 52 (1995) 3793.

[56] G. J. Feldman and R. D. Cousins, Phys. Rev. D 57 (1998) 3873.

[57] P. Belli et al., Il Nuovo Cim. 103A (1990) 767.

[58] P. Belli et al., Il Nuovo Cim. C 19 (1996) 537.

[59] P. Belli et al., Astrop. Phys. 5 (1996) 217.

[60] P. Belli et al., Phys. Lett. B 387 (1996) 222 and Phys. Lett. B 389 (1996) 783 (erratum).

[61] R. Bernabei et al., New J. Phys. 2 (2000) 15.1.

[62] R. Bernabei et al., Eur. Phys. J.-direct C11 (2001) 1.

[63] R. Bernabei et al., Phys. Lett. B 436 (1998) 379.

[64] R. Bernabei et al., in the volume "Beyond the Desert 2003", Springer (2003) 365.

[65] R. Bernabei et al., Nucl. Instr. & Meth. A482 (2002) 728.

[66] R. Bernabei et al., Phys. Lett. B 546 (2002) 23.

[67] F. Cappella, PhD Thesis, Università di Roma "Tor Vergata", 2005.

[68] R. Bernabei et al., Phys. Lett. B 527 (2002) 182.

[69] P. Belli et al., Phys. Rev. D 61 (2000) 117301.

[70] P. Belli et al., Phys. Lett. B 465 (1999) 315.

[71] R. Bernabei et al., Phys. Lett. B 493 (2000) 12.

[72] R. Bernabei et al., Eur. Phys. J. A 27 s01 (2006) 35.

[73] R. Bernabei et al., in the volume "Cosmology and particle Physics", AIP ed. (2001) 189.

[74] V.I. Tretyak, Yu.G. Zdesenko, At. Data Nucl. Data Tables **61**, 43 (1995); **80**, 83 (2002).

[75] M. Hirsch et al., Z. Phys. A 347 (1994) 151.

[76] G. Audi, A.H. Wapstra, C. Thibault, Nucl. Phys. A **729**, 337 (2003).

[77] J.K. Bohlke et al., J. Phys. Chem. Ref. Data **34**, 57 (2005).

[78] I. Bikit et al., Appl. Radiat. Isot. **46**, 455 (1995).

[79] H. Kiel et al., Nucl. Phys. A **723**, 499 (2003).

[80] F.A. Danevich et al., Nucl. Instr. Meth. A 544 (2005) 553.

[81] H.J. Kim et al., Nucl. Phys. A 793 (2007) 171.

[82] P. Belli et al., Phys. Lett. B 658 (2008) 193.

[83] S. Agostinelli et al., Nucl. Instr. Meth. A **506**, 250 (2003);
J. Allison et al., IEEE Trans. Nucl. Sci. **53**, 270 (2006).

[84] O.A. Ponkratenko et al., Phys. At. Nucl. **63**, 1282 (2000);
V.I. Tretyak, to be published.

[85] F.A. Danevich et al., Phys. Rev. C 68 (2003) 035501.

[86] P. Domin, S. Kovalenko, F. Simkovic, S.V. Semenov, Nucl. Phys. A **753**, 337 (2005).

[87] E.-W. Grewe et al., Phys. Rev. C **77**, 064303 (2008).

[88] P. Belli et al., Nucl. Phys. A 806 (2008) 388.

[89] M. Krcmar et al., Phys. Rev. D 64 (2001) 115016.

[90] E.B. Norman, Phys. Rev. C 31 (1985) 1937.

[91] P. Belli et al., in the volume *"Current problems in Nuclear Physics and Atomic energy"*, ed. INR-Kiev (2006) 479.

[92] P. Belli et al., KINR-annual report 2008.

The GERDA experiment

M. Allardt[c], A.M. Bakalyarov[l], M. Balata[a], I. Barabanov[j], M. Barnabe-Heider[f],
L. Baudis[q], C. Bauer[f], E. Bellotti[g,h], S. Belogurov[k,j], S.T. Belyaev[l], A. Bettini[n,o],
L. Bezrukov[j], F. Boldrin[n,o], V. Brudanin[d], R. Brugnera[n,o], D. Budjas[f],
A. Caldwell[m], C. Cattadori[g,h], E.V. Demidova[k], A. Denisiv[j], A. Di Vacri[a],
A. Domula[c], A. D'Andragora[a], V. Egorov[d], A. Ferella[q], F. Froborg[q], N. Frodyma[b],
A. Gangapshev[j], A. Garfagnini[n,o], S. Gazzana[f], A. Glück[m], R. Gonzalea de
Orduna[e], P. Grabmayr[p], G.Y. Grigoriev[l], K.N. Gusev[l,d], V. Gutentsov[j],
A. Hagen[p], W. Hampel[f], M. Heisel[f], G. Heusser[f], W. Hofmann[f], M. Hult[e],
L. Ioannucci[a], L.V. Inzhechik[l], J. Janicsko[m], M. Jelen[m], J. Jochum[p], M. Junker[a],
S. Kionanovsky[j], I.V. Kirpichnikov[k], A. Klimenko[d,j], M. Knapp[p], K-T. Knoepfle[f],
O. Kochetov[d], V.N. Kornoukhov[k,j], V. Kusminov[j], M. Laubenstein[a], V.I. Lebedev[l],
D. Lenz[m], S. Lindemann[f], M. Lindner[f], I. Lippi[o], J. Liu[m], X. Liu[m],
B. Lubsandorzhiev[j], B. Majorovits[m], G. Marissens[e], G. Meierhofer[p],
I. Nemchenok[d], S. Nisi[a], L. Pandola[a], K. Pelczar[b], A. Pullia[i], S. Riboldi[i],
F. Ritter[p], C. Rossi Alvarez[o], R. Santorelli[q], J. Schreiner[f], J. Schubert[m],
U. Schwan[f], B. Schwingenheuer[f], S. Schönert[f], M. Shirchenko[l], H. Simgen[f],
A. Smolnikov[d,j], L. Stanco[o], F. Stelzer[m], H. Strecker[f], M. Tarka[q],
A.V. Tikhomirov[l], C.A. Ur[o], A.A. Vasenko[k], S. Vasiliev[d,j], M. Weber[f],
M. Wojcik[b], E. Yanovich[j], S.V. Zhukov[l], F. Zocca[i], K. Zuber[c], and G. Zuzel[f].
Spokespersons: S. Schönert, C. Cattadori

[a]) INFN Laboratori Nazionali del Gran Sasso, LNGS, Assergi, Italy
[b]) Institute of Physics, Jagellonian University, Cracow, Poland
[c]) Institut für Kern- und Teilchenphysik, Technische Universität Dresden, Dresden, Germany
[d]) Joint Institute for Nuclear Research, Dubna, Russia
[e]) Institute for Reference Materials and Measurements, Geel, Belgium
[f]) Max Planck Institut für Kernphysik, Heidelberg, Germany
[g]) Dipartimento di Fisica, Università Milano Bicocca, Milano, Italy
[h]) INFN Milano Bicocca, Milano, Italy
[i]) Dipartimento di Fisica, Università degli Studi di Milano e INFN Milano, Milano, Italy
[j]) Institute for Nuclear Research of the Russian Academy of Sciences, Moscow, Russia
[k]) Institute for Theoretical and Experimental Physics, Moscow, Russia
[l]) Russian Research Center Kurchatov Institute, Moscow, Russia
[m]) Max-Planck-Institut für Physik, München, Germany
[n]) Dipartimento di Fisica dell'Università di Padova, Padova, Italy
[o]) INFN Padova, Padova, Italy
[p]) Physikalisches Institut, Eberhard Karls Universität Tübingen, Tübingen, Germany
[q]) Physik Institut der Universität Zürich, Zürich, Switzerland

Abstract

The GERmanium Detector Array (GERDA) experiment searches for neutrinoless double beta decay ($0\nu\beta\beta$) of the isotope ^{76}Ge. The goal is to reduce the background by about two orders of magnitude compared to existing experiments and hence to improve the sensitivity by an order of magnitude. For this, a new shielding concept was chosen using pure liquids (water and liquid argon). In 2009, major parts of the hardware were finished and the cryostat was filled.

1 Introduction

The observation of neutrinoless double beta decay ($0\nu\beta\beta$) is the most sensitive experimental method to test whether the neutrino is its own antiparticle. GERDA [1], currently under construction in Hall A of LNGS, uses the isotope ^{76}Ge to search for this decay. Germanium diodes made out of enriched material ($\approx 86\%$ ^{76}Ge) will be immersed in a 65 m^3 cryostat filled with liquid argon. These diodes are both source and detector of the decay. Since no neutrino is emitted, the signal is a line at the Q value of the decay. The excellent energy resolution of the detectors helps to suppress backgrounds.

Argon is radiopure[1] and serves to cool the detectors to their operating temperature and to shield against the radioactivity of the cryostat and the environmental activity of the laboratory. The cryostat is surrounded by three meters of water as additional shield and - with the installation of photo multipliers (PMT) - as Cherenkov muon veto. A model of the experimental setup is shown in figure 1.

Above the water tank is a clean room for diode handling and at its center a lock for transferring the detectors to the argon atmosphere. The lock includes the mechanics for lowering the detectors and electrical feedthroughs. The building next to the water tank contains all the infrastructure like the electronics for operating the diodes, a water purification plant and safety devices for the cryostat.

The GERDA collaboration was founded in 2004 and has now about 100 authors from 15 institutions located in 6 countries. In 2009, most parts of the hardware were finished and the commissioning started with the filling of the cryostat.

2 Goal of the experiment

So far, all experiments searching for $0\nu\beta\beta$ are background limited. A background reduction is a prerequisite for an improved sensitivity. Especially advantageous is a quasi background free situation since the sensitivity on the life time $T_{1/2}$ scales then linearly with time and detector mass. This is the goal of GERDA.

Part of the Heidelberg-Moscow collaboration claims evidence for the observation of $0\nu\beta\beta$ [2]. For an integrated statistics of 71.7 kg·years, a signal of 28.75±6.86 was reported which corresponds to a half-life of ^{76}Ge of about $T_{1/2} = 1.2 \cdot 10^{25}$ years. Other experiments which use different isotopes are so far not sensitive enough to refute or confirm this claim. This is partially due to the fact that theoretical calculations for nuclear matrix elements are needed to relate the life times of different isotopes.

---

[1]The Q value of ^{39}Ar is far below the one of $0\nu\beta\beta$.
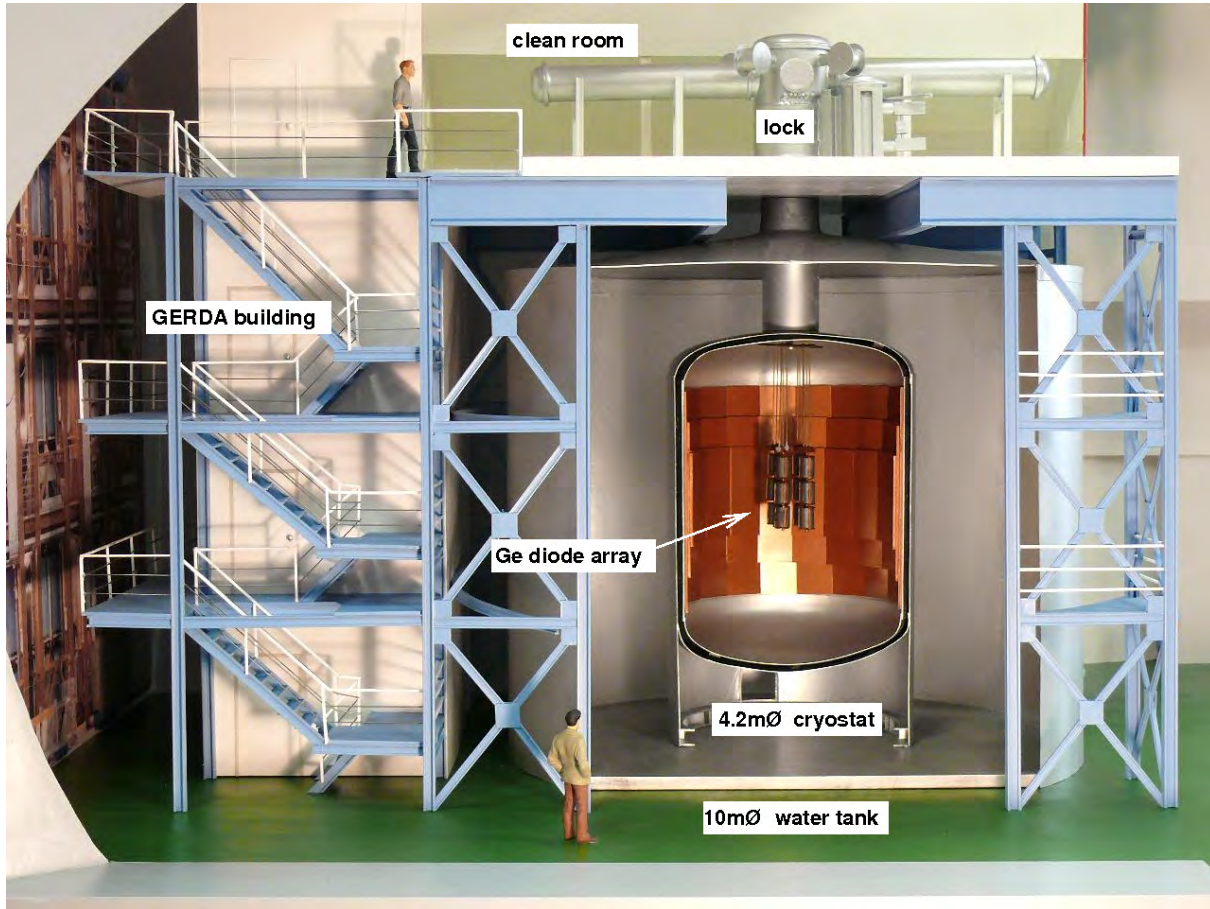
Figure 1: Model of the GERDA experiment.

In a first phase, diodes used by the previous Heidelberg-Moscow and IGEX experiments will be deployed. These have a total mass of 17.7 kg and a background rate below 0.01 cts/(keV·kg·y) is expected, which is an order of magnitude lower than for previous experiments.

Since the background index for Phase I is expected to be a factor of 10 lower, even with moderate statistics of 15 kg·years, GERDA should find six events above a background of one event in the region of interest. This allows us to scrutinize the claim with a good confidence level.

Additional diodes made out of newly bought enriched material will be operated in a second phase. Due to additional background suppression techniques like segmented read-out or enhanced pulse shape analysis, the goal background is then 0.001 cts/(keV·kg·y). For an integrated statistics of 100 kg·years, the exclusion sensitivity is about $T_{1/2} > 1.4 \cdot 10^{26}$ years at 90% confidence level, i.e. a factor of 10 better than for the previous Heidelberg-Moscow and IGEX experiments.

3 Diodes and readout

The diodes of Heidelberg-Moscow and IGEX were tested and then removed from their original cryostat. After refurbishment by Canberra, Belgium, they were mounted in the final low mass holder and tested for leakage current and energy resolution. Currently they are stored underground in vacuum. The detectors made out of natural germanium from Genius-TF are also available. The characteristics of the detectors can be found in table 1.

Table 1: Characteristics of the enriched detectors from Heidelberg-Moscow (ANG 1-5) and IGEX (RG 1-3) and non-enriched diodes from Genius-TF (GTF 32, 42, 44). The results are obtained in liquid argon with the diodes mounted in their low-mass holders. The mass is the total mass of the diode, the leakage current and the spectroscopic performance (FWHM) for the 1.332 MeV ^{60}Co line are measured at the given high voltage. The energy resolution ranges between 2.5 and 5.1 keV. Tests showed that better energy resolution can be achieved by improving the HV contact via further polishing of the diode surface. This procedure will be used for ANG 4-5 and RG 1-2 which show inferior energy resolution despite of their low leakage current. ANG 3 will be reprocessed by Canberra before its is deployed.

name	mass (g)	voltage (V)	current (pA)	resolution (FWHM) (keV)
ANG 1	958	3500	235	2.6
ANG 2	2833	4000	65	2.5
ANG 3	2391	3000	200	5.1
ANG 4	2372	3000	40	4.4
ANG 5	2746	1800	60	4.0
RG 1	2110	4500	65	4.4
RG 2	2166	4000	60	4.1
RG 3	2087	3500	800	3.5
GTF 32	2321	3200	50	2.5
GTF 42	2467	3000	55	3.2
GTF 44	2465	3500	55	3.0

Three detectors will be connected to form one string. About 35 cm above the highest detector is a cuflon PCB which holds the charge sensitive amplifiers for the 3 channels. The distance is given by the radioactivity of the PCB which is exclusively due to the passive components.

A conventional charge sensitive amplifier for diode readout is built with discrete components. It can not be operated in liquid argon which is a requirement of GERDA and it has high mass which also means high radioactivity. GERDA therefore decided to build a custom made chip (ASIC) in CMOS technology which is the ideal choice. The current version is called PZ0. It has a good intrinsic energy resolution of 1.2 keV for a pulser signal equivalent to an energy deposition of 1 MeV in germanium and for a 33 pF capacitor
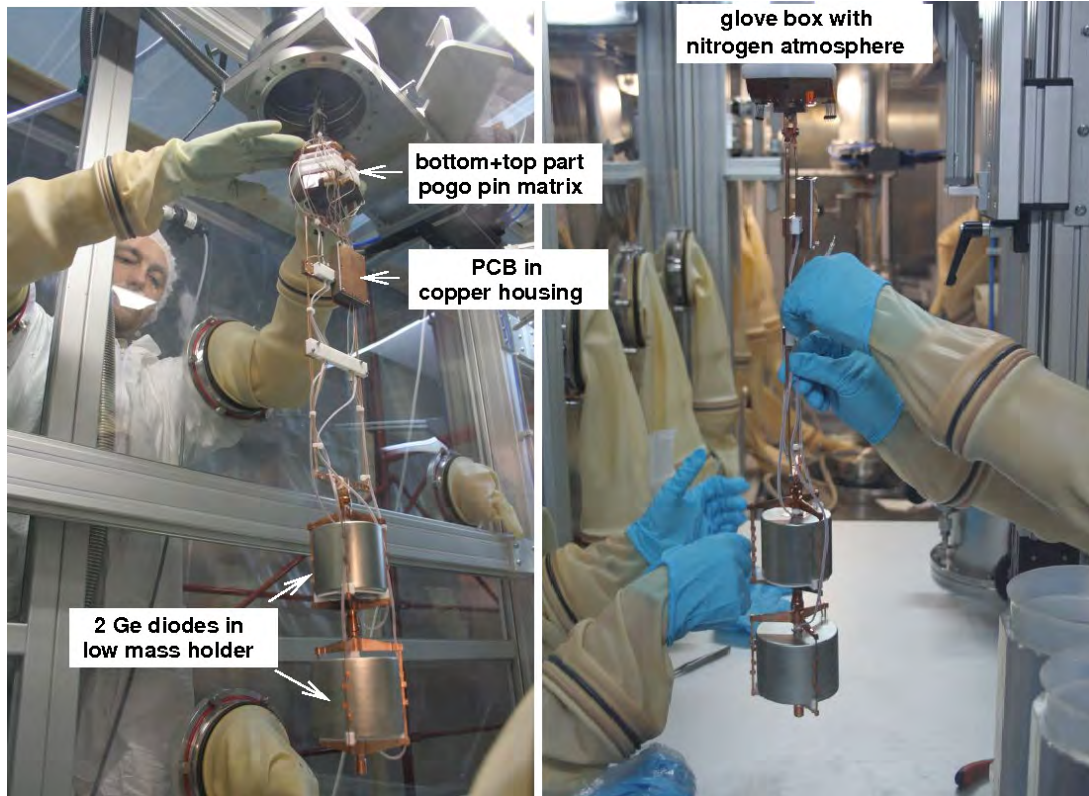
Figure 2: The string with two diodes during the commissioning in Hall di Montaggio.

at the input. To reduce the cross talk between different channels on the same ASIC and to improve its capability to drive a 50 Ohm 10 m long output cable, a new version was designed in 2009.

Above the PCB is the bottom part of the so-called pogo pin matrix. The latter is the removable part of the mechanical and electrical interface between the string and the support and cables inside the lock. The string is assembled in a clean bench in nitrogen atmosphere and then transferred to the lock.

In 2009, a preliminary version of the lock was built and assembled in Hall di Montaggio. This setup allowed to operate a string with two detectors and helped to identify and fix several problems. This commissioning lock will be used in the first start-up of GERDA.

A picture of the assembled string can be seen in figure 2. The detector performances are shown in figure 3. The measured resolutions of full width half maximum (FWHM) of 2.9 keV are quite satisfactory. The cross talk is about 1% between the two readout channels and needs further study.

For detector calibration we use a ^{228}Th source. To reduce neutrons from (α, n) reactions in the ceramic package of commercial sources, GERDA has ordered a source in a gold package. At PSI, Switzerland, the $ThCl_4$ solution was converted to oxide and the packaging and certification was done by Eckert&Ziegler, Prague. The (α, n) threshold of gold is 9.9 MeV and therefore higher than all α energies of the thorium decay chain. For the 20 kBq source produced, a neutron rate of (0.017 ± 0.003) n/s was measured.
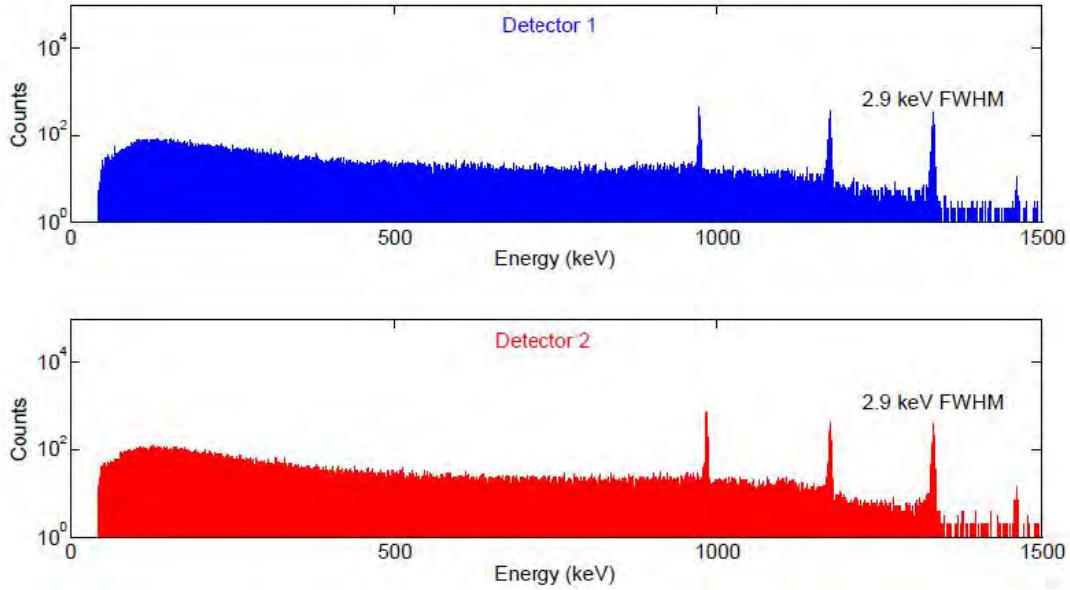
Figure 3: ^{60}Co energy spectrum of the two detector string. The line at 1 MeV is from a pulser and has FWHM of 2.2 keV.

4   Detectors for Phase II

In 2006, GERDA purchased 37.5 kg of germanium enriched to about 87% in ^{76}Ge in form of GeO$_2$. Since we did not find a manufacturer to grow n-type crystals, we contacted the Institut für Kristallzüchtung (IKZ) in Berlin. IKZ is in the process to pull high-purity crystals suitable for detector production using the float-zone and Czochralski method.

The conversion from oxide to metal with 6N purity - the input quality for crystal growing - was successfully demonstrated in 2009 by the company PPM Pure Metal, Germany. A yield of more than 90% was achieved simply by reducing the oxide in a hydrogen atmosphere and by zone refinement, i.e. no chemistry was required to reach the required purity and yield. No degradation of the enrichment was observed. This procedure was tested with depleted material which was collected during the enrichment process and which was processed chemically in the same way.

To improve the rejection power for background events from internal and external gammas, the outer surface diode contact can be segmented and individually read out. Gammas of a few MeV energy have a mean free path of typically one cm while about 90% of the signal events deposit all energy within a few mm. Coincidence signals in several segments can therefore be used to identify background.

Several 18-fold segmented n-type diodes (true coaxial detectors) have been purchased from Canberra, Lingolsheim, and tested for their background rejection capabilities [3, 4, 5]. These detectors have been operated with stable performance over the period of 3 and 5 months in liquid argon and nitrogen, respectively.

The time variation of the diode current signal can also be used to detect energy deposits originating from different radii, i.e. to reject photon backgrounds. The total background rejection and signal efficiency for such a diode is given in table 2 for a ^{228}Th source

Table 2: Background rejection and signal efficiency for an 18-fold segmented detector and a BEGe detector. For the BEGe detector a pulse shape analysis based on the ratio of maximal current over total charge in an event is used. For the segmented detector a combination of pulse shape analysis and segment anti-coincidence cut is used. The numbers are for a ^{228}Th source and the double escape peak (DEP) efficiency is typical for the signal efficiency. The events rejected at the energy $Q_{\beta\beta}$ are multiple scattering Compton events from the 2.6 MeV line.

energy	BEGe	segmented detector
DEP	90%	82%
1.62 MeV γ line	12%	19%
2.6 MeV γ line	10%	15%
$Q_{\beta\beta}$	42%	48%
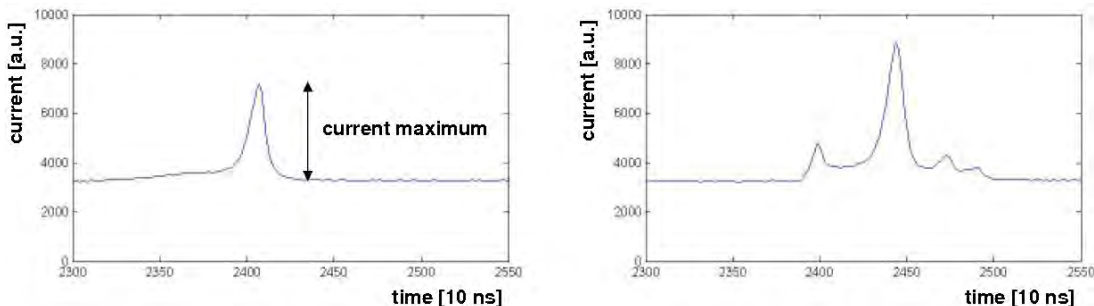
Figure 4: Current pulses for two events as recorded with a BEGe detector. Left: for a single site event. Right: for an event with multiple energy depositions which is characteristic for background events.

spectrum. The double escape peak (DEP) of the 2.6 MeV line mimics the behaviour of signal events.

In 2009, GERDA also exploited another diode type [6]. The thick-window Broad Energy GErmanium detectors (BEGe) from Canberra, Belgium, are p-type diodes with cylindrical shape and a small contact on one front face. The electric field strength is largest close to the contact and the current signal is therefore largest when the drifting holes reach the contact. The drift time depends on the position of the energy deposition and the identification of several current pulse therefore indicates background from gammas. This is shown in figure 4 for an event with a single current pulse (single site event) and an event with multiple pulses. A cut on the maximum of the current over the total charge can therefore select signal events. The rejection power of such a detector mounted in a standard cryostat is summarized in table 2. We successfully operated a BEGe detector also in a low mass holder in liquid argon without performance deterioration in energy resolution, pulse shape discrimination and stability.

To test the feasibility not only of the detector technology but of the entire production chain starting from the enriched material to the fabrication of the diodes, GERDA

has ordered for both diode types detectors. We start with depleted material which was processed by PPM. The metal was then sent to Canberra in Oak Ridge and to IKZ for growing p-type and n-type crystals, respectively. In January 2010, we received the first three crystals slices from Canberra which are now being processed in Belgium. At IKZ, a small n-type crystal with an acceptable net charge carrier level of $4 \times 10^{10}/\text{cm}^3$ was grown with the float-zone method. The Czochralski puller turned out to be contaminated with arsenic, i.e. impurities have been an order of magnitude too large. It was completely electro-polished and crystals are expected to be pulled in 2010.

5   Cryostat and water tank

After the cryostat completion in 2007, the water tank was built around it and then the GERDA building followed. In 2009, the clean room was finished and the cryogenic infrastructure which includes cryogenic storage tanks for argon and nitrogen, transfer lines, control valves and safety valves, a water - argon gas heat exchanger and the connection to the LNGS ventilation system were built. The heater is used to heat up the cold gas in case of an emergency before discharging it to the ventilation.

The infrastructure installed inside the cryostat includes temperature sensors, two copper heat exchangers for cooling of the liquid argon with liquid nitrogen and different fill level sensors.

By Christmas 2009, the cryostat was filled with liquid argon and it is operated stably since then. The active cooling with nitrogen avoids argon losses.

The water purification plant was finished in 2009. For filling, the water is taken from the BOREXINO water plant and then flows through a filter with 4.5 μm pore size before it enters the GERDA tank. We will constantly recirculate the water with a rate of 2-4 m^3/h through the above mentioned filter and an ionic resin. The water should have a resistivity above 17 MΩ·cm at 25 ^{o}C (to keep radioactive contaminations at a low level) and a level of Total Organic Carbon below 20 ppb (to ensure good optical properties). Above the water level is a nitrogen gas buffer at a small overpressure (30 mbar) to avoid air entering the water.

For the safety of LNGS it is important to drain the 600 m^3 water within two hours. A first test in 2009 showed that the installed flow regulators could not guarantee this. New devices and tests are needed before the water tank can be filled.

6   Muon veto

The water acts not only as passive shield against gammas and neutrons but is also equipped with PMTs to veto muons [7]. In 2009, the walls were covered with VM2000 foil which acts as reflector and wavelength shifter. Then, 66 PMTs were mounted at the cylindrical wall, the bottom surface and below the cryostat inside its support skirt. Figure 5 shows pictures taken inside the water tank before and after the installation.

To cover also the central part of the experiment, plastic panels of 1.5 cm thickness will be positioned on top of the clean room and cover the central 4 m^2.
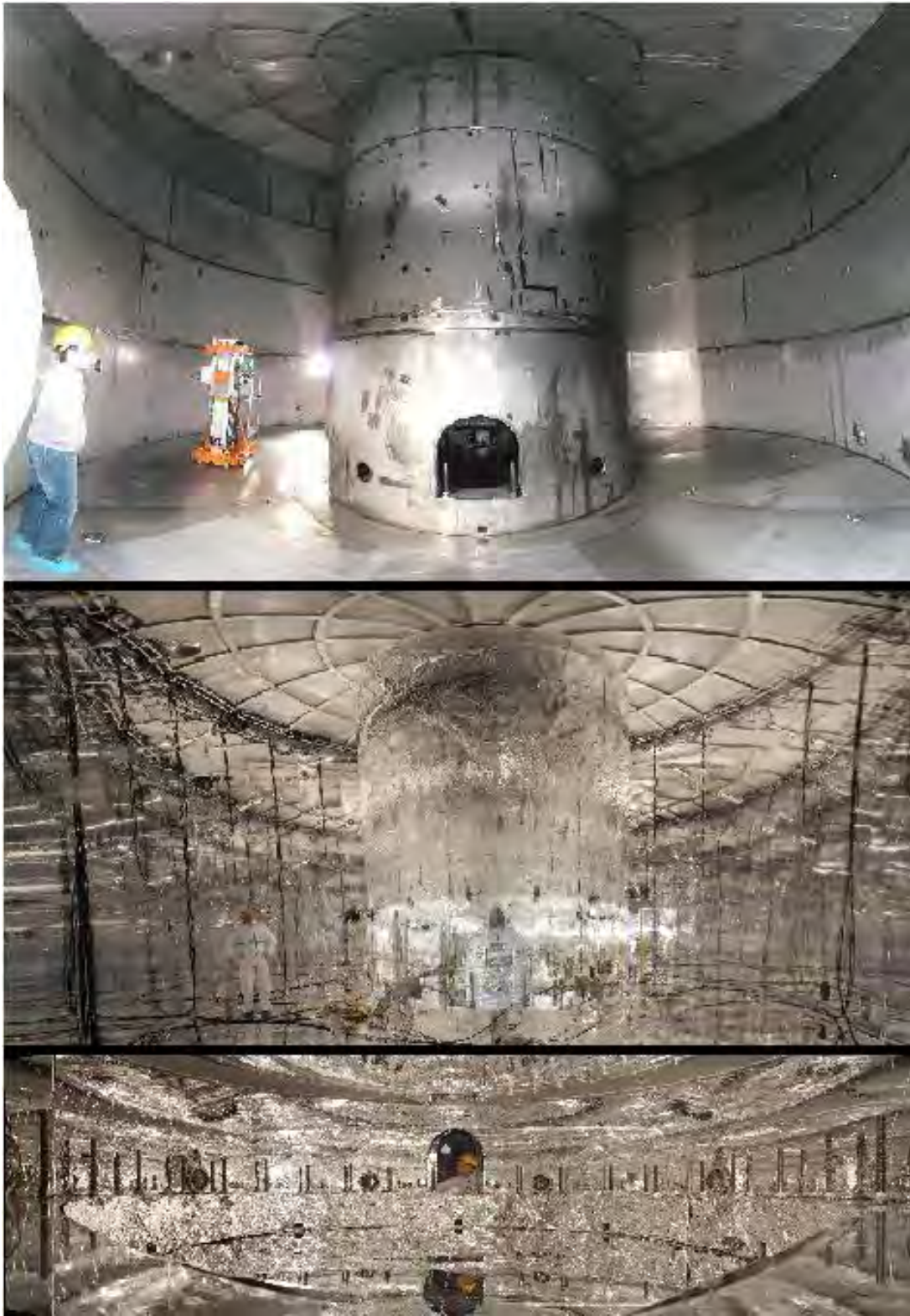
Figure 5: Pictures taken before (top) and after the installation of the VM2000 foil and the PMTs (middle). The bottom picture shows a 360° view of the volume below the cryostat.

In total, a veto efficiency above 99% is expected for those muons which deposit energy in a diode.

7   Low-background test stand LArGe

An additional background reduction can be achieved if the energy deposited in the liquid argon can be measured and used in anti-coincidence to the signal in the germanium detectors. Since argon scintillates, the light can be read out with PMTs.

First tests with a small 19 kg setup showed the potential of this method [8, 9]. To test this option in a more realistic assembly, a 1 m^3 copper cryostat was installed in 2009 in the underground Germanium Detector Laboratory (GDL). The inner cryostat walls are covered with VM2000. Nine PMTs with low internal radioactivity view the volume from the top and a string of germanium diodes can be deployed into the center. Figure 6 shows pictures taken during the installation of the cryostat. The cryostat is shielded with (from inside to outside) copper, lead, steel and polyethylene. The cryostat also allows cooling of the argon with liquid nitrogen and hence to compensate any thermal losses.

The commissioning of this setup is ongoing and a lock will be installed in 2010. It allows to transfer the diodes into the argon atmosphere and contains all electrical feedthroughs.
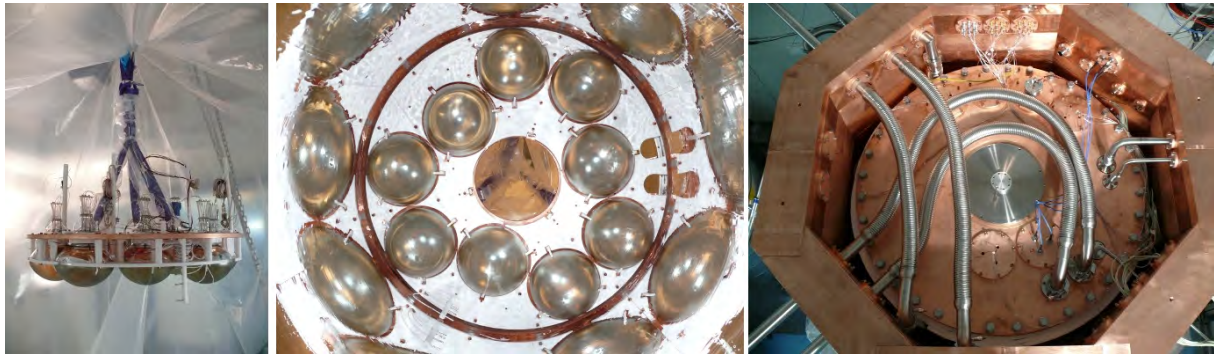
Figure 6: Integration of the low-background test stand LArGe in GDL. **Left:** View of the PMT bank prior to installation inside the cryostat. **Center:** View from the inside of the cryostat on the PMT bank and the reflecting wavelength shifting foil covering the internal walls of the cryostat. **Right:** View on the top flange of the cryostat with the vacuum insulated cryogenic lines and signal feed throughs.

8   Material screening

During the construction, GERDA relied heavily on several gamma screening facilities at LNGS, the MPI for Nuclear Physics in Heidelberg, the Institute for Reference Materials and Measurements in Geel and the Russian screening facility in Baksan (see e.g. [10]).

All are operated by members of the collaboration. During 2009, mainly the electronics components of the PCB have been screened.

The emanation of ^{222}Rn of most materials inside the argon gas volume has been measured. Samples were stored in a container with a clean buffer gas. After a period of 1-2 weeks, the buffer gas was extracted together with the radon atoms. Radon was then trapped in cold charcoal filters and eventually transferred to a proportional counter where α decays of the radon chain were detected.

The cryostat emanation has been measured at different times. For such a measurement the entire cryostat is filled with clean nitrogen gas. After the grow-in period, part of the gas is extracted and radon is detected as discussed before. For the empty cryostat, the emanation was 14 ± 2 mBq which is quite low for the size of the container. After the installation of all pipes, the value increased to 55 ± 4 mBq. There is evidence that the additional contributions are located in the top part of the cryostat which is in the gas phase [11].

The behaviour of radon and its daughters in gaseous and liquid nitrogen has been studied. Radon and its daughters - when emanated into the gas phase - prefer to stick to cold walls rather than to dissolve into the liquid. However surfaces on high voltage (like the diode surfaces) attract radon daughters. We have therefore installed a cylinder made out of 30 μm thick copper foil around the position of the germanium array. This cylinder is electrically isolated from the cryostat and can act as attractor for radon daughters.

An electrostatic radon monitor with a volume of 711 liters was built and installed in 2009. It will be connected to the exhaust gas of the cryostat and measure online the emanation. The sensitivity is estimated to be 70 μBq.

9   Neutron capture cross sections

Neutron induced reactions are among the most dangerous background sources for $0\nu\beta\beta$ searches. Inelastic scattering of neutrons in excess of 4 MeV can excite levels in ^{76}Ge which during decay emit gammas in the vicinity of $Q_{\beta\beta}$. Similarly, after neutron capture the instable ^{77}Ge is formed, which undergoes beta decay to ^{77}As, followed by a second beta emission to ^{77}Se. Furthermore, the prompt gamma intensities in ^{77}Ge are known for about 15% of the total strength.

While not important in phase I, the neutron induced background will become significant at later stages. Thus, a thorough program has been started to measure the capture cross section on ^{76}Ge (and ^{74}Ge) and the decay of $^{77(75)}$Ge . Included is the determination of the prompt spectrum. The analysis is hampered by the poor knowledge of branching ratios which keep up the systematic errors while the statistics could be strongly improved with the new measurements at the cold neutron facility reactor FRM2 in Munich. For details of the present results see references [12, 13].

10   Data acquisition

The analog data will be digitized by 100 MHz flash ADCs. For the muon PMTs, a commercial VME based solution was chosen while a special NIM based hardware with PCI

bus readout was built for the germanium diodes. Both systems have similar specifications, e.g. both use the same clock and have a trapezoidal filter implemented in hardware for triggering.

All hardware including a stable pulser for the germanium diodes, high voltage and low voltage power supplies and a calibration system for the PMTs is available.

11 Simulation

The simulation of an experiment by Monte Carlo methods is mandatory from the very beginning. For the design of GERDA, all different background contributions had to be simulated and this process continued over the years in more detail. To ensure reliable results, we decided to base our simulation mainly on GEANT4 which is widely used. A framework called MaGe was developed in cooperation with the MAJORANA collaboration [14].

The activities during 2009 include a new Monte Carlo campaign to generate a library of background contributions from all sources for a close to final geometry. The sum of all spectra with a proper weighting for the individual contributions is a realistic expectation for the experiment. Vice versa, the spectrum seen in GERDA for the individual diodes is the weighted sum from all background sources and the calculation of the weights is an important part of the analysis. A toolkit was developed for this task.

Another activity focuses on the simulation of the current pulses. Starting from electric field calculations for a BEGe detector for a given impurity distribution, the displacement current was simulated for the energy depositions calculated by MaGe. Finally, the measured impulse response function of the electronics was used and included in the full simulation. Figure 7 shows as an example the simulated (solid blue) and data (crosses and dashed line) integrated current signals for an ^{241}Am source. The low energy gamma of 59.5 keV deposits all energy locally, i.e. all pulses look similar.

12 Summary

In 2009, the construction of all major hardware items was finished. To speed up the commissioning of the final installation, a test stand was built in Hall di Montaggio. Two diodes were operated successfully. The operation of the cryostat started by filling it with liquid argon.

In 2010, the commissioning setup from Hall di Montaggio will transfer to the GERDA site. It allows to operate up to 12 diodes and we expect first results on the background level of the experiment by deploying the diodes of Heidelberg-Moscow and IGEX.

13 List of GERDA related publications in 2009

1. I. Abt et al, *Operation of an 18-fold segmented n-type HPGe detector in liquid nitrogen*, J. of Instrumentation (JINST) 4 (2009) P11008.
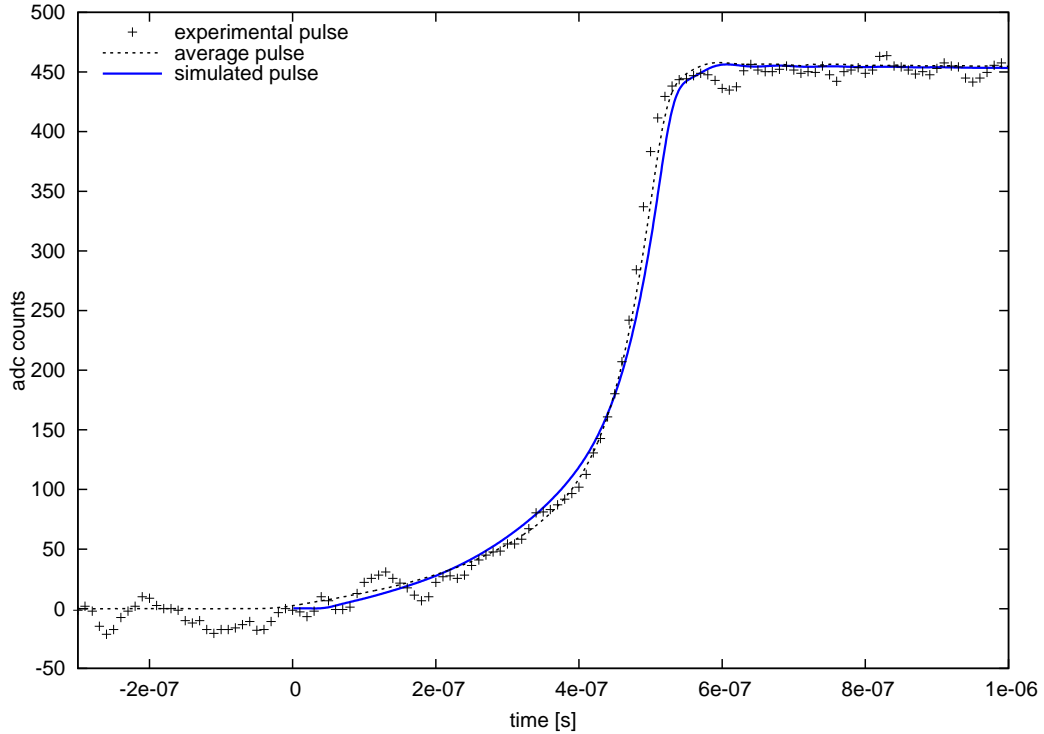
Figure 7: Comparison between an experimental charge pulse (crosses), the average experimental pulse (dashed line) and the simulated pulse (blue solid line) for a BEGe detector. Data have been collected with a collimated ^{241}Am source placed on the top surface of the detector. The deviations of the simulated signal from the average signal are small than the single event noise fluctuations.

2. D. Budjas et al, *Pulse shape discrimination studies with a Broad-Energy Germanium detector for signal identification and background suppression in the GERDA double beta decay experiment*, J. of Instrumentation (JINST) 4 (2009) P10007.

3. I. Barabanov et al, *Shielding of the GERDA experiment against external gamma background*, Nucl. Instr. Methods A 606 (2009) 790.

4. J. Marganiec et al, *Neutron capture cross sections of ^{74}Ge, ^{76}Ge and ^{75}As at 25 keV*, Phys. Rev. C 79 (2009) 065802

5. B.P. Kay et al, *Nuclear structure relevant to neutrinoless double beta decay: The valence protons in ^{76}Ge and ^{76}Se*, Phys. Rev. C 79 (2009) 021301(R).

6. M. Laubenstein and G. Heusser, *Cosmogenic radionuclides in metals as indicator for sea level exposure history*, Applied Radiation and Isotopes 67 (2009) 750.

7. G. Meierhofer et al, *Thermal neutron capture cross-section of ^{76}Ge*, Eur. Phys. J. A 40 (2009) 61-64.

8. H. Simgen and G. Zuzel, *Analysis of the ^{222}Rn concentration in argon and a purification technique for gaseous and liquid argon*, Appl. Rad. Isot. 67 (2009) 922-925.

9. G. Zuzel and H. Simgen, *High Sensitivity Radon Emanation Measurements*, Appl. Rad. Isot. 67 (2009) 889-893.

10. D. Budjas et al., *Optimisation of the MC-model of a p-type Ge-spectrometer for the purpose of efficiency determination*, Appl. Rad. Isot. 67 (2009) 706-710.

11. M. Heisel et al., *Statistical analysis of low-level material screening measurements via gamma-spectroscopy for MC background estimations in $0\nu\beta\beta$ experiments*, Appl. Rad. Isot. 67 (2009) 741-745.

12. M. Laubenstein et al., *Gamma-ray spectrometry of ultra low levels of radioactivity within the material screening program for the* GERDA *experiment*, Appl. Rad. Isot. 67 (2009) 755-758.

13. M.Knapp et al, *The* GERDA *muon veto Cherenkov detector*, Nucl. Instrum. Meth. A610 (2009) 280-282.

References

[1] www.mpi-hd.mpg.de/GERDA

[2] H.V. Klapdor-Kleingrothaus, I.V. Krivosheina, A. Dietz and O. Chkvorets, *Search for neutrinoless double beta decay with enriched ^{76}Ge in Gran Sasso 1990-2003*, Phys. Lett. B 586 (2004) 198-212.

[3] I. Abt et al, *Operation of an 18-fold segmented n-type HPGe detector in liquid nitrogen*, J. of Instrumentation (JINST) 4 (2009) P11008.

[4] I. Abt et al, *Neutron interactions as seen by a segmented germanium detector*, Eur. Phys. J. A 36 (2008) 139-149.

[5] I. Abt et al, *Test of pulse shape analysis using single Compton scattering events*, Eur. Phys. J. C 54 (2008) 425-433.

[6] D. Budjas et al, *Pulse shape discrimination studies with a Broad-Energy Germanium detector for signal identification and background suppression in the GERDA double beta decay experiment*, J. of Instrumentation (JINST) 4 (2009) P10007.

[7] M.Knapp et al, *The* GERDA *muon veto Cherenkov detector*, Nucl. Instrum. Meth. A610 (2009) 280-282.

[8] P. Peiffer et al, *Pulse shape analysis of liquid argon scintillation signals for radioactive background identification and suppression*, J. of Instrumentation (JINST) 3 (2008) P08007.

[9] M. Di Marco et al, *LArGe: Background suppression using liquid argon scintillation for $0\nu\beta\beta$ decay search with enriched germanium detectors*, Nucl. Phys. Proc. Suppl. 172 (2007) 45-48.

[10] W. Maneschg et al, *Measurements of extremely low radioactivity levels in stainless steel for* GERDA, Nucl. Instr. Methods A 593 (2008) 448-453.

[11] G. Zuzel and H. Simgen, *High Sensitivity Radon Emanation Measurements*, Appl. Rad. Isot. 67 (2009) 889-893.

[12] J. Marganiec et al, *Neutron capture cross sections of ^{74}Ge, ^{76}Ge and ^{75}As at 25 keV*, Phys. Rev. C 79 (2009) 065802

[13] G. Meierhofer et al, *Thermal neutron capture cross-section of ^{76}Ge*,Eur. Phys. J. A 40 (2009) 61-64.

[14] Yuen-Dat Chan et al, *MaGe - a Geant4-based Monte Carlo framework for low-background experiments*, arXiv:0802.0860.

The ICARUS T600 Experiment

The ICARUS Collaboration

A. Ankowski[o], M. Antonello[c], P. Aprili[d], F. Arneodo[d], M. Armenante[b],
B. Baiboussinov[a], M. Baldo Ceolin[a], G. Battistoni[f], P. Benetti[h], E. Calligarich[h],
N. Canci[c], F. Carbonara[b], F. Cavanna[c], P. Cennini[j], S. Centro[a], A. Cesana[k,f],
D.B. Cline[m], K. Cieślik[n], A.G. Cocco[b], A. Dąbrowska[n], R. Dolfini[h], C. Farnese[a],
A. Fava[a], A. Ferrari[j,f], G. Fiorillo[b], S. Galli[c], D. Gibin[a], K. Graczyk[o], A. Guglielmi[a],
J. Holeczek[g], C. Juszczak[o], D. Kiełczewska[q], J. Kisiel[g], T. Kozłowski[p], M. Lantz[f],
G. Mannocchi[t], M. Markiewicz[n], A. Menegolli[h], G. Meng[a], P. Mijakowski[p],
C. Montanari[h], S. Muraro[f], O. Palamara[d], T.J. Palczewski[p], L. Periale[t],
G. Piano Mortari[c], A. Piazzoli[h], P. Picchi[t], F. Pietropaolo[a], W. Półchłopek[v],
M. Posiadala[q], M. Prata[h], P. Przewłocki[p], A. Rappoldi[h], G.L. Raselli[h], E. Rondio[p],
M. Rossella[h], C. Rubbia[1d], P. Sala[f], D. Scannicchio[h], A. Scaramelli[f], E. Segreto[c],
F. Sergiampietri[m,w], J. Sobczyk[o], D. Stefan[n], J. Stepaniak[p], R. Sulej[x], M. Szeptycka[p],
M. Szarska[n], M. Terrani[k,f], F. Varanini[a], S. Ventura[a], C. Vignoli[h], H. Wang[m],
T. Wachala[n], A. Zalewska[n]

[a]Università di Padova e INFN, Padova, Italy
[b]Università Federico II di Napoli e INFN, Napoli, Italy
[c]Università dell'Aquila e INFN, L'Aquila, Italy
[d]INFN - Laboratori Nazionali del Gran Sasso, Assergi, Italy
[f]Università di Milano e INFN, Milano, Italy
[g]Institute of Physics, University of Silesia, Katowice, Poland
[h]Università di Pavia e INFN, Pavia, Italy
[j]CERN, Geneva, Switzerland
[k]Politecnico di Milano (CESNEF), Milano, Italy
[m]Department of Physics, UCLA, Los Angeles, USA
[n]H.Niewodniczański Institute of Nuclear Physics, Kraków, Poland

---

[1]Spokesman of the ICARUS Collaboration

[o]Institute of Theoretical Physics, Wrocław University, Wrocław, Poland

[p]A.Sołtan Institute for Nuclear Studies, Warszawa, Poland

[q]Institute of Experimental Physics, Warsaw University, Warszawa, Poland

[r]Institute of Mechanics and Machine Design, Cracow University of Technology, Kraków, Poland

[t]INFN Laboratori Nazionali di Frascati, Frascati, Italy

[v]University of Mining and Metallurgy, Kraków, Poland

[w]INFN, Pisa, Italy

[x]Warsaw University of Technology, Warszawa, Poland

1   Introduction

The technology of the Liquid Argon Time Projection Chamber (LAr TPC), first proposed by C. Rubbia in 1977 [1], was conceived as a tool for a completely uniform imaging with high accuracy of massive volumes. The operational principle of the LAr TPC is based on the fact that in highly purified LAr ionization tracks can be transported practically undistorted by a uniform electric field over macroscopic distances. Imaging is provided by a suitable set of electrodes (wires) placed at the end of the drift path continuously sensing and recording the signals induced by the drifting electrons.

Non–destructive read–out of ionization electrons by charge induction allows to detect the signal of electrons crossing subsequent wire planes with different orientation. This provides several projective views of the same event, hence allowing space point reconstruction and precise calorimetric measurement.

A large volume detector (about 450 m^3 corresponding to more than 600 t of LAr), the T600 detector, has been built and tested (Pavia 2001). Successively it has been transported to LNGS (Hall B) and re-assembly of the cryogenics infrastructure took place over the last past few years. Completion of the whole experimental set-up has been achieved during 2009 and the first step of commissioning phase (namely the cryostat evacuation by vacuum pumping) is currently under way.
Liquid Argon filling and start of operation is expected by spring 2010.

2   Activity in Hall-B (LNGS)

During 2009 an intense hardware activity has been performed aiming at the completion of the ICARUS T600 cryogenic plant and ancillary instrumentation. This activity is briefly summarized in the following sub-sections.

2.1   Liquefaction Plant (Stirling)

Dedicated tests showed the incorrect functioning of the LN$_2$ transfer circuit to the storage dewars located on the top floor of the Icarus structure. It was therefore necessary a re-shaping of the pumping system. A new design has been proposed and after realization and

installation, it was successfully tested in June 2009. Since then this part of the cryogenic plant is under continuous operation.

2.2 Process Control

From a careful survey of the (cryogenic) "Process Control" system, it was identified the need of a further hw/sw redundancy to reach full reliability. The hw instrumentation necessary for this issue has been quickly provided. In particular, final test of the correct alignment between the ICARUS-Air Liquide (AEI) process control system and the LNGS supervisor system (SCADA-LNGS) is presently (end of 2009) under way.

2.3 Insulation panel replacement

During a detector survey on May 13, 2009 a damaged evacuated insulation panel was found. Behind the grid of the north wall, the lower part of the insulation panel turned out to be deformed. No vacuum loss was however detected.

- According to AirLiquide investigations, the accident was due to a wrong mounting of a fraction of the honeycomb structure of the panel.

- An *ad-hoc* INFN committee, including ICARUS members, proposed to replace the full honeycomb insulation panel with a new insulation material (*Divinycell*) which does not require vacuum.

- The new solution implies an increase of the heat loss from 7 to 17 W/m^2 from the panel surface. The overall heat load of the cryostat is however practically unaffected.

- AirLiquide agreed on the proposal and included a new monitoring system of the stability and deformations of the vertical pannels.

Replacement of the insulation panel has been completed by Dec. 2009. Additional displacement sensors have been mounted to check for deformations of the panels (data included in the Process Control system).
In parallel, the vacuum tightness of the other insulation panels (base and lateral walls) has been checked. Leakage He-tests have been performed, and two minor leaks have been found and repaired. After this operation, vacuum of the insulation panels reached the design level ($2 \div 4 \times 10^{-2}$ mbar at room temperature).

2.4 Signal feed-through flange replacement

In the first tests in over-pressure seal casualties were recorded at the flexible connection of gas recirculation and (most important) substantial losses on the signals feed-through flanges (these lead to the decision of complete replacement, for a total of about 100 pieces (see next section).

The T600 signal flanges had been designed by the ICARUS collaboration and built and tested by an external company (DG-Technology, Parma, Italy). They are composed of a stainless body, shaped as a CF200 flange (Conflat).

The stainless bulk has been machined to obtain 9 slots each housing a printed circuit
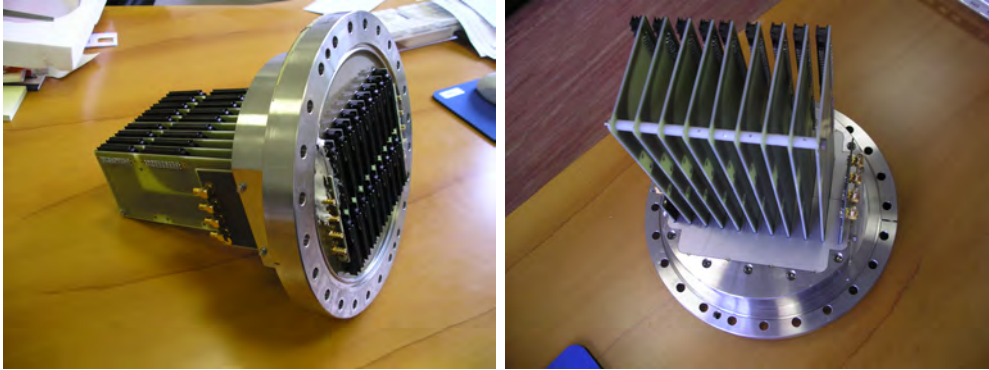
Figure 1: *[Left] Signal feed-through flange - old type, external view. [Right] internal view.*

equipped with two connectors at both ends. Each connector holds 32 signal leads and the corresponding screens. As a whole the flange holds 576 channels. Two additional printed circuits housed in smaller lateral slots hold 4 coaxial channels each, equipped with SMA connectors.

Stycast epoxy glue (by Emerson & Cumming) fills the slots holding the printed circuit in place and should provide the vacuum tightness. The flanges were tested by DG-Technology before delivery and tested again in Pavia in 2001, before being installed on the first T600 half module. Flange is shown in Fig.1.

Tests done with overpressure in the T600, after its installation at the LNGS, made evident an important flange leak problem, on at least half of them. As a consequence it was decided to replace all the flanges with new ones realized according to a design developed within the collaboration and granted by a registered patent.

The new flanges, designed by INFN-Padova and composed of a sandwich of printed circuit boards (PCB) strengthened by carbon fiber sheets. Inner layers hold metallized passing-through holes, while the outer layers have metallized blind holes electrically connected with the inner ones but out of axis with respect to them, to insure the vacuum tightness. The photographs in Fig.2 show the PCB hosting the connectors and insuring the vacuum tightness.

2.4.1 Tests of the new flanges

The complete new flange is shown in Fig.3 (external and internal sides respectively). After connectors soldering araldite is poured on the surfaces not to improve the vacuum tightness but to mechanically protect the soldered contacts, having adopted the SMT (Surface Mounting Technology) technique as shown in Fig.3. Being polarized to the wire
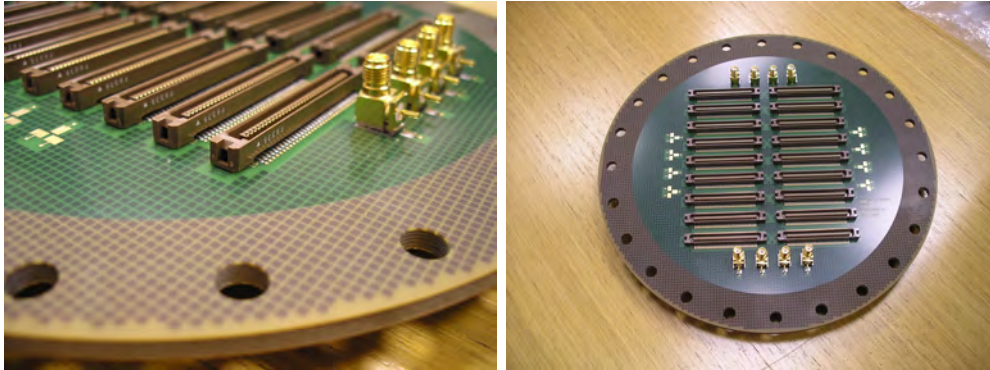
Figure 2: *Signal feed-through flange - new type, G10 (vetronite) frame*

potential unprotected contacts could accumulate dust and lose their insulation with time. After gluing the stainless rings, flanges are tested to check their vacuum tightness. During
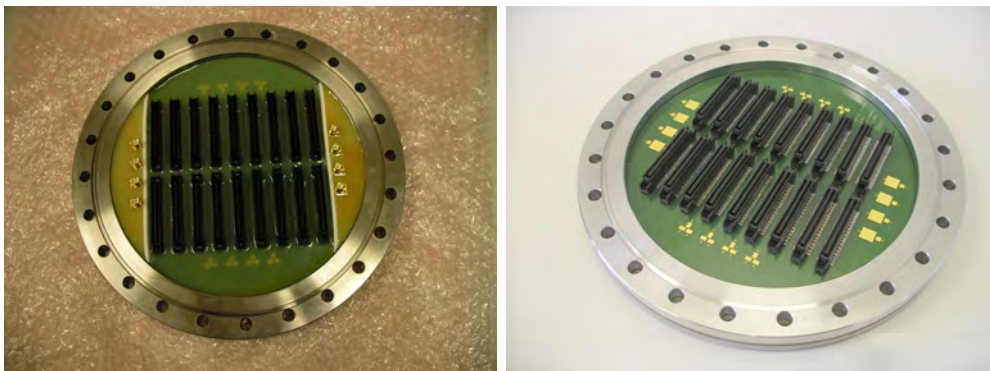
Figure 3: *[Left] Signal feed-through flange - NEW type, external view. [Right] internal view..*

the test the detected leak was required to be better than $1. \times 10^{-9}$ mbar l/s operating with a vacuum of 2×10^{-3} mbar.

During second half of October '09 all the old design flanges have been removed and replaced by the new ones. The replacement required also the use of a small adapting board and a short cable on the inner side to match the existing inner cables to the new connectors equipping the flange: the details are shown in Fig.4.

After the complete installation of the new flanges, leak tests confirmed the vacuum tightness of the new design flanges. Details of the replacement of the flanges on the detector chimneys are shown in Fig.5.

2.5 Cryostats Vacuum tightness and cleaning

After signal feed-through flanges replacement, over-pressure leak test, and then, primary vacuum tests indicated the persistence of significant losses attributable (after careful and
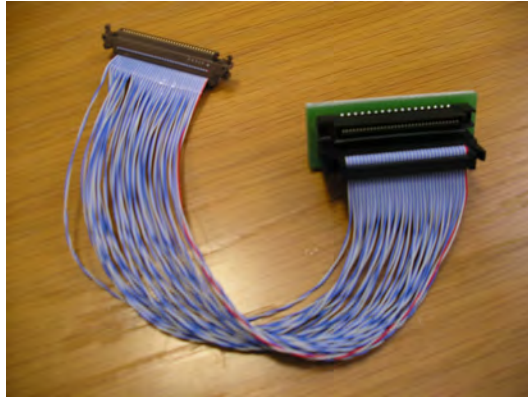
Figure 4: *Adapting board and cable.*
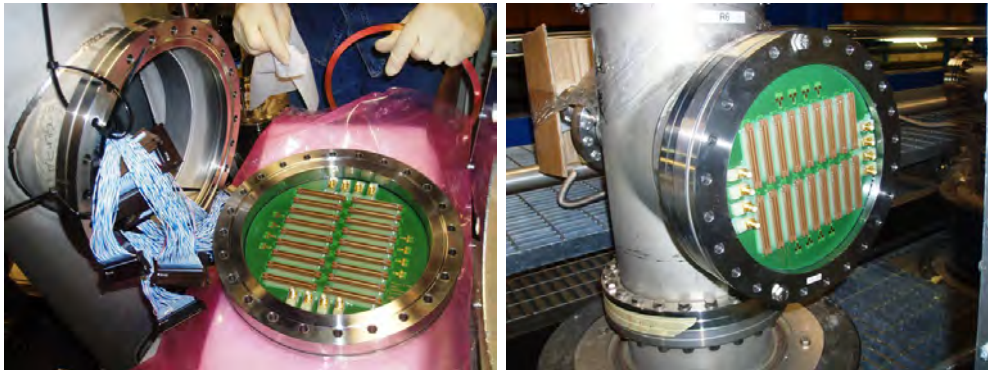
Figure 5: *Signal feed-through flange - NEW type: mounting on the signal chimneys.*

repeated measures) to other flanges, or to the flexible recirculation circuit. It was decided to test the seal of the flanges of closure of the manholes. Thus we noted the imperfect closure of the latter and decided to intervene with an operation of welding. This step was completed at the end of December.

Commissioning of the two cryostat with vacuum pumping was therefore finally started.

The displacement of the walls of the cryostats (in arbitrary units) as a function of pressure, is illustrated in Fig.6. It is evident from the linearity of the displacement that it was operating under elastic conditions. The evolution of the pressure in cryostats is shown in Fig.7, as well as the partial pressures of gas extracted.

The conditions achieved are very good. The pumping will be continued until the cooling phase will begin.
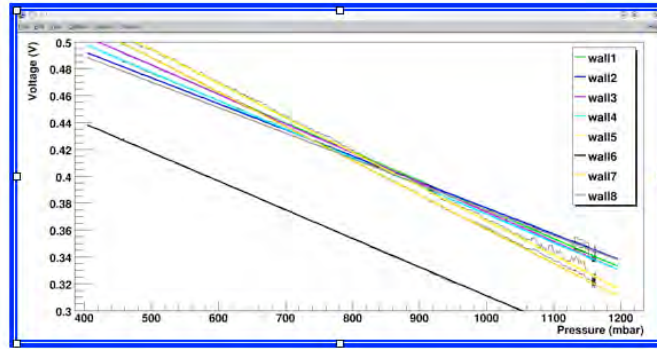
Figure 6: *Displacement of the walls (Arb. Units) of the cryostats as a function of pressure.*

2.6 Detector read-out test

A campaign of tests of the read-out electronics was conducted in December 2009, injecting test pulse signals in the decoupling boards, to measure the electronic noise, perform an initial calibration of different channels and check the linearity of the response. Unfortunately, it was not possible to create suitable low noise conditions of the system. Because of the concurrent work to verify the operation of the cryostats, the top floor (where the electronics is located) was not accessible and therefore it was not possible to close the electrostatic screens of the cables from the flanges to the decoupling boards. Moreover, all the activities related to vacuum pumping and check (pumps, UPS and other equipment on top of the detector) introduced severe additional noise on the front-end electronics, that deteriorated the measures. Overall, 33 electronics cabinets were acquired out of 40 of the second half-module, varying the amplitude and duration of the injected signal. Only 10 % of these had acceptable noise conditions. The test has however allowed to verify the operation of algorithms of automatic analysis and extraction of calibration constants.

As an example, Fig.8 [Left] shows, for the boards in a group of three consecutive cabinets, the value of the amplitude of the signal in response to a test-pulse, while Fig.8 [Right] shows the linearity of the response of a card by changing width of the step-signal used to inject the test pulse.

2.7 Off-line software

The current software is an evolution of what already developed and used for the data from the Pavia test. Developments, either completed or under final validation, are:

- Root data sharing;

- Mysql data sharing, for databases handling (online and offline);

- DAta Compression decoding;

103
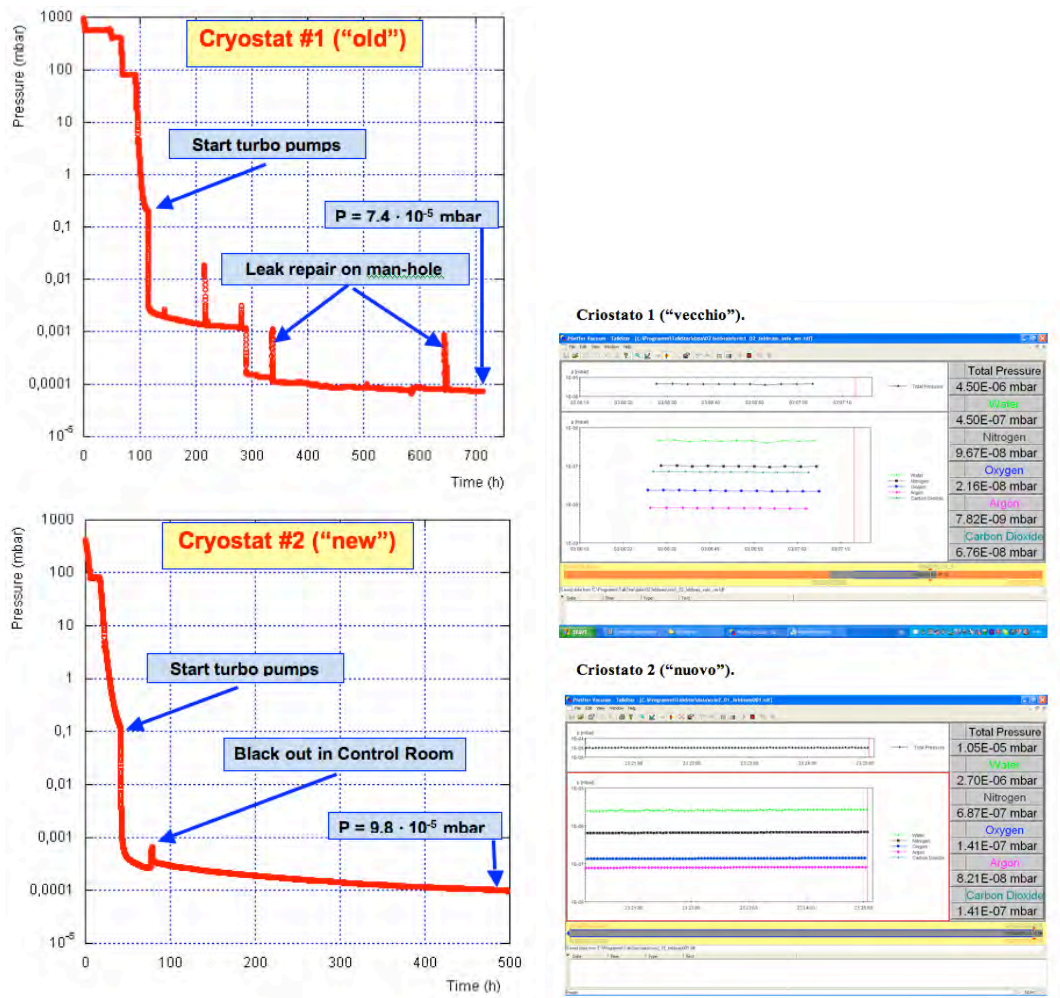
Figure 7: *[Left] Behavior of pressure during vacuum pumping. [Right] partial pressures of gas extracted*

- Automatic search algorithms for track and vertex;

- Full 3D reconstruction;

- Automatic analysis of calibration data;

- Muon momentum determination by multiple scattering;

- LAr purity determination with crossing muon tracks;

- Light signal analysis from PMTs;

- ElM. shower reconstruction: lateral and longitudinal profile.
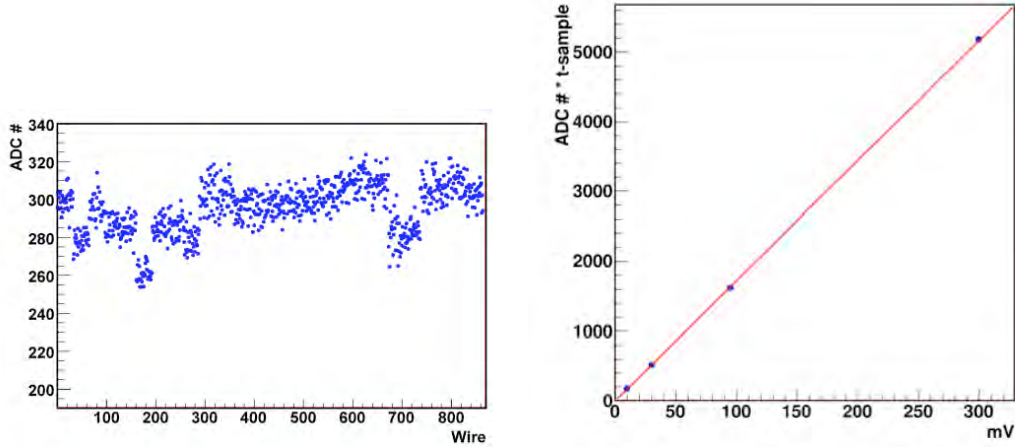
Figure 8: *[Left] Collection boards response in a group of three consecutive cabinets. [Right] Linearity of the response.*

3 Development of a new real time algorithm for track finding

A new hit finding algorithm has been developed aiming at a higher efficiency signal identification with respect to the one implemented in the DAEDALUS chip, both for collection and induction wires.

In the ICARUS detector the signal produced by ionization on a single wire, after shaping by front end electronics, corresponds to a peak of duration 30-40 t-samples (1 t-sample equal to 400 ns) whose height is about 15 ADC counts (1 ADC count $\sim$ 1000 electrons). The signal is immersed in noise with both low frequency components, baseline modulation of amplitude up to 15 ADC counts, and high frequency components that look like short peaks of about 5 t-sample duration and amplitude of 3-4 ADC counts. Due to the baseline oscillation it is not easy to identify efficiently the signal with simple threshold discrimination.

Therefore the signal extraction requires estimating the baseline and subtracting it. At the same time to reduce identification of the fake hits it is required to reduce the high frequency noise while preserving the signal amplitude as much as possible. To fulfill these two tasks an algorithm based on double rebinning of the wire signals has been developed. It is based on the method of sliding window , choosing a window width of 8 t-samples ($\leq$ that a typical signal duration) for short rebinning size and 128 for long rebinning ($\geq$ than the signal duration), and threshold 6 ($\sim$ one half of a mip signal).

The algorithm has been tested on the data collected in 2001 in Pavia. Efficiency in hit finding above 99 % has been found while fake identification remain less than 1%.

Recently the algorithm has been implemented on XILINX-FPGA's that has been used to replace the daedalus chips on some CAEN-V789 ICARUS DAQ boards acting on 32 wires simultaneously, for real-time hit finding on single wires. The LAr-TPC test facility at LNL (Icarino) has been equipped with these modified DAQ boards (3 in collection
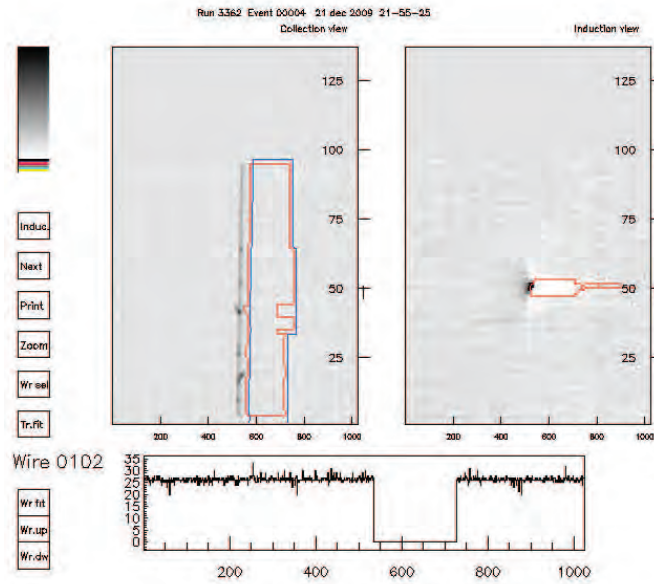
Figure 9: *Vertical through-going muon event in the LNL LAr-TPC. The red contour areas are the stretched hit found peak, while the blue contour include a majority parameter ($\geq$ 8 out of 32 wires).*

mode and 3 for induction for a total of 96+96 wires). Efficiency, tested with exposure to cosmic rays, has been found in full agreements with off-line results both for collection and induction.

Additional programmable features (time-above-threshold, peak-stretching, signal majority) have been added to the algorithm to perfect its use in terms of self triggering. This filtering procedure can be applied also to the search for negative signal, setting a parameter called polarity.

As an example, Figure 9 shows a typical crossing muon event. The red contour areas are the stretched hit found peak, while the blue contour include a majority parameter ($\geq$ 8 out of 32 wires).

Fig.10 [Left] and [Right] show the efficiency as a function of threshold for the collection and induction wires respectively. Fake hits are shown in Fig.11 [Left] and [Right]. A fake rate less than 1 % is reached with a threshold of 6 which guarantees an efficiency better than 99 % both in induction and collection. As a further test on the algorithm quality, a "solar neutrino trigger" has been implemented, requiring signal hit found only on the central 32 wires and nothing on the adjacent 32 + 32. Fig.12 [Left] shows an event, Fig.12 [Right] shows the energy distribution (in the MeV threshold) of the events selected by this trigger.

Given the excellent performance of the algorithm and the FPGA implementation well suited for on-line signal extraction, the possibility to replace all the DAEDALUS chips on the T600 DAQ boards is under serious investigation.

106
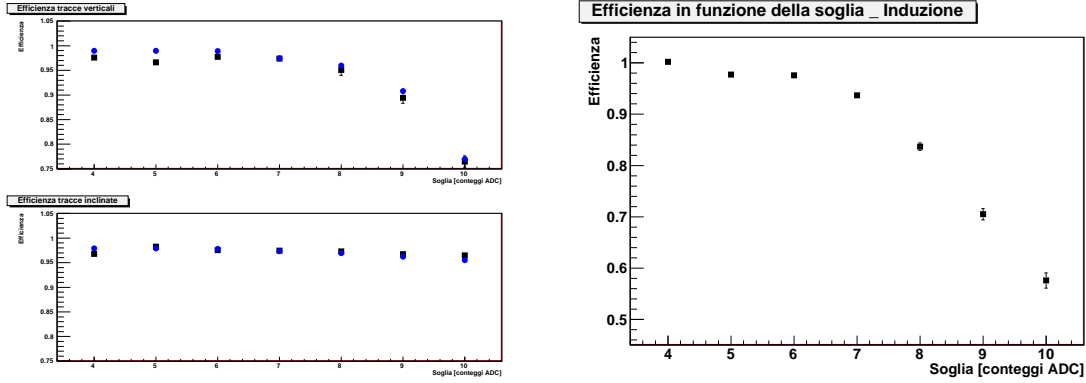
Figure 10: *[Left] Detection efficiency in the collection plane both for straight and inclined muon tracks (black dots), compared with the off-line algorithm results (in blue). [Right] Detection efficiency in the induction plane.*
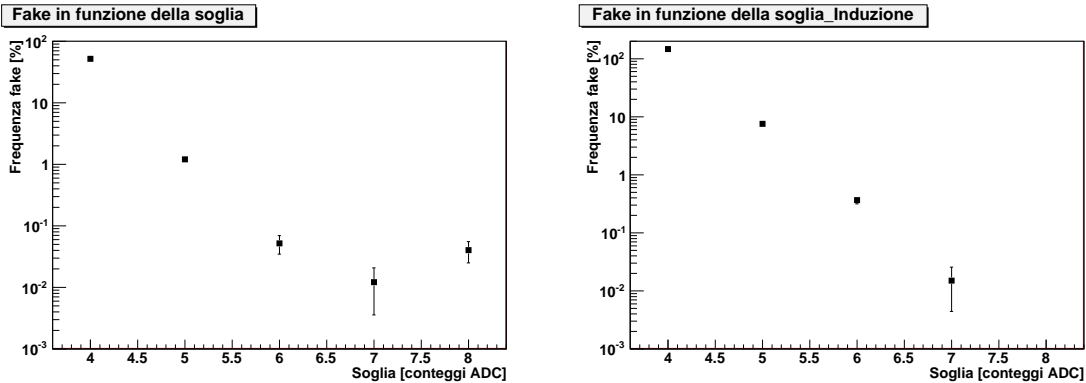
Figure 11: *[Left] Fake hits rate for the collection plane. [Right] Fake hits rate for the induction plane.*

4 Conclusions

The ICARUS T600 detector, a large–mass Liquid Argon TPC, is now completely installed in the underground Gran Sasso Laboratory.

The commissioning phase has been finally started with the first step of the vacuum pumping in the two vessels. Vacuum pumping is expected to last few months (down to the 10^{-5} mbar range), and successively the cooling step and the final LAr filling step will take place (presumably by spring 2010).

Publications in 2009
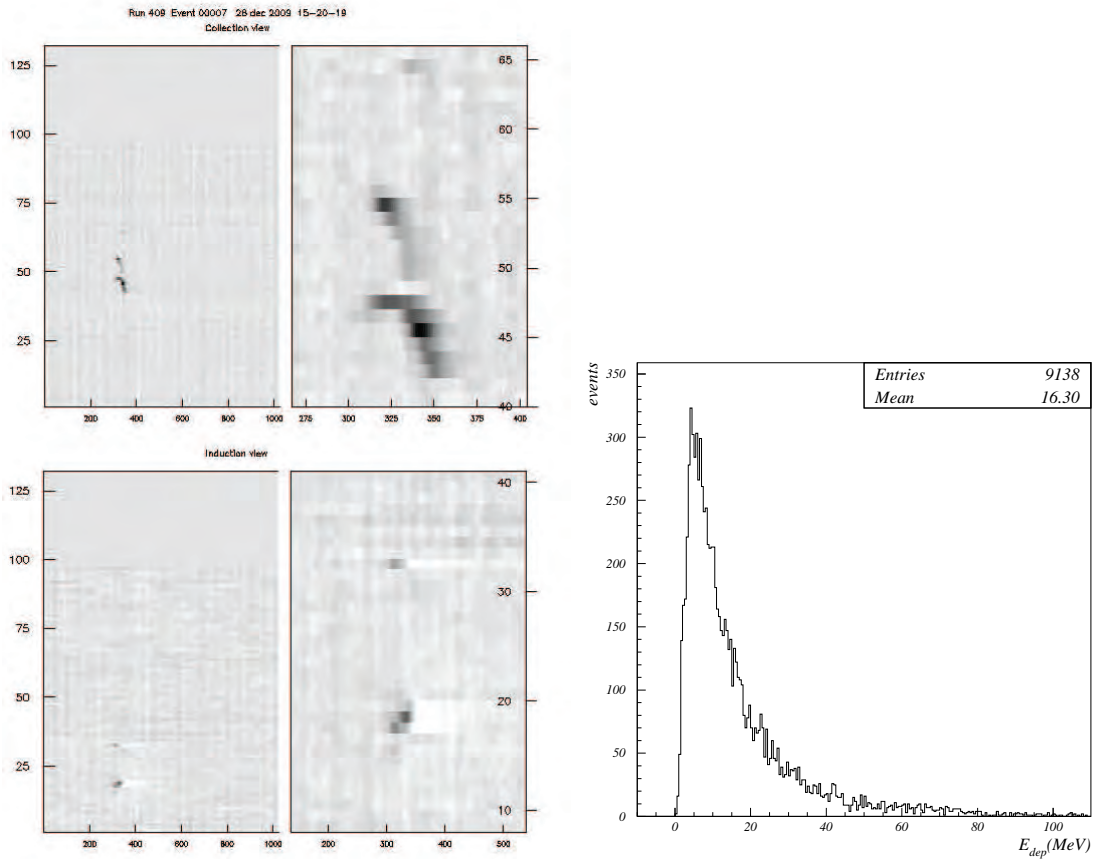
Figure 12: *[Left] Isolated low energy event selected with the "solar neutrino trigger". [Right] Energy spectrum of the isolated low energy events obtained requiring at least four wires hit (majority 4).*

References

[1] A. Ankowski *et al.*, *ENERGY RECONSTRUCTION OF ELECTROMAGNETIC SHOWERS FROM π^0 DECAYS WITH THE ICARUS T600 LIQUID ARGON TPC* Acta Phys. Pol. B 41(2010), 103.

References

[1] C. Rubbia, *The Liquid-Argon Time Projection Chamber: A New Concept For Neutrino Detector*, CERN–EP/77–08, (1977).

[2] S. Bonetti *et al.* [ICARUS Collaboration], *A Study Of The Electron Image Due To Ionizing Events In A Two-Dimensional Liquid Argon Tpc With A 24-Cm Drift Gap*, Nucl. Instrum. Meth. A **286**, (1990) 135.

[3] A. Bettini *et al.* [ICARUS Collaboration], *A Study Of The Factors Affecting The Electron Lifetime In Ultrapure Liquid Argon*, Nucl. Instrum. Meth. A **305**, (1991) 177.

[4] P. Benetti *et al.* [ICARUS Collaboration], *A 3 Ton Liquid Argon Time Projection Chamber*, Nucl. Instrum. Meth. A **332**, (1993) 395.

[5] P. Benetti *et al.* [ICARUS Collaboration], *Argon Purification In The Liquid Phase*, Nucl. Instrum. Meth. A **333**, (1993) 567.

[6] P. Cennini *et al.* [ICARUS Collaboration], *Performance Of A 3 Ton Liquid Argon Time Projection Chamber*, Nucl. Instrum. Meth. A **345**, (1994) 230.

[7] P. Benetti *et al.* [ICARUS Collaboration], *A 3D Image Chamber For The Lar Tpc On Multilayer Printed Circuit Board*, Nucl. Instrum. Meth. A **346**, (1994) 550.

[8] ICARUS Collaboration, *A First 600 Ton ICARUS Detector Installed At The Gran Sasso Laboratory*, Addendum to Proposal by the ICARUS Collaboration, LNGS–95/10, (1995).

[9] P. Cennini *et al.* [ICARUS Collaboration], *A Neural Network Approach For The Tpc Signal Processing*, Nucl. Instrum. Meth. A **356**, (1995) 507.

[10] P. Cennini *et al.* [ICARUS Collaboration], *Improving The Performance Of The Liquid Argon Tpc By Doping With Tetramethyl Germanium*, Nucl. Instrum. Meth. A **355**, (1995) 660.

[11] F. Arneodo *et al.* [ICARUS Collaboration], *Performance Evaluation Of A Hit Finding Algorithm For The Icarus Detector*, Nucl. Instrum. Meth. A **412**, (1998) 440.

[12] P. Cennini *et al.* [ICARUS Collaboration], *Detection Of Scintillation Light In Coincidence With Ionizing Tracks In A Liquid Argon Time Projection Chamber*, Nucl. Instrum. Meth. A **432**, (1999) 240.

[13] F. Arneodo *et al.* [ICARUS Collaboration], *First Observation Of 140-Cm Drift Ionizing Tracks In The Icarus Liquid-Argon Tpc*, Nucl. Instrum. Meth. A **449**, (2000) 36.

[14] F. Arneodo *et al.* [ICARUS Collaboration], *Determination Of Through-Going Tracks' Direction By Means Of Delta-Rays In The Icarus Liquid Argon Time Projection Chamber*, Nucl. Instrum. Meth. A **449**, (2000) 42.

[15] F. Arneodo *et al.* [ICARUS Collaboration], *Performance Of The 10 m^3 Icarus Liquid Argon Prototype*, Nucl. Instrum. Meth. A **498**, (2003) 293.

[16] F. Arneodo *et al.* [ICARUS Collaboration], *Observation Of Long Ionizing Tracks With The ICARUS T600 First Half–Module*, Nucl. Inst. Meth., A **508**, (2003) 287.

[17] F. Arneodo *et al.* [ICARUS Collaboration], *Detection Of Cerenkov Light Emission In Liquid Argon*, Nucl. Instrum. Meth. A **516** (2004), 348.

[18] S. Amoruso *et al.* [ICARUS Collaboration], *Analysis Of The Liquid Argon Purity In The ICARUS T600 TPC*, Nucl. Inst. Meth., A **516**, (2004) 68.

[19] S. Amoruso *et al.* [ICARUS Collaboration], *Measurement Of The Muon Decay Spectrum With The ICARUS T600 Liquid Argon TPC*, Eur. Phys. J., C 33 (2004) 233.

[20] S. Amoruso *et al.* [ICARUS Collaboration], *Study Of The Electron Recombination In Liquid Argon With The ICARUS TPC*, Nucl. Inst. Meth., A 523 (2004) 275.

[21] S. Amerio *et al.* [ICARUS Collaboration], *Design, construction and tests of the ICARUS T600 detector*, Nucl. Inst. Meth., A 527 (2004) 329.

[22] A. Ankowski *et al.*, [ICARUS Collaboration], *Characterization of ETL 9357 FLA Photomultiplier Tubes for cryogenic temperature applications*, Nucl. Inst. and Meth. A 556 (2005) 146.

[23] A. Ankowski *et al.*, [ICARUS Collaboration], *Measurement of through-going particle momentum by means of multiple scattering with the ICARUS T600 TPC*, Eur. Phys. J. C 48 (2006), 667.

[24] F. Arneodo *et al.*, [ICARUS-Milano Collaboration], *Performance of a liquid argon time projection chamber exposed to the CERN West Area Neutrino Facility neutrino beam*, Physical Review D (2006) (Vol. 74, No. 11).

[25] M. Antonello *et al.*, *Analysis of Liquid Argon Scintillation Light Signals with the ICARUS T600 Detector*, ICARUS-TM/06-03 (to be published).

LUNA. Laboratory for Underground Nuclear Astrophysics

D. Bemmerer[a], C. Broggini[b], A. Caciolli[c], V. Capogrosso[d], P. Corvisiero[e],
H. Costantini[e], Z. Elekes[f], M. Erhard[b], A. Formicola[g], Zs. Fülöp[f], G. Gervino[h],
A. Guglielmetti[d], C. Gustavino[g], Gy. Gyürky[f], G. Imbriani[i], M. Junker[g], R. Kunz[j],
A. Lemut[e], B. Limata[i], M. Marta[a], C. Mazzocchi[d], R. Menegazzo[b], P. Prati[e],
V. Roca[i], C. Rolfs[j], C. Rossi Alvarez[b], E. Somorjai[f], O. Straniero[k], F. Strieder[j],
F. Terrasi[l], H.P. Trautvetter[j]
SPOKESPERSON: A. GUGLIELMETTI

[a]Forschungszentrum Dresden-Rossendorf, Dresden, Germany
[b]INFN, Padova, Italy
[c]Università degli Studi di Padova and INFN, Padova, Italy
[d]Università degli Studi di Milano and INFN, Milano, Italy
[e]Università degli Studi di Genova and INFN, Genova, Italy
[f]Institute of Nuclear Research (ATOMKI), Debrecen, Hungary
[g]INFN, Laboratori Nazionali del Gran Sasso (LNGS), Assergi (AQ), Italy
[h]Università degli Studi di Torino and INFN, Torino, Italy
[i]Università degli Studi di Napoli "Federico II", and INFN, Napoli, Italy
[j]Institut für Experimentalphysik III, Ruhr-Universität Bochum, Bochum, Germany
[k]Osservatorio Astronomico di Collurania, Teramo, and INFN Napoli, Italy
[l]Seconda Università di Napoli, Caserta and INFN, Napoli, Italy

Abstract

The principal goal of the LUNA experiment is the measurement of thermonuclear fusion cross sections relevant for stellar nucleosynthesis. In the course of the year 2009, the reaction ^{15}N(p,γ)^{16}O was measured and a feasibility study on the D(α,γ)^{6}Li reaction was performed. Moreover, the data analysis of the ^{25}Mg(p,γ)^{26}Al was finished and results are going to be published. In this report, a brief description of the future reaction to be measured, namely the proton capture on ^{17}O, is also given.

1 ^{15}N(p,γ)^{16}O

The CNO cycles dominate the energy production in stars more massive than our Sun, belonging to second or later generation and with an appreciable abundance of CNO isotopes. The CNO cycles are characterized by sequences of radiative capture reactions and β decay processes. The proton capture at ^{15}N introduces a reaction branch linking the first CNO or CN cycle with the second CNO or NO cycles. The ratio between the reaction rate of the ^{15}N(p,γ)^{16}O and the ^{15}N(p,$\alpha\gamma$)^{12}C reactions directly determines the nucleosynthesis of the oxygen isotopes ^{16}O, ^{17}O and ^{18}O. The reaction rate at stellar energies is dominated by two broad low-energy resonances at E$_p$ = 335 and 1028 keV and the associated interference terms [1]. In addition, it is expected to have a strong non-resonant direct capture component which may significantly contribute to the reaction cross-section at stellar energies. Before the LUNA measurements, the cross section was studied from E$_p$ = 150 to 2500 keV [2, 3] but at energies corresponding to the interference region between the two resonances and for energies E$_p$ < 300 keV the uncertainty of the data is rather large bringing to a big error on the extrapolated reaction rate. New precision experimental data at these energies are therefore extremely important.

In a first effort, a re-analysis of the data acquired during a past measurement of the ^{14}N(p,γ)^{15}O reaction with a high efficiency BGO detector was performed, exploiting the fact that the gas target was composed of natural nitrogen (0.3% ^{15}N). The data covered only a limited energy range (90-230 keV) and were affected by large uncertainties at low energy [4].This measurement was already described in the 2008 LNGS Annual Report. Then, a systematic study using enriched ^{15}N solid targets and HPGe detectors over a wide energy range was undertaken, in collaboration with the University of Notre Dame (USA).This is described in subsection 1.1. Finally, the lowest energies were reached with an high efficiency BGO detector and enriched solid targets. This is described in subsection 1.2.

1.1 Measurement of ^{15}N(p,γ)^{16}O over a wide energy range in collaboration with the University of Notre Dame, USA (P. J. LeBlanc, J. Görres and M. Wiescher)

Three different accelerators were used during this phase, namely the 4 MV and the 1 MV Van der Graff accelerators at the University of Notre Dame and the LUNA II 400 kV Cockroft Walton machine at LNGS. The first was used in the energy range from 700 to 1800 keV with low intensity, the second from 285 to 700 keV with medium intensity and the last from 130 to 400 keV with high intensity. The energy range of each machine was chosen in order to overlap with that of another machine. The Ti- ^{15}N targets were fabricated in Karlsruhe by reactive sputtering of Ti in a Nitrogen atmosphere enriched in ^{15}N to 99.95%. Isotopical abundances were experimentally verified by comparing the yield of the ^{14}N(p,γ)^{15}O 278 keV resonance [5] from the enriched targets with that obtained using a target produced with a natural nitrogen gas. At Notre Dame, the γ-rays were observed using a HPGe Clover detector consisting of four HPGe crystals contained in the same cryostat. At Gran Sasso, a single crystal, 126% HPGe detector was used. The detectors were put at an angle of 45deg in order to minimize any possible angular distribution
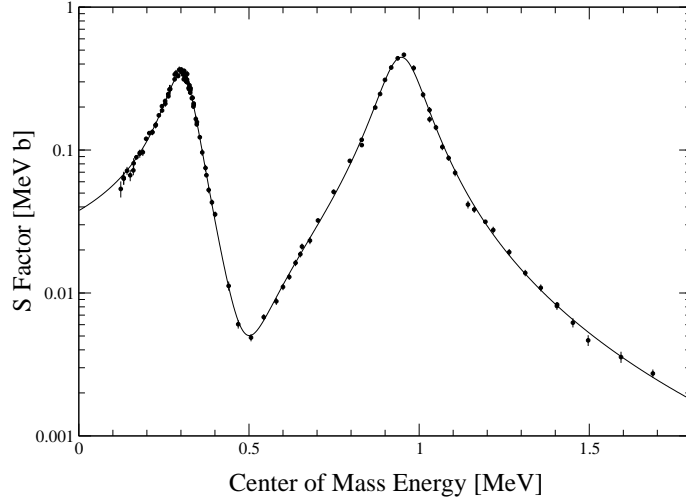
Figure 1: Astrophysical S-factor of the ^{15}N(p,γ)^{16}O reaction obtained in the LUNA-NotreDame joint experiment together with the AZURE R-matrix fit.

effect and allow the detector to be as close as possible to the reaction spot. The relative efficiency of the detectors were measured using radioactive sources and well known proton capture reaction, according to the procedure described in [5]. The excitation function for the ground state transition of the reaction ^{15}N(p,γ)^{16}O was measured from 131 to 1800 keV. An R-matrix analysis with the code AZURE [6] was performed including the two broad 1^- resonances plus a direct capture contribution. Figure 1 shows the astrophysical S-factor data as a function of the center of mass energy together with the R-matrix fit. The results on the lowest energy resonance agree with those of ref [2] while those on the highest energy one are compatible with those of ref [3].

1.2 Measurement of ^{15}N(p,γ)^{16}O at LUNA with solid state targets and BGO detector

Based on the experience gained with the spin-off analysis of the data acquired during the measurement of the ^{14}N(p,γ)^{15}O reaction [4] and in the experimental phases described in sec. 1.1, the LUNA collaboration started an additional experiment on ^{15}N(p,γ)^{16}O. In this approach, solid state targets similar to those used for the measurements described in sec.1.1 have been produced by reactive plasma deposition of TiN onto Ta backings at FZ Karlsruhe, Germany, and at the Laboratori Nazionali di Legnaro (LNL), Italy. These targets have been mounted inside the LUNA BGO detector (Figure 2) where they have been bombarded with protons provided by the LUNA 400kV accelerator. The BGO detector consists in six separated segments which digitized separately and stored on disk event by event [7]. The trigger of the ADCs is given by the sum of all six elements which must be higher than approximately 2 MeV, low enough compared to the gamma ray of 12.4 MeV emitted by the studied reaction. The data have been calibrated and summed off line. A typical spectrum obtained with this setup is shown in Figure 3.

The use of the high efficiency BGO detector allowed to extend the energy range of the

113
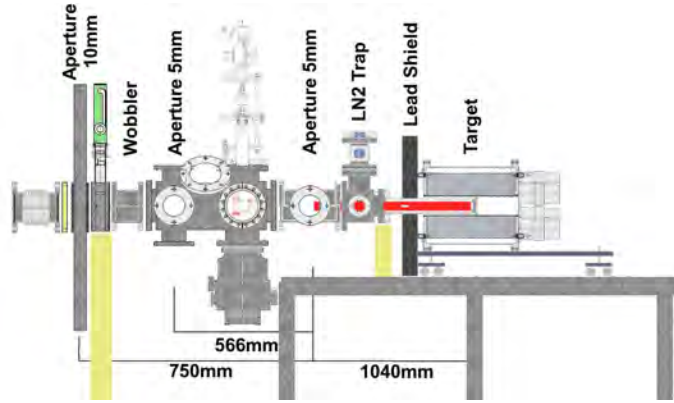
Figure 2: Setup used for investigating the ^{15}N(p,γ)^{16}O reaction with solid state targets and a BGO detector.
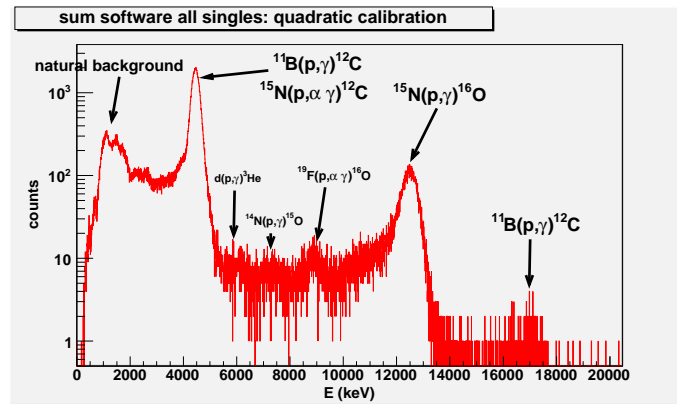
Figure 3: Typical BGO spectrum obtained during the ^{15}N(p,γ)^{16}O experiment with a beam energy $E_p = 250$keV and a beam current of $I = 200\mu$A. The most relevant background lines are indicated in the spectrum.
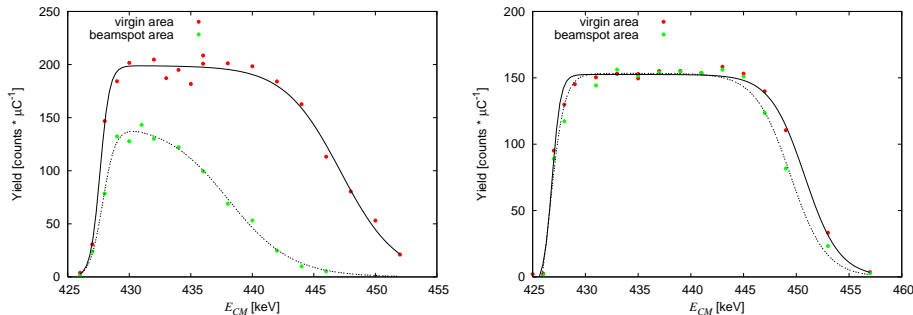
Figure 4: Resonance scans performed at FZD on two different Ti^{15}N targets bombarded in the course of the experiment with 46 C (left) and 10 C (right). The red (green) points indicate the scans performed before (after) irradiation at LUNA.

measurement down to 70 keV, the lowest energy data point obtained for this reaction. This energy corresponds to the Gamow peak for ^{15}N(p,γ)^{16}O in Novae and AGB stars. As a consequence, after the conclusion of these measurements no extrapolation will be any more needed for these astrophysical environments.

One major problem faced in the course of this experiment is the limited energy range of the LUNA 400kV accelerator, as for this reaction no narrow reference resonance for systematic determination of target stoichiometry and thickness is available below $E_p = 400$ keV: The resonance at $E_p = 335$ keV has a width of 91 keV and is thus too broad to serve this aim. For this reason, the resonance at $E_p = 429.57$ keV with a width of 0.1 keV is normally used for normalization. However this resonance is out of the energy range of the LUNA 400kV accelerator.

To overcome the shortcoming, all targets have been studied with the $E_p = 429.57$ keV resonance before and after the measurements at LUNA using the 3MV Tandetron accelerator of the Forschungszentrum Dresden (FZD). Typical results are displayed in Figure 4. The modification of the target quality as a function of the total amount of charge accumulated on a given target is clearly visible. In the course of the data analysis it turned out that, in particular in the energy region of the 335 keV resonance, an exact knowledge of the target profile is of paramount importance also to determine the effective reaction energy [8, 9].

In addition, selected targets have been analyzed by Elastic Recoil Detection (ERD) at the University of Munich in order to independently verify the target stoichiometry assumed to be Ti/N = 1. An additional test engaging a Secondary Nuclear Mass Spectroscopy (SNMS) at ATOMKI (Hungary) did not provide useful information due to the rough target backings and to the background of ^{14}N caused by the residual gas in the SNMS apparatus.

The efficiency of the setup has been determined by a Geant 4 based Monte Carlo Code. The simulation has been tested using the reaction ^{11}B(p,γ)^{12}C which emits gamma rays in the same energy range as the reaction ^{15}N(p,γ)^{16}O. Simulated and measured spectra are in good agreement giving confidence on the obtained efficiency (Figure 5).

After the conclusion of the data taking in November 2009, the data are now being analyzed by two different groups of the collaboration and a publication of the final results
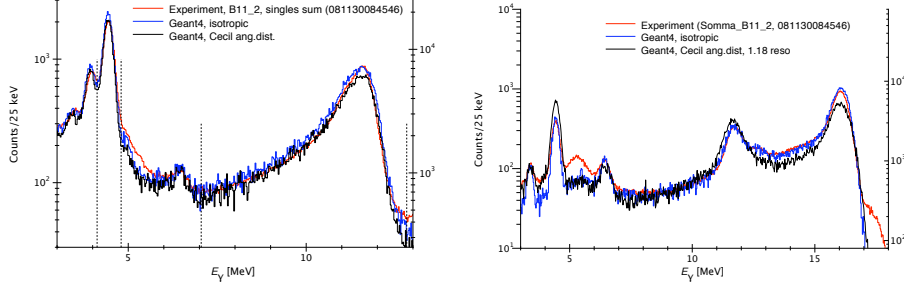
Figure 5: Simulations (black and blue) compared with measurements (red) of the reaction ^{11}B(p,γ)^{12}C performed to check the efficiency obtained with GEANT 4. The spectrum on the left panel has been obtained by first constructing off–line the spectra for each element of BGO detector and then summing them together. The spectrum on the right panel is obtained by summing event by event the energies deposited in the six elements. The difference between the red and the black curve is caused by different angular distributions assumed in the simulations.

is foreseen in 2010.

2 $D(\alpha, \gamma)^6Li$ reaction

In its standard picture,the Big Bang nucleosynthesis occurs during the first three minutes of universe, with the formation of light elements such as D, ^3He, ^4He, ^6Li and ^7Li, through the reaction chain shown in figure 6. Due to its outstanding importance in the Big Bang Nucleosynthesis, the $D(\alpha, \gamma)^6Li$ reaction is part of the LUNA scientific program approved by the LNGS Scientific Committee for the next five years [10]. Its reaction rate determines the amount of primordial ^6Li abundance in the universe. In spite of its importance, this reaction has not been directly measured in the region of interest. In fact, the reaction yield of this reaction is very low, probably being a weak, non resonant electric quadrupole transition. On the other hand, theoretical calculations differ by two orders of magnitude, leaving a noticeable uncertainty in the calculation of primordial ^6Li [11].
The direct measurement of the $D(\alpha, \gamma)^6Li$ reaction can be performed at the LUNA 400 kV accelerator using an α-beam, a deuterium gas-target and a HPGe detector (135% efficiency) mounted in close geometry. The intrinsic beam induced background associated to this reaction is a side effect that has to be dealt with. In fact, the $D(\alpha, \alpha)d$ Rutherford scattering induces the $D(d, n)^3He$ and $D(d, p)t$ reactions (see figure 7). While the $D(d, p)t$ reaction is not a problem in this context, the neutrons produced by the $D(d, n)^3He$ reaction ($E_{n(c.m.)} = 2450\ keV$) induce $(n, n'\gamma)$ reactions in the HPGe detector and in the surrounding materials, generating a beam-induced background in the $\gamma - ray$ spectrum, and, in particular, in the energy region around 1.6 MeV, where the capture transition to the ground state of ^6Li is expected. An analytical code simulation has been developed to calculate the neutron yield in different experimental conditions [12], and a test measurement has been performed in march 2009 [13]. The set-up used for the test is schematically shown in figure 8. Inside the scattering chamber a silicon detector was installed to mea-

116
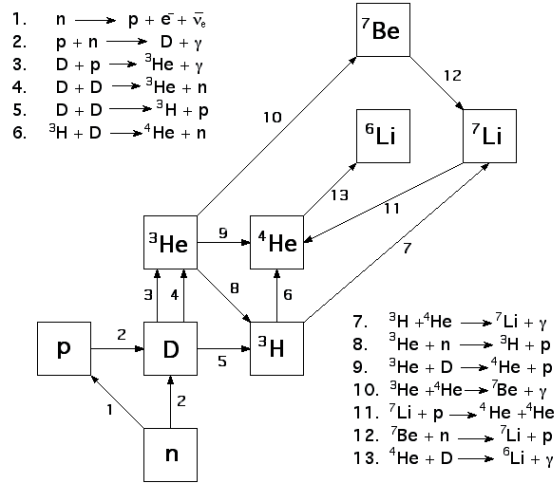
Figure 6: Simplified scheme of the BBN reaction chain.
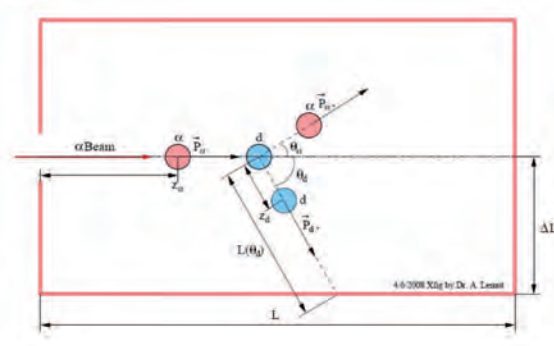
Figure 7: Schematic of the $D(\alpha, \alpha)d$ Rutherford scattering of the α beam particles on the deuterium target.

sure the protons generated in the $D(d,p)t$ reaction. Since the cross sections for both the $D(d,p)t$ and $D(d,n)^3He$ reactions are known, the measurement of the number of protons detected can be related to the number of neutrons produced. The efficiency of the silicon detector was computed with the LUNA Monte Carlo simulation code [14]. Figure 9 shows the obtained simulated spectrum of the Silicon detector: the peak at about 3 MeV is due to the protons of the $D(d,p)t$ reaction ($E_{p(c.m.)} = 3022$ keV). Outside the chamber, a HPGe detector was placed at a distance of 9 cm from the beam axis to measure the background induced by the beam in the γ-ray spectra. The experimental contitions during the test were: beam energy $E_\alpha = 330$ keV, average current $I_\alpha = 130$ μA and two different target pressures $P_{Deuterium} = 0.5$ and 1.0 $mbar$. Figure 10 shows the spectrum acquired by the silicon detector at the two different pressures. The result is in good agreement with our calculations (see figure 9). As foreseen, the production of protons (and neutrons) is approximately proportional to the squared target density. The recorded HPGe spectra
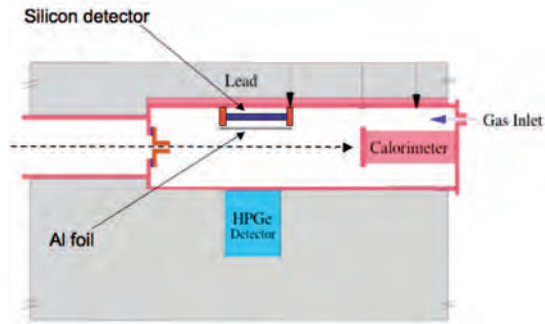
Figure 8: Schematic diagram of the experimental set-up used in March 2009 for the $D(\alpha,\gamma)^6Li$ test.

are shown in figure 11. Various γ transitions due to the interaction of neutrons with the Germanium and the surrounding materials (Fe, Pb, Cu) can be identified as well as the dependence of the beam-induced background on the pressure. The peak at $E_\gamma = 693 \; keV$, is due to the interaction of neutrons with the germanium atoms of the detector itself [15].

The test of march allowed to define the set-up for the $D(\alpha,\gamma)^6Li$ reaction. A new chamber has been realized in the LNGS mechanical workshop (see figure 12. It consists of a steel box properly shaped to host the HPGe detector at a distance of 2 cm from the beam axes. Inside the chamber is inserted a tube 16 cm long, with a square cross section of $2x2 \; cm^2$. The tube strongly reduces the effective gas volume and therefore the $D(d,n)^3He$ reaction yield. Finally, two silicon detectors are faced to the gas target volume to monitor the running conditions through the detection of protons generated in the $D(d,p)t$ reaction. The new chamber has been successfully tested at the end of 2009, implementing the set-up with a lead shield and a radon box, to minimize the natural background. The measurement of $D(\alpha,\gamma)^6Li$ reaction should start in the middle of 2010. The reaction chamber can be considered a neutron source with an intensity up to few tens of neutron/second. For this reason, an external shield of borated paraffin 10 cm thick will be mounted.

3 Study of low-energy (p,γ) resonances on Magnesium isotopes

Observations from satellites [16] have mapped the Sky in the light of the prominent γ-ray line at $E_\gamma = 1809$ keV of the β-decay of ^{26}Al ($T_{1/2} = 7 \times 10^5$ yr). The intensity of the line corresponds to about 6 solar masses of ^{26}Al in our galaxy [17]. The presence of ^{26}Al in the interstellar medium has been determined from the observation of ^{26}Mg isotopic enrichment (extinct ^{26}Al) in carbonaceous meteorites [18]. While the observations from COMPTEL and INTEGRAL provided evidence that ^{26}Al nucleosynthesis is still active on a large scale, the Mg isotopic variations show that ^{26}Mg must have been produced within the last 4.6 billion years since the condensation of the solar-system. Any astrophysical
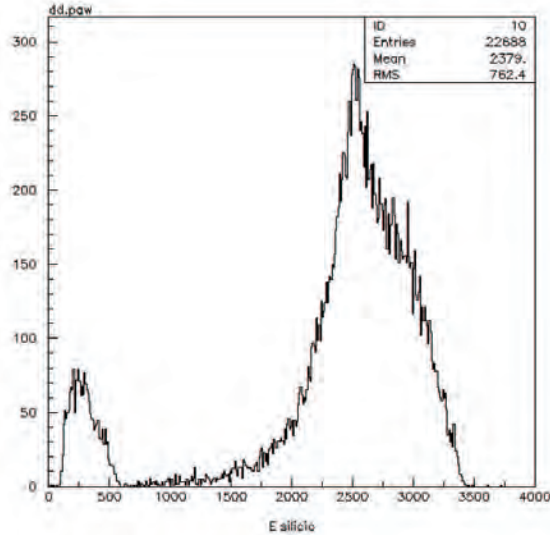
Figure 9: Simulated proton spectrum of the $D(d,p)t$ reaction obtained with the LUNA Monte Carlo simulation code with a pressure of 1 mbar at $E_\alpha = 330\ keV$.

scenario for [26]Al nucleosynthesis must be concordant with both observations. The [26]Al is produced mainly via the [25]Mg(p,γ)[26]Al capture reaction. The most important site for the activation of this reaction is the hydrogen-burning shell in off-main-sequence stars of any mass [19].

Moreover, a global anticorrelation between the abundances of Mg and Al has been observed, e.g. in Globular Cluster stars [20]. This observation is to the present knowledge coupled to the nucleosynthesis processes involving the Mg-Al cycle occurring in the H-burning shell of the primeval generation of AGB and massive stars. A detailed knowledge of these processes is a fundamental step toward a general understanding of the formation of the building blocks of our Galaxy.

The uncertainties in the present stellar models are closely related to a precise evaluation of the relevant reactions of the Mg-Al cycle, e.g. [24]Mg(p,γ)[25]Al and [25]Mg(p,γ)[26]Al. The reaction [25]Mg(p,γ)[26]Al is dominated by narrow resonances. These resonances decay in complex γ-ray cascades either to the ground state of [26]Al or an isomeric state at $E_x = 228$ keV. Only the ground state transition is of astrophysical relevance since the ground state decays into the first excited state of [26]Mg with the subsequent γ-ray emission observed by the satellite telescopes. The strengths of these [25]Mg(p,γ)[26]Al resonances have been experimentally studied down to an energy of E = 190 keV [21]. Nevertheless, the present uncertainty is insufficient for precise models. At LUNA resonances down to an energy of E = 93 keV are accessible with a largely improved precision compared to previous experiments. In particular, a disagreement between resonance strengths measured by γ-ray spectroscopy and delayed AMS (Accelerator Mass Spectrometry) detection of the [26]Al nuclei after a proton irradiation of [25]Mg target at the relevant energies has been recently reported [22]. The nuclear reaction rate of [24]Mg(p,γ)[25]Al at astrophysical energies has a contribution by a low-energy resonance at E = 214 keV. Moreover, a
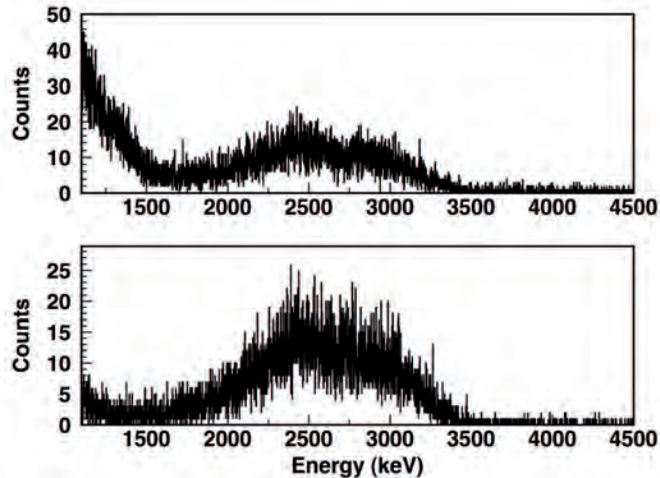
Figure 10: Experimental proton spectra of the $D(d, p)t$ reaction recorded in the silicon detector with $E_\alpha = 330 \ keV$ and two different pressures $P = 0.5$ (top panel) and $1.0 \ mbar$ (bottom panel).

strong direct capture component dominates the resonance contribution. The estimate of the latter contribution is solely based on the experimental data from [23]. Additionally, the E = 214 keV resonance strength carries a large systematic discrepancy between the existing data [24].

At LUNA-400 kV new measurements of the strengths of some resonances in proton captures on Mg isotopes were performed. The resonances were studied using Mg targets with the well known isotopic composition of natural Mg as well as enriched ^{25}Mg target. In order to reduce the systematic uncertainties arising from the detection technique, several independent methods have been used. The absolute value of the resonance strengths were measured with both a high resolution HPGe detector and a high efficiency 4π BGO summing crystal. The latter setup was used also for the low-energy studies.

As an alternative method - only in case of the ^{25}Mg(p,γ)^{26}Al resonance at E = 304 keV - an enriched Mg target was irradiated with a proton beam and after a proper chemical treatment the number of produced ^{26}Al nuclei were counted by means of the AMS (Accelerator Mass Spectrometry) technique, using the CIRCE (Center for Isotopic Research on Cultural and Environmental Heritage) facility in Caserta, Italy.

We have completed the analysis (strengths $\omega\gamma$ and branching ratios) for the E = 214, 304, and 326 keV resonances in the reactions ^{24}Mg(p,γ)^{25}Al, ^{25}Mg(p,γ)^{26}Al, and ^{26}Mg(p,γ)^{27}Al, respectively. These new results together with selected previous work are used to calculate updated recommended values for the resonance strengths. The full results will be published soon [25]. We stress that the new results were obtained from measurements with partly independent approaches, yielding a remarkable agreement among them. Moreover, particular attention was paid to the critical problem of target stoichiometry and its variation under beam bombardment: a severe problem for Mg targets.

The ^{25}Mg(p,γ)^{26}Al resonance strength given by NACRE [1] is basically confirmed

120
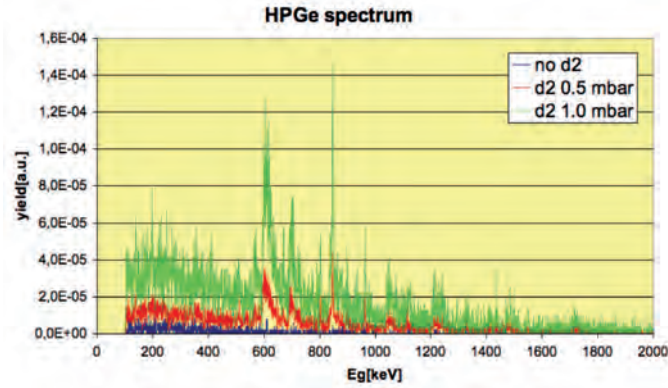
Figure 11: γ-ray spectra of the $D(\alpha,\gamma)^6Li$ reaction recorded at $E_\alpha = 330\ keV$ with a HPGe detector. The blu curve represents a background spectrum with N_2 at $P = 1\ mbar$ in the target. The red curve corresponds to the spectrum at $P_{deuterium} = 0.5\ mbar$, while the green one is the spectrum observed at $P_{deuterium} = 1\ mbar$.

by the present experiment. We suggest to use the NACRE rate until the results for low-energy ^{25}Mg(p,γ)^{26}Al resonances, i.e. the resonances at E = 93 and 190 keV for which the analysis is already far advanced, will be available. However, the uncertainty of the E = 304 keV resonance could be reduced to 4%. This is important since this resonance serves as a normalization for the measurements at low-energies and, thus, those results will benefit strongly from the present work. Furthermore, the primary branching ratios have been measured with high accuracy and the ground state feeding probability could be extracted. The additional AMS measurement based on an irradiation performed simultaneously to a γ-ray detection showed no systematic difference between both detection techniques and is a strong evidence for the internal consistency of the present approach. The case of ^{24}Mg(p,γ)^{25}Al is rather complex. The present recommended $\omega\gamma$ of the lowest resonance in this reaction is lower by more than 10% compared to the latest published measurement [24]. However, a strong direct capture component dominates the resonance contribution and a reanalysis of the reaction at astrophysical energies by using an R-matrix formalism may proof worthwhile. The reaction ^{26}Mg(p,γ)^{27}Al proceeds very fast at all temperatures compared to the other Mg-Al cycle reactions and, therefore, its astrophysical implications are negligible. Nevertheless, an apparent discrepancy in the literature [1] has been solved and the strength of the E = 326 keV ^{26}Mg(p,γ)^{27}Al resonance was measured with a high accuracy.

4 Future measurements: the study of ^{17}O(p,γ)^{18}F and ^{17}O(p,α)^{14}N

The ^{17}O+p thermonuclear reaction rate is of paramount importance for understanding hydrogen burning in a number of different stellar environments, including Red Giants, Massive stars [26], Asymptotic Giant Branch (AGB) stars [27] in the stellar temperature
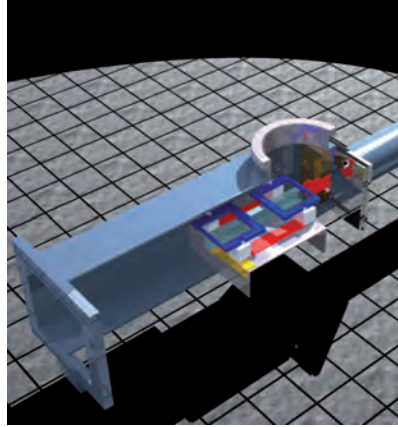
Figure 12: Drawing of the chamber realized at the LNGS mechanical workshop for the $D(\alpha,\gamma)^6Li$ measurement, tested at the end of 2009.

range T=0.03-0.1 GK and Classical Novae [28] in the stellar temperature range T=0.1-0.4 GK. These temperature ranges correspond to Gamow peak energy ranges of 26-140 keV and 70-370 keV, respectively. Moreover, the knowledge of the process $^{17}O(p,\gamma)^{18}F$, followed by the ^{18}F β^+ decay, is related to the ^{19}F production during the AGB phase. The origin of Fluorine is a longstanding problem in nuclear astrophysics. The $^{17}O(p,\gamma)^{18}F$ and $^{17}O(p,\alpha)^{14}N$ reactions have an impact on all these issues governing the destruction of ^{17}O and the production of ^{18}F [28]. As pointed out by [29], varying the $^{17}O(p,\gamma)^{18}F$ and $^{17}O(p,\alpha)^{14}N$ reaction rates within the adopted uncertainty intervals produce a change of the ^{17}O and ^{18}F isotopic abundances by more than a factor 2 in Nova nucleosynthesis.

The ^{18}F energy level scheme is quite complex: the low resonances at $E_{R,lab}$=70 and 193 keV are believed to dominate the Nova energy region. The minimum energy explored up to now in nuclear physics laboratories is well above the region of interest implying that values used in stellar model calculations are based on extrapolations.

The first experimental phase at LUNA will focus on the study of the properties of the γ-cascade and of any possible contaminant reaction (proton captures on ^{11}B, ^{12}C, ^{19}F, ^{23}Na) with a HPGe detector. The second phase will instead use a high efficiency BGO detector to reach the lowest energies, down to E_p=90 keV. At such energy, assuming a target density of 10^{18} atoms/cm^2 and an average current of 200 μA, the counting rate is expected to be about 30 counts/day. The targets will be produced in the LNGS chemistry laboratory by an anodization process of thick tantalum backings in ^{17}O enriched (70%) water. The procedure is well established [30]: stable targets with well defined stoichiometry Ta_2O_5 are expected. Through a variation of the anodizaton voltage different thicknesses can be obtained.

5   List of publications

- *"Direct measurement of the $^{15}N(p,\gamma)^{16}O$ total cross section at nova energies",*

D. Bemmerer, A. Caciolli, R. Bonetti, C. Broggini, F. Confortola , P. Corvisiero , H. Costantini , Z. Elekes, A. Formicola, Zs Fulop, G. Gervino , A. Guglielmetti., C. Gustavino , Gy. Gyurky, M. Junker , B. Limata , M. Marta , R. Menegazzo , P. Prati , V. Roca , C. Rolfs , C. Rossi Alvarez, E. Somorjai and O. Straniero (The LUNA collaboration),
J. Phys. G: Nucl. Part. Phys. 36 (2009) 045202.

- *"Ultra-sensitive in-beam gamma-ray spectroscopy for nuclear astrophysics at LUNA"*, A. Caciolli, L. Agostino, D. Bemmerer, R. Bonetti, C. Broggini, F. Confortola, P. Corvisiero, H. Costantini, Z. Elekes, A. Formicola, Zs. Fulop, G. Gervino, A. Guglielmetti, C. Gustavino, Gy. Gyurky, G. Imbriani, M. Junker, M. Laubenstein, A. Lemut, B. Limata, M. Marta, C. Mazzocchi, R. Menegazzo, P. Prati, V. Roca, C. Rolfs, C. Rossi Alvarez, E. Somorjai, O. Straniero, F. Strieder, F. Terrasi and H. P. Trautvetter,
Eur. Phys. J. A 39 (2009) 179.

6   Conference and seminar contributions

- D. Bemmerer, "Nuclear Physics Underground", invited talk at the VIII Latin American Symposium on Nuclear Physics and Applications, December 2009, Santiago de Chile, Chile.

- D. Bemmerer, "The ^{15}N(p,gamma)^{16}O reaction studied at LUNA", poster at the EPS European Nuclear Physics Conference 2009, March 2009, Bochum, Germany.

- D. Bemmerer, "Sensitive in-beam gamma-ray spectroscopy for nuclear astrophysics at LUNA", poster at the international conference Nuclear Physics in Astrophysics IV, June 2009, Frascati, Italy.

- C. Broggini, "LUNA and the Sun", invited talk at the International Conference Nuclear Structure and Dynamics, May 2009, Dubrovnik, Croatia.

- C. Broggini, "LUNA and the Sun", invited seminar at the International School of Nuclear Physics, 31st course, September 2009, Erice, Italy.

- A. Caciolli, "Study of the ^{15}N(p,γ)^{16}O reaction at the LUNA accelerator with a BGO detector", oral presentation at the international conference Nuclear Physics in Astrophysics IV, June 2009, Frascati, Italy.

- A. Caciolli, "Study of the ^{15}N(p,γ)^{16}O reaction at the LUNA accelerator with a gas target setup", oral presentation at the V European School of Astrophysics of S.Tecla, September 2009, S.Tecla (CT), Italy.

- H. Costantini, "Nuclear Astrophysics at the Gran Sasso Underground Laboratory, oral presentation at the European Nuclear Physics Conference, March 2009, Bochum, Germany.

- H. Costantini, "Nuclear Astrophysics at the Gran Sasso Underground Laboratory, seminar at APC, Paris, France, February 2009.

- H. Costantini, "Nuclear Astrophysics at the Gran Sasso Underground Laboratory, seminar at CPPM, Marseille, France, February 2009.

- Zs. Fulop, "The LUNA experiment: an overview", talk at the VII Tours Symposium on Nuclear Physics and Astrophysics, November 2009, Kobe, Japan.

- Zs. Fulop, "Nuclear Astrophysics at Surface Facilities", invited talk at the Workshop on Nuclear Astrophysics Opportunities at the Underground Laboratory in Canfranc, February 2009, Barcelona, Spain.

- A. Guglielmetti, "Progress of LUNA, invited talk at the international conference Nuclear Physics in Astrophysics IV, June 2009, Frascati, Italy.

- G. Imbriani, "Why to go underground to study the stars", lecture at the V European School of Astrophysics of S.Tecla, September 2009, Santa Tecla (CT), Italy.

- C. Mazzocchi, "Nuclear astrophysics deep underground: the case of the ^{15}N(p,γ)^{16}O reaction at LUNA, oral presentation at the 12th Int. Conf. on Nuclear Reaction Mechanisms, June 2009, Varenna, Italy.

- C. Mazzocchi, "Nuclear astrophysics deep underground: the LUNA experiment, seminar at the Department of Physics and Astronomy, University of Tennessee, Knoxville-TN, USA, August 2009.

- C. Mazzocchi, "Astrofisica nucleare in laboratori sotterranei: l'esperimento luna, seminar at Laboratori Nazionali del Sud, Catania, Italy, July 2009.

- O. Straniero, "Nuclear reactions in stellar interiors" invited talk at the meeting HELAS, Synergies between solar and stellar modelling, June 2009, Rome, Italy.

- F. Strieder, "Direct Measurements of the low energy resonances in ^{25}Mg(p,γ)^{26}Al", oral presentation at the EuNPC Meeting, March 2009, Bochum, Germany.

References

[1] C. Angulo et al., Nucl. Phys. A 656, 3 (1999)

[2] D.F. Hebbard, Nucl. Phys. A 15, 289 (1960)

[3] C. Rolfs and W. Rodney, Nucl. Phys. A 235,450 (1974)

[4] D. Bemmerer et al., J. Phys. G 36, 045202 (2009)

[5] G. Imbriani et al, Eur. Phys. J. A 25 (2005) 455

[6] R.E. Azuma et al., submitted to PRC, 2010.

[7] A.Ordine et al., IEEE Transaction in Nuclear Science 45 No.3, 873 (1998)

[8] C.Rolfs and W.S.Rodney, Cauldrons in the Cosmos (University of Chicago Press, 1988)

[9] A. Lemut, Eur. Phys. J. A36, 233 (2008)

[10] XXVII Meeting of the Gran Sasso Scientific Committee (April 18-19, 2007).

[11] P. D. Serpico et al., JCAP 0412 (2004) 010 [arXiv:astro-ph/0408076].

[12] P. Corvisiero, C. Gustavino and A. Lemut: Report on the $D(\alpha,\gamma)^6Li$ at LUNA.

[13] P. Corvisiero and C. Gustavino: $D(\alpha,\gamma)^6Li$ measurement at LUNA: results of the test performed in March 2009 for the 2010 experiment, July 24th, 2009.

[14] C. Arpesella et al., Nucl. Instr. and Meth in Phys. Res. A360 (1995) 607.

[15] G. F. Knoll, Radiation Detection and Measurement (Third Edition), (Wiley, New York, 2000).

[16] C. Winkler, T.C. Courvoisier, G. Di Cocco et al., A&A, 411 (2003) L1.

[17] R. Diehl et al., Nature 439 (2006) 45.

[18] G.J. Wasserburg, in Protostars and planet II, edited by D.C. Black and M.S. Matthews (Universirty of Arizona Press, Tucson, 1985), p.703.

[19] O. Straniero, R. Gallino, S. Cristallo, Nucl. Phys. A 777 (2006) 311.

[20] E. Carretta et al., Astron. Astroph. 505 (2009) 139.

[21] C. Iliadis et al., Nucl. Phy. A 512 (1990) 509.

[22] A. Arazi et al., Phys. Rev. C 74 (2006) 025802.

[23] H.-P. Trautvetter and C. Rolfs, Nucl. Phys. A 242 (1975) 519.

[24] D.C. Powell et al., Nucl. Phys. A 660 (1999) 349.

[25] The LUNA collaboration, Phys. Rev. C (in preparation, 2010).

[26] R.D. Hoffman et al., Astrophys. J. 549, 1085 (2001)

[27] A. I. Boothroyd et al., Astrophys. J. 430, L77 (1994)

[28] A. Coc et al., Astron. Astrophys. 357, 561 (2000)

[29] C. Iliadis et al., Astrophys. J. Suppl. Ser. 134, 151 (2001)

[30] D. Phillips et al., Nucl. Instr. and Meth. A 135, 389 (1976)

2009 LVD STATUS REPORT

The LVD Collaboration

N.Yu.Agafonova[9], M.Aglietta[14], E.D.Alyea[7], P.Antonioli[1], G.Badino[14], G.Bari[1], M.Basile[1], V.S.Berezinsky[9], M.Bertaina[14], R.Bertoni[14], V.V.Boyarkin[9], A. Bonardi[14], G.Bruni[1], G.Bruno[5], G.Cara Romeo[1], A.Chiavassa[14], J.A.Chinellato[3], L.Cifarelli[1], F.Cindolo[1], A.Contin[1], V.L.Dadykin[9], E.A. Dobrynina[9], L.G.Dos Santos[3], R.I.Enikeev[9], W.Fulgione[14], P.Galeotti[14], M.Garbini[1], P.L.Ghia[5,14], P.Giusti[1], F.Gomez[14], F.Grianti[4], G.Iacobucci[1], E.Kemp[3], E.V.Korolkova[9], V.B.Korchaguin[9], V.V.Kuznetsov[9], M.Luvisetto[1], A.A.Machado[5], A.S.Malgin[9], H.Menghetti[1], N.Mengotti Silva[3], A.Molinario[14], C.Morello[14], R.Nania[1], K.Okei[10], L.Periale[14], R.Persiani[1], A.Pesci[1], P.Picchi[14], I.A.Pless[8], A.Porta[14], A.Romero[14], V.G.Ryasny[9], O.G.Ryazhskaya[9], O.Saavedra[14], K.Saitoh[13], G.Sartorelli[1], M.Selvi[1], N.Taborgna[5], N.Takahashi[12], V.P.Talochkin[9], G.C.Trinchero[14], S.Tsuji[11], A.Turtelli[3], P.Vallania[14], S.Vernetto[14], C.Vigorito[14], L.Votano[4], R.Weinstein[6], M.Widgoff[2], V.F.Yakushev[9], G.T.Zatsepin[9], A.Zichichi[1,*]

[1]University of Bologna and INFN-Bologna, Italy
[2]Brown University, Providence, USA
[3] University of Campinas, Campinas, Brazil
[4] INFN-LNF, Frascati, Italy
[5] INFN-LNGS, Assergi, Italy
[6] University of Houston, Houston, USA
[7] Indiana University, Bloomington, USA
[8] Massachusetts Institute of Technology, Cambridge, USA
[9] Institute for Nuclear Research, Russian Academy of Sciences, Moscow, Russia
[10] Okayama University, Okayama, Japan
[11] Kawasaki Medical School, Kurashiki, Japan
[12] Hirosaki University, Hirosaki, Japan
[13] Ashikaga Institute of Technology, Ashikaga, Japan
[14] IFSI-INAF, Torino; University of Torino and INFN-Torino, Italy

Spokesperson of the LVD experiment

Abstract

The Large Volume Detector (LVD) in the INFN Gran Sasso National Laboratory (LNGS), Italy, is a ν observatory mainly designed to study neutrinos from core collapse supernovae. The experiment has been monitoring the Galaxy since June 1992, under increasing larger configurations: in January 2001 it has reached its final active mass $M = 1$ kt. No burst candidate has been found over 5618 days of livetime, the resulting 90% c.l. upper limit to the rate of gravitational stellar collapses in the Galaxy ($D \leq 20$ kpc) is 0.15 y^{-1}.

Since July 2005 LVD participates to the Supernovae Early Warning System (SNEWS), the network of SN neutrino observatories whose main goal is to provide the astronomical community with a prompt alert for the next galactic core collapse supernova explosion.

Since 2006 LVD acts as a far beam monitor for the Cern Neutrinos to Gran Sasso (CNGS) project, the high energy, wide band ν_μ beam, set up at Cern and sent towards the LNGS.

The study of the seasonal modulation of the cosmic muon flux during 2001-2008 has been completed. An annual modulation with average amplitude 1.5% and maximum intensity in July has been found, in agreement with previous measurements at LNGS.

The low threshold channel of the LVD electronics, dedicated to the detection of gammas from (n,p) capture, is continuously monitored to keep under control the detector performance during long periods allowing to measure the environmental conditions. The analysis of these data during 1997-2009 shows the existence of a seasonal modulation with the maximum occurring at the end of August due to changes of the radon concentration in the experimental hall.

1 The LVD experiment

The Large Volume Detector (LVD), located in the hall A of the INFN Gran Sasso National Laboratory, Italy, consists of 1000 tons of liquid scintillator arranged in a modular geometry. The major purpose of LVD is the search for neutrinos from Gravitational Stellar Collapses (GSC) in our Galaxy [1].

The detector consists of an array of 840 scintillator counters, 1.5 m^3 each. The whole array is divided in three identical "towers" with independent power supply, trigger and data acquisition. In turn, each tower consists of 35 "modules" hosting a cluster of 8 counters. Each counter is viewed from the top by three photomultipliers (PMTs).

The main neutrino reaction in LVD[1] is $\bar{\nu}_e p \rightarrow e^+ n$, which gives two detectable signals: the prompt one, due to the e^+, followed by the signal from the (n,p) capture ($E_\gamma = 2.2$ MeV) with a mean delay of $\simeq 185$ μs.

The trigger logic is optimized for the detection of both products of the inverse beta decay and is based on the three-fold coincidence of the PMTs of a single counter. Each PMT is discriminated at two different thresholds resulting in two possible levels of coincidence between a counter's PMTs: H and L, corresponding to $\mathcal{E}_H \simeq 4$ MeV and $\mathcal{E}_L \simeq 500$ KeV.

---

[1]LVD is also sensitive to $\overset{(-)}{\nu}_i + e^- \rightarrow \overset{(-)}{\nu}_i + e^-$ scattering; $(\nu_e + \bar{\nu}_e)$ c.c. interactions and $\overset{(-)}{\nu}_i$ n.c. interactions with carbon.

The iron support structure of the detector can also act as a target for neutrinos and antineutrinos. The products of the interaction can exit iron and be detected in the liquid scintillator. The amount of neutrino-iron interactions can be as high as about 20% of the total number of interactions.

The signal observable in LVD, in different reactions and due to different kinds of neutrinos, besides providing astrophysical informations on the nature of the collapse, is sensitive to intrinsic ν properties, as oscillation of massive neutrinos and can give an important contribution to define some of the neutrino oscillation properties still missing.
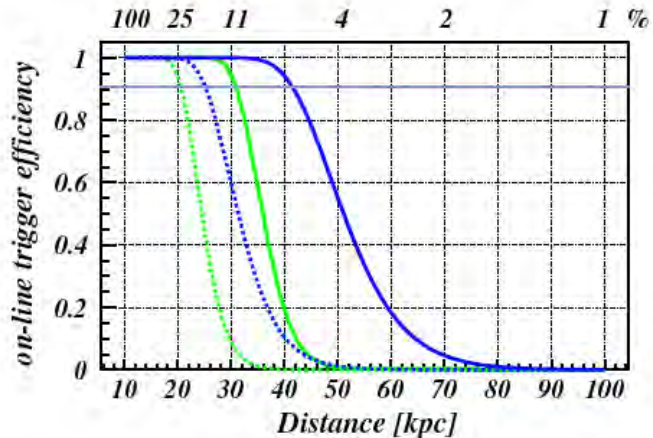
Figure 1: *On-line trigger efficiency versus distance (lower scale) and percentage of SN1987A signal at 10 kpc (upper scale) for E_{cut}=7-10MeV (light green and dark blue lines, respectively) and M=300t (dotted) and 1000t (continuous) for LVD stand alone.*

We have studied [2] how neutrino oscillations affect the signal detected by LVD and also evaluated the impact on the signal of the astrophysical parameters of the supernova explosion mechanism, such as the total energy emitted in neutrinos, the star distance, the neutrino–sphere temperatures and the partition of the energy among the neutrino flavors. However, being aware of the fact that the astrophysical parameters of the supernova mechanism are up to now not well defined, to compute the detector sensitivity expressed in terms of source distance or emitted neutrino flux we adopted the following conservative values for the astrophysical parameters [3], [4]: average $\bar{\nu}_e$ energy $\langle E_{\bar{\nu}_e} \rangle$=14 MeV; total radiated energy $E_b = 2.4 \cdot 10^{53}$ erg and average non-electron neutrino energy 10% higher than $\bar{\nu}_e$ [5].

Concerning neutrino oscillations we conservatively considered normal mass hierarchy. Taking into account Poisson fluctuations in the cluster multiplicity, we derived the trigger efficiency shown in figure 1 as a function of the distance (lower scale) for LVD working stand-alone (the trigger efficiency, as a function of neutrino luminosity in terms of percentage of SN1987A one is shown in the upper scale). The trigger efficiency for LVD working in the SNEWS network [6] is shown in figure 2 [7].
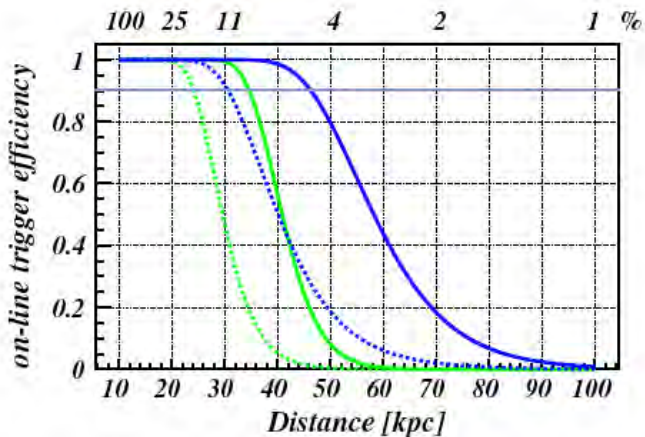

Figure 2: *Same as figure 1 for LVD in the SNEWS.*

2   LVD: experimental activity

2.1   Supernova physics

2.1.1   Monitoring the Galaxy

LVD has been taking data since June 1992 with increasing mass configurations (sensitive mass being always greater than 300 t), enough to monitor the whole Galaxy ($D \leq 20$ kpc)[2]. In figure 3 we show the sensitive mass of the experiment during the period 2001-2009. The LVD duty cycle, in the same period, was greater than 99.5%.

The search for ν burst candidates is performed by studying the temporal sequence of triggers and looking for clusters. Preliminary cuts are applied to reject muons and events with an energy release lower than 7 MeV or higher than 100 MeV. The off-line neutrino burst candidate selection, widely discussed in [9], consists of the analysis of each cluster of triggers of duration up to 200 seconds.
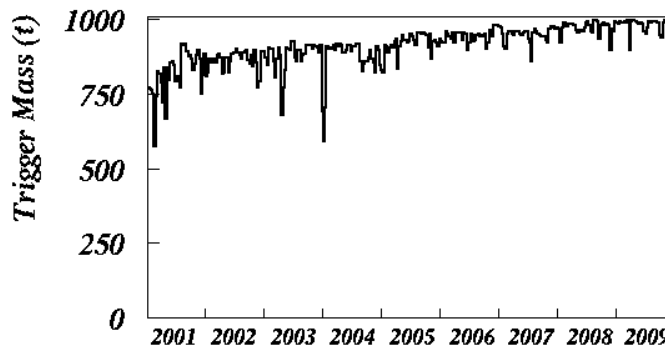
Figure 3: *LVD sensitive mass during 2001-2009.*

For each cluster, with multiplicity m and duration Δt, the imitation frequency F_{im} is calculated as a function of the background rate. After this pure statistical selection a complete analysis of each detected cluster with $F_{im} \leq 1$ y^{-1} is performed, to test its consistency with a ν burst through the study of the topological distribution of pulses inside the detector. Additional information will come from the study of: *a)* the energy spectrum of the events in the cluster; *b)* the time distribution of the events in the cluster and *c)* the time distribution of delayed low energy pulses.

No candidates have been found since 1992, see detail in table 1. Since the LVD sensitivity is higher than expected from GSC models (even if the source is at a distance of 20 kpc and for soft neutrino energy spectra), the resulting 90% c.l. upper limit to the rate of gravitational stellar collapses in the Galaxy ($D \leq 20$ kpc) is 0.15 y^{-1} (to be compared with the result obtained by SuperKamiokande of 0.32 y^{-1} ($D \leq 100$ kpc)[10].

2.1.2   The Supernova On-line Monitor and SNEWS

Since the first, and unique, observation of ν's from gravitational stellar collapse was guided by the optical observation and since the optical observation of a stellar collapse in our Galaxy has a 20% probability, the detector capabilities of identifying a ν burst in the absence of an "external trigger" must be carefully demonstrated. In the presence of an electromagnetic counterpart, on the other hand, the prompt identification of the neutrino

---

[2]The results of this search have been periodically updated and published in the ICRC and Neutrino Conference Proceedings, since 1993 till 2009. [8].

Table 1: LVD run.

Run	start	end	days	up (%)	mass (t)
1	6-6-1992	5-31-1993	285	60	310
2	8-4-1993	3-11-1995	397	74	390
3	3-11-1995	4-30-1997	627	90	400
4	4-30-1997	3-15-1999	685	94	415
5	3-16-1999	12-11-2000	592	95	580
6	12-12-2000	3-24-2003	821	98	842
7	3-25-2003	2-4-2005	666	> 99	881
8	2-4-2005	5-31-2007	846	> 99	936
9	5-31-2007	4-30-2009	669	> 99	967
Σ	6-6-1992	4-30-2009	5618	94	

signal could alert the worldwide network of observatories allowing study of all aspects of the rare event from its onset.

The SNEWS (SuperNova Early Warning System) [6] project is an international collaboration including several experiments sensitive to a core-collapse supernova neutrino signal in the Galaxy and neighbourhood. Its goal is to provide the astronomical community with a prompt and confident alert of the occurrence of a Galactic supernova event, generated by the coincidence of two or more active detectors. In July 2005, after a few years of tuning, the charter members of SNEWS (i.e., LVD, Super-K and SNO[3]) together with the newly joined Amanda/IceCube, started the effective operation of the network, which means that the alert is really sent to the list subscribers, in the case of an at least two-fold coincidence (see *http://snews.bnl.gov* to get your own SN alert !).

Since 2001 a fast and reliable on-line ν-burst monitor has been implemented, the algorithm is based on the search for clusters of triggers within a fixed time window, Δt=20 s. The candidate is simply characterized by its multiplicity m, i.e. the number of pulses detected in Δt. All the other characteristics of the cluster are left to a subsequent independent analysis. The search for burst candidates is performed, on-line, simultaneously for two values of the energy cut: $E_{cut} = 7$ MeV ($f_{bk} = 0.2$ Hz) and $E_{cut} = 10$ MeV ($f_{bk} = 0.03$ Hz). The chosen imitation frequencies, F_{im}, below which the detected cluster will be an on-line candidate supernova event, is 1 per 100 year working stand-alone while it is relaxed to 1 per month working in coincidence with other detectors (SNEWS), and 1 per day for monitoring task. The corresponding detection efficiency are shown in figure 1 and 2, details are discussed in [7].

2.2 CNGS beam monitor

The Cern Neutrinos to Gran Sasso (CNGS) project is a high energy, wide band ν_{μ} beam set up at Cern and sent towards the LNGS. Its main goal is the observation of the ν_{τ}

---

[3]At present the SNO experiment is stopped and decommissioned.

appearance, through neutrino flavour oscillation. As shown in [11], due to its large area and active mass, LVD can act as a beam monitor, detecting the interaction of neutrinos inside the detector and the muons generated by the ν interaction in the rock upstream the detector. The monitor capabilities have been confirmed during the first CNGS run in August 2006 [12], fall 2007 and 2008 [13].

2.2.1 MC simulation of the expected events

The CNGS events in LVD can be subdivided into two main categories:

- ν_μ charged current (CC) interactions in the rock upstream the LNGS; they produce a muon that can reach LVD and be detected,

- ν_μ CC and neutral current (NC) interactions in the material (liquid scintillator and iron of the support structure) of LVD.

A full Montecarlo simulation has been developed including the generation of the neutrino interaction products, the propagation of the muon in the Gran Sasso rock and the response of the LVD detector. The details of the simulation are described in [11]. The resulting number of expected events, at the nominal intensity $4.5 \; 10^{19}$ p.o.t./y is 33400/y, equivalent to $7.422 \; 10^{-16}$ events per p.o.t. (considering 200 effective days per year it corresponds to ~ 165 CNGS events per day): 78% are muons from the rock, 17% are CC interactions in the detector and 5% are NC.

2.2.2 CNGS detected events

The LVD events are filtered using a very loose selection cut: we require to have at least one scintillation counter with an energy release larger that 100 MeV. The resulting rate is quite stable, with an average value of about 0.13 Hz, and it is mainly due to cosmic muon events.

Among this sample the selection criteria is based on the coincidence of the LVD event time with the beam spill time written in the DB: we search for the CNGS events in the interval $[-15, +25]$ μs around the start time of the beam spill. An example of this distribution, corresponding to the data collected during 2008, is shown in figure 4: it reflects the 10.5 μs width of the beam spill.In figure 5 we show the comparison between the expected and detected event rate per each day of data acquisition in 2009.
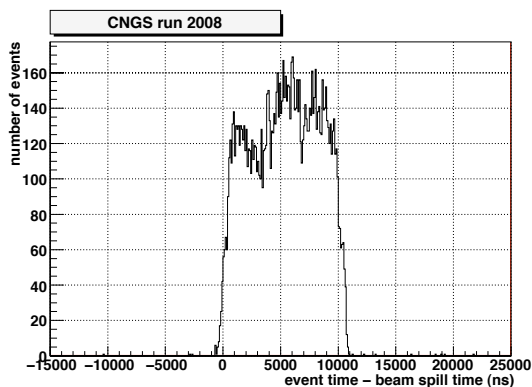
Figure 4: *Distribution of the detection time of the CNGS events, with respect to the initial time of the beam spill.*
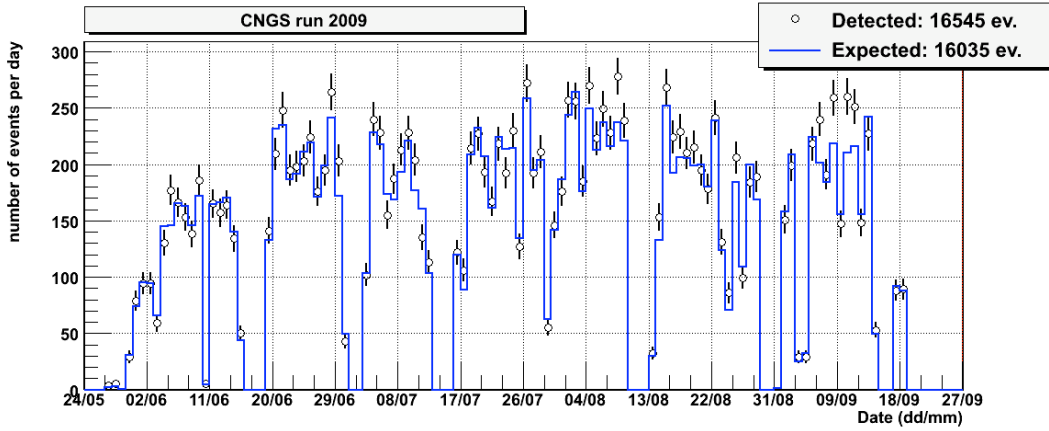
Figure 5: *Number of events per day: observed (black circles) and expected (blue line).*

The background, estimated considering: the 0.13 Hz rate of events among which the CNGS events are searched for, the time window around the beam spill time, 40 μs wide, and the number of useful spills in the DB, is practically negligible.

3 Other Topics

During 2009 we have completed the following studies:

3.1 Analysis of the seasonal modulation of the cosmic muon flux

It is well known that the flux of cosmic muons underground is related to the temperature of the Earth atmosphere (the higher the temperature, the higher the muon flux underground) because the change in the air density implies a variation in the decay and interaction rate of the parent mesons. Typically, in the boreal hemisphere, the muon flux reach the maximum in July and the minimum in January. This effect has been previously measured by various experiments deep underground: MACRO [14], AMANDA [15] and MINOS [16], however their data cover respectively 4, 1 and 3 years. In this work we have analyzed the whole available data set with the detector in its final configuration, starting in January 2001 and ending in December 2008. The LVD geometrical acceptance (averaged over the cosmic muon arrival directions in the LNGS) is A = (298 ± 3) m^2, the number of detected muons per day is of the order of ~ 8000 (~ 0.1 Hz). The total number of muons in the full data is about 21.5 millions. The muon intensity measured day by day since 2001 till 2008 is shown in figure 6. A modulation is clearly visible; fitting the distribution with the following function:
$I^\mu = I_0^\mu + \delta I^\mu \ cos \left(\frac{2\pi}{T} \cdot (t - t_0) \right)$
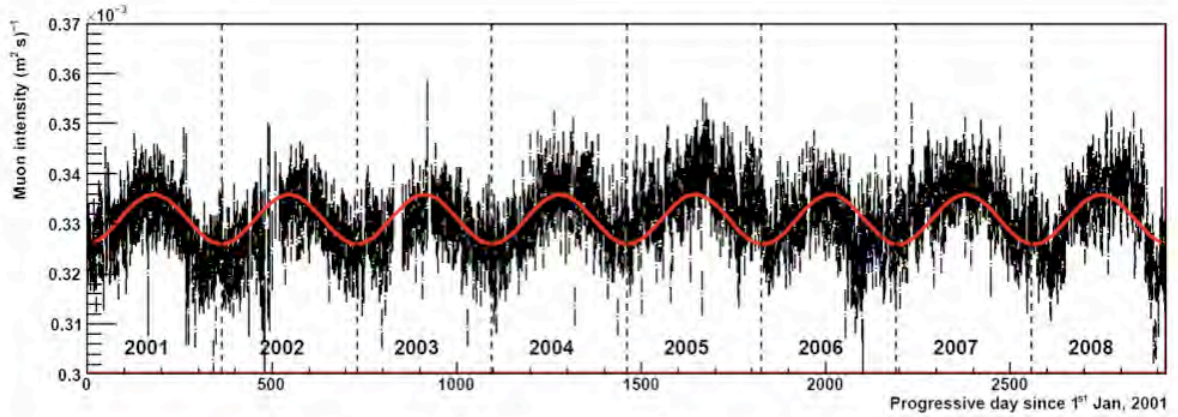
Figure 6: *Muon intensity along the 8 years of data acquisition. Each bin corresponds to one day, starting from 1st January, 2001 to 31st December, 2008. The error bars are the statistical uncertainty. The solid red curve is the result of a cosinusoidal fit to the data. The vertical dashed lines separate each solar year.*

we obtain an average intensity $I_0^\mu = (3.31 \pm 0.03)\ 10^{-4}\ (\mathrm{m}^2\ \mathrm{s})^{-1}$ and a period T = (367 $\pm$ 15) days, i. e., compatible with one year.

The amplitude of the modulation δI^μ and the phase t_0 are better evaluated projecting and averaging the results of the eight years of analysis into one single year, as shown in figure 7. We obtain, fitting again with fixed period T = 1 year, $\delta I^\mu = (5.0 \pm 0.2)\ 10^{-6}\ (\mathrm{m}^2\ \mathrm{s})^{-1}$, corresponding to 1.5%. The phase is $t_0 = (185 \pm 15)$ days, corresponding to a maximum intensity at the beginning of July and the minimum at the beginning of January.

These results have been presented at the last International Cosmic Ray Conference [26]. The analysis of the direct correlation of the daily muon intensity in LVD with the atmosphere temperature, to calculate the temperature coefficient, is ongoing and will be published in a separate work.
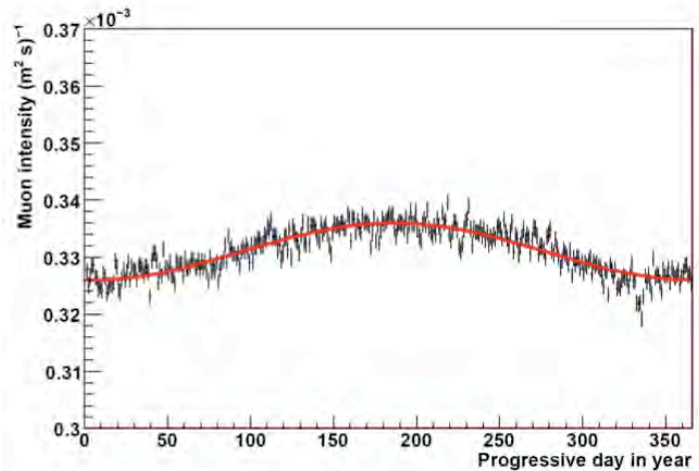
Figure 7: *Superposition of the mean daily intensity for the averaged total data set 2001-2008 into one year.*

134

3.2 Long-term study of low energy counting rate

Neutrinos interact in scintillator mainly trough inverse beta decay (IBD) reaction: $\bar{\nu}_e p \to e^+ n$. In LVD signals coming from each pmt are discriminated at two different thresholds (L and H), corresponding to the energies $\mathcal{E}_L \simeq 0.5$MeV and $\mathcal{E}_H \simeq 4$MeV. The H three-fold coincidence of the PMTs of any counter represents the scintillator trigger condition and enable the L coincidence channel that allows the detection of the signal due to np,d gamma capture, whose time delay is 185±5 μs.

The single counter rate at the low energy threshold (LTCR) is measured by a system of 840 scalers enabled, every 10 min for 10 s, by a dedicated trigger, designed for monitoring purpose.

The rate per counter is around 50 Hz, and it is mainly due to gammas from rock radioactivity and decays of radon products. To study the long-term behavior of the low-energy counting rate we consider scaler data between 1997 and 2009. We limit the analysis to counters that shows a stable behavior versus time. The definition of stability is based on the counting rate deviation from its average. The LTCR time series obtained averaging the contribution of a subset of selected counters is shown in figure 8. The selection is updated every two years and the subset is never smaller than 50 tanks.

Each peak of fig. 8 shows a well structured shape if observed in detail. An example is reported in fig. 9 where the behavior of the counting rate (black-thick line) in 5 days in 2008 is shown, together with data recorded by an alpha radon-meter (green-light line) located just inside the LVD experiment.In this particular case the increase observed is due to a scheduled switch off of the ventilation system. The LTCR and radon-meter series are clearly correlated as we have already demonstrated in [19].
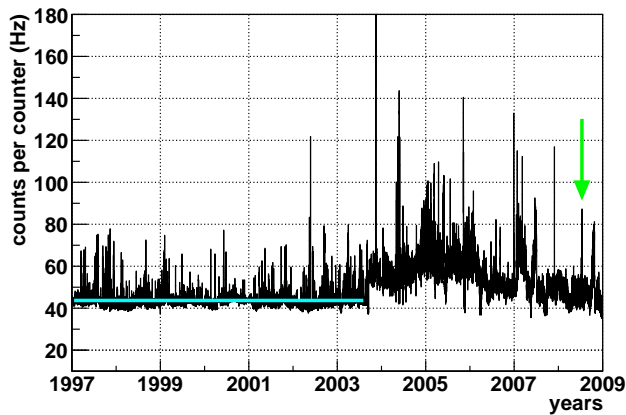
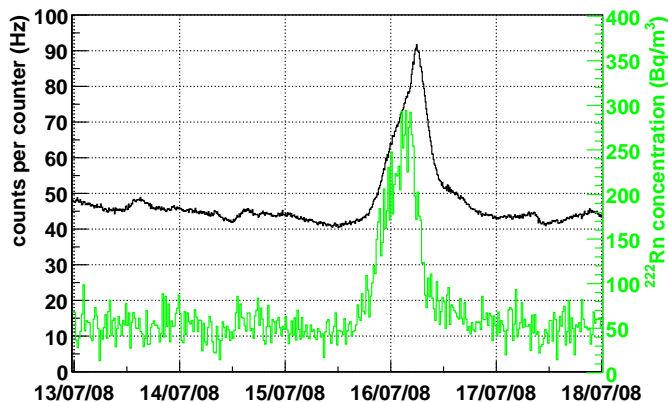Figure 8: *Average LTCR collected in the period 1997-2009.*

Figure 9: *Average LTCR (black-thick line) since July 13th to 18th, 2008, compared with the radon-meter data (green-light line).*

As highlighted by other authors [20], the radon concentration in the laboratory strongly depends on the conditions of the ventilation system. The change in the average counting rate visible in fig. 8, just before the beginning of the 2004, is related to modifications of the ventilation system. Mean value and weekly behavior of LTCR are influenced by these change as shown in figure 10 and 11.

The visible pattern is well explained by the anti-correlation between pressure and radon emanation from rock in caves [21]: in the LVD hall the pressure changes due to the opening/closing of the main entrance door in correlation with the start/end of human working activity. The opposite behavior between fig. 10 and 11 is due to an inversion of the pressure gradient between inside and outside the hall A.
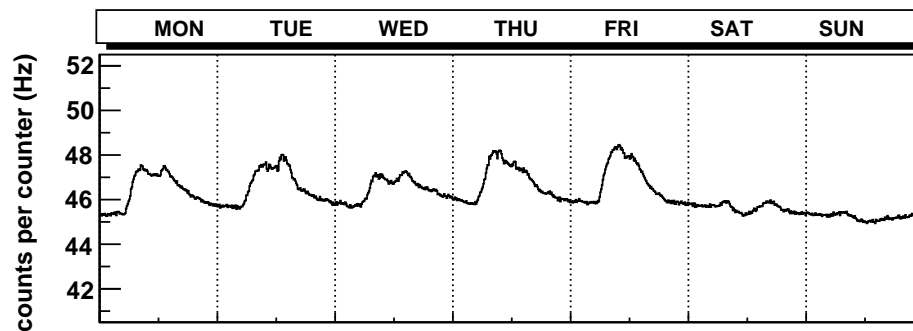
Figure 10: *Average counting rate on a weekly time-base during: 2001-2002.*
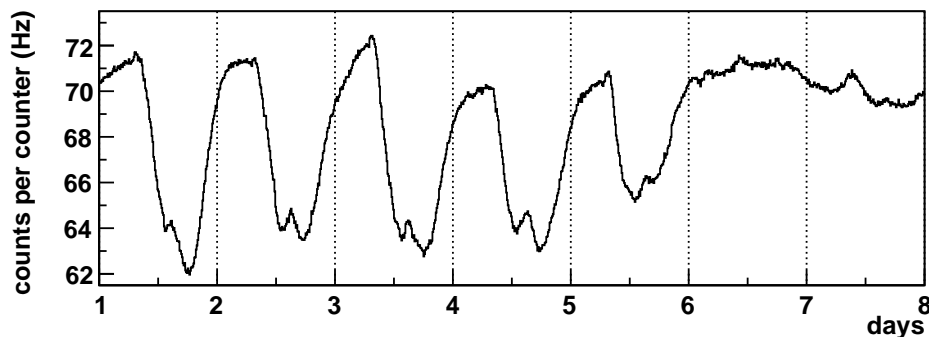
Figure 11: *Average counting rate on a weekly time-base during: 2004-2005.*
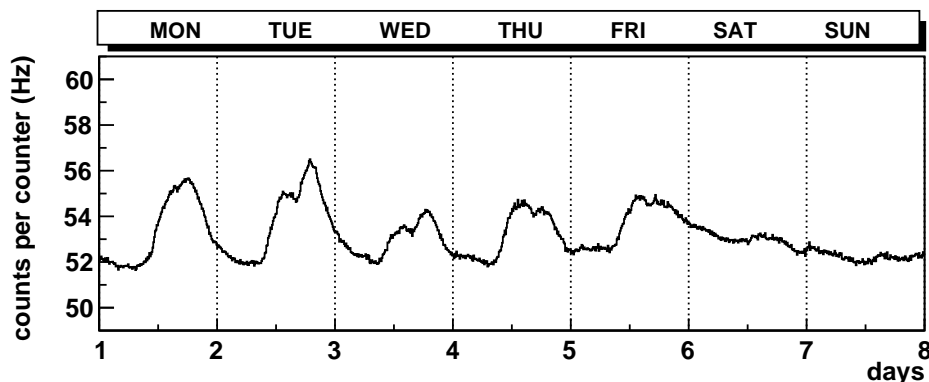
Figure 12: *Average counting rate on a weekly time-base currently up to april 2009.*

Indeed, during 2004-2005, the ventilation system was configured to maintain hall A de-pressurized assuring air re-circulation between the experimental halls and then ejecting outside the laboratory hot air through an extractor located on the northern side of the hall A [22]. From fig. 12 we can argue that at present the environmental conditions of the Hall A are returned to their original conditions.
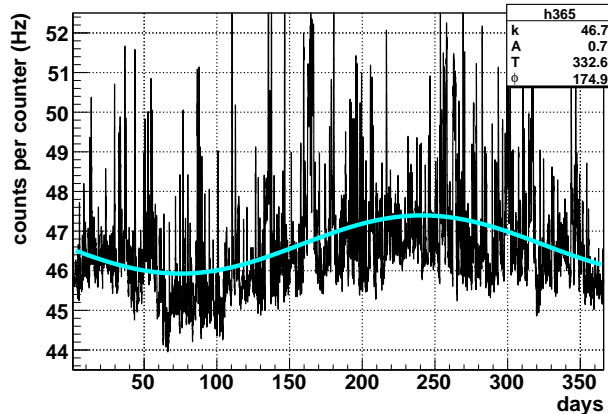
To study long-term modulations in the counting rate, we limit ourselves to the period up to beginning of 2003, when the counting rate was more homogeneous. The analysis is carried out applying Discrete Fourier Transform (DFT) algorithm and the obtained power spectrum shows evidence of a seasonal variation.

To better visualize the modulation we plot in figure 13 the yearly rate averaged over 6 years. The seasonal modulation shows the maximum at day 241±32, corresponding to the end of August. The phase of this modulation is consistent with the one found by the analysis of data from the radon-meter located inside LVD, see figure 14. The details of this analysis are discussed in [23].

Figure 13: *Yearly LTCR averaged over 6 years (1997-2002) and fitted with the function $k + A \cdot sin(\frac{2\pi}{T}(x + \phi))$.*
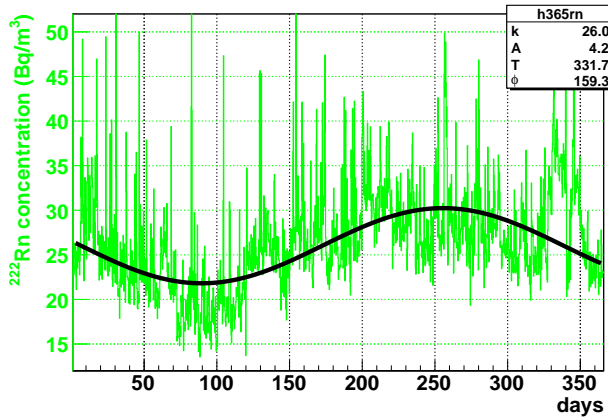
Figure 14: *Yearly Rn concentration (B) averaged over 6 years (1997-2002) and fitted with the function $k + A \cdot sin(\frac{2\pi}{T}(x + \phi))$.*

4   R&D

During the last years we have investigated possible upgrades of the detector. In particular we studied:

- the possibility to improve the detector capability in distinguish different neutrino interactions by adding Gd to the liquid scintillator;

- the performance of the LVD detector as a powerful active shielding and veto with respect to an internal region that we call 'Core Facility'.

4.1 Gd doped scintillator

Doping the liquid scintillator with a small ($\sim 0.15\%$ in weight) quantity of Gd definitely improves the performance of the LVD tank in the neutron detection, because Gd has a huge cross section for n-capture due, essentially, to the two isotopes ^{155}Gd and ^{157}Gd; in particular the mean n-capture time results highly shortened. It can be seen that, for the quoted Gd concentration, the mean n-capture time results $\tau_n < 23\mu$s, 8 times shorter than the one obtained with undoped liquid scintillator. These results have been obtained by a set of experiments described in [24].

On the other hand, the maximum achievable n-capture detection efficiency, that in the standard LVD tank, operated with the present electronics, is 60%, becomes η_n=79.0±1.5%. Moreover n-captures on Gd generate a gamma cascade up to about 8 MeV to be compared with 2.23 MeV of gamma quanta from (n,p) captures. Accordingly, doping with Gd the LVD liquid scintillator, we could increase the signal to noise ratio of a factor of several hundreds maintaining the present neutron capture detection efficiency, simply increasing the energy threshold for neutron detection and shortening the time window for the coincidence.

However Gd doped liquid scintillators showed, in the past, a degradation of the light transmittance that makes necessary a survey over numerous doped counters.

4.2 The LVD Core Facility

It is well known that the muon-induced fast neutrons limit the possibility of searches for rare events, like neutrinoless double beta decay or WIMP dark matter interactions. Underground laboratories provide the overburden necessary to reduce this background, by attenuating cosmic-ray muons and their progenies. If the depth of the underground laboratory is not enough to reach the necessary background reduction, the fast neutron flux can be shielded and/or actively vetoed.

An inner region inside the LVD structure ("LVD Core Facility") has been identified with a volume of about 30 m^3: its realization causes a negligible impact on LVD operation and sensitive mass. The LVD Core Facility could be effectively exploited by a compact experiment for the search of rare events, such as double beta decay or dark matter [25]. We have evaluated the shielding power of LVD working both as an active veto for muons that generate high energy neutrons, and as a passive shield and moderator for the low energy gamma and neutron background. From the results of a dedicated simulation [26] it appears that, with LVD behaving as a muon veto, the flux of high energy un-vetoed neutrons at the surface of the core facility is reduced by a factor 50, that is equivalent to the muon-induced neutron flux at the equivalent vertical depth of 6 km w.e (i.e. the Sudbury mine).

Concerning low energy gamma and neutron background, a set of measurements have been performed inside and outside the LVD structure showing that the radioactive contamination, in the core facility, is reduced by more than a factor of 10, see figure 15 [27].
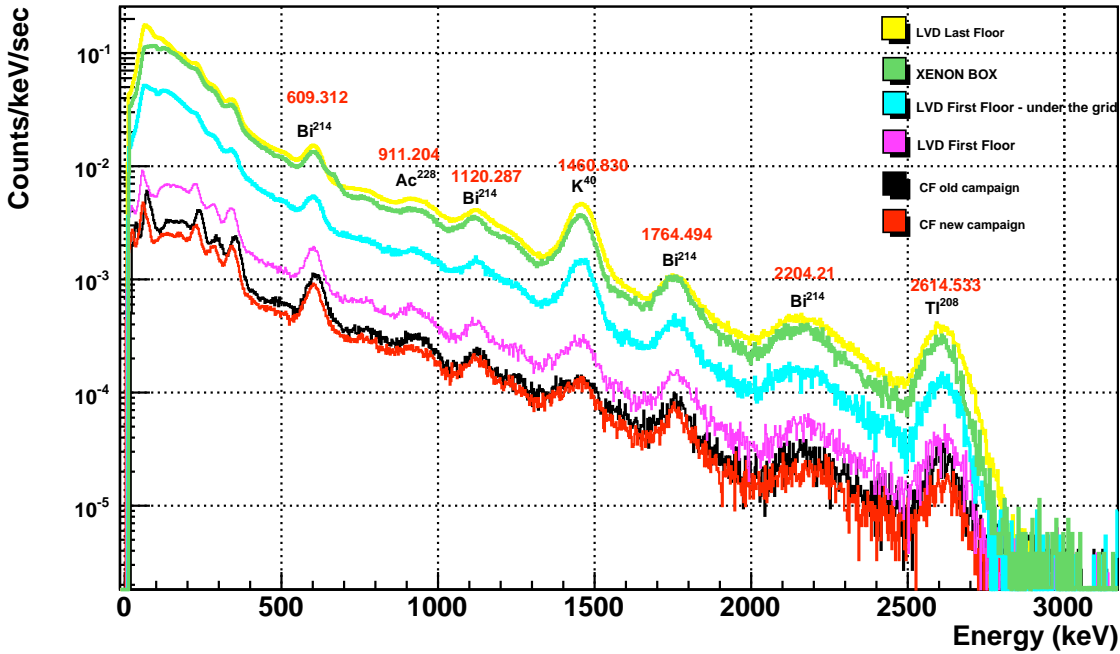
Figure 15: Gamma spectra measured in different places inside the LNGS. Hall A outside the LVD structure (yellow), LVD Core Facility (Black).

5   List of publications in 2009

- *Search for neutrino bursts with LVD detector at Gran Sasso national laboratory*
  C.Vigorito et al., (LVD Collaboration), Proceedings of the 31st ICRC (2009)

- *Analysis of the seasonal modulation of the cosmic muon flux in the LVD detector during 2001-2008.*
  M.Selvi for the LVD Collaboration, Proceedings of the 31st ICRC (2009)

- *The μ^+/μ^- Ratio at the Depth of 3000 m w.e.*
  N.Yu. Agafonova et al., (LVD Collaboration), Proceedings of the 31st ICRC (2009)

- *Long-term study of low energy counting rate with the Large Volume Detector.*
  G.Bruno for the LVD Collaboration, Proceedings of TAUP2009 (Roma)

Acknowledgements

References

[1] LVD Collaboration, Il Nuovo Cimento **A105** (1992) 1793

[2] N. Yu. Agafonova *et al.*, *Study of the effect of neutrino oscillations on the supernova neutrino signal in the LVD detector*, Astropart. Phys. **27**, 254-270 (2007) [arXiv: hep-ph/0609305].

[3] G. Pagliaroli, F. Vissani, M. L. Costantini, and A. Ianni, Astropart. Phys. **31**, 163 (2009)

[4] M.L. Costantini, A. Ianni and F. Vissani, Phys. Rev. D **70** (2004) 043006.

[5] M.T.Keil, G.G.Raffelt and H.T.Janka, Astrophys. J. **590** (2003) 971.

[6] P. Antonioli *et al.*, New Journal of Physics **6** (2004) 114; http://hep.bu.edu/∼snnet/

[7] N. Yu. Agafonova *et al.*, *On-line recognition of supernova neutrino bursts in the LVD detector*, Astropart. Phys. **28**, 516-522 (2008) [arXiv:0710.0259].

[8] LVD Collaboration, Proceedings of the 31st ICRC, 2009 and reference therein.

[9] W.Fulgione, N.Mengotti-Silva, L.Panaro NIM A 368 (1996)

[10] M.Ikeda *et al.*, The Astrophysical Journal, 669:519-524, 2007

[11] M. Aglietta et al., *CNGS beam monitor with the LVD detector*, Nuclear Instruments and Methods in Physics Research **A 516**, 96 (2004).

[12] N. Yu. Agafonova et al., *First CNGS events detected by LVD*, Eur. Phys. J. **C 52**, 849-855 (2007) [arXiv:0710.1536 hep-ex].

[13] N. Yu. Agafonova et al., *The Large Volume Detector*, in the 2007 and 2008 LNGS Annual Report, p. 114 (2007).

[14] M. Ambrosio et al. (MACRO collaboration), Astrop. Phys, **24** (1997) 109.

[15] A. Bouchta et al. (AMANDA collaboration), Proceedings of the 26th ICRC (1999) HE.3.2.11

[16] E. W. Grashorn et al. (MINOS collaboration), Proceedings of the 30th ICRC (2007) [arXiv: 0710.1616]

[17] M.Selvi et al. (LVD Collaboration) Proceedings of the 31st ICRC (2009)

[18] A Bettini 2008 *J. Phys.: Conf. Series* **120** 082001

[19] G Bruno, H Menghetti et al. (LVD Collaboration) 2006 *J. Phys.: Conf. Series* **39** 278-280

[20] A Bassignani et al. 1995 *Radiation Measurements* **Vol. 25** Nos 1-4, pp.557-560

[21] *Radon Measurements By Etched Track Detectors*, Saeed A Durrani & Radomir Ilic

[22] Ing. D. Franciotti, Private communication

[23] G.Bruno et al. (LVD Collaboration) Proceedings of TAUP2009 (Roma) in press

[24] I.R. Barabanov et al., e-Print: arXiv:0803.1577 [physics.ins-det]

[25] F.Arneodo and W.Fulgione JCAP02(2009)028

[26] M.Selvi et al., IDM 2008: 7th International Workshop on the Identification of Dark Matter 2008, Stockholm, Sweden, 18-22 Aug 2008. e-Print: arXiv:0811.2884 [hep-ex]

[27] F. Arneodo, G. Bruno, S. Fattori and W. Fulgione, LNGS preprint, LNGS-EXP-02-08 (2008).

OPERA

N. Agafonova[1], A. Anokhina[2], S. Aoki[3], A. Ariga[4], T. Ariga[4], L. Arrabito[5], D. Autiero[5], A. Badertscher[6], A. Bagulya[7], F. Bersani Greggio[17], A. Bertolin[9], M. Besnier[10], D. Bick[11], V. Boyarkin[1], C. Bozza[12], T. Brugière[5], R. Brugnera[13,9], G. Brunetti[14,15], S. Buontempo[16], E. Carrara[13,9], A. Cazes[5], L. Chaussard[5], M. Chernyavsky[7], V. Chiarella[17], N. Chon-Sen[18], A. Chukanov[16], M. Cozzi[14], G. D'Amato[12], F. Dal Corso[9], N. D'Ambrosio[19], G. De Lellis[20,16], Y. Déclais[5], M. De Serio[21], F. Di Capua[16], D. Di Ferdinando[15], A. Di Giovanni[22], N. Di Marco[22], C. Di Troia[17], S. Dmitrievski[23], A. Dominjon[5], M. Dracos[18], D. Duchesneau[10], S. Dusini[9], J. Ebert[11], O. Egorov[24], R. Enikeev[1], A. Ereditato[4], L. S. Esposito[19], J. Favier[10], G. Felici[17], T. Ferber[11], R. Fini[21], D. Frekers[25], T. Fukuda[8], C. Fukushima[26], V. I. Galkin[2], V. A. Galkin[27], A. Garfagnini[13,9], G. Giacomelli[14,15], M. Giorgini[14,15], C. Goellnitz[11], T. Goeltzenlichter[18], J. Goldberg[28], D. Golubkov[24], Y. Gornoushkin[23], G. Grella[12], F. Grianti[17], M. Guler[29], C. Gustavino[19], C. Hagner[11], T. Hara[3], M. Hierholzer[30], K. Hoshino[8], M. Ieva[21], K. Jakovcic[31], B. Janutta[11], C. Jollet[18], F. Juget[4], M. Kazuyama[8], S. H. Kim[35], M. Kimura[26], B. Klicek[31], J. Knuesel[4], K. Kodama[32], D. Kolev[33], M. Komatsu[8], U. Kose[29], A. Krasnoperov[23], I. Kreslo[4], Z. Krumstein[23], V.V. Kutsenov[1], V.A. Kuznetsov[1], I. Laktineh[5], C. Lazzaro[6], J. Lenkeit[11], A. Ljubicic[31], A. Longhin[13], G. Lutter[4], A. Malgin[1], K. Manai[5], G. Mandrioli[15], A. Marotta[16], J. Marteau[5], V. Matveev[1], N. Mauri[14,15], F. Meisel[4], A. Meregaglia[18], M. Messina[4], P. Migliozzi[16], P. Monacelli[22], K. Morishima[8], U. Moser[4], M. T. Muciaccia[34,21], N. Naganawa[8], M. Nakamura[8], T. Nakano[8], V. Nikitina[2], K. Niwa[8], Y. Nonoyama[8], A. Nozdrin[23], S. Ogawa[26], A. Olchevski[23], G. Orlova[7], V. Osedlo[2], D. Ossetski[27], M. Paniccia[17], A. Paoloni[17], B. D Park[8], I. G. Park[35], A. Pastore[34,21], L. Patrizii[15], E. Pennacchio[5], H. Pessard[10], V. Pilipenko[25], C. Pistillo[4], N. Polukhina[7], M. Pozzato[14,15], K. Pretzl[4], P. Publichenko[2], F. Pupilli[22], R. Rescigno[12], D. Rizhikov[27], T. Roganova[2], G. Romano[12], G. Rosa[36], I. Rostovtseva[24], A. Rubbia[6], A. Russo[20,16], V. Ryasny[1], O. Ryazhskaya[1], A. Sadovski[23], O. Sato[8], Y. Sato[37], V. Saveliev[27], A. Schembri[36], W. Schmidt Parzefall[11], H. Schroeder[30], H. U. Schütz[4], J. Schuler[18], L. Scotto Lavina[16], H. Shibuya[26], S. Simone[34,21], M. Sioli[14.15], C. Sirignano[12], G. Sirri[15], J. S. Song[35], M. Spinetti[17], L. Stanco[13], N. Starkov[7], M. Stipcevic[31], T. Strauss[6], P. Strolin[20,16], V. Sugonyaev[13], S. Takahashi[8], V. Tereschenko[23], F. Terranova[17], I. Tezuka[37], V. Tioukov[16], P. Tolun[29], V. Tsarev[7], R. Tsenov[33], S. Tufanli[29], N. Ushida[32], V. Verguilov[33], P. Vilain[38], M. Vladimirov[7], L. Votano[17], J. L. Vuilleumier[4], G. Wilquet[38], B. Wonsak[11] V. Yakushev[1], C. S. Yoon[35], Y. Zaitsev[24], A. Zghiche[10], and R. Zimmermann[11].

1. INR-Institute for Nuclear Research of the Russian Academy of Sciences, RUS-117312 Moscow, Russia
2. SINP MSU-Skobeltsyn Institute of Nuclear Physics of Moscow State University, RUS-119992 Moscow, Russia
3. Kobe University, J-657-8501 Kobe, Japan
4. Centre for Research and Education in Fundamental Physics, Laboratory for High Energy Physics (LHEP), University of Bern, CH-3012 Bern, Switzerland
5. IPNL, Université Claude Bernard Lyon 1, CNRS/IN2P3, F-69622 Villeurbanne, France
6. ETH Zurich, Institute for Particle Physics, CH-8093 Zurich, Switzerland
7. LPI-Lebedev Physical Institute of the Russian Academy of Sciences, RUS-117924 Moscow, Russia
8. Nagoya University, J-464-8602 Nagoya, Japan
9. INFN Sezione di Padova, I-35131 Padova, Italy
10. LAPP, Université de Savoie, CNRS/IN2P3, F-74941 Annecy-le-Vieux, France
11. Hamburg University, D-22761 Hamburg, Germany
12. Dipartimento di Fisica dell'Università di Salerno and INFN, I-84084 Fisciano, Salerno, Italy
13. Dipartimento di Fisica dell'Università di Padova, I-35131 Padova, Italy
14. Dipartimento di Fisica dell'Università di Bologna, I-40127 Bologna, Italy
15. INFN Sezione di Bologna, I-40127 Bologna, Italy
16. INFN Sezione di Napoli, 80125 Napoli, Italy
17. INFN - Laboratori Nazionali di Frascati dell'INFN, I-00044 Frascati (Roma), Italy
18. IPHC, Université de Strasbourg, CNRS/IN2P3, F-67037 Strasbourg, France
19. INFN - Laboratori Nazionali del Gran Sasso, I-67010 Assergi (L'Aquila), Italy
20. Dipartimento di Fisica dell'Università Federico II di Napoli, 80125 Napoli, Italy
21. INFN Sezione di Bari, I-70126 Bari, Italy
22. Dipartimento di Fisica dell'Università dell'Aquila and INFN, I-67100 L'Aquila, Italy
23. JINR-Joint Institute for Nuclear Research, RUS-141980 Dubna, Russia
24. ITEP-Institute for Theoretical and Experimental Physics, RUS-117259 Moscow, Russia
25. University of Münster, D-48149 Münster, Germany
26. Toho University, J-274-8510 Funabashi, Japan
27. Obninsk State University, Institute of Nuclear Power Engineering, RUS-249020 Obninsk, Russia
28. Department of Physics, Technion, IL-32000 Haifa, Israel
29. METU-Middle East Technical University, TR-06531 Ankara, Turkey
30. Fachbereich Physik der Universität Rostock, D-18051 Rostock, Germany
31. IRB-Rudjer Boskovic Institute, HR-10002 Zagreb, Croatia
32. Aichi University of Education, J-448-8542 Kariya (Aichi-Ken), Japan
33. Faculty of Physics, Sofia University "St. Kliment Ohridski", BG-1000 Sofia, Bulgaria
34. Dipartimento di Fisica dell'Università di Bari, I-70126 Bari, Italy
35. Gyeongsang National University, 900 Gazwa-dong, Jinju 660-300, Korea
36. Dipartimento di Fisica dell'Università di Roma "La Sapienza" and INFN, I-00185 Roma, Italy
37. Utsunomiya University, J-321-8505 Tochigi-Ken, Utsunomiya, Japan
38. IIHE, Université Libre de Bruxelles, B-1050 Brussels, Belgium

Abstract

The OPERA neutrino detector at the underground Gran Sasso Laboratory (LNGS) was designed to perform the first detection of neutrino oscillations in appearance mode through the study of $\nu_\mu \to \nu_\tau$ oscillations. The apparatus consists of a lead/emulsion-film target complemented by electronic detectors. It is placed in the high-energy long-baseline CERN to LNGS beam (CNGS) 730 km away from the neutrino source. Runs with CNGS neutrinos were successfully conducted in 2007 and 2008 for a total luminosity of 1.864×10^{19} p.o.t. (*proton on target*). In 2009 a new CNGS run has been conducted, from the end of May till November 23rd. The total collected luminosity in 2009 has been of 3.522×10^{19} p.o.t. After a brief

description of the beam and of the experimental apparatus we report on the first data and related analysis results.

1   Introduction

The solution of the long-standing solar and atmospheric neutrino puzzles has come from the hypothesis of neutrino oscillations. This implies that neutrinos have non vanishing and non-degenerate mass eigenstates, and that their flavor eigenstates involved in weak interaction processes are a superposition of the mass eigenstates.

Several experiments carried on in the last decades with solar and reactor neutrinos, as well as with atmospheric and accelerator neutrinos, contributed to build-up our present understanding of neutrino mixing. Atmospheric neutrino oscillations have been studied mainly by the Kamiokande, MACRO, Super-Kamiokande and SOUDAN2 experiments. Long baseline experiments with accelerator neutrinos (K2K and MINOS) confirmed the oscillation scenario first pointed out by the Super-Kamiokande experiment supporting the $\nu_\mu \to \nu_\tau$ oscillation channel for atmospheric neutrinos, while the CHOOZ and Palo Verde reactor experiments excluded the $\nu_\mu \to \nu_e$ channel as the dominant one.

However, the direct appearance of a different neutrino flavor is still an important open issue. This is the main goal of the OPERA experiment [1, 2] that uses the long baseline (L=730 km) CNGS neutrino beam from CERN to LNGS. The challenge of the experiment is to measure the appearance of ν_τ from ν_μ oscillations in an almost pure muon-neutrino beam. This requires the detection of the short-lived τ lepton ($c\tau = 87.11$ μm) produced in the charged-current interaction of a ν_τ. This sets two conflicting requirements: a large target mass needed to have sufficient statistics and an extremely high accuracy detector technique to observe the short-lived τ lepton.

The τ is identified by the detection of its characteristic decay topologies either in one prong (electron, muon or hadron) or in three prongs. The τ track is measured with a large-mass active target made of 1 mm thick lead plates (target mass and absorber material) inter-spaced with thin nuclear emulsion films (high-accuracy tracking devices). This detector is historically called Emulsion Cloud Chamber (ECC). Among past applications it was successfully used in the DONUT experiment for the first direct observation of the ν_τ.

The OPERA detector [2] is made of two identical Super Modules (SM) each consisting of a target section of about 625 tons made of lead/emulsion-film ECC modules (hereafter called "bricks"), of a scintillator tracker detector (TT) needed to trigger the read-out and pre-localize neutrino interactions within the target, and of a muon spectrometer (Figure 1). A single SM has longitudinal dimensions of about 10 m. The detector is equipped with an automatic machine (the Brick Manipulator System, BMS) that allows the on-line removal of bricks from the detector. Ancillary facilities exist for the handling, the development and the scanning of the emulsion films. The film scanning is performed with two independent types of scanning microscopes: the European Scanning Sytem (ESS) in Europe and the S-UTS in Japan.

A target brick consists of 56 lead plates of 1 mm thickness interleaved with 57 emulsion films [4]. The plate material is a lead alloy with a small calcium content to improve its
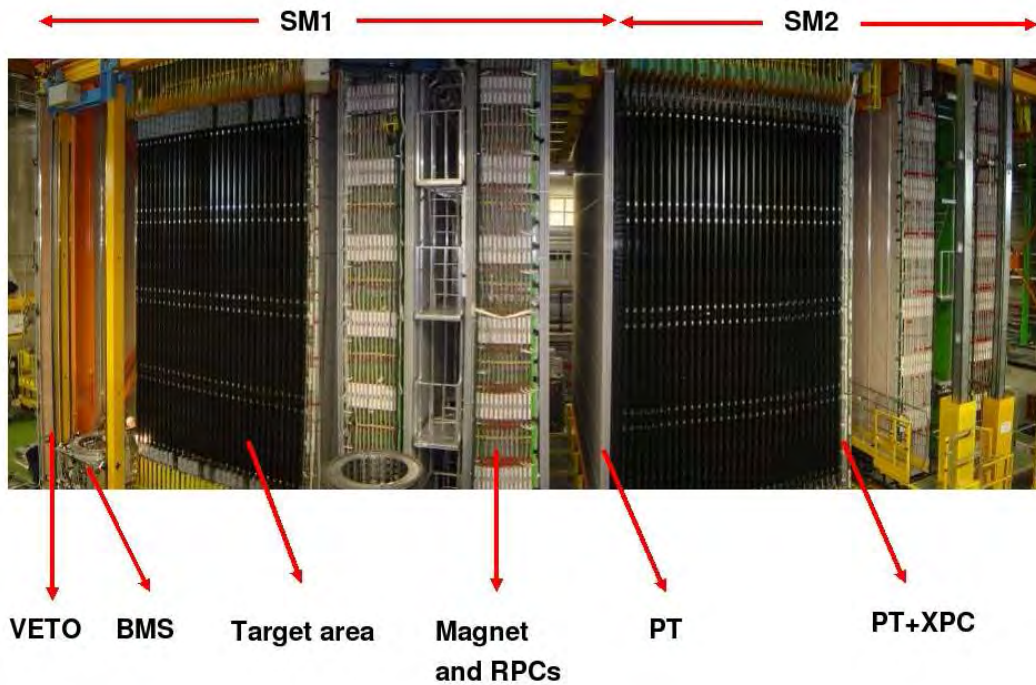
Figure 1: Fish-eye view of the OPERA detector. The upper horizontal lines indicate the position of the two identical supermodules (SM1 and SM2). The "target area" is made of walls filled with ECC bricks interleaved with planes of plastic scintillators (TT). Arrows also show the position of the VETO planes, the drift tubes (PT), the RPC with diagonal strips (XPC), the magnets and the RPC installed between the magnet iron slabs. The Brick Manipulator System (BMS) is also visible. See [2] for more details.

mechanical properties [5]. The transverse dimensions of a brick are 12.8×10.2 cm^2 and the thickness along the beam direction is 7.9 cm (about 10 radiation lengths). The construction of more than 150,000 bricks for the neutrino target has been accomplished by an automatic machine, the Brick Assembly Machine (BAM) operating underground in order to minimize the number of background tracks from cosmic-rays and environmental radiation. The BAM was delivered at LNGS in July 2006 and made operational in September 2006. The production lasted from March 2007 to June 2008 with an average rate of 650 assembled bricks/day. In this period, the brick production at the BAM was based on two shifts/day of 8 hours each, 5 working days a week. Each shift involved 7 operators plus 1 site manager. At the end of mass production the BAM had assembled 146621 bricks (June 2008). A few thousand more have been produced at the beginning of 2009 after the delivery of the remaining lead, delayed by an accident which occurred at lead producing factory (JL Goslar, Germany) in June 2008. The bricks have been inserted in the detector target by BMS and housed in a light support structure placed between consecutive TT walls. The support structure has been designed with the requirement of minimizing the material along the neutrino beam direction in order to reduce to the 0.1% level the number of interactions in regions not instrumented with emulsion films or scintillators.

In order to reduce the emulsion scanning load the use of Changeable Sheets (CS) [6], successfully applied in the CHORUS experiment, was extended to OPERA. Tightly packed doublets of emulsion films are attached to the downstream face of each brick and can be removed without opening the brick. Charged particles from a neutrino interaction in the brick cross the CS and produce a trigger in the TT scintillators. Following this trigger the brick is extracted and the CS developed and analyzed in the scanning facilities at LNGS and in Nagoya. The information of the CS is used for a precise prediction of the position of the tracks in the most downstream films of the brick, hence guiding the so-called *scan-back* vertex finding procedure.

The brick, CS and TT layout [6] is schematically shown in Figure 2.

A charged-current event, as reconstructed in the emulsion films, is shown in the bottom panel of Figure 3. In this case the detected event dimensions are of the order of a few millimeters, to be compared with the > 10 m scale of the whole event reconstructed with the electronic detectors (top panel of Figure 3).

First data were collected by the OPERA detector in 2006 with the electronic detectors alone, in 2007 with reduced target and in 2008 and 2009 with the full target installed (around 150000 bricks).

2   Real time detection of CNGS Beam

The CNGS neutrino beam was designed and optimized for the study of $\nu_\mu \to \nu_\tau$ oscillations in appearance mode, by maximizing the number of charged current (CC) ν_τ interactions at the LNGS site. For a detailed description of the CNGS beam we refer to [2].

After the beam commissioning run in 2006, the CNGS run started on September 2007 at rather low intensity. The first event inside the OPERA target was observed on October
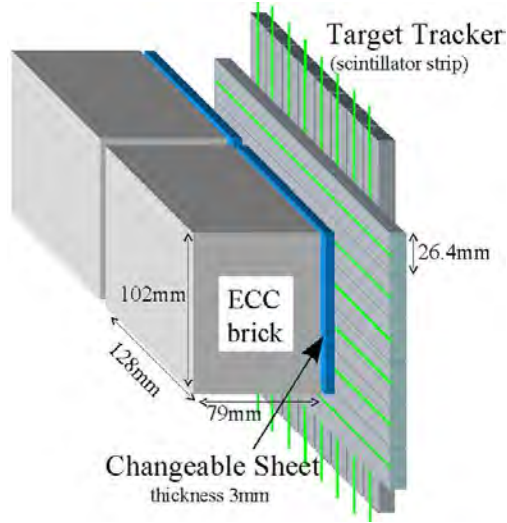
Figure 2: Schematic view of two bricks with their Changeable Sheet and target tracker planes.

3rd. Unfortunately, due to a fault of the CNGS facility, the physics run lasted only a few days. During this run 0.082×10^{19} p.o.t were accumulated with a mean value of 1.8×10^{13} protons per extraction: this represented 3.6 effective nominal days of run. With such an integrated intensity about 32 neutrino interactions in the bricks and about 3 events in the scintillators of the target tracker were expected. This has to be compared with the 38 on time events collected as originating in the target region (bricks plus target tracker).

A longer run took place in 2008 [3] when 1.782×10^{19} protons were delivered on the CNGS target. OPERA collected about 10100 events on time with the arrival of the beam at the Gran Sasso and among them around 1700 interactions in the bricks. The other events originate outside the target region (spectrometer, OPERA supporting structures, rock surrounding the cavern, hall structures). The scanning of these events is almost completed and the status of the measurements is shown in TABLE I.

In 2009 the CNGS beam started on May the 30th and lasted until November the 23rd. The beam intensity per extraction is shown in Figure 4 and was normally higher than 2×10^{13} POT/extraction. The holes in the intensity distribution are due to machine development periods and to some minor accidents which occurred in the linac/PS/SPS accelerator complex. The 2009 CNGS integrated proton on target intensity as a function of time is shown in Figure 5. The final integrated intensity was 3.522×10^{19} p.o.t. The total number of events recorded in time with the CNGS spill was 21428, of which 3693 are tagged as internal events. The scanning of these events is going on and the situation at the end of January 2010 in shown in TABLE II.

During the 2007, 2008 and 2009 CNGS runs, all electronic detectors were operational. The trigger rate was ~ 15 Hz and the live time of the Data Acquisition system exceeded 99%. The selection of the beam related events is based upon a time stamp, thanks to the time synchronization accuracy between the CERN beam GPS tagging and the OPERA
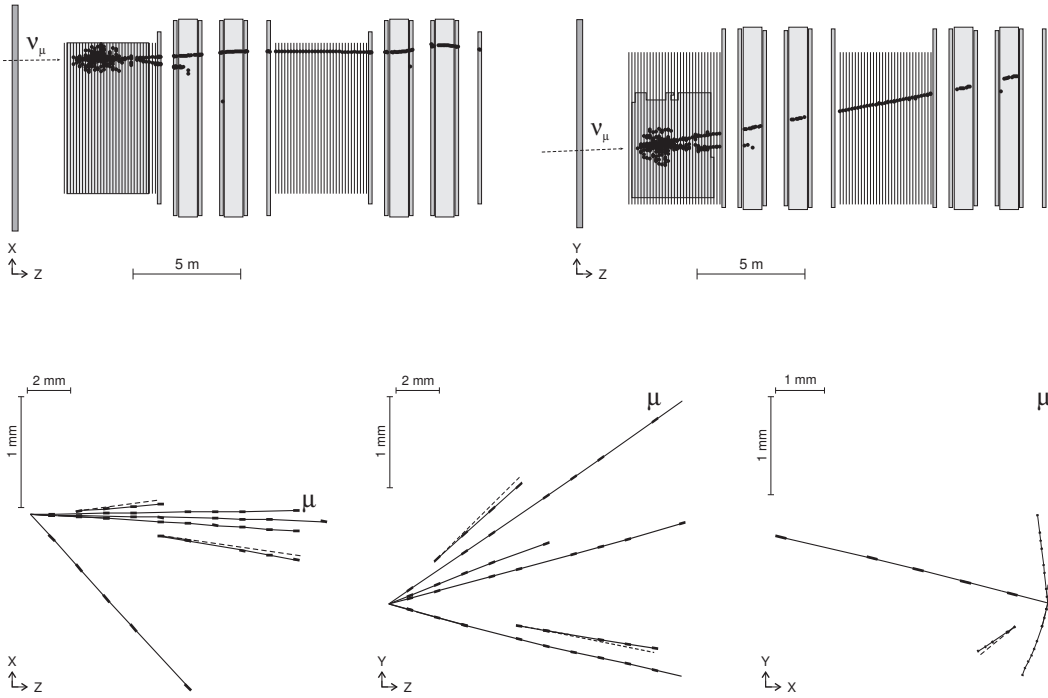
Figure 3: Top panel: on line display of an event seen by the OPERA electronic detectors (side and top views): a ν_μ interacts in one of the first bricks of the first supermodule (SM) yielding hadrons and a muon which is seen in both SMs and whose momentum is measured by the magnets of the two SMs. Bottom panel: the vertex of the same event observed in the emulsion films (side, top and front views). Note the two $\gamma \to e^+e^-$ vertices: the opening angle between them is about 300 mrad. By measuring the energy of the γ's one obtains a reconstructed invariant mass of 110 ± 30 MeV consistent with the π^0 mass.
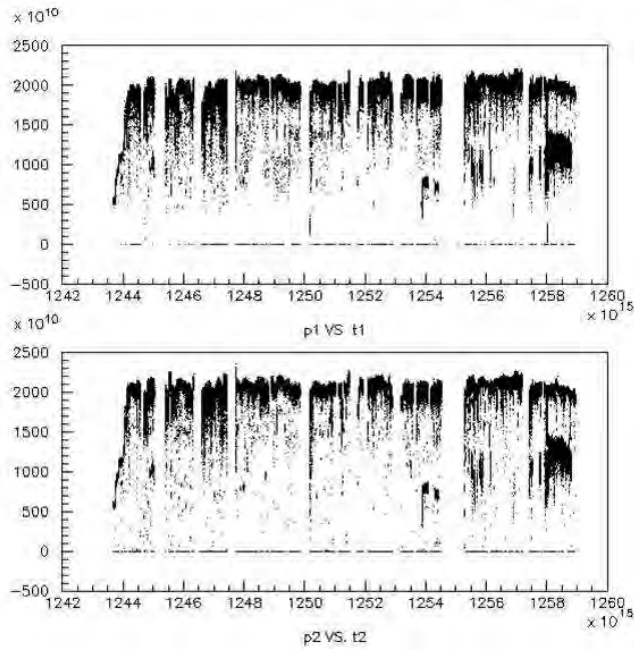
Figure 4: Beam intensity per extraction as a function of time for the 2009 CNGS run (June-November). The intensity/extraction was normally higher than 2×10^{13} p.o.t./extraction; the holes correspond to CNGS stop periods.
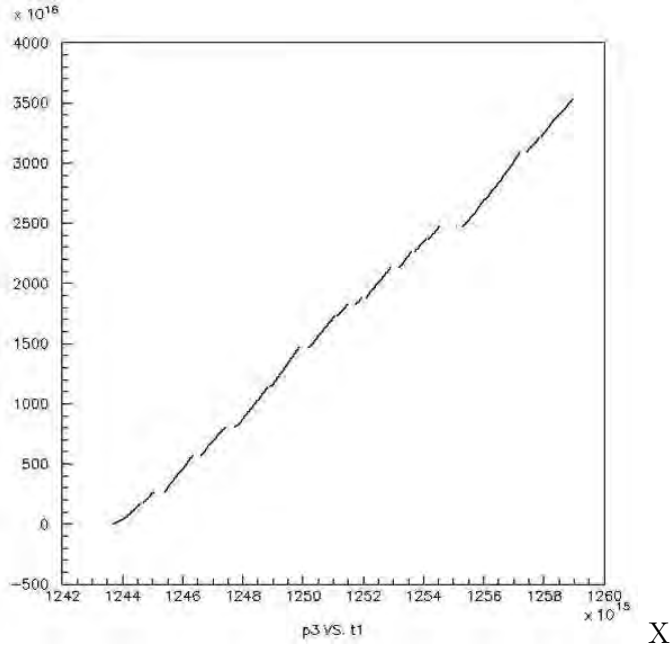

Figure 5: Integrated protons on target intensity as a function of time for the 2009 CNGS run (June-November). The final integrated intesity obtained was 3.522×10^{19} p.o.t.

150

Run 2008 status			
	0mu	1mu	All
Events predicted by electronic detector	401	1288	1689
Found CS	261 (65%)	1025 80%)	1286 (76%)
Neutrino interactions in the bricks	152	788	940
Located in dead material	5	30	35
Interaction in the upstream brick	8	32	40

Table 1: Event location in the bricks for the 2008 Run (emulsion scanning almost completed)

Run 2009 status			
	0mu	1mu	All
Events predicted by electronic detector	745	1932	2677
CS scanned	575	1583	2158
Found CS	287	968	1255
Neutrino interactions in the bricks	55	294	349
Located in dead material	1	10	11
Interaction in the upstream brick	3	31	34

Table 2: Event location in the bricks for the 2009 Run (emulsion scanning still in progress)

timing system which is about 100 ns.

The interactions in the material surrounding the OPERA target were analyzed and used for the monitoring of the CNGS beam and of the OPERA detector.

The classification algorithm was implemented to provide very high efficiency in the selection of neutrino interactions inside the OPERA target both for CC and NC events, to the expense of a slightly low purity in the rejection of neutrino interactions in the external material.

The beam direction estimated by the averaged angle is found to be tilted vertically by $(3.5 \pm 0.2)°$ in agreement with the value of $3.3°$ expected from geodesy.

3 Event Identification: from ECC Extraction to Kinematical Reconstruction

In the following the breakdowns of the different steps which are carried out to analyze the neutrino interaction events are described: from the identification of the "fired" brick up to the detailed kinematical analysis of the vertex in the emulsion films.

Once a trigger in the electronic detectors is selected to be compatible with an interaction inside the brick, the following procedure, named "Brick Handling", is applied:

1. the whole electronic detector data are processed by the reconstruction program and the most probable brick, inside which the neutrino interaction may have occurred, is selected;

Figure 6: Left: Two of the six chains of the film development facility at the LNGS external laboratory. Right: The European CS Scanning Station at LNGS.

2. the brick is removed from the detector by the BMS and exposed to X-rays for film-to-film alignment. There are two independent X-ray exposures: the first one ensures a common reference system to the CS films doublet and the brick (frontal exposure); the second produces thick lateral marks on the brick edges used for internal alignment and film numbering;

3. after first X-ray exposures the CS doublet is detached from the brick and developed underground while the brick is stored underground in a box with 5 cm thick iron shielding to reduce the radioactivity background.

4. if the CS scanning is successful in locating tracks compatible with those reconstructed in the electronic detectors, the brick is brought to the surface laboratory and exposed to cosmic-rays for about 24 hours inside a pit. The pit has been built to select high-energy particles in order to provide straight tracks in the bricks for a refined (sub-micrometric) film-to-film alignment;

5. the brick emulsion films are then developed in the OPERA developing laboratory at LNGS (Figure 6) and dispatched to the various scanning laboratories. Half of the removed bricks are sent to Japan for emulsion measurement, the other half is measured in the European laboratories. The CS of the European bricks are all measured at the LNGS Scanning Station (Figure 6) for event confirmation and localization.

The overall efficiency for the selection of bricks with neutrino interactions inwards depends of the convolution of several effects and measurements. We address here the issues on the two most important ones, the Changeable Sheet measurement and the Brick Finding. For the time being preliminary results have been obtained from the analysis of the first samples of events in 2007, 2008 and 2009 runs.

The ability in selecting the "fired" brick is the convolution of several effects and measurements. Here we discuss the two most important ones, the Brick Finding procedure and the Changeable Sheet measurement, for which preliminary results have been obtained from the analysis of partial samples of already scanned events.

The tracking efficiency of single emulsion films can be measured by exposure to high-energy pion beams [7]. However, the measurement of the CS doublet efficiency in situ, in the OPERA detector, is by far more challenging, given the coarse resolution in the extrapolation of tracks from the electronic detectors to the CS.

At the present, we are studying the CS tracking efficiency by two independent approaches: (a) all tracks produced in already located neutrino vertices are followed downstream and searched for in the corresponding CS doublet; (b) muon tracks reconstructed by the electronic detectors and found in the CS are normalized to the total number of CC events where at least one track (not necessarily the muon) is found in the CS. The two methods yield a preliminary efficiency for finding a track in both films of the CS doublet which is compatible with the conservative expectation of $\sim 90\%$ on a single film.

The brick finding algorithm exploits the tracking capabilities of the OPERA electronic detectors and, by combining this information with the output of a Neural Network for the selection of the most probable wall where the interaction occurred, provides a list of bricks with the associated probability that the interaction occurred therein. A preliminary estimate of the brick finding efficiency, limited to the extraction of the most probable brick, is compatible with the Monte Carlo estimate of $\sim 70\%$ computed for a standard mixture of CC and NC events. A higher efficiency can be obtained by extracting also bricks ranked with lower probabilities.

All tracks measured in the CS are sought for in the most downstream films of the brick and followed back until they are not found in three consecutive films. The stop is considered as the signature of a primary or secondary vertex. The vertex is then confirmed by scanning a volume with a transverse size of 1 cm^2 for 11 films in total, upstream and downstream of the stopping point. Preliminary results on the vertex location efficiency as measured with the data are in agreement with the Monte Carlo expectations of $\sim 90\%$ and $\sim 80\%$ for CC and NC events, respectively.

Typical NC and CC events are shown in Figures 7 and 8, respectively.

In the subsample of located neutrino interactions charm and tau decay topologies were searched for. This search is systematically going on. Up to now 19 charm decay candidates have been found, but a systematic analysis of the possible decay topologies is still going on in the measured sample of 2008 and 2009 events.

4   Conclusions

The 2007, 2008 and 2009 CNGS successful runs constitute an important milestone for the OPERA experiment at LNGS. First neutrino interaction events with lead/emulsion bricks have been collected and these events allowed to check the complete analysis chain starting from the trigger to the neutrino vertex location in the emulsions and then to the topological and kinematical characterization of the event.

The major achievements can be summarized as follows:

- all electronic detectors performed excellently allowing the precise localization of the brick hit by the neutrino;
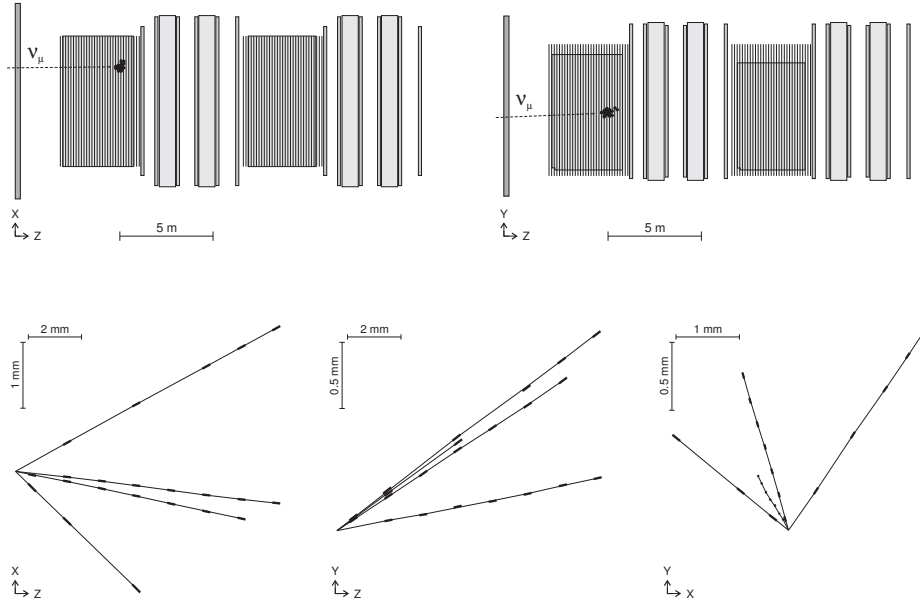
Figure 7: Online display of one NC event seen by the OPERA electronic detectors. The emulsion reconstruction is shown in the bottom panels: top view (bottom left), side view (bottom center), front view (bottom right).
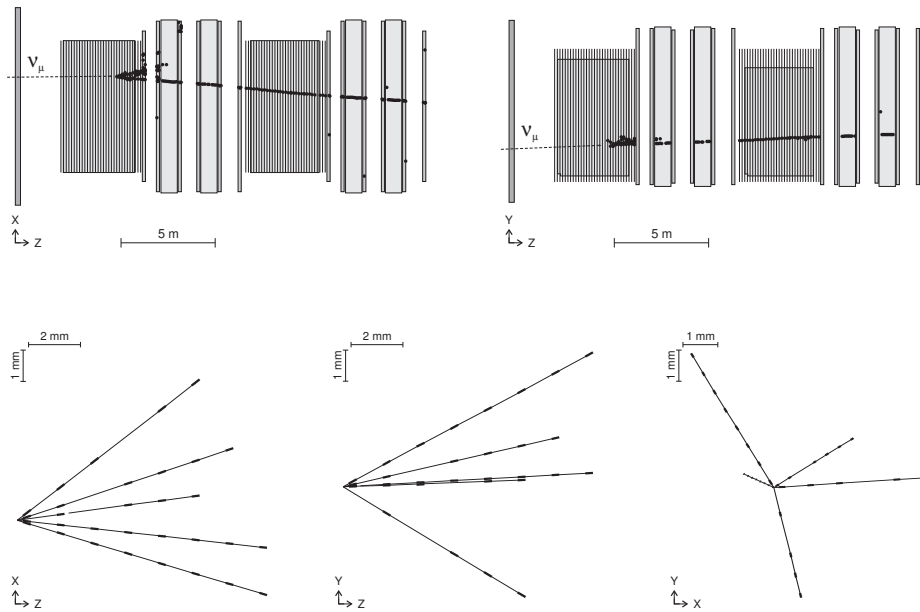
Figure 8: Online display of one CC event seen by the OPERA electronic detectors. The emulsion reconstruction is shown in the bottom panels: top view (bottom left), side view (bottom center), front view (bottom right).

- the electronic detector event reconstruction was tuned to the brick finding procedure, operated for the first time with real neutrino events. Identification of the brick where the interaction occurred has been done by using real data providing satisfactory results;

- all experimental activities that go from brick removal upon identification to the X and cosmic-ray exposures, brick disassembly and emulsion development, have been successfully accomplished. So far a rate of more than 100 brick per week can be routinely handled;

- the interface emulsion (CS) scanning was performed with the expected efficiencies. In particular, the track finding efficiency in a CS doublet was measured in OPERA and is in agreement with test beam results;

- the vertex location was successfully attempted for both CC and NC, although a quantitative estimate of the efficiency is still under evaluation;

- the topological and kinematical analyses of the vertices were successfully exploited and led to an unambiguous interpretation of neutrino interactions. In particular, in the reported analyzed event sample, 19 events with charm-like topologies were found. This shows that the experiment is capable of detecting events with short living particles produced at the neutrino interaction vertex, with topologies very similar to τ production.

References and list of publications

[1] R. Acquafredda *et al.* [OPERA Collaboration], "First events from the CNGS neutrino beam detected in the OPERA experiment,"New J. Phys. **8** (2006) 303 [arXiv:hep-ex/0611023].

[2] R. Acquafredda *et al.* [OPERA Collaboration] "The OPERA experiment in the CERN to Gran Sasso neutrino beam", JINST 4:P04018,2009.

[3] N. Agafonova *et al.* [OPERA Collaboration] "The Detection of neutrino interactions in the emulsion/lead target of the OPERA experiment", JINST 4:P06020,2009.

[4] T. Nakamura *et al.*, "The Opera Film: New Nuclear Emulsion For Large-Scale, High-Precision Experiments," Nucl. Instrum. Meth. A **556** (2006) 80.

[5] A. Anokhina *et al.* [OPERA Collaboration], "Study of the effects induced by lead on the emulsion films of the OPERA experiment," JINST **3** P07002 (2008).

[6] A. Anokhina *et al.* [OPERA Collaboration], "Emulsion sheet doublets as interface trackers for the OPERA experiment," JINST **3** (2008) P07005

[7] L. Arrabito *et al.*, "Track reconstruction in the emulsion-lead target of the OPERA experiment using the ESS microscope," JINST **2** (2007) P05004

[8] K. Kodama *et al.*, "Momentum measurement of secondary particle by multiple Coulomb scattering with emulsion cloud chamber in DONuT experiment," Nucl. Instrum. Meth. A **574** (2007) 192.

THEORY GROUP

The research is organized in the six working groups: FA51, GS51, CT51, PD51, PI12, PI21, that are generically denoted as IS (from "Iniziative Specifiche"). It concerns as main areas: astroparticle physics (mainly FA51), phenomenology of Planck scale physics (GS51), supernova neutrinos (CT51), cosmology, large scale structures and dark matter (PD51), computer simulations of gauge theories (PI12), particle physics phenomenology (mainly PI21). There is a tradition of collaboration between the LNGS theory group and several experimental groups. In this report, we describe the activities of the theory group in 2009.

Members of the group: R. Aloisio, Z. Berezhiani, V. Berezinsky, D. Boncioli, G. Di Carlo, A. Gazizov, A.F. Grillo, E. Luzio, A. Maiezza, F. Nesti, G. Pagliaroli, P. Panci, L. Pilo, N. Rossi, F.L. Villante, F. Vissani.

Updated information and further info at: `http://theory.lngs.infn.it/index.html` .

— QCD at Finite Temperature and Density (PI12) —

Member: Giuseppe Di Carlo, who works in collaboration with Vicente Azcoiti, Eduardo Follana e Alejandro Vaquero from Departamento de Fisica Teorica - Universidad de Zaragoza.

Scientific work

Our main interest is the study of lattice theories with sign problem, in particular Lattice QCD at non-zero baryon density; we are currently working on an improved monomer-dymer algorithm that we hope to extend outside the strong coupling regime. This is only a member of a class of possible new geometric algorithms for simulating fermion models. Another field of interest are non abelian gauge theories with theta term in the action.

Our activity during 2009 mainly regarded the study of models presenting the so-called sign problem. We are trying to extend the old monomer-dymer algorithm ideas (up to now applied only in the infinite strong coupling limit, $\beta = 0$) to simulate the system for larger beta. The work on the new geometric algorithm is reported in ref. [2].

Apart from this, we have reconsidered an old problem on realization of discrete symmetries in lattice QCD, using an approach that some of us introduced few years ago. In this line we have analysed the structure of the Aoki Vacua in Lattice QCD with Wilson fermions; a paper on the subject has been published in Phys. Rev. D in early 2009 [1] and the results have also been presented to the annual Lattice Conference (Proceedings in ref. [3]).

Publications in journals, proceedings and preprints

[1] "QCD with two flavors of Wilson fermions: The QCD vacuum, the Aoki vacuum, and other vacua"
V. Azcoiti, G. Di Carlo, A. Vaquero
Phys. Rev. D79 (2009) 014509

[2] "Geometric Algorithm for Abelian-Gauge Models"
V. Azcoiti, G. Di Carlo, E. Follana, A. Vaquero
JHEP 0908:008,2009

[3] "Understanding the Aoki phase"
V. Azcoiti, G. Di Carlo, E. Follana, A. Vaquero
arXiv:0910.0947 to be published in PoS(Lattice '09)

──── Particle Physics Phenomenology (PI21) ────

Members: Z. Berezhiani, F. Nesti, P. Panci, L. Pilo, N. Rossi, F. Villante.

Scientific work

One research line was dedicated to the particle interaction/mixing phenomena between the ordinary particles and the particles of the hypothetical gauges sectors that could give rise to the dark matter of the Universe. We further studied the neutron-mirror neutron oscillation features in the background of the magnetic fields and analyzed the consequences of experimental data on the search of these oscillations [1]. We also studied the cosmological bounds on the photon-mirror photon kinetic mixing that translates into the bound on the electric charges of the mirror species [2].

Another line of the research was devoted to the following topics: large distance modifications of gravity (also known as massive gravity) that can change our views on the problem of dark matter and dark energy [3, 4, 5]. In particular, we studied the massive phase of gravity realized by coupling the metric of the general relativity to additional twin metric related to the twin (mirror) matter, in conditions the Lorentz symmetry breaking. We have shown that this gives rise to the Yukawa type modification of the gravity at large distances and we studied the implications of the mirror twin gravity for the galactic rotational curves [3, 4]. We also studied he stability of the massive gravity theories in curved space, proving a viable window of stability in a universe with very small curvature as is ours [5]. The extensions of the gauge group of gravity, that allow the unification with the other interactions, and proved that a realistic fermion content can be accomodated in a unifying group, were studied in [6, 7].

Conferences, seminars and other activities

Int. *ENTApP Dark matter Workshop*, CERN, Geneve, Feb. 2009 (talks of Z. Berezhiani and F. Nesti), Int. Workshop *"Hot Topics in Modern Cosmology"* SW3, Cargese, France, April 2009 (talks of Z. Berezhiani, F. Nesti and N. Rossi); CERN Theory Institite "SM and BSM physics at the LHC", Aug. 2009, (seminar of Z. Berezhiani); Int. Workshop "Searching for New Physics at the LHC", Sept. 2009, Galileo Galilei Institute for Theoretical Physics, Florence, Italy (seminar of Z. Berezhiani); Int. Conf. "Cosmo 2009",CERN Geneve, Sept. 2009 (F. Nesti and L. Pilo participants); 3rd UniverseNet School Particle Astrophysics and Cosmology, Barcelona, Spain, Sept. 2009 (talks of P. Panci and N. Rossi); Invited seminars at the Univ. of Helsinki, at the EPFL Lausanne and at the ICTP Triest (Z. Berezhiani) and at Oslo Univ. (F. Nesti).

Z. Berezhiani was one of the organizers of the Int. Workshop *"Hot Topics in Modern Cosmology"* SW3, Cargese, France, April 2009.

Publications in journals, proceedings and preprints

[1] Z. Berezhiani.
More about neutron - mirror neutron oscillation.
Eur. Phys. J. C 64, 421-431 (2009).

[2] Z. Berezhiani, A. Lepidi.
Cosmological bounds on the 'millicharges' of mirror particles.
Phys. Lett. B 681, 276-281 (2009).

[3] Z. Berezhiani, F. Nesti, L. Pilo, N. Rossi,
Gravity Modification with Yukawa-type Potential: Dark Matter and Mirror Gravity.
JHEP 0907, 083 (2009).

[4] Z. Berezhiani, L. Pilo, N. Rossi,
Mirror Matter, Mirror Gravity and Galactic Rotational Curves.
e-Print: arXiv:0902.0146 [astro-ph.CO]

[5] D. Blas, D. Comell, F. Nesti, L. Pilo.
Lorentz Breaking Massive Gravity in Curved Space.
Phys. Rev. D 80, 044025 (2009).

[6] F. Nesti.
Standard Model and Gravity from Spinors.
Eur. Phys. J. C 59, 723-729 (2009).

[7] F. Nesti, R. Percacci.
Chirality in unified theories of gravity.
e-Print: arXiv:0909.4537

[8] M. Cirelli, P. Panci.
Inverse Compton constraints on the Dark Matter e+e- excesses.
Nucl. Phys. B821, 399-416 (2009).

[9] M. Cirelli, F. Iocco, P. Panci.
Constraints on Dark Matter annihilations from reionization and heating of the inter-galactic gas.
JCAP 0910, 009 (2009).

[10] M. Cirelli, P. Panci, P.D. Serpico.
Diffuse gamma ray constraints on annihilating or decaying Dark Matter after Fermi.
e-Print: arXiv:0912.0663

[11] F. L. Villante and F. Vissani.
Cosmic Rays And Neutrinos From Supernova Remnants From VHE Gamma Ray Data.
Nucl. Phys. Proc. Suppl. 188 (2009) 261.

⎯⎯⎯⎯⎯ Supernova Neutrinos (CT51) ⎯⎯⎯⎯⎯

Members in 2009: G. Pagliaroli, F.L. Villante, F. Vissani. They worked in collaboration with F. Rossi-Torres (PhD student at UNICAMP) long term visitor at LNGS; P. Lipari (Rome University); F. Aharonian (High Energy Astrophysics Theory Group, Heidelberg and Dublin Institute for Advanced Studies) and member of HESS experiment; A. Ianni of Borexino; A. Drago (Ferrara U.); W. Fulgione (Turin U.) and other members of the LVD team; E. Coccia and other members of VIRGO team.

Scientific work

This research group aims at exploring the scientific potential of supernova neutrino observations.

We proposed a new model to parameterize the electron antineutrino emission from supernova in [1]. We used it to argue that SN1987A provides a 2.5 σ evidence for an initial, very luminous phase of emission lasting about 0.5 seconds, which corresponds quite closely to the expectations of the standard neutrino emission (also termed neutrino assisted, delayed, or Bethe and Wilson scenario).

A quite broad survey of SN1987A data, arguing for the fact that they *do not* contradict the standard neutrino emission, is presented in [2], where we also discuss the impact of SN1987A data on the search of relic supernova neutrinos.

We wrote a note [3] to clarify the likelihood that should be adopted in supernova neutrino analyses, correcting in this way one of the most authoritative previous analysis of SN1987A neutrino, due to Loredo and Lamb.

Finally, we outlined a method to profit of the data collected by supernova neutrino telescopes for the search of a burst of gravity waves [4].

For a general review and more details of this part of the research activity, see the PhD thesis of Giulia Pagliaroli [5].

Another activity regards the more general field of neutrino astronomy. This is documented in the review works [6, 7, 8]. It can be noted that in the appendix of [6] a new approach to the study of the rate of galactic supernovae is proposed.

Conferences, seminars and other activities

F. Vissani gave a series of lectures on "Neutrinos" at the *ICTP Summer School on particle physics in the era of LHC.*

He also gave invited talks at the national meeting *Incontri di Fisica delle Alte Energie,* Bari (Sugli obiettivi della astronomia neutrinica, Apr. 2009); at the Int. conference *The sun, the stars, the universe and general relativity, (rst Galileo-Xu Guangqi meeting),* Shanghai, China (Potential of neutrino detectors as monitors of gravitational core collapses, Oct. 2009). Giulia Pagliaroli gave invited talks at *NPAIV 2009*, Rome, June 2009 and at *TAUP 2009*, Rome, July 2009.

F. Vissani presented the results of this activity at the *VESF Council Meeting,* Osservatorio di Monte Porzio Catone (Neutrinos from supernovae as trigger for GW search, Apr. 2009); at the *Commissione Scientifica Nazionale II, INFN,* Rome, to contribute to the discussion on perspects of neutrino astronomy (A candidate for observations: RX J1713.7-3946, Sep. 2009); and discussed the potential of neutrino detectors as monitors of gravitational core collapses in seminars given at the ICTP, Trieste and at the IJS, Ljubljana (Slovenia).

F. V. became the referent person of the Italian Physics Society (SIF) at LNGS and coordinator for LNGS of the Virgo-EGO Science Forum (VESF) since April 2009.

Publications in journals, proceedings and preprints

[1] **"Improved analysis of SN1987A antineutrino events"**
G. Pagliaroli, F. Vissani, M. L. Costantini and A. Ianni
Astropart. Phys. **31**, 163 (2009)

[2] **"Features of Kamiokande-II, IMB and Baksan observations and their interpretation in a two-component model for the signal"**
G. Pagliaroli and F. Vissani
Astron. Lett. **35**, 1 (2009)

[3] **"The likelihood for supernova neutrino analyses"**
A. Ianni, G. Pagliaroli, A. Strumia, F. R. Torres, F. L. Villante and F. Vissani
Phys. Rev. D **80**, 043007 (2009)

[4] **"Neutrinos from Supernovae as a Trigger for Gravitational Wave Search"**
G. Pagliaroli, F. Vissani, E. Coccia and W. Fulgione
Phys. Rev. Lett. **103**, 031102 (2009)

[5] **"Analysis of supernova neutrinos: astrophysics, particle physics and implications for gravitational wave search"**

G. Pagliaroli
PhD thesis, L'Aquila University, defended with success on April 2009.

[6] **"On the Goals of Neutrino Astronomy"**
F. Vissani, G. Pagliaroli and F. L. Villante
Il Nuovo Cimento C **32**, 351 (2009)

[7] **"Neutrini dallo Spazio (discutendo gli obiettivi di una nuova astronomia)"**
G. Pagliaroli, F. L. Villante and F. Vissani
Il Nuovo Saggiatore **25**, no.3-4, 1 (2009)

[8] **"Cosmic Rays And Neutrinos From Supernova Remnants From Vhe Gamma Ray Data"**
F. L. Villante and F. Vissani
Nucl. Phys. Proc. Suppl. **188**, 261 (2009)

—————— Astroparticle Physics (FA51) ——————

The Astroparticle group of LNGS in 2009 included R.Aloisio, V.Berezinsky, A.Gazizov and visitors V.Dokuchaev (Institute for Nuclear Research, Moscow), Yu.Eroshenko (Institute for Nuclear Research, Moscow), B.Hnatyk (Lviv University, Ukraine), S.Grigorieva (Institute for Nuclear Research, Moscow). The group worked in close collaboration with P.Blasi (Arcetri Observatory, Firenze), A.Vilenkin (Tufts University, USA), M.Kachelriess (NUST, Trondheim, Norway), S.Ostapchenko (Karslrue, Germany) and others.

Scientific work

The main field of the work is astroparticle physics, including ultra high energy cosmic rays, and high energy neutrino and cosmology. From the works of 2009 one may be explicitly mentioned: R. Aloisio, V. Berezinsky, A. Gazizov, Superluminal problem indiffusion of relativistic particles and its phenomenological solution, Astrophys. J. **693**, 1275, (2009).

The problem of appearance of superluminal signal in non-relativistic diffusion equation, e.g. in thermal conductivity, viscous motion of gases etc. is known for about 100 years. In this work it is studied and phenomenologically solved for diffusion of cosmic rays. The phenomenological solution of this problem is found with the help of the generalized Juettner propagator, originally proposed for relativization of the Maxwellian gas distribution. The solution obtained is very general for diffusion of particles. The applications are considered for ultra-high energy cosmic rays, where the superluminal problems are shown to be eliminated.

Conferences, seminars and other activities

R.Aloisio works as the scientific secretary of the LNGS scientific committee and as the organizer of LNGS seminar.

V.Berezinsky works as a member of Int. Advisory board of JEM-EUSO.

R.Alosio presented invited talk at Int. Conference "Searching for the origin of Cosmic Rays" in Trondheim, Norway, 15 - 18 June, 2009.

V. Berezinsky presented the invited talks at Int. Conferences "Searching for the origin of Cosmic Rays" in Trondheim, Norway, 15 - 18 June, 2009. "Callenges in Theoretical Cosmology" in Talloires (France), 2 - 5 September 2009, 13th Chalogne Cosmology Colloquium in Torino, 21 - 24 October 2009, XCV Italian Phys. Soc. Congress in Bari Sept. 28 - Oct 4 and at EUSO meeting in Paris 12 - 14 May, 2009

A. Gazizov presented invited talk at Int. Conferences "Searching for the origin of Cosmic Rays" in Trondheim, Norway, 15 - 18 June, 2009.

Publications in journals, proceedings and preprints

[1] R. Aloisio, V. Berezinsky, A.Gazizov
Superluminal problem in diffusion of relativistic particles and its phenomenological solution.
Astrophys.J. 693, 1275-1282, 2009

[2] V.Berezinsky, K.Olum, E.Sabancilar, A. Vilenkin
UHE neutrinos from superconducting cosmic strings.
Phys. Rev. D80:023014, 2009.

[3] V. Berezinsky
Ultra High Energy Cosmic Ray Protons: Signatures and Observations
Nucl. Phys. B (Proc. Suppl.) 188, 227-232, 2009.

[4] R. Aloisio, V. Berezinsky, A.Gazizov
Ultra High Energy Cosmic Rays: The disappointing model
arXiv:0907.5194

⎯⎯⎯⎯ Cosmology and Dark Matter (PD51) ⎯⎯⎯⎯

Members: Z. Berezhiani, F. Nesti, P. Panci, L. Pilo, N. Rossi, F.L. Villante and F. Vissani. They worked in collaboration with D.Comelli (INFN-Ferrara), M. Cirelli (CERN and CNRS), A. Drago (University of Ferrara), R. Percacci (SISSA), D. Blas (IPT, Lausanne), P. Salucci (SISSA)

Scientific work

The research activity has been focused on the following topics:

i) Modifications of gravity. We have studied models of gravity modification at large distances and their impact on dark energy and dark matter. We have discussed, in particular, the general features of massive gravity around a cosmological backgrounds. We have also studied the stability of these theories in curved space, proving a viable window of stability in a universe with very small curvature. We have, finally, considered the deviation from a universal gravitational law at large scale in the context of the "multigravity" theories where "Lorentz invariance" is broken.

ii) Direct and Indirect dark matter search. We have discussed some astrophysical implications of the dark matter interpretation of the PAMELA e+/e- excess. We have discussed the limits on the dark matter properties that can be obtained by indirect dark matter searches. We have analyzed the possibility that "mirror matter" can provide a relevant component of the dark matter of our universe in view of the recent DAMA/Lybra results.

Conferences, seminars and other activities

International *ENTApP Dark matter Workshop*, CERN, February 2009 (talk di F. Nesti) International Workshop on *Hot topics in cosmology* SW3, Cargese, France, April-May 2009 (talks di Z. Berezhiani, N.Rossi, F. Nesti) International Conference on *Topics in Astroparticle and Underground Physics* TAUP, Rome, Italy, July 2009 (talk of F.L. Villante). F Nesti presented the talk "Exact black hole solutions in massive gravity" at Lausanne U.

F. L. Villante gave an invited lecture about *Neutrino in Physics and Astrophysics* at *2009 2D-IDAPP meeting*, Varenna, Italy, June 2009. P. Panci and N. Rossi partecipated to the 3rd UniverseNet School *Particle Astrophysics and Cosmology*, Barcellona (Spain), September-October, 2009. Z. Berezhiani gave talks at Int. *ENTApP Dark matter Workshop*, CERN, Geneve, Feb. 2009; CERN Theory Institute "SM and BSM physics at the LHC", Aug. 2009; Int. Workshop "Searching for New Physics at the LHC", Sept. 2009, Galileo Galilei Institute for Theoretical Physics, Florence, Italy; and presented invited seminars at the Univ. of Helsinki, at the EPFL Lausanne, at the ICTP, Triest.

F. L. Villante and F. Vissani were members of the Organizing Commitee of the Internation Workshop on *Weak Interaction and Neutrinos* WIN09, Perugia, Italy, September 2009.

Publications in journals, proceedings and preprints

[1] Z. Berezhiani, F. Nesti, L. Pilo and N. Rossi, "Gravity Modification with Yukawa-type Potential: Dark Matter and Mirror Gravity", JHEP 0907 (2009) 083

[2] D. Blas, D. Comelli, F. Nesti and L. Pilo, "Lorentz Breaking Massive Gravity in Curved Space", Phys. Rev. D 80 (2009) 044025

[3] F. Nesti, R. Percacci, "Chirality in unified theories of gravity" Phys. Rev. D 81 (2010) 025010

[4] "The dark matter density at the suns location" P. Salucci, F. Nesti, Submitted.

[5] F. Nesti, "Standard Model and Gravity from Spinors", Eur.Phys.J. C59 (2009) 723.

[6] Z. Berezhiani and A. Lepidi, "Cosmological bounds on the 'millicharges' of mirror particles," Phys. Lett. B 681 (2009) 276

[7] M. Cirelli, P. Panci, P.D. Serpico "Diffuse gamma ray constraints on annihilating or decaying Dark Matter after Fermi"

[8] M. Cirelli, F. Iocco, P. Panci, "Constraints on Dark Matter annihilations from reionization and heating of the intergalactic gas." JCAP 0910 (2009) 009

[9] M. Cirelli, P. Panci, "Inverse Compton constraints on the Dark Matter e+e- excesses.", Nucl.Phys.B 821 (2009) 399

[10] Z. Berezhiani, L. Pilo and N. Rossi. "Mirror Matter, Mirror Gravity and Galactic Rotational Curves" arXiv:0902.0146 [astro-ph.CO]

[11] F. L. Villante and F. Vissani, "Cosmic Rays And Neutrinos From Supernova Remnants From VHE Gamma Ray Data", Nucl. Phys. Proc. Suppl. 188 (2009) 261.

[12] A. Ianni, G. Pagliaroli, A. Strumia, F. R. Torres, F. L. Villante and F. Vissani, "The likelihood for supernova neutrino analyses", Phys. Rev. D 80 (2009) 043007

[13] F. L. Villante and B. Ricci, "Linear Solar Models", arXiv:0912.4696 [astro-ph.SR].

The WArP Experiment

The WArP Collaboration

R.Acciarri[a], M.Antonello[b], B. Baibussinov[c], M.Baldo-Ceolin[d], P.Benetti[e], F. Boffelli[e], F.Calaprice[f], E.Calligarich[g], M.Cambiaghi[e], N.Canci[a], F.Carbonara[h], F.Cavanna[a], S. Centro[d], A.G.Cocco[i], F.Di Pompeo[a], G.Fiorillo[h], C.Galbiati[f], L.Grandi[b], A.Menegolli[e], G. Meng[c], C.Montanari[g], O.Palamara[b], L.Pandola[b], F. Pietropaolo[c], G.L.Raselli[g], M.Roncadelli[g], M.Rossella[g], C.Rubbia[1][b], E.Segreto[b], A.M.Szelc[j,b], S. Ventura[c], C.Vignoli[g]

[a] *Università dell'Aquila e INFN, L'Aquila, Italy*
[b] *INFN - Laboratori Nazionali del Gran Sasso, Assergi, Italy*
[c] *INFN - Sezione di Padova, Padova, Italy*
[d] *Universitá di Padova e INFN, Padova, Italy*
[e] *Universitá di Pavia e INFN, Pavia, Italy*
[f] *Princeton University - Princeton, New Jersey, USA*
[g] *INFN - Sezione di Pavia, Pavia, Italy*
[h] *Universitá di Napoli e INFN, Napoli, Italy*
[i] *INFN - Sezione di Napoli, Napoli, Italy*
[j] *IFJ PAN, Krakow, Poland*

---

[1]Spokesman of the WArP Collaboration

1 WArP-100 detector Technical Commissioning

The activity of the WArP Collaboration in 2009 has been almost entirely dedicated to the commissioning, tests and related actions on the WArP-100 lt detector. This activity is here briefly summarized. Construction and assembly of the WArP-100 detector have been completed by December 2008 and immediately after deployed into the cryostat, positioned in Hall-B at LNGS inside the Lead & Polyethylene external shield for gamma and neutron background suppression.
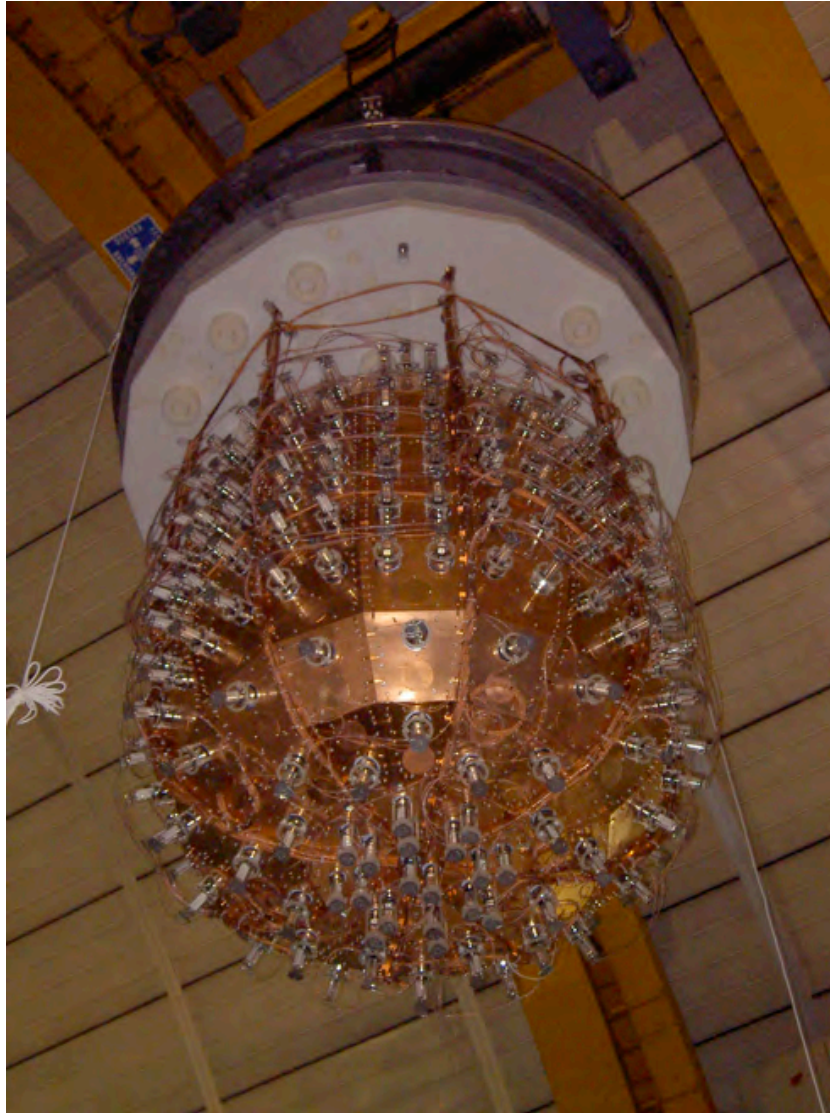
Phase-1

Phase-1 of the Detector Commissioning was started on Dec. 22nd with the vacuum pumping of the cryostat internal volume, combined with a number of cycles of inert gas flushing (N_2 at room temperature) for the reduction of the residual H_2O content of the

internal materials. This phase lasted about five months (from Dec. 23rd to May 5th, 2009).

Initially, leak search, localization and repairs required about one month and successively vacuum pumping lasted up until the design residual pressure was reached as measured by the pressure probes located in various points of the cryostat.

During this period external cabling of the PMTs and of the slow-control sensors (LAr levels, T, P,) has been completed. A full test of the PMT signal and HV mapping has been then performed and validated. The assembly of the lateral walls of the Lead shield was also completed and the installation of the most external n-shield well advanced In
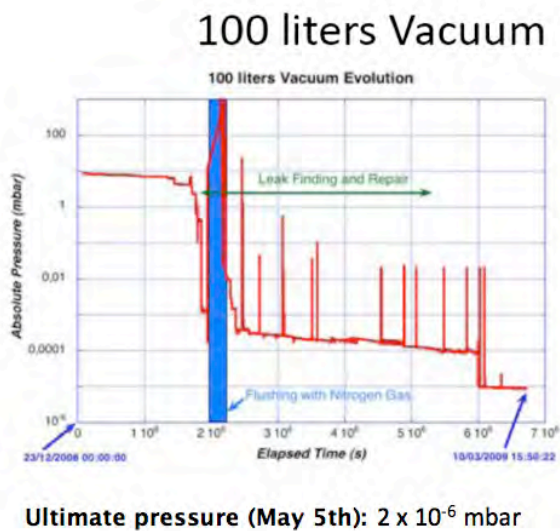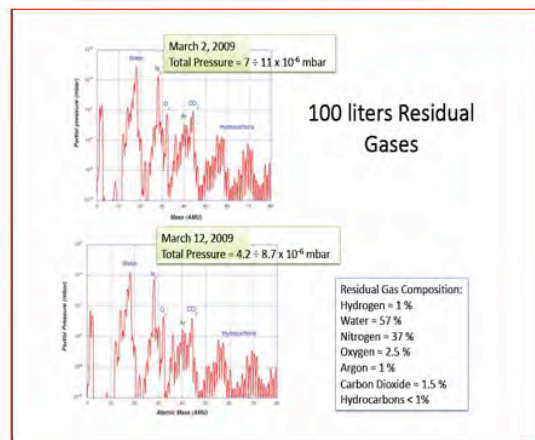
this Phase-1 of the Commissioning the composition of the residual gas has been continuously monitored by mass spectrometry. Air components (from residual leaks) and water (from material outgassing) have been identified and monitored during their progressive decrease (e.g H_2O outgassing rate: 6×10^{-5} mbar lt/sec). The vacuum pumping period was assumed as completed when the residual pressure reached the design value in the range $2 \div 6 \times 10^{-6}$ mbar (end of March, 2009).

Phase-2

Phase 2 of the Commissioning procedure (inner detector Cooling and LAr Filling) was started on May 5th, the first day of resuming into normal operation at LNGS underground after the suspension of activity due to the earthquake (during the month of April, vacuum pumping indeed continued without interruptions)

The Cooling phase lasted less than 3 days via low-quality LAr forced recirculation in the piping system inserted in the vacuum jacket of the cryostat, in thermal contact with

169

the internal wall. This produced ensured a smooth cooling down of the materials inside the cryostat to less than 200 K (in the innermost element of the detector), thus stopping the water outgassing (as seen by the drop of the H_2O partial pressure). The ultimate residual pressure just below 1×10^{-6} mbar was then reached.

The following step with the LAr filling lasted four more days. Good-quality LAr (equivalent to 5.5 grade) at a speed of about 300 lt/hr was conveyed inside the cryostat through a dedicated vacuum insulated filling line from a movable LAr storage. The line included a large two-stages filter (Oxygen reactant for O_2 removal and molecular sieves for H_2O trapping). During the first day of the Filling Phase all the inner components (internal Polyethylene shield and detector) were cooled down to LAr temperature and successively the LAr level inside the cryostat has grown up to the detector operation design level (full immersion of the active veto detector).

On May 13th, the WArP-100 detector Technical Commissioning was successfully completed.

2 WArP-100 detector Technical Run

A technical run of the WArP 100lt detector started with the activation of the various components of the detector and of the cryogenic system (May-July, 2009):

- GAr recirculation (liquefaction and purification) activated, allowing direct measurement of the actual total heat load of the system (estimated at a level of 1 kW, in agreement with design value).

170

- GAr/LAr precise level configuration for the two-phase 100lt inner detector successfully established (gas Argon pocket generated and maintained by resistive heaters inside the bell-shaped immersed cryostat).

- PMT activation with voltage bias at nominal value with slow HV ramp and individual test:

  – 37/37 PMTs of the inner detector correctly functional (1 slightly noisy)
  – 298/302 PMTs of the veto system correctly functional (2 PMT: faulty connection at the feed-through, 2 PMT: broken printed circuit of the resistor divider)

- DAQ & Trigger for 100lt detector, after initial debugging phase, in run with progressive tuning and optimization of the performance.

- Off-line event reconstruction successfully tested and used for first data analysis.

- HV system for the Inner Detector (connection from external power supply to inner detector cathode): while ramping up the HV a major discharge occurred inside the cryostat along the connection line and this broke the HV injection system. This unforeseen event prevented to establish the EF in the LAr volume of the 100 lt detector, necessary for operation in two-phase configuration.

Due to the HV problem, after repeated attempts to rescue the HV connection, the Run was stopped on August 13th and the cryostat emptied to proceed to the HV feed-through/cable replacement. During these three months several data taking runs (limited to recording signals from the 37 PMTs of the inner 100lt detector) were collected outside the periods of interventions on the HV system with the chamber in null Electric Field configuration. Most of these runs were dedicated to achieve lowest possible Electronic Noise configuration and to define Single Electron Response (SER) of the individual PMTs (and to monitor SER stability in time). Finally a limited number of data acquisition runs, in best configuration and steady state, have been collected to measure the Light Yield and the Time Constants of Light Signal, characterizing the 100 lt detector performance during this technical run.
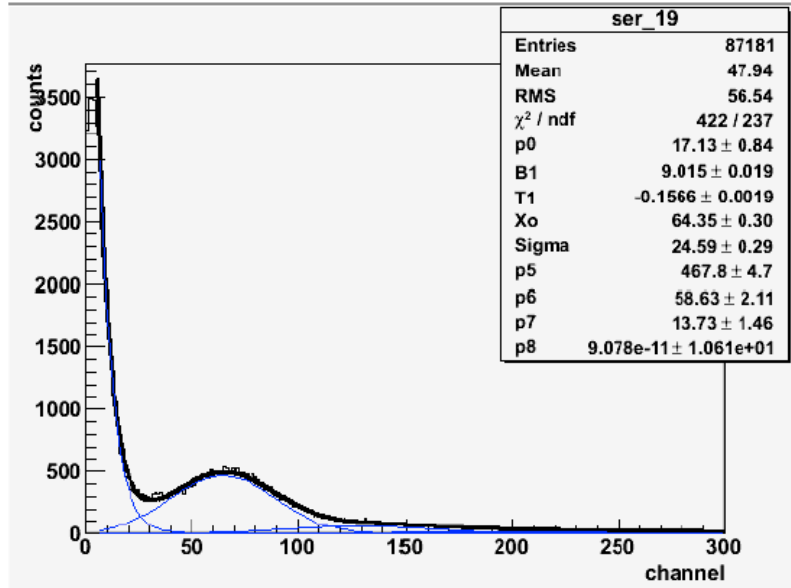
2.1 Data Analysis from the Technical Run

Single Electron Response: for each PMT the SER distribution has been evaluated. This has been done by searching for isolated peaks in each collected PMT waveform (sampled at 1GHz). The area under the detected peaks, which is proportional to the charge collected by the PMT, was evaluated after having subtracted a running baseline[2].

---

[2]In order to evaluate the local baseline the algorithm requires that in a 50 ns window (baseline window) starting at 25 ns after the peak no other peaks are observed. If a second peak is found it is merged with the previous one, the baseline window is set at 25 ns from the second peak and the check is performed again. This algorithm results in a distribution of areas that represent multiple photoelectrons together with the single photoelectron line.

The SER spectrum of each PMT is hence fitted by the sum of an exponential function (describing the dark counts distributions) and the sum of four Gaussian functions with a fixed ratio of the means in order to reproduce the peaks associated to 1, 2, 3 and 4 photoelectrons. The mean value of the first gaussian is taken as the SER value of the PMT. A typical SER spectrum is shown in the figure below.

ser_19	
Entries	87181
Mean	47.94
RMS	56.54
χ^2 / ndf	422 / 237
p0	17.13 ± 0.84
B1	9.015 ± 0.019
T1	-0.1566 ± 0.0019
Xo	64.35 ± 0.30
Sigma	24.59 ± 0.29
p5	467.8 ± 4.7
p6	58.63 ± 2.11
p7	13.73 ± 1.46
p8	9.078e-11 ± 1.061e+01

Light Yield: data from selected acquisition runs have been (individually) analysed to obtain estimates of the Light Yield. For example, results from Run #3229 are reported here. Collected events are mostly from beta decay of ^{39}Ar (Trigger logic: majority 8 PMT with at least 1 phe each). For each event, the individual PMT recorded waveform is first running-baseline subtracted and then integrated in a 7 μs window from the onset (two slightly different integration methods have been employed in the analysis code). The single PMT integrated signals are normalized using the corresponding SER values and then summed (over 36 out of the 37 PMT of the 100lt detector)[3] up to form a sum integrated signal. The amplitude of the sum integrated signal, proportional to the total number of detected photoelectrons, is the primary scintillation signal value, indicated as $S1$ (in phel units).

The $S1$ experimental distribution, after having removed the saturated events, is shown in the figure below (in linear scale and log scale). A fit function was defined by best fitting of the expected spectrum obtained by full simulation of the100 lt detector in presence of the internal ^{39}Ar contamination with GEANT4-based Monte Carlo code (8-th degree polynomial in the energy region 100-650 keV). The free parameters of the fit include the Light Yield. The fit result (red line) is also shown in the figure. The obtained Light Yield

---

[3]One PMT, though functional, was excluded from the sum because the SER peak determination was unstable due to higher noise level.
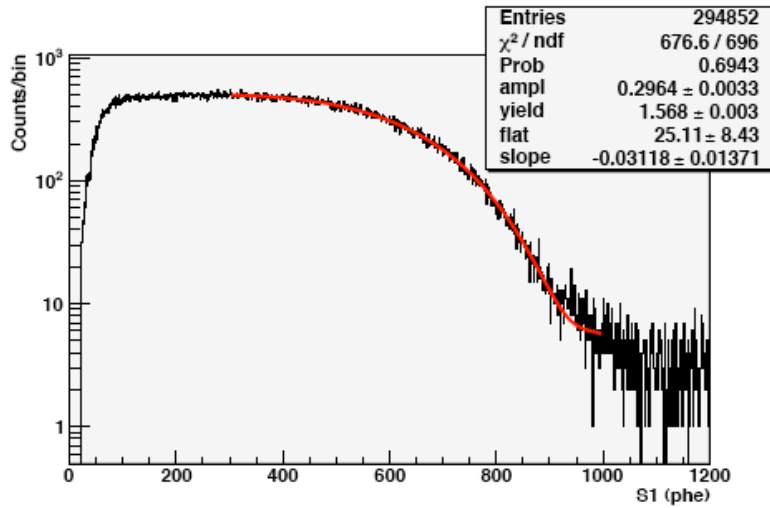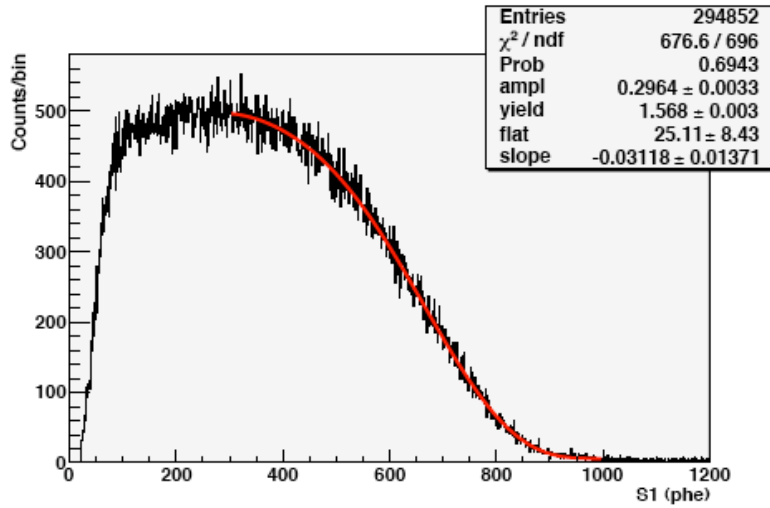
is:

$$Y_{3229} = 1.630 \pm 0.002 phel/keV \tag{1}$$

where only the statistical error is reported. (A slightly lower value $Y_{3229} = 1.568$ has been obtained with the other waveform integration methods implemented in the off-line code). The stability in time of the Light Yield value has been controlled by comparison with equivalent results obtained from the analysis of other two data samples acquired during this technical run. A higher LY value (in the range around 2.5 hel/keV) was expected from simulations and available data on intrinsic parameters of the optical system (wavelength shifter, reflector layer and PMT efficiency.) The lack of LY has been investigated and at present ascribed $\sim$ 15?20 % to apparent reduction of ETL 3PMTs performance and $\sim$ 15?20 % to sub?optimal performance of wavelength shifter (TPB film deposit on reflector foils).

LAr purity measurement through scintillation light decay time: indication about purity level of the liquid has been obtained by analysis of the scintillation (average)

173

signal shape. In particular the long decay time constant τ_T of the LAr scintillation light emission is subject to decrease due to quenching processes in two-body collision of impurities with the Ar_2^* excimer states.

Averaged signal from a data sample has been evaluated and the signal shape fitted to obtain the characteristic time constants of the exponential scintillation light emission (as shown in the figure).

The long decay time constant obtained from the fit was:

$$\tau_T \simeq 1.3 \pm 0.1\mu s \tag{2}$$

This is in agreement with the intrinsic τ_T value of LAr, indicating that a satisfactory level of purity of the liquid was achieved at the filling time and maintained by the GAr recirculation system over the technical run period.
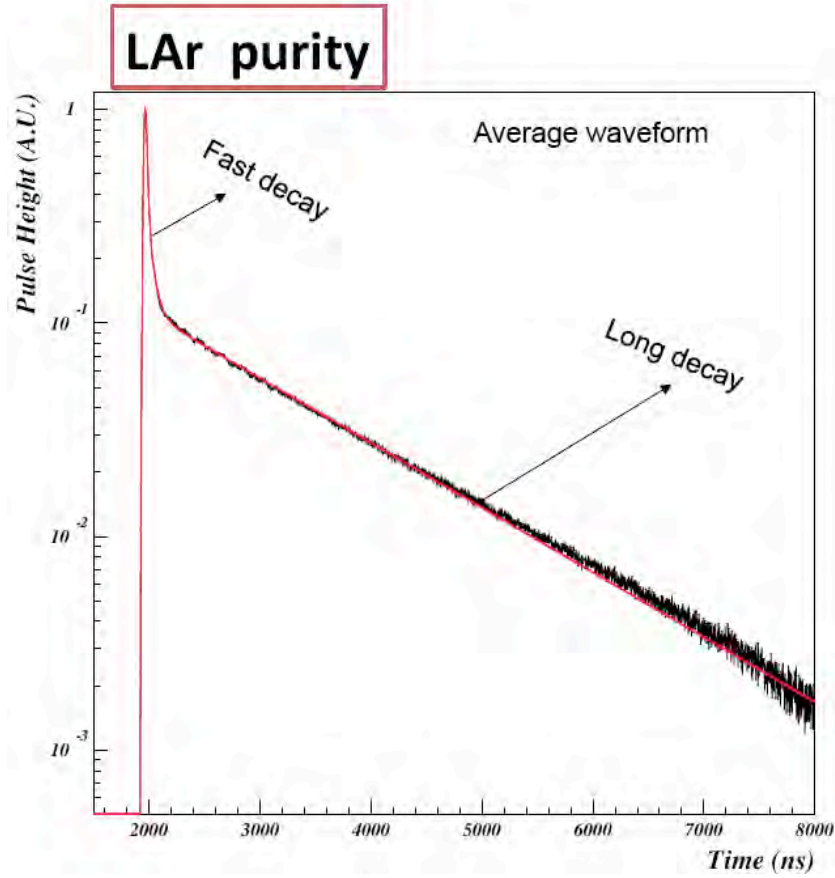
3 Projected sensitivity to WIMP search

Considering the measured Light Yield of 1.63 phel/keVee (at null field), the sensitivity to WIMP search has been projected (according to the standard adopted recipe), yielding

174

for 1 yr running a limit of $10^{?44}$ cm^2 (a factor 2 lower than design sensitivity of $5 \times 10^{?45}$ cm^2). However, this is (still) about 10 times better than present (2009) best published limit.
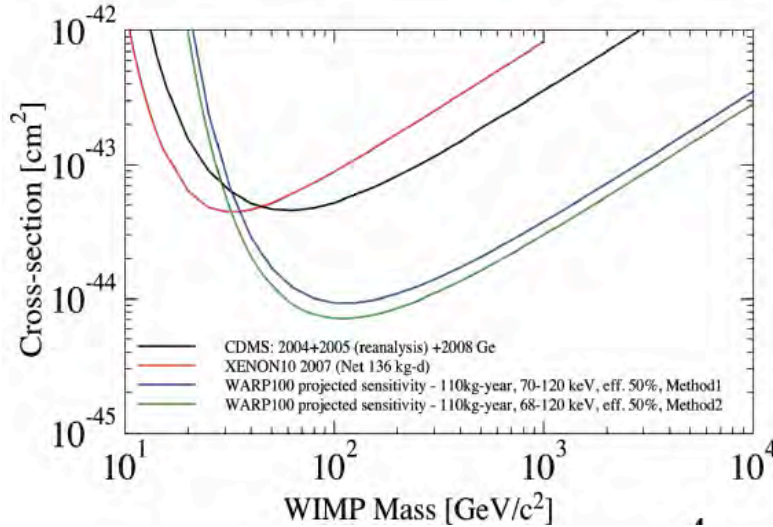
4 Present status and Conclusions

The technical run was stopped on August 13th and the cryostat slowly emptied to proceed to the HV feed-through/cable replacement. Warming up to room temperature (avoiding air/humidity back diffusion into the cryostat) lasted about one month and then the top flange of the cryostat has been opened and the detector moved back into the WArP clean room in Hall B.

Inspection of the HV system confirmed the presence of a crack along the HV cable insulation, connecting the HV feedthrough (internal side) to the detector cathode, where the discharge occurred in the gas phase volume just above the liquid argon surface level.

The HV cable insulation (H.D. PolyEthylene) mechanically cracked at LAr temperature due to internal stresses introduced by a thermal treatment of the HV cable.

A limited portion of the veto detector has been dismounted to allow removal of the HV cable.

A new HV cable and feed-through design has been drawn and realized. It has already been successfully tested at LAr temperature with 100 kV supply in several cycles.

The faulty PMT connections (4 PMTs) have been fixed.

Investigations are also actively on going to identify the origin of the lack of light yield (compared to expectations) experienced during the technical run. In particular, attention is being paid to possible variations of the quality of the TPB film deposit on the reflector foils covering the internal surfaces of the 100 lt detector. Tests of the optical system (reflector and TPB coating) have been performed as well in view of a detector remounting.

Start of the WArP 100 lt detector new commissioning is foreseen by January 2010. About two months of vacuum pumping are required. After LAr filling (March), back to operation is expected in April 2010. After common detector issues (detector/electronics/DAQ debugging, analysis optimization, background studies, etc.), an extended calibration run with gamma and neutron sources is foreseen, just before starting a long duration Physics run.

In parallel, a run with the 2.3 liters prototype with Depleted Argon in Hall B at LNGS is included in the WArP program for 2010. The prototype will make use of a new type of High QE PMT developed to work at LAr temperature to reach the highest light yield.

References

[1] C. Rubbia *et al.*, A programme to search for WIMP particles in Liquid Argon at the LNGS, Letter of intent, Univ. of Pavia, July 1999.

[2] WArP Collaboration, Status Report of the current progress of the WArP Experiment, **LNGS-EXP 32/05** (2005);

[3] WArP Collaboration, First results from a dark matter search with liquid argon at 87 K in the Gran Sasso underground laboratory, Astropart. Phys. **28** (2008), 495.

[4] WArP Collaboration, Measurement of the specific activity of ^{39}Ar in natural argon, Nuclear Instruments and Methods in Physics Research A 574, 83 (2007).

[5] D. Acosta-Kane *et al.* (WArP Collaboration), Discovery of underground argon with low level of radioactive 39Ar and possible applications to WIMP Dark Matter detectors, arXiv:0712.0381v1 [astro-ph] (Dec 2007), Nucl. Instr. and Meth. A 587 (2008), 46.

[6] WArP Collaboration, Effects of Nitrogen contamination in Liquid Argon, arXiv [nucl-ex]0804.1217v, to be submitted to *JINST*

[7] WArP Collaboration, Oxygen contamination in liquid Argon: combined effects on ionization electron charge and scintillation light, arXiv [nucl-ex]0804.1222v, to be submitted to *JINST*

The XENON100 Dark Matter Experiment

E. Aprile[a] [*], K. Arisaka [g], F. Arneodo[c],
A. Askin[b], L. Baudis[b], M. Beck[h], A. Behrens [b], E. Brown [g], J. Cardoso[e],
B. Choi[a], D. Cline [g], L. Coelho[e], J.-P. Cussonneau[i], S. Fattori[c] [f],
A. Ferella[b], K.L. Giboni[a], V. Hannen[h], K. Hugenberg[h], A. Kish[b], J. Lamblin[i]
R. Lang[a], K.E. Lim[a], J.A.M. Lopes[e], T. Marrodan-Undagoitia [b],
Y. Mei[d] , A.J. Melgarejo[a], K. Ni[j], U. Oberlack[d], S. Orrigo[e],
E. Pantic [g], G. Plante[a], A. Ribeiro[e], J. Santos[e], R. Santorelli[b],
M. Schumann[d], P. Shagin[d], A. Teymourian [g],
D. Thers[i], H. Wang [g], C. Weinheimer[h]

[a] Department of Physics, Columbia University, New York, NY 10027, USA
[b] Physics Department, University of Zurich, Switzerland
[c] INFN, Laboratori Nazionali del Gran Sasso, Assergi, 67100, Italy
[d] Department of Physics and Astronomy, Rice University, Houston, TX 77251, USA
[e] Department of Physics, University of Coimbra, R. Larga, 3004-516, Coimbra, Portugal
[f] Dipartimento di Fisica, Università de L'Aquila, Italy
[g] University of California, Los Angeles
[h] Institut für Kernphysik, Wilhelms Universität, 48149 Münster, Germany
[i] Subatech Laboratory, University of Nantes, 44307 Nantes, France
[j] Shanghai Jiao Tong University, Shanghai, China

[*] Spokesperson

Abstract

The XENON100 experiment aims to detect cold dark matter particles via their elastic collisions with xenon nuclei. During 2009 the commissioning phase of the detector has been completed and calibration runs have been carried out, prior to he start of data taking which occurred in January, 2010. We briefly review the status of the project.

1   Introduction

XENON100 is a two-phase liquid/gas time projection chamber (TPC) aiming to directly detect dark matter by observing nuclear recoils from WIMPs scattering off xenon nuclei. As its predecessor XENON10, which has established some of the best limits on WIMP-nucleon interactions so far [2], the experiment is located in the interferometer tunnel of LNGS. It has about 10 times more target mass than XENON10, and the gamma background was improved by 2 orders of magnitude by optimizing the detector design and careful selection of all detector materials.

A liquid xenon (LXe) two-phase TPC is a powerful tool for rare event searches since it combines excellent self-shielding capabilities with 3D event position reconstruction and signal to background discrimination, based on the simultaneous detection of the scintillation light (S1) and the charge signal (S2) of an interaction.

Even though the experiment itself was not affected at all by the earthquake in April, we had to reduce the number of permanent people on site due to a lack of housing and general infrastructure. However, the progress of XENON100 is not affected by this measure.

The commissioning of XENON100 has been completed in 2009. The detector has been filled with 170kg of ultra pure Xenon, through a distillation column to remove 85-Kr. The detector is now (early 2010) in data taking and will accumulate data for a dark matter search throughout the year. With a raw exposure of 6000 kg-days, free of background events, XENON100 will reach $\sigma \sim 2 \times 10^{-45}$ cm^2 at 100 GeV, more than a factor of 20 better than current limits [2, 1].

2   The XENON100 Detector

The XENON100 detector uses the same principle of operation and many design features successfully tested in the XENON10 prototype. A detailed description of Xenon 10 and its performances can be found in [3]. Here we only recall a few characteristics of the detector. XENON100 is a position-sensitive XeTPC, with the sensitive LXe volume viewed by two arrays of photomultiplier tubes (PMTs), to detect simultaneously the primary scintillation signal (S1) and the ionization signal via the proportional scintillation mechanism (S2). The sensitive target can be "fiducialized" to keep only the inner core free of background. In addition, the high ionization density of nuclear recoils in LXe leads to an enhancement in S1 and reduction in S2, compared to electronic interactions. The S2/S1 ratio therefore discriminates WIMP nuclear recoils from γ and β backgrounds with an efficiency of 99.5–99.9%, as demonstrated with XENON10 [2].

A schematic drawing of the XENON100 detector and a photo are shown in Fig.1 (right). The active volume contains 65 kg of LXe and is instrumented with 178 PMTs in two arrays, 98 in the gas and 80 in the liquid. All PMTs are Hamamatsu R8520-06-Al 1" square, optimized for Xe 178 nm light and selected for low radioactivity. The quantum efficiency (QE) of these tubes was also improved from $\sim 24\%$ to $\sim 35\%$. The active target is enclosed in a PTFE cylinder of 15 cm radius and 30 cm height. This PTFE cylinder reflects scintillation light with high efficiency [6], and optically separates the LXe target from the surrounding LXe which is necessary to separate the TPC with its electric field
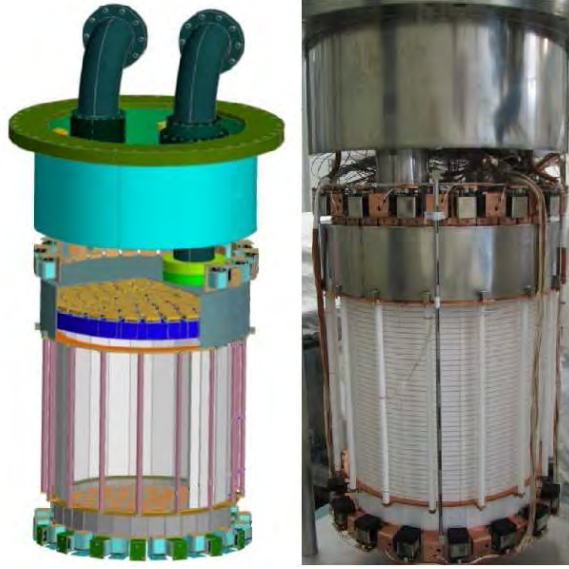
Figure 1: Drawing and a photo of the XENON100 TPC.

from the walls of the vessel. 64 PMTs turn this outer LXe volume into an active LXe, with a total mass of 105 kg, including LXe layers above the top and below the bottom PMT arrays. The cooling system is based on a 170 W pulse tube refrigerator (PTR), originally developed for the MEG experiment [5]. The PTR is used to liquefy Xe and to maintain the liquid temperature during operation.

3 Xe Gas Handling, Purification and Kr Removal System

The XENON100 detector requires a total of 170 kg of Xe to fill the target and the active veto. The gas is stored in four aluminum cylinders connected by high pressure valves, that can be cooled with LN_2 during recovery from the detector.

To reduce electronegative impurities in commercial Xe well below 1 part per billion (ppb) O_2 equivalent that is required for long electron lifetime and long VUV photons absorption length, we are using the system developed for XENON10, based on continuous Xe gas circulation with purification through a high temperature metal getter (SAES). The ~ 2 ms electron lifetime demonstrated with XENON10 data [3] correspond to four meters drift length, much longer than the 30 cm maximum drift in XENON100.

LXe, as a condensed noble gas, is readily purifiable for most radioactive impurities. The one notable exception is ^{85}Kr, present in commercial Xe gas at the ppm level. Beta decays of ^{85}Kr (687 keV end point, 10.76 years of half life) presents a serious background for a dark matter search. The gas used in XENON100 was processed by the Spectra Gases Company to reduce the Kr concentration to ~ 5 ppb, using their cryogenic distillation plant. This level has been achieved in XENON10 [3] with gas also processed by the same company, and verified by positive identification of the beta-gamma coincidences with

Figure 2: Picture of the Kr distillation column in commissioning.

1.46 μs time difference from decays ^{85}Kr(β) $\rightarrow^{85m}$Rb(γ) $\rightarrow^{85}$Rb at a 0.454% branching ratio. During the first background run with XENON100, we identified these "delayed-coincidence" events and inferred a Kr/Xe level of 7 ppb, consistent with the value of Spectra Gases.

In order to reduce the ^{85}Kr level to <50 ppt, required by the XENON100 sensitivity goal (50 ppt of ^{85}Kr contribute a rate of 10^{-3} evts/kg/keV/day), we have purchased a cryogenic distillation column made by Taiyo-Nippon Sanso. The column has been commissioned at LNGS and has been used to purify the XENON100 gas. It is 3 m tall and is designed to deliver a factor of 1000 reduction in Kr at a purification speed of 0.6 kg/hour.

4   Activity in 2009

Year 2009 has been characterized by an intense activity aimed at the final commissioning of the detector, which, at the end of the year, started the final set of calibration runs.

4.1   Light and Charge Signals

During early Spring 2009, we realized that we had some gas permeation through a seal of the cryostat. After the exchange of the seal under N_2 atmosphere, the detector was prepared for filling by baking and by recirculation of warm xenon gas though the detector and the getter. The analysis of the residual gas showed that the gas permeation into the detector had been reduced by 2 orders of magnitude. The decrease of the water content
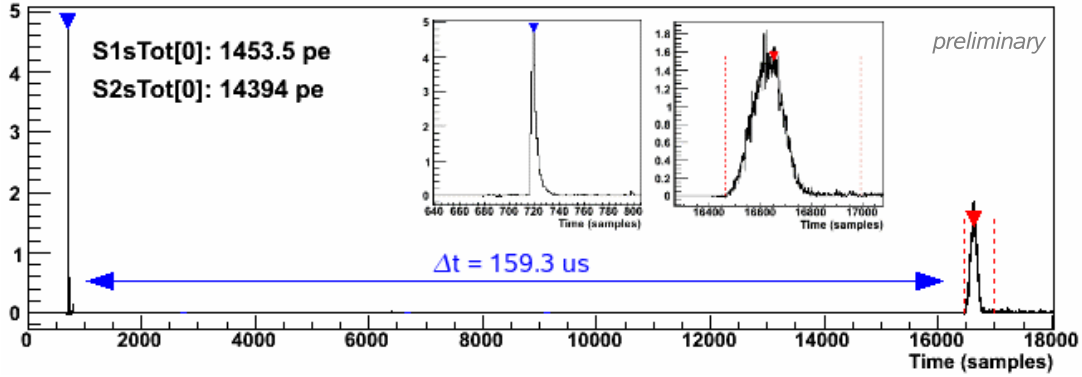
Figure 3: Example of a XENON100 event with almost maximum drift time: The interaction happened close to the cathode. One time sample corresponds to 10 ns. The narrow pulse at 720 is the prompt S1 scintillation light, the broader peak at 16600 is the charge signal (S2).

in the xenon gas was monitored with a dedicated device (TigerOptics HALO). The final value was about 1 ppb, the sensitivity of the device. In August 2008 a recirculation through the distillation column has been performed, lasting approximately 20 days.

Whereas the previous runs showed an increase in light yield during the first weeks after detector filling until a maximum value was reached, we now observe the maximum light yield basically immediately. Furthermore, with the improved leak-tightness of the detector and the improved outgassing, we also observe charges from interactions in the LXe that are drifted across the TPC and get extracted into the gas phase. The loss of ionization electrons with drift length, described by the *electron lifetime* as we measure the drift length in microseconds, is directly related to the number of remaining electronegative impurities in the LXe. The lifetime increases with continuous Xe purification and we are able to detect S2 signals from all parts of the TPC (cf. Fig. 3). The highest value reached so far is 240 μs.

Position Reconstruction; Position Dependence of Light Signal The calibration data have been used to fully exploit the 3D interaction position reconstruction capabilities of the TPC: The z-coordinate is given by the drift time (since the drift velocity for a given drift field is a constant number), and the xy-position is derived from the hit pattern on the top PMT array, located in the gas volume. We have developed 3 different reconstruction techniques, based on neural networks, support vector machines, and χ^2-minimization, that are continuously tested, compared, and improved. A test of the reconstruction quality with a strongly collimated point source gives a measured uncertainty of ± 3 mm in the reconstructed position, where the error is dominated by the positioning of the source.

The position information for every event also permits to measure the position dependence of the light yield (that is directly correlated to the light collection efficiency, LCE), and to calculate the average light yield of the detector: From the analysis of a high statistics ^{137}Cs data set, we obtain an energy corrected average of 4.5 PE/keV at 122 keV (zero field). This is 80% of the XENON10 light yield as expected from detector design. The z-dependence of the light yield agrees with the Monte Carlo simulations of the LCE
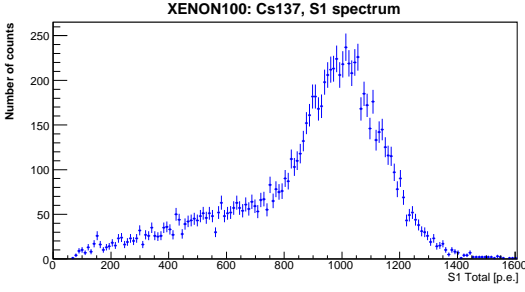
Figure 4: Prelim. scintillation light (S1) spectrum of ^{137}Cs corrected for position dependent light collection efficiencies. An active veto cut has been applied.

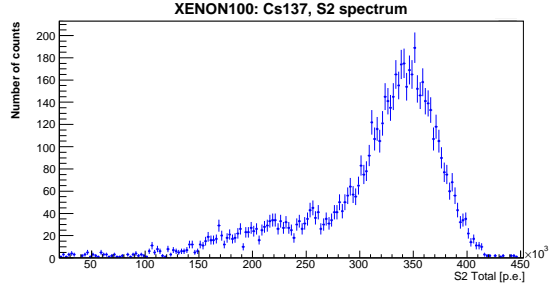Figure 5: Preliminary charge (S2) spectrum of ^{137}Cs corrected for the finite electron lifetime. An active veto cut has been applied.

(cf. Fig. 6).

With light and charge signal at hand many other analyses are possible since all position dependent corrections can be applied (cf. Figs 4, 5). Work on the energy resolution for S1, S2 signals, and the combined energy scale are in progress. The same holds for calibrations of the gamma and neutron bands as a prerequisite for the discrimination between electron- and nuclear recoils based on their different S2/S1 ratios.

5 Purification from ^{85}Kr

Xenon itself has no long-lived radioactive isotope, however, commercially available xenon gas always contains some krypton at the ppm–ppb level. About 10^{-11} of this is the radioactive isotope ^{85}Kr ($T_{1/2} = 10.76$ a). In order to reach the full design sensitivity of XENON100, the Kr concentration in Xe has to be about 50 ppt, leading to less than 1 event from ^{85}Kr in the WIMP search region within 180 days.

Since both elements are noble gases, Kr cannot be separated chemically from Xe.
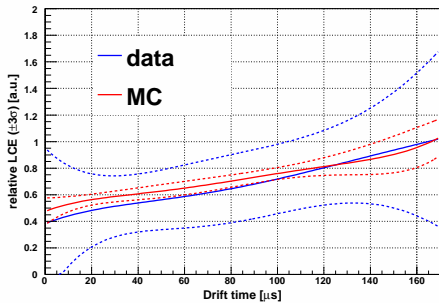
Figure 6: Comparison of the measured z-dependence of the light yield (blue) with the expectation from a Monte Carlo simulation of the light collection efficiency (red). Shown is the mean value and the $\pm 3\sigma$ contours. The agreement is very satisfactory.
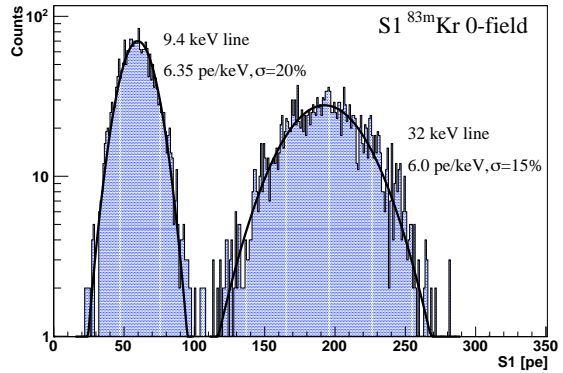

Figure 7: The low energetic gamma lines at 9.4 keV and 32.1 keV from the delayed coincidence decay of ^{83}Kr. Figure from [4].

Therefore we have procured a dedicated Kr-distillation column to decrease the Kr concentration. A first test run in September 2008 has proven that the column works. A second purification run to reach the required Kr-level was performed in July/August 2009. The data has been analyzed using a delayed coincidence decay channel with 0.434% branching ratio, and a preliminary confidence interval of 15 to 550 ppt for the Kr concentration has been obtained. At these low concentrations, a large amount of data are necessary for the analysis and more statistics is needed in order to improve the limit. Since there are also events from other sources that show a similar pattern, the delayed coincident analysis might reach its limit at some point, so that the background spectrum at low energies will have to be used to give the final limit. A new method based on trace analysis of trapped Kr atoms has been proposed by the Columbia group and funded by NSF, but will take some time to develop.

6   R&D for Calibration at low Energies

The excellent self shielding capability of LXe has the drawback that the target volume of XENON100 cannot be calibrated with low energetic gamma rays from the outside: their mean free path is simply too short and all photons are stopped in the LXe veto layer. However, the whole detector volume has to be calibrated in the region of interest for the Dark Matter search at low energies. In XENON10, neutron activated xenon with two metastable isotopes with half-lifes around 10 days was added to the detector for a volume calibration. The drawback of this method is the fairly long half life of the activated nuclei, the possible creation of other radioactive isotopes, and the rather high energy of the gamma lines (164 keV and 236 keV).

Two small prototype two-phase TPCs have been developed in Zurich and Columbia to investigate 83mKr for energy calibration. 83mKr is introduced into the liquid xenon detectors through the gas system and it provides a uniform calibration source. At the same time it has two transitions at the energies: 32.1keV and 9.4keV being the second in the dark matter region of interest. Both lines are separated by only 154ns which makes the identification easy even for a detector that is not design for low background. The short half-life of 83mKr only 1.83 hours allows for a short turnaround time following dark matter measurement.

Data from the successful implementation of this source in the Zurich test prototype have been published [4]. They provide new information on the scintillation light emission for low energy events as well as the dependence of the light yield on an applied electric drift field. As the applied field is increased, more and more electrons leave the interaction point, suppressing the recombination process that contributes photons to the scintillation signal.

83mKr is a decay product of a 83Rb source which emit gamma rays mainly at 520keV. In this setup, a possible contamination of the liquid xenon with rubidium has been studied and no contamination has been found. This measurement provides an upper limit on the level of 83Rb contamination introduced to the system of $< 120\mu$Bq/h exposure. In the context of the next generation of LXe dark matter direct detection searches, this upper limit translates to a maximum introduced background far below the intrinsic backgrounds.

7 List of Publications during 2009

- Constraints on inelastic dark matter from XENON10. By XENON10 Collaboration (J. Angle et al.). Oct 2009. (Received Dec 1, 2009). 8pp. Published in Phys.Rev.D80:115005,2009. e-Print: arXiv:0910.3698 [astro-ph.CO]

- Aprile et al. Design and Performance of the XENON10 Dark Matter Experiment. arXiv (2010) vol. astro-ph.IM

- Aprile et. al "New Measurement of the Relative Scintillation Efficiency of Xenon Nuclear Recoils Below 10 keV", Phys. Rev. C 79, 045807 (2009)

- E. Aprile & L. Baudis, "Liquid Noble gases" in *Particle Dark Matter*, Edited by Gianfranco Bertone, Cambridge University Press, 2009

- E. Aprile and S. Profumo, "Dark Matter and Particle Physics", Focus Issue for New Journal of Physics, 2009

References

[1] Z. Ahmed *et al.* [CDMS Collaboration], arXiv:0802.3530 [astro-ph].

[2] J. Angle *et al.* [XENON Collaboration], Phys. Rev. Lett. **100**, 021303 (2008).

[3] Aprile et al. Design and Performance of the XENON10 Dark Matter Experiment. arXiv (2010) vol. astro-ph.IM

[4] A. Manalaysay et al., arXiv:0908.0616 (2009).

[5] T. Haruyama *et al.*, in: *Cryocoolers 13*, Springer, New York, 689 (2005).

[6] M. Yamashita *et al.*, NIM A **535**, 692 (2004).

ERMES
Uranium groundwater monitoring: from the neutron flux background to the L'Aquila earthquake, 6th April 2009

Wolfango Plastino[a][b], Francesco Bella[a],
Stefano Nisi[c], Luca Ioannucci[c], Piergiorgio Aprili[c],
Marco Balata[c], Massimiliano De Deo[c], Mario De Vincenzi[a][b],
Giuseppina Giusti[c], Matthias Laubenstein[c],
Federico Ruggieri[b], Ludovico Tortora[b]

[a] Dep. of Phys., Univ. of Roma Tre, I-00146 Rome, Italy
[b] INFN, Section of Roma Tre, I-00146 Rome, Italy
[c] INFN, Gran Sasso National Laboratory,I-67010 Assergi (AQ), Italy

Abstract

The possible sources analyzed up to now for the neutron flux background at the Gran Sasso National Laboratory are the natural radioactivity in the rock, the concrete, as well as the induced part coming from interaction of cosmic ray muons with the rock or the detector material itself. Water was considered only as moderator in concrete, due to its variable concentration and its radioactivity as additional source for neutron flux modulation. Therefore, the water-rock interaction and its spatial-temporal variation induced by hydrological pattern of the Gran Sasso aquifer are taken into account [1]. Monitoring of chemical and physical groundwater parameters has been carried out worldwide in seismogenic areas with the aim to test possible correlations between their spatial and temporal variations and strain processes. Uranium groundwater anomalies were observed during the preparation phases of the recent L'Aquila earthquake of 6th April 2009 in the cataclastic rocks near the overthrust fault crossing the deep underground Gran Sasso National Laboratory. The obtained results suggest that uranium may be used as a potential strain indicator of geodynamical processes occurring before the seismic swarm and the main earthquake shock [2].

1 Introduction

The neutron flux background plays a key-role in several research activities for Neutrino Physics and Dark Matter detection in underground environment. The neutron sources considered at deep underground are (α, n) reactions on light elements (e.g., Li, F, Na, etc.), spontaneous fission, mainly of ^{238}U [3], and those induced by cosmic ray muons. The Gran Sasso National Laboratory - National Institute of Nuclear Physics (LNGS-INFN) is located inside the largest aquifer of central Italy. The natural radioactivity in rock and materials used for the internal structures of the LNGS-INFN has been studied in detail [4] [5], and the specific activities of natural radionuclides are known with high accuracy for the characterization of neutron background at the LNGS-INFN [5]. Moreover, numerical simulations [3] and neutron flux measurements were carried out inside the LNGS-INFN [5] [6] [7] [8] [9] [10] [11]. Nevertheless, the contribution of the natural radioactivity in the ground water and its spatial-temporal variations induced by the water-rock interaction and the hydrological properties of the Gran Sasso aquifer have never been considered. The measurements of the neutron flux made during the years at the LNGS-INFN revealed differences of orders of magnitude [3], but it is difficult to correlate them with the aquifer properties at that time. Within the framework of the INFN scientific program ERMES (Environmental Radioactivity Monitoring for Earth Sciences) environmental radioactivity measurements were performed inside the LNGS-INFN: particularly, radon [12] [13], radiocarbon [14], and tritium [15]. These measurements have shown the existence of different chemical-physical and fluid dynamical characteristics in the ground water. The measurements of the neutron flux [5] [6] [7] [8] [9] [10] [11] and the numerical simulations [3] have been performed in time intervals not exceeding the temporal and spatial variations of environmental radioactivity detected by ERMES. The results of the ground water radioactivity monitoring show temporal modulations induced by ground water variations due to percolation effect related to snow melting, and spike-like events due to rainfall and/or diffusive processes through the structural discontinuities [16]. Therefore, this work is a preliminary study focusing on the importance of ground water radioactivity as additional source for neutron flux variation. The ability to predict earthquakes has been of great interest for the Earth Sciences and the society. Radon has been suggested as one of possible precursors, and its groundwater anomalies associated with earthquakes and water-rock interactions were detected in several seismogenic areas worldwide indicating possible transport of radon through microfractures or the crustal gas fluxes along active faults [12] [13] [17] [18] [19] [20] [21] [22] [23] [24] [25]. The physical processes associated with radon groundwater anomalies are based on changes of radon emanation rates occurring due to strain signal near the earthquake's nucleation point. In the geological environment the radon concentration depends on the isotopic abundance of its parents (^{238}U and ^{226}Ra), and on their geochemical patterns with reference to environmental redox and pH characteristics. The geodynamical processes induced by earthquakes can modify radon migration patterns in groundwater as a potential strain meter probe. However, the activity of radon in fractured lithologies is difficult to predict and the measurement of radon concentration does not uniquely constrain the rock deformation or the chemical inhomogeneity [26], as well as its relationship with the transient crustal strain signals from 'aseismic' fault slip near the earthquake's nucleation point [27]. Moreover, non-tectonic

factors related to variations of chemical and physical groundwater parameters may be of importance [2] [28], requiring proper geological, hydrological and hydrogeological settings [29], so only the variations induced by stress-strain processes should be considered in evaluations. Important issues are the stability and reliability of the monitoring system which should be checked continuously during the measurement time [12] or the development of new detectors independent of environmental noise parameters such as temperature, acid concentrations, humidity, and air pressure [30]. The LNGS-INFN is located inside the largest aquifer of central Italy, within the limestones formation of the upturned syncline, near the main overthrust fault. This separates water masses belonging to two distinct creeks: the first one, where the main laboratories are excavated, flows in well drained cretaceous formations, while the latter is within not drained and poorly permeable dolomitic formations [11].

2 Discussion

The high peaks in the uranium concentration [1] were induced prevalently by geodynamical processes through the fault and hydrological pattern due to the high permeability of the cretaceous limestone forming of the Gran Sasso massif. The water-rock interaction and ground water geochemistry modulate these variations. The thorium concentration could not be determined and gave only upper detection limits. This can be understood as thorium compounds are generally very poorly soluble in water. These studies have emphasized a complex structure of the aquifer due to geological and structural discontinuities, induced by the distensive tectonic phase that characterizes the Gran Sasso area. The presence of semi-permeable and impermeable structures near these discontinuities produces hydrostatic gradients as well as different hydrologic and geochemical properties in the various compartments of the aquifer. In particular, the main overthrust fault is separating water masses belonging to two distinct creeks [1] [13]: the first one in which are embedded the main laboratories, flows in well-drained cretaceous formations, while the latter is lying within not-drained and poorly permeable dolomitic formations. The area under investigation was from November 2008 to December 2009 marked by a seismic swarm with the main shock occurring at 01:33 UT on April 6th, 2009 (Mw=6.3), located about 18 km far from LNGS-INFN. In the period 2002-2007 the local seismicity was widespread in the NW sector of the epicentral area of the L'Aquila earthquake with depths ranging from 10 to 20 km and magnitudes from 0.8 to 3.5. The L'Aquila sequence started in November 2008 close to the main event of 6th April, 2009. The depths were between 8 - 12 km and the magnitudes were up to 4.1 (less of 2,000 events). After 6th April, 2009 the seismicity continued, migrating to the North and SE sectors with 2 aftershocks of Mw=5.2 and Mw=5.4 [2]. Uranium groundwater monitoring was carried out from June 2008 with the aim to better define the radon groundwater transport processes through the overthrust fault [2] [12] [13], as well as to check its contribution to the neutron background at the LNGS-INFN [1]. The uranium groundwater results obtained between June 2008 and December 2009 showed two different water groups, which were also supported by stable isotope ($\delta^2 H$,δ^{18}O), ^{14}C and ^{3}H analyses [2] [31]. This indicates that the uranium groundwater changes strongly depend on the position of monitoring

stations and the overthrust fault [2]. The observed uranium variations [2] were pointing out a seasonal trend of the water table in the Gran Sasso aquifer due to its recharge modulated by percolation effect related to snow melting during summer period, and some spike-like anomalies not related to hydrological and geochemical patterns. These uranium anomalies in groundwater were detected until beginning of March, 2009 about one month before the L'Aquila earthquake of 6th April, 2009. However, during the main shock and aftershocks the variations in the uranium content were small. Groundwater pH and Eh do not support the observed uranium anomalies. The flow rate observed at the Traforo spring located in the tunnel close to the monitoring area, which collected percolation water from the LNGS-INFN and the highway tunnel, showed a seasonal trend due to snow melting during summer period. This trend was modified, however, from November 2008 with starting of the seismic swarm located about 20 km far from the spring, and drastically during the main shock on 6th April, 2009 with a jump-like anomaly of about 120 l/s. This behavior emphasized hydrological links between the Gran Sasso aquifer and seismic activities before, during and after the main shock [2]. A correlation between the shear strain in cataclastic rocks and the uranium content of groundwater was investigated, suggesting a progressive increase in uranium enrichment with deformation [32]. This behaviour was detected in thermal waters and environments characterized by uranium concentrations of rocks of several parts per million. The Gran Sasso karst aquifer, however, does not have similar characteristics, and the uranium content of the rock is very low [3] [4]. The fluids are crucial for the mechanics of faults [33], as they play both passive and active role during deformations. Variations in the fluids flux was observed during seismic sequences, likely associated with variations in the state of stress of the crust. Moreover fluids (CO_2) can increase pore pressure, and thus trigger a fault rupture along asperities [34]. The crustal rupture may follow the fault-valve behaviour [33], with cyclic changes in the transit, accumulation and release of fluids. As fluids decrease the friction on the fault plane, their variation in time could control the episodic activity of faults.

3   Conclusion

The characterization of the neutron flux background at the LNGS-INFN was done until now considering as possible sources: (a) the radioactivity in the rock and the concrete, and (b) the induced radioactivity from cosmic ray muons interaction with rock or detector itself. Water was considered only as neutron moderator, due to its presence in the concrete. Therefore, only an expected steady-state neutron background was evaluated. Nevertheless, the radioactivity in the ground water showed spatial-temporal variations at the LNGS-INFN; for a better characterization of neutron flux background new piece of information should be considered. In particular, the fluid dynamics properties in fractured porous rock play an important role to define the uranium pattern in the ground water [1]. The uranium groundwater anomalies observed before the seismic swarm and the main shock, which occurred on 6th April, 2009 in L'Aquila, were probably associated with geodynamical processes occurring before the earthquake, which triggered diffusion processes through the overthrust fault. The observed uranium anomalies cannot be re-

lated with geochemical and/or hydrological variations of the Gran Sasso aquifer. This would indicate that more attention should be devoted to the pre-earthquake studies of geodynamical processes, especially on characteristics of fluids, filling the fractures before the main shock. Uranium in groundwater can be used therefore as a potential indicator of pre-earthquake processes as it may be associated with geodynamics of preparation phases of earthquakes [2].

4 Acknowledgments

References

[1] W. Plastino et al., J. Radioanal. Nucl. Chem. 813, 809 (2009)

[2] W. Plastino et al., J. Environ. Radioactiv. 101, 45 (2010)

[3] H. Wulandari et al., Astropart. Phys. 22, 313 (2004)

[4] A. Esposito, M. Pelliccioni, Nucl. Sci. J. 22, 291 (1985)

[5] E. Bellotti, Nucl. Instr. Meth. 264, 1 (1988)

[6] A. Rindi et al., Nucl. Instr. Meth. A 272, 871 (1988)

[7] R. Aleksan et al., Nucl. Instr. Meth. A 274, 203 (1989)

[8] P. Belli et al., Nuovo Cimento 101A, 959 (1989)

[9] M. Cribier et al., Astropart. Phys. 4, 23 (1995)

[10] F. Arneodo et al., Nuovo Cimento 112A, 819 (1999)

[11] H. Menghetti, Nuovo Cimento 29C, 345 (2006)

[12] W. Plastino, F. Bella, Geophys. Res. Lett. 28, 2675 (2001)

[13] W. Plastino, In Radionuclides in the Environment, P. P. Povinec, J. A. Sanchez-Cabeza. Eds. (Elsevier, Oxford, UK, 2006), pp. 335-342.

[14] W. Plastino et al., Radiocarbon 43, 157 (2001)

[15] W. Plastino et al., Radiat. Meas. 42, 68 (2007)

[16] M. Caputo, W. Plastino, Geophys. J. Int. 158,:385 (2004)

[17] V. I. Ulomov, B. Z. Mavashev, Dokl. Akad. Sci. USSR, Earth Sci. Sec. 174, 9 (1968).

[18] C. H Scholz, L. R. Sykes, Y. P. Aggarwal, Science 181, 803 (1973).

[19] H. Wakita, Y. Nakamura, K. Notsu, M. Noguchi, T. Asada, Science 207, 882 (1980).

[20] E. Hauksson, J. Geophys. Res. 86, 9397 (1981).

[21] Wakita, G. Igarashi, Y. Nakamura, Y. Sano, K. Notsu, Geophys. Res. Lett. 16, 417 (1989).

[22] M. M. Monnin, J. L. Seidel, Nucl. Instr. Meth. A 314, 316 (1992).

[23] H. S. Virk, B. Singh, Geophys. Res. Lett. 21, 737 (1994).

[24] G. Igarashi et al., Science 269, 60 (1995).

[25] C. Y. King, N. Koizumi, Y. Kitagawa, Science 269, 38 (1995).

[26] T. Torgersen, J. Beniot, D. Mackie, Geophys. Res. Lett. 17, 845 (1990).

[27] E. Roeloffs, Nature 399, 104 (1999).

[28] M. H. Shapiro, A. Rice, M. H. Mendenhall, D. Melvin, T. A. Tombrello, Pure and Appl. Geophys. 122, 309 (1985).

[29] . Trique, P. Richon, F. Perrier, J. P. Avouac, J. C. Sabroux, Nature 399, 137 (1999).

[30] W. Plastino, P. De Felice, F. De Notaristefani, Nucl. Instr. Meth. A 486, 146 (2002).

[31] K. Rozanski, Private communication.

[32] A. McCaig, Nature 340, 600 (1989).

[33] R. H. Sibson, Tectonophysics 211, 283 (1992).

[34] S. Miller et al., Nature 427, 724 (2004).

GIGS. The Interferometric Station at LNGS

Antonella Amoruso[a,b], Luca Crescentini[a,b,c]

[a] Dip.to di Fisica Univ. di Salerno, Salerno - Italy
[b] INFN - Gruppo collegato di Salerno, Salerno - Italy
[c] Spokeperson

Abstract

Since several years two geodetic extensometers are working at LNGS. Both instruments are unequal-arm Michelson interferometers, using a 90-m long measurement arm and a <40-cm long reference arm, and sharing the same stabilized HeNe laser source. Nominal sensitivity is $\sim 10^{-12}$ and, in the present configuration, recording rate is 600Hz ([1]). The two interferometers are monitoring extension along two orthogonal directions, striking N66E (BC interferometer) and N24W (BA interferometer). During 2009 the activity has been mainly devoted to the analysis of the data produced by the interferometers before and after the occurrence of the April 6th earthquake. We have already obtained definitive results related to the slow slip propagation occurred on the earthquake causative fault in the hours immediately after the main shock, and afterslip on a stationary region of the same fault occurred in the first few days after the event ([2]). Preliminary results from the analysis of pre-seismic data, in search of precursors of the earthquake, give unprecedentedly tight limits on the size and strength of a possible preparatory zone and on the amount of released pre-seismic moment. Data related to the post-seismic phase are still under investigation.

1 The April 6th 2009 L'Aquila earthquake: The first few days following the event

During the April 6th 2009 LAquila earthquake the interferometers never lost optical alignment (Figure 1) and have produced unusually clean recordings of postseismic strain (Figure 2). Unfortunately, low-pass filters in the electronics made the interferometers blind during major shaking preventing the recording of coseismic offsets during the main shock and major aftershocks, thus any coseismic offset has been removed from the plots.

From Figure 2 it is clear that after 1.5 days postseismic strain on the two strainmeters is monotonic and quite similar. In contrast, the initial (several hour long) transient is quite different for BA and BC: in the case of BA fast initial compression is followed by extension
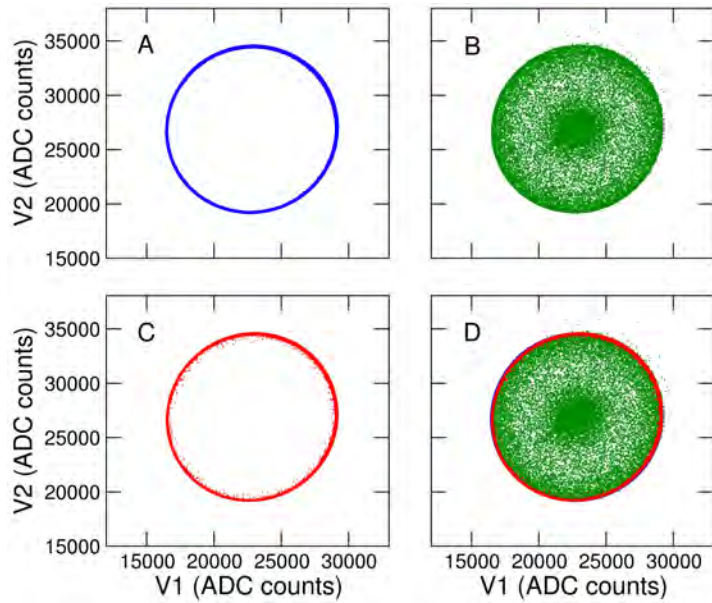
191

Figure 1: Lissajous figures given by the two outputs of interferometer BA (600 samples per second) (A) during 2000 s immediately before the earthquake, (B) 58 s throughout major shaking, (C) 880 s immediately after it, and (D) for the whole period A to C.
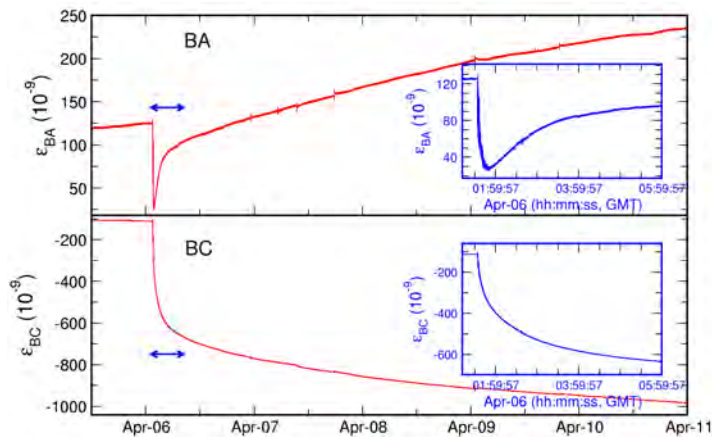

Figure 2: Low-passed (cut-off frequency = 0.25 Hz) re-sampled (1 s) strain data recorded by the two interferometers (labeled as BA and BC) after removal of Earth tides and environmental (air pressure and temperature) effects. Extension is positive. About 80 s starting from the main shock ("blind" time for the interferometers, see text) are missing. Any coseismic offset has been removed. Blue insets, enlargement of the signals inside the arrowed lines. Uncut remnant oscillations originate the seeming slight uptick in the insets. Note the very different (between the two interferometers) initial post-seismic transient and the monotonic similar behavior after about 1.5 days from the main shock.

after about 15 minutes, while BC shortens monotonically. Such features suggest that the initial phase (hours) is dominated by a different phenomenon or a different phase of the same phenomenon with respect to the longer term (days) deformation. After modeling pore-pressure transients and viscous relaxation in a layered (poro-elastic and visco-elastic respectively) half-space, using different source models, we find that neither process can account for the recorded signals, because predicted deformation is much smaller and slower than observed for any reasonable choice of the Earth model parameters. Thus, we conclude that deformation after about 1.5 days is probably attributable to afterslip on a stationary region of the fault plane, but the non-monotonic behaviour of ϵ_{BA} excludes the possibility that such a mechanism is the dominant one during the hours immediately following the earthquake. We test for consistency with our measurements the strain arising from aseismic slip on a plane containing the source fault (Figure 3).
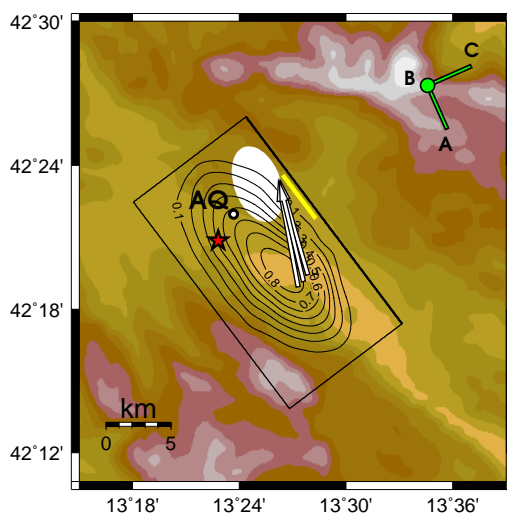
Figure 3: Map of the epicentral region of the 6 April 2009 LAquila earthquake with the fault geometry and slip distribution from the work by [11]. Green solid circle (B), location of the two interferometers; green solid lines (BA and BC), directions of the interferometers. Red star, earthquake epicenter ([4]); yellow thick solid line close to the fault trace, approximate location of surface ground fractures. White ellipse, probable source region of the afterslip occurred in the first days following the earthquake. The white black-contoured arrows exemplify the class of minimum-misfit slow slip diffusion paths over the fault plane.

Figure 4 shows the expected amplitude and sign of deformation at both interferometers due to very small subfaults located in different positions on the fault plane, using a simple homogeneous half-space approximation. All areas of the fault rupture that had significant slip (see Figure 3 and [11]) cause negative BC deformation (contraction), while the fault plane is divided by a nodal line for deformation as recorded by BA (Figure 4). We consequently model the initial phase of the recorded signals by means of a slow 1D slip propagation from the fault region giving BA contraction and negative $\epsilon_{BC} - \epsilon_{BA}$ toward the
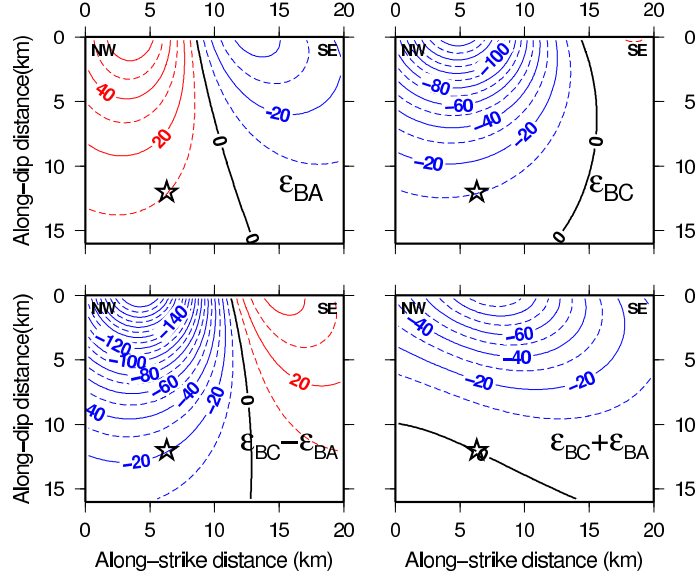
Figure 4: Strain (in units of 10^{-9}) generated at the interferometers by a small rectangular source (M $= 2.5 \times 10^{16}$ N m, same focal mechanism as the main shock) located in different positions on the fault plane. Star, earthquake hypocenter.

fault region giving BA extension. We consider two propagation mechanisms along straight paths: a constant propagation velocity, and a diffusive process. For both mechanisms the along-path linear density of the seismic moment is optimized with respect to the observed signals at the interferometers. Because of the model simplicity, we test the consistency of different (starting point, length, direction) paths against observations (35000 seconds in duration) by means of a gridding technique instead of searching for the optimal (from the misfit point of view) model. The diffusive model is fully consistent with observations, while the constant propagation velocity model is unable to fit timing or shape of the minimum observed in BA (Figure 5).

The linear density of the seismic moment decreases roughly linearly with distance along the path (like the steady-state solution of 1D diffusive processes) and the seismic moment increases with time following a quasi-exponential law (Figures 6 and 7).

The cumulative seismic moment is 2.5×10^{17} N m, i.e., about 10% of the main shock seismic moment ([4]). Similar computations performed using other fault models give analogous results. Intriguingly, the shallower part of the propagation path is close to mapped cm-wide surface ground fractures, with lengths of about 5 km during the days following the main shock. The fault area at the end of the propagation path is the only one where $\epsilon_{BC} \sim 2\epsilon_{BA}$ (see Figure 4 and the white ellipse in Figure 3) and is thus a potential source area for later afterslip. Our results are consistent with published slip models from geodetic data, derived from InSAR images acquired a few days after the main shock (see e. g. Figure 3). Indeed, our interpretation of our strainmeter data appears to explain the discrepancy between the slip distribution derived from InSAR data and even if we cannot completely exclude other possibilities for interpreting the recorded postseismic deformation, our model and observed data are fully consistent.
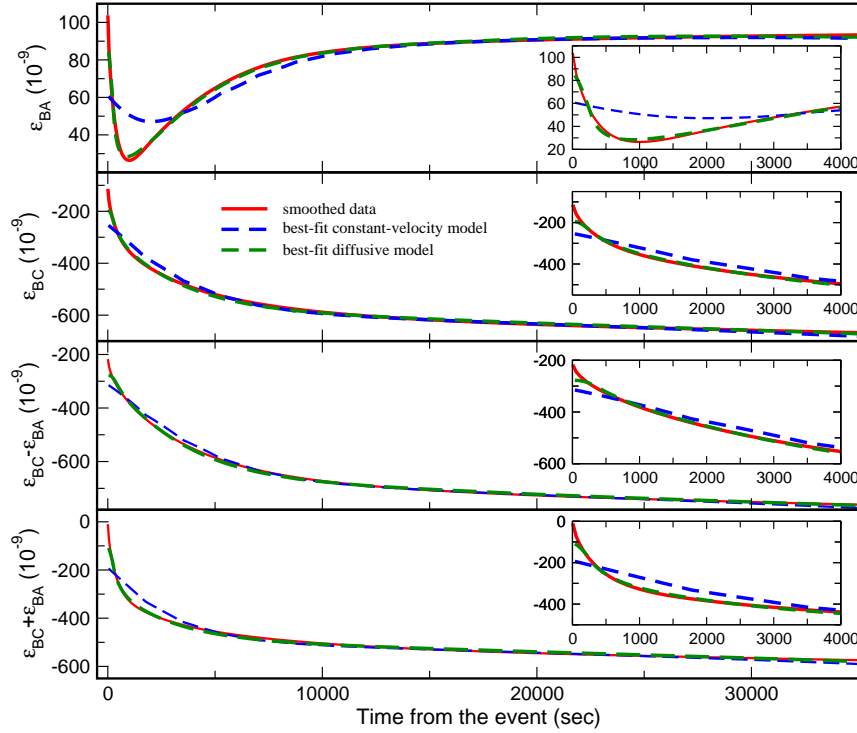
Figure 5: Initial (35000 seconds) smoothed detrended postseismic transient recorded at the two interferometers (red solid lines) after removal of Earth tides and environmental effects. Blue dashed lines, predicted strain history for the best constant propagation-velocity model. Green dashed lines, predicted strain history for the best diffusive model.
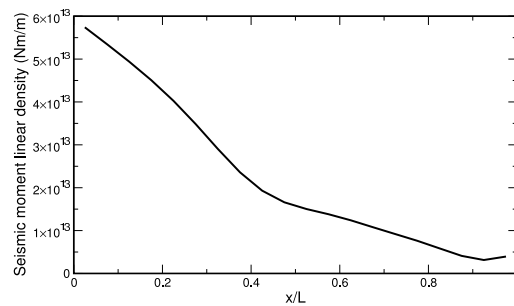

Figure 6: Linear density of the seismic moment released along the path by the slow slip diffusive process following the 2009/04/06 L'Aquila earthquake. Total seismic moment amounts to about 2.5×10^{17} N m, i. e. 10% of the main shock seismic moment. The quasi-linear decrease with distance along the path strongly resembles the asymptotic steady-state temperature profile in the case of heat diffusion across a slab.
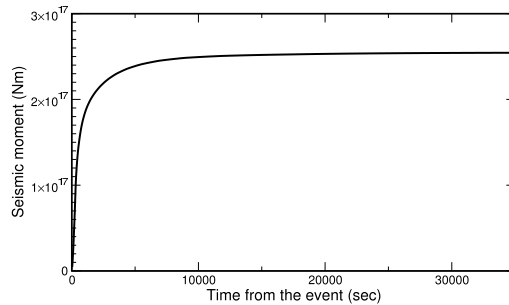
Figure 7: Retrieved seismic moment history for the slow slip diffusive process following the 2009/04/06 L'Aquila earthquake.

Slip propagation similar to heat diffusion has been suggested ([5]; [8]) to explain the observed scaling law between amplitude and duration of slow earthquakes, but our results give its first observational evidence.

2   April 6th 2009 L'Aquila earthquake: Clues on preseismic phenomena

As regards the 2009 L'Aquila earthquake, claimed earthquake precursors and preparation-phase-related phenomena include radon anomalies ([7]), radio anomalies ([3]), and uranium groundwater anomalies ([10]).

The analysis of pre-seismic deformation data, briefly described in what follows, gives tight limits on the amount of released pre-seismic slip and on the size and strength of a possible preparation zone. Numerical results given here are to be considered preliminary and subject to possible changes.

We do not observe strain changes greater than 2×10^{-9} during two days before the event, 2×10^{-10} during one hour before the event, 5×10^{-11} during one minute before the event, and 2×10^{-12} during two seconds before the event. Moreover, prerupture nucleation slip in the hypocentral region is constrained to have a moment less than (conservative estimate) 2×10^{15} Nm during two days before the event, 2×10^{14} during one hour before the event, 1×10^{14} Nm during one minute before the event, and 2×10^{12} Nm during two seconds before the event, to be compared with the earthquake seismic moment (about 3.5×10^{18} Nm; [4]).

Since radon and groundwater anomalies are usually related to earthquake models where at a certain preparation stage a region with many cracks is formed, we have tested the model by [6], after adapting the formulas to an extensional tectonic environment. In [6] the appearance of an inclusion affect the deformation field caused by the regional tectonic stress. We have computed the expected preseismic deformation at the strainmeter site and

196

its surroundings, for an extensional tectonic strain $\sigma \sim 100$ MPa and a 10% decrease of the shear modulus inside the soft inclusion. Predicted deformation is orders of magnitude greater than observational threshold, and no anomalous behaviour has been envisaged.

Changes in earth tidal response were rst suggested by [9]) as a possible means for earthquake prediction. Also recently, strain tidal changes up to 20% in amplitude have been reported several tens of kms from the epicenter of magnitude-6 earthquakes ([12]). Signal-to-noise ratio of the Gran Sasso strainmeters in the tidal band is very high, thus we have determined the tidal response for the two years prior to L'Aquila earthquake ($M_w \sim$ 6.3; epicentral distance about 20 km). No change in tidal response is apparent in the data before the earthquake, within 1% in amplitude and 1° in phase (for BA interferometer).

A detailed analysis is the subject of a manuscript in preparation.

3   April 6th 2009 L'Aquila earthquake: Work in progress on post-seismic phenomena

The deformative phenomenon following the April 6th 2009 event has continued for a long time, and we are still working on the interpretation of the data produced by the interferometers. Besides the post-seismic deformation induced by the earthquake itself, our signals have also the signature of the hydrological changes occurred in the Gran Sasso area. Both contributions deserve attention: the former would shed more light on the event and on the depth-dependent viscoelastic structure of the Earth's ductile regions, the latter would draw some features of the complex Gran Sasso aquifer. In fact, an earthquake occurring in an (idealized) elastic region of the upper crust is followed by relaxation of the underlying viscoelastic regions (post-seismic deformation). Moreover, earthquakes affect the direction, quantity, and rate of surface and subsurface water flow, and variety of mechanisms have been proposed to explain hydrological responses to earthquakes. The joint study of hydrological and deformation data collected before and after the 2009 L'Aquila earthquake would give new insights into these processes, both as regards the transient coseismic response and the sustained postseismic one.

These analyses are inserted in an already active co-operation with R. Adinolfi Falcone, A. Falgiani, M. Petitta, and M. Tallini, aimed to study possible correlations between strain data and local hydrology (spring discharge in the Gran Sasso area, hydrochemical and isotope data of groundwater collected within LNGS, fracture network in the Gran Sasso massif).

4   Acknowledgments

References

[1] Amoruso, A., and L. Crescentini, *J. Geodyn.*, **48**, 120–125, doi:10.1016/j.jog.2009.09.025, 2009.

[2] Amoruso, A., and L. Crescentini, *Geophys. Res. Lett.*, **36**, L24306, doi:10.1029/2009GL041503, 2009.

[3] Biagi, P. F., L. Castellana, T. Maggipinto, D. Loiacono, L. Schiavulli, T. Ligonzo, M. Fiore, E. Suciu, and A. Ermini, *Nat. Hazards Earth Syst. Sci.*, **9**, 1551–1556, 2009.

[4] Cirella, A., A. Piatanesi, M. Cocco, E. Tinti, L. Scognamiglio, A. Michelini, A. Lomax, and E. Boschi, *Geophys. Res. Lett.*, **36**, L19304, doi:10.1029/2009GL039795, 2009.

[5] Crescentini, L., A. Amoruso, and R. Scarpa, *Science*, **286**, 2132–2134, 1999.

[6] Dobrovolsky, I.P., S.I. Zubkov, and V.I. Miachin, *Pure Appl. Geophys.*, **117**, 1025–1044, 1979.

[7] Giuliani, G. G., R. Giuliani, G. Totani, G. Eusani, and F. Totani, *Eos Trans. AGU*, **90(52)**, Fall Meet. Suppl., Abstract U14A-03, 2009.

[8] Ide, S., G. C. Beroza, D. R. Shelly, and T. Uchide, *Nature*, **447**, 76–79, doi:10.1038/nature05780, 2007.

[9] Nishimura, E., *Trans. Am. Geophys. Union*, **31**, 357–376, 1950.

[10] Plastino, W., P. P. Povinec, G. De Luca, C. Doglioni, S. Nisi, L. Ioannucci, M. Balata, M. Laubenstein, F. Bella, and E. Coccia, *J. Environ. Radioact.*, doi:10.1016/j.jenvrad.2009.08.009, 2009.

[11] Walters, R. J., J. R. Elliott, N. DAgostino, P. C. England, I. Hunstad, J. A. Jackson, B. Parsons, R. J. Phillips, and G. Roberts, *Geophys. Res. Lett.*, **36**, L17312, doi:10.1029/2009GL039337, 2009.

[12] Zhang, Y., J. Jian, J. Qian, J. Chen, S. He, Y. Zhang, and P. He, *Acta Seismologica Sinica*, **15(1)**, 113–118, 2002.

TELLUS Experiment.
Detection of transient phenomena associated with thunderstorms.

V. Sgrigna[a], L. Conti[a], D. Zilpimiani[b]

[a] Dipartimento di Fisica e Sezione INFN, Università Roma Tre, Rome, Italy.
[b] Institute of Geophysics, Georgian Academy of Sciences, Tbilisi, Georgia.

Abstract

A set of instruments has been planned to detect in the near-Earth space TLEs and TGFs phenomena associated with thunderstorms as well as X/γ rays from sun and cosmic rays and fluxes of high-energy particles from the inner radiation belt. The instrumental set includes optical and UV photometers and video cameras as well as X/γ and particle detectors. Such instruments are planned to be installed on board a LEO satellite or the ISS in order to study the large energy transfer from the troposphere to the atmosphere, ionosphere and magnetosphere regions and the temporal stability of the Van Allen radiation belts. Also geomagnetic cavity perturbations produced by sun and cosmic rays can be investigated by these instruments. During the year 2009 also three patents were produced by the TELLUS team.

1   The Tellus experiment

Aim of the experiment is to detect tropospheric TLEs, lightnings and TGFs, to contribute to the understanding of TLEs interaction mechanisms with TGFs, to study the large energy transfer ($\simeq 250MW \div 1GW$ per event) produced by TLEs and TGFs from the troposphere to the atmosphere/ionosphere/magnetosphere and investigate the temporal stability of the Van Allen radiation belts. At this purpose specific instruments have been planned to be installed on board a LEO satellite and/or the International Space Station (ISS). The processes storm in the upper atmosphere generates intense luminous phenomena called TLEs (Transient Luminous Events). Observations of TLE have shown the existence of an intense dynamics of impulsive transfers of energy between the atmosphere and ionosphere. The most commonly observed from the ground are the "red sprites" (Stratospheric/mesospheric Perturbations Resulting from Intense Thunderstorm Electrification), a manifestation of electrical breakdown in the mesosphere. A graphic representation of the main TLEs phenomena is reported in figure 1 with a few details concerning Red Sprite characteristics. References are reported in the reference list.
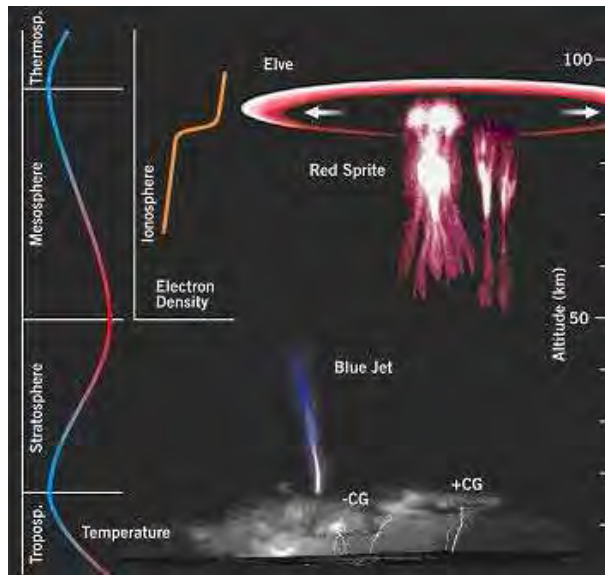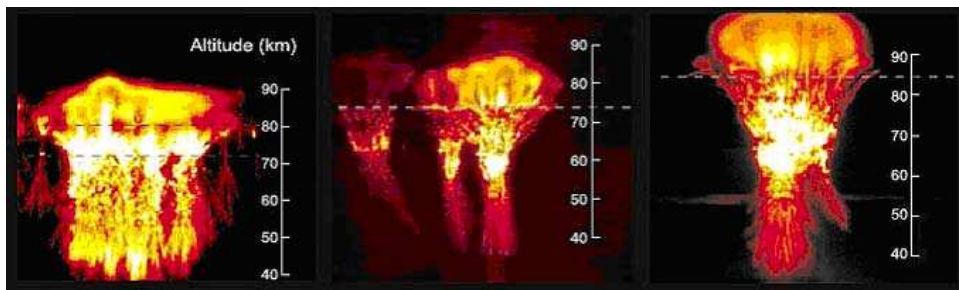
(a)
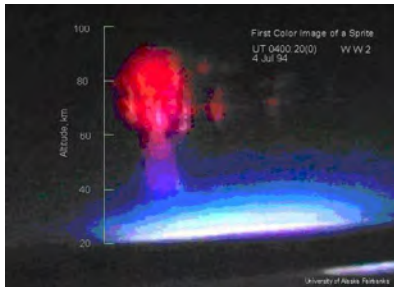
(b)

(c)

(d)

Figure 1: [a] Main tropospheric TLEs phenomena; [b] First imagine of a red sprite event detected by NASA in 1994 during the night between July 3 and 4; [c] Colored imagine of a sprite event over an intense lightning occurred in Africa at an altitude of 80-90 km; [d] Characteristic spatial dimensions of a red sprite event.

Above the storm formations intense emission of X/γ rays are observed. They are the so-called Terrestrial Gamma ray Flashes (TGF). The first detection of TGF above areas with thunderstorm has also provided the evidence of the flow of relativistic electrons in the upper atmosphere. A TGFs geographic distribution is given in figure 2. Adding information can be found in the publications reported in the reference list.

2 Intruments

For detecting TLEs and Lightnings two blocks of optical-UV instruments have been considered, one of which is nadir pointing and the other one limb oriented. Each block is constituted by 2 video cameras and 4 photometers with filters adapted to mainly detect red sprites, blue jets and lightnings, respectively. The main characteristics and a pictorial view of these instruments are reported in table 1 and figure 3 respectively.
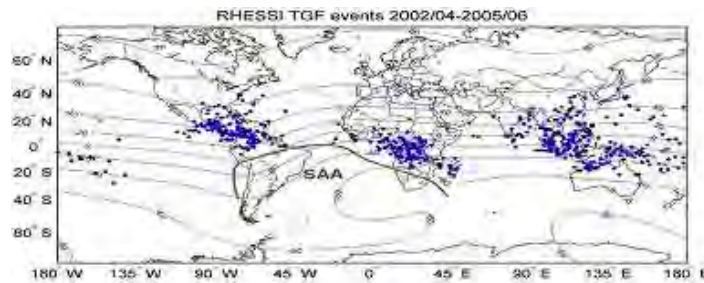
Figure 2: Geographical distribution of TGF events.

Two instrumental units have been designed to detect TGFs, one of which is nadir pointing and the other one tangent to the satellite orbit. Each unit (figure 4) consists of two different instruments combined and assembled together: an X/γ ray detector and a charged particle detector. The X/γ ray detector measures tropospheric X/γ emissions (studying the characteristics and sources of TGFs and their correlations with TLEs) and detect X/γ rays from sun and cosmic rays, thus investigating the effects of these radiations to the magnetospheric cavity. The charged particle detector may detect fluxes of high-energy charged particles from the inner radiation belt, which gives information about particle precipitation mechanisms and sources as well as stability of the Van Allen radiation belts.

Instrument	Function / Mode	Pointing mode	Run period	λ (nm)	Transition	FOV (deg) (nadir / limb)	Resolution (pixels)	Bit	Sampling Rate
Video Camera	Sprite camera	Nadir + Limb	Night	762±5		55 / 20	1024 x1024	10	30 fr/s
Video Camera	Lightning camera			600-800		55 / 20	1024 x1024	10	30 fr/s
Photometer	Trigger / Acquisition			762±5	O_2 (0,0)	55 / 20		12	50 - 20 μs
Photometer	Trigger / Acquisition			337±5	N_2 (2P)	55 / 20		12	50 - 20 μs
Photometer (single or 8 x 8 pixels)	Trigger / Acquisition			150-280	FUV / N2 LBH	55 / 20		12	50 - 20 μs
Photometer	Study of AGW/ Event acquisition			600-800	N1(1P) and OH	55 / 20		12	50 - 20 μs

Table1. Characteristics of video cameras and photometers planned to detect TLEs and lightnings.
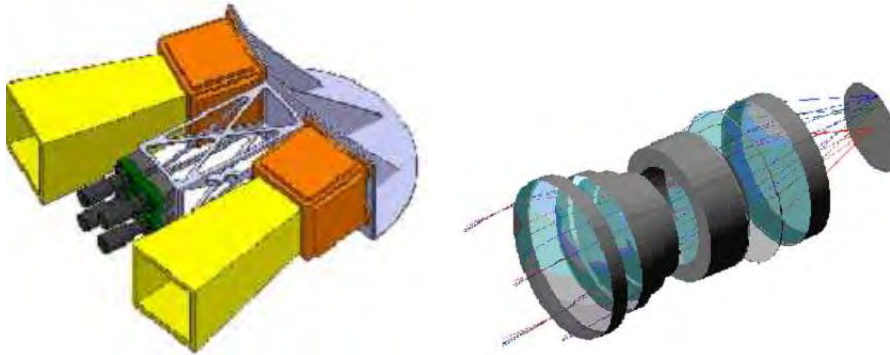
Figure 3: Photometers and video cameras layout (left) and optical design (right).

3   Conclusions.

Optical-UV instruments (photometers and video cameras), as well as an X/γ ray detector and a charged particle detector have been considered and planned to be installed on board a LEO satellite and/or the ISS to investigate tropospheric TLEs, lightnings and TGFs. Aim of the experiment is to contribute to the understanding of TLEs interaction mechanisms with TGFs, study the large energy transfer produced by TLEs and TGFs from the troposphere to the atmosphere/ionosphere/magnetosphere region of the near-Earth space and investigate the temporal stability of the Van Allen radiation belts. Also perturbations produced by sun and cosmic rays to the geomagnetic cavity will be considered in the study. The activity carried out in 2009 by the TELLUS team includes three patents.
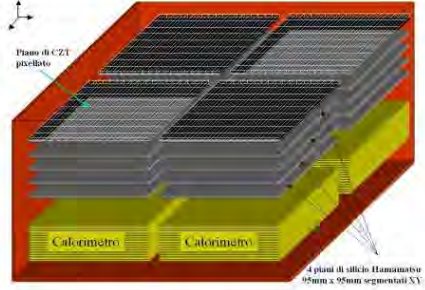
Figure 4: Structure and characteristics of a TGF instrumental unit.

List of references including publications and patents during the year 2009

1. Sgrigna, V. and Conti, L., 2009. Earthquake preparation and warning: science, methods and technologies, Novapublishers, in press.

2. Sgrigna, V., Buzzi, A., Conti, L., Stagni L., Zilpimiani, D., 2008. TELLUS. A new electromagnetic strainmeter for the monitoring of groundfield deformations, Laboratori Nazionali del Gran Sasso, INFN, Annual Report 2008, LNGS/EXP-01/09, June 2009, pp.187-192.

3. Mende, S.B., Y.S. Chang, A.B. Chen, H.U. Frey, H. Fukunishi, S.P. Geller, S. Harris, H. Heetderks, R.R. Hsu, L.C. Lee, H.T. Su, and Y. Takanashi, Spacecraft based studies of transient luminous events, in "Sprites, elves and intense lightning discharges", M. Fullekrug et al. editors, Springer, 2006.

4. Cummer, S.A., H.U. Frey, S.B. Mende, R.R. Hsu, H.T. Su, A.B. Chen, H. Fukunishi, and Y. Takahashi, Simultaneous radio and satellite optical measurements of high altitude sprite current and lightning continuing current, J. Geophys. Res., 111, A10315, 2006

5. Cummer, and S.A., and W.A. Lyons, Implications of lightning charge moment changes for sprite initiation, J. Geophys. Res., 110, A04304, 2005.

6. Blanc, E., T. Farges, R. Roche, D. Brebion, T. Hua, A. Labarthe, and V. Melnikov, Nadir observations of sprites from the International Space Station, J. Geophys. Res., 109, A02306, doi:10.1029/2003JA009972, 2004

7. Smith, D.M., L.I. Lopez, R.P. Lin, and C. Barrington-Leigh, Terrestrial gamma ray flashes observed up to 20 Mev, Science, 307, 1085-1088, 2005a.

8. Dwyer, J.R., and D.M. Smith, A comparison between Monte Carlo simulations of runaway breakdown and terrestrial gamma ray flashes observations, Geophys. Res. Let, 32, L22804, 2005.

9. Enell, C.-F., Chemical perturbations from sprites and energetic particle radiation, CAL third year meeting, Cambridge, England, 2006.

10. Heavner, M.J., D.D. Sentman, D.R. Moudry, E. M. Wescott, C. L. Siefring , J. S. Morrill, and E. J. Bucsela, Sprites, Blue Jets, and Elves: Optical evidence of energy transport across the stratopause, AGU Monograph 123 "Atmospheric science across the stratopause," 69-82, 2000.

Patents

1. Year 2009. Title: A new technique for the signal waveform reconstruction by multi-channel selection and retroaction variable differential amplification (patent pending RM2009A000001). Authors: Conti, L., Sgrigna, V., and Zilpimiani, D.

2. Year 2009. Title: Amplification calibration system for acquisition devises of analog signals (patent pending RM2009A000200). Authors: Conti, L., Sgrigna, V., and Zilpimiani, D.

3. Year 2009. Title: Signal conditioning board for filtering and feedback multichannel amplification in data acquisition systems of analog signals (patent pending RM2009A000207). Authors: Conti, L., Sgrigna, V., and Zilpimiani, D.

UNDERSEIS - Underground Seismic Array

C. Fischione[b,*], G. Saccorotti[a], R. Scarpa[b]

[a] Istituto Nazionale di Geofisica e Vulcanologia, Sez. di Pisa, Italy
[b] Dipartimento di Matematica e Informatica, Università di Salerno, Italy
[*] Spokesperson

Abstract

This report describes a geophysical instrument installed in the underground physics laboratories of Gran Sasso (LNGS-INFN), located in the seismic zone of central Apennines, Italy. This instrument is aimed to monitor seismic radiation with very high sensitivity; it is a small aperture seismic array composed by 19 three-components short period seismometers (Lennartz 3D-LITE, 1 Hz) and 1 broad-band Guralp GMC-40 T seismometer.

1   Introduction

The physics of earthquakes is based on the measurements of radiated seismic waves and ground displacement associated with this phenomena. The inertial pendulum is the oldest and most diffused instrument used to measure the main features of seismic waves. The advantages of this instrument are the simplicity of the theory, the high sensitivity, the robust design and the simple calibration methods, in spite of the quite reduced frequency band and linearity (Wielandt, 1983). Other instruments based on different physical principles, such as strainmeters and gyroscopes, are only partially used by seismologists (Benioff, 1935; Farrell, 1969; Aki and Richards, 1980). Networks of short period seismometers are as far the most diffused system to monitor local and regional seismicity (Lee and Stewart, 1981). Broad-band instruments make up a powerful system to study the details of seismic sources and also to study large earthquakes at global scale (Lee and Wallace, 1995). Strainmeters and tiltmeters (Agnew, 1986) are used to study the lower frequencies radiated from seismic sources and allow to detect slow earthquakes and strain steps (i.e. anelastic deformations around seismic sources). Moreover arrays of seismometers and accelerometers are used to study the Earth structure at global, regional and local scale (Green, 1965; Kedrov and Ovtchinnikov, 1990; Mikkeltveit, 1985), earthquake source process (Spudich and Oppenheimer, 1986; Goldstein and Archuleta, 1991), nuclear underground explosions (Bolt, 1976; Chouet, 1996) and, more recently, for the analysis of

complex signals associated to the volcanic activity (see f.i. Goldstein and Chouet, 1994; Chouet *et al.*, 1997; Almendros *et al.*, 1991). The main advantage of the seismic arrays consists in their ability to detect small signals through multichannel waveform stacking (Capon, 1969). The seismicity of the area is associated with the mainly distensive tectonics affecting the Apennines since the late Pliocene (D'Agostino *et al.*, 2001; Galadini *et al.*, 2003). Historical events include the 1915, Ms=6.8 Fucino earthquake, which caused about 32000 casualties; recent studies (Amoruso *et al.*, 1998) have modelled this event in terms of a normal fault striking along the Apennine direction (NNW-SSE). In addition, swarms of low-to moderate-size earthquakes occur quite frequently, such as those of 1992, 1994, 1996 (De Luca *et al.*, 2000), and 2006 (this study). The most recent activity is dominated by the Mw=6.3 earthquake which, on April 6th, 2009, stroke the city of L'Aquila and surroundings, causing more than 300 casualties. This catastrophic event was part of an energetic seismic sequence which began as of early January, 2009 (Chiarabba *et al.*, 2009). This relevant rate of seismicity, joint to the low-noise conditions and site response associated to the underground setting, make the Gran Sasso underground laboratories an ideal site for high-resolution seismic observations (De Luca *et al.*, 1998).

2   The Underground Seismic Array

A seismic array is a set of seismographs distributed over an area of the Earth's surface at spacing narrow enough so that the signal waveform may be correlated between adjacent seismometers (Aki and Richards, 1980).
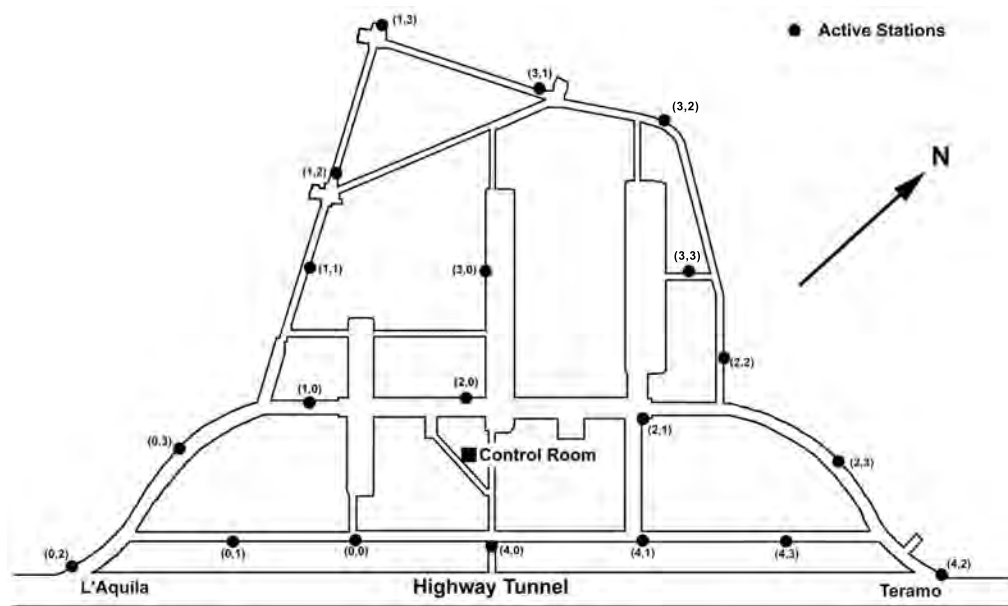

Figure 1: Map of the Underground Seismic Array. The notation (n,m) shows the line number (n) and the station number (m).

The design of the UnderSeis hardware and software components began on the late

90's; over the following years, major upgrades were developed under a technological effort jointly carried out by engineers from the University of Granada (Spain), University of L'Aquila (now the team moved to the University of Salerno), and INGV - Osservatorio Vesuviano. The array become fully operative since May, 2002. In its present configuration, it consists of 19 elements, each equipped with a Lennartz 3D-LITE, 1 Hz, 3-component seismometers and 1 broad-band Guralp GMC-40 T seismometer. The average sensor spacing is on the order of 90 m, and the largest distance among sensors is about 400 m. Seismic signals are digitized locally at each individual seismometer with a dynamic range of 24 bits and sampling frequency of 100 Hz. Data synchronization is achieved via a Master Oscillator which transmit the UTC synchronized pulses from an atomic clock to the different ADC boards. The synchronized data packets are then sent via serial cable connection to a set of five nodal PCs, which are in turn connected via an Ethernet network to a central data server and an on-line processor (Scarpa *et al.*, 2004).

3 Data analysis and results

Our data span the 2005-2008 time interval, and are associated with the same seismogenic region which caused the destructive Mw=6.3 earthquake of April 6th, 2009. The seismic sequence including the destructive April 6th, 2009 event is still ongoing, likely including several tens of thousands of detections. While the analysis of this massive data set is left for future studies, in this paper we describe the activity of the UnderSeis array during the 2.5 year long period (July, 2005 - December, 2008) preceding the onset of the sequence. In particular, we focus on the array performances in terms of detection capabilities-catalogue completeness. A distance-dependent, catalogue-completeness relationship is found which is well fitted by a generic attenuation function. We then describe the seismicity recorded during the analysed time interval, and discuss the obtained locations with reference to the structural setting and recent seismicity of the region. These locations exhibit a significant discrepancy with respect to those obtained by the National Centralized Seismic Network (RSNC). The systematic pattern of backazimuth differences between the two set of locations is attributed to a combination of (a) the intrinsic error of the multichannel directional measurements associated with the array geometry, and (b) the presence of marked, lateral velocity anomalies inducing significant ray bending and multipathing.

3.1 Catalogue completeness and detection capabilities

During the analysed time interval, UnderSeis detected more than 1600 earthquakes. For this data set, Figure 2 illustrates the temporal distribution of the daily number of events, the stress release and the magnitude. The average detection rate is on the order of 1-2 events/day, with peaks of up to 50 events/day in association with two swarms on February and August, 2006 (Fig. 2a). Magnitudes are generally lower than 3 (Fig. 2b). The catalogue completeness and detection capabilities are estimated by plotting the magnitude as a function of epicentral distance (Fig. 3). The lower envelope of the scatter plot may be taken as a distance-varying detection threshold of the array. This envelope

is well fitted by a simple relationship of the form:

$$M_{min} = log(\Delta) - b$$

where M_{min} is the minimum magnitude which can be observed at the epicentral distance Δ, and b is a constant taking the value of 2.75. In order to compare the detection capabilities of the array with those of INGV's RSNC, we computed the number of earthquakes detected by the two systems as a function of the distance from the array. The results, reported in Figure 4, indicate that UnderSeis detection performances are better than, or comparable to those of the RSNC up to epicentral ranges on the order of 25 km.
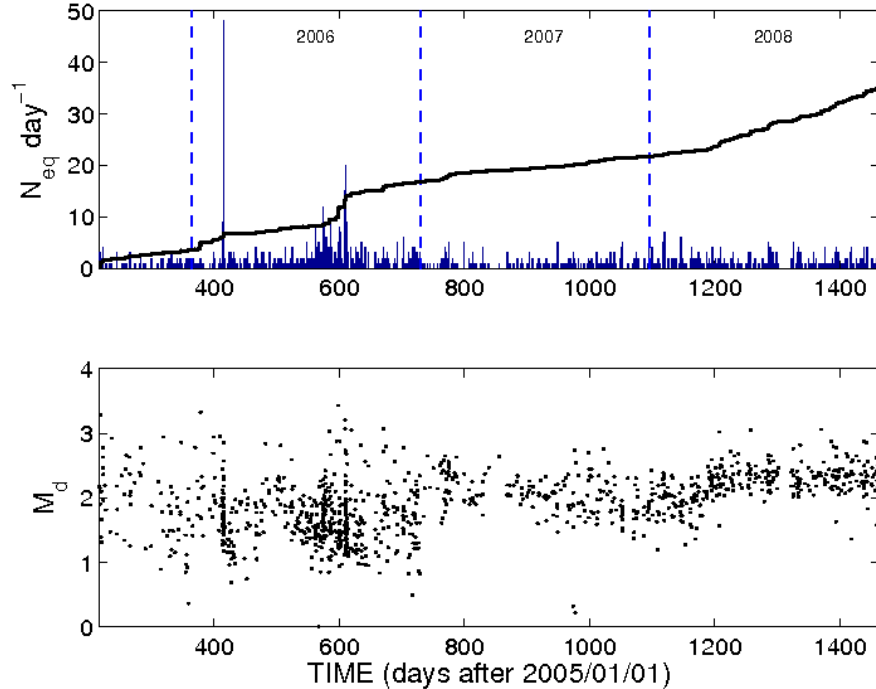
Figure 2: (a) Time series of the daily number of events and stress release for 1688 earthquakes recorded by UnderSeis during the August 2005-December 2008 time interval. (b) Temporal evolution of the duration Magnitudes.

3.2 Spatial distribution of the recent regional seismicity

Events selected by the automatic procedure are then subjected to the refined multichannel analysis as described in previous report (The 2006 Annual report). For each slowness estimate, we consider an error bound given by the range of slownesses associated with those region of the spectrum which power is greater than 95% of the peak power. For each event, we iterate the location procedure using all these slownesses, and by randomly varying the estimated $S - P$ time differences according to a Gaussian distribution with $2\sigma = 0.1s$. In this manner, each event has associated a cloud of points which are taken

208

as samples of the 95% confidence region of the probability density function for epicentral location.
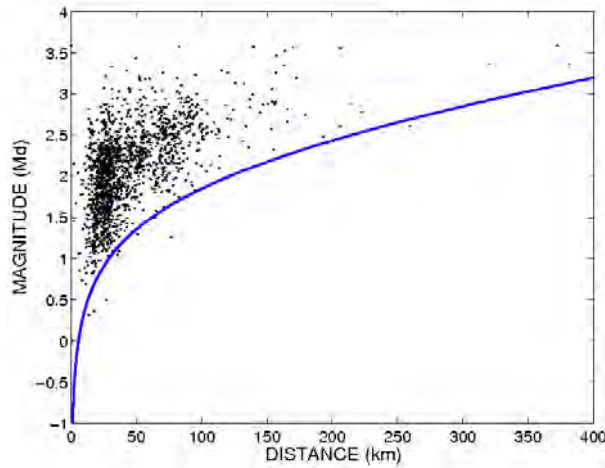

Figure 3: Magnitude of UnderSeis detections as a function of epicentral distance. The solid line indicates the empirical relationship relating distance to minimum detectable magnitude.
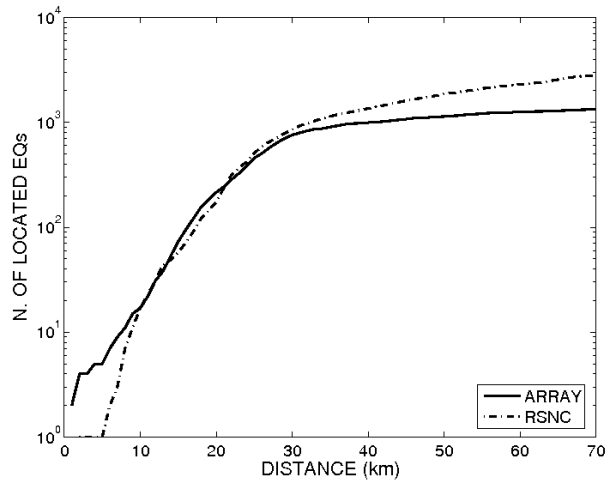

Figure 4: Number of earthquakes reported by the UnderSeis and INGV-RSNC catalogues (bold and dashed lines, respectively) as a function of distance from the array.

We then stacked all the probability maps associated with individual locations, and eventually calculated the earthquake density (Number of Earthquakes for unit area) for a 50 x 50 km square region centered at the array site (Fig. 5). The array seismicity distribution is substantially different from that of the RSNC catalog. In particular, one of the most prominent feature of the UnderSeis location map is a peak of earthquake location very close to the hypocenter of the April 6th, 2009 mainshock (Fig. 5a). This

peak, associated with epicenters from the two 2006 swarms, is substantially absent in the RSNC location map, where the 2006 epicenters are shifted some $15 - 20km$ to the NW.
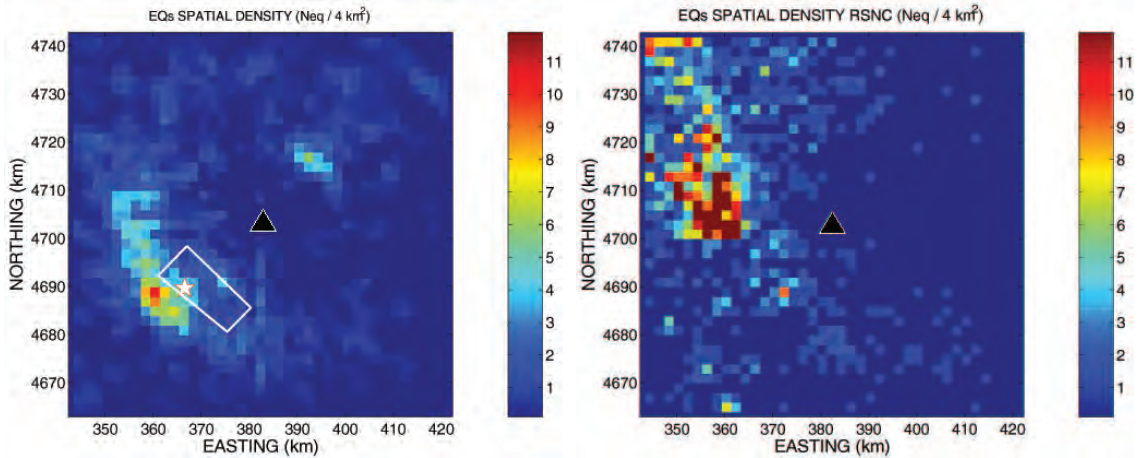

Figure 5: (a) Earthquake Density obtained from stacking individual maps of location probability. The triangle marks the array site; the star indicates the epicenter of the April 6th, 2009, $M_W = 6.3$ destructive event. (b) The same as in (a), but using data from the RSNC catalogue. The colour scale is clipped to the maximum value of the map in (a).

Using a subset of about 700 events for which we found an unambiguos corrispondence of origin times between UnderSeis and RSNC locations, we compared the array backazimuths retrieved from slowness analysis with those expected on the basis of RSNC locations. The disagreement between the two data sets assumes both positive and negative values depending on the expected azimuth (Fig. 6). Over the $N - N50°E$ angular range, Backazimuths (measured clockwise from the North) from multichannel analysis are greater than those associated with RSNC locations. These epicenters correspond to the cluster located some $15km$ NE of the array (Fig. 5a), which is not present in the RSNC location map (Fig. 5b). The opposite occurs for backazimuths in the range $N90°W - N40°W$, for which the measured backazimuths are lower than those predicted on the base of the RSNC locations (Fig. 6). These data correspond to the aforementioned 2006 earthquakes, which RSNC epicenters are shifted NW with respect to those measured by UnderSeis. Such anomalies can be attributed to one or a combination of the following 2 factors: (1) uncertainties of either RSNC or UnderSeis locations, and (2) a propagation effects due to lateral variations of velocity. To better constrain these two hypothesis, we examined in detail the largest ($M_d = 2.85$) shock of the February 2006 swarm. We measured the slownesses associated with the first few cycles of the P-wave using a plane-wave-fitting of the interchannel delay times estimated via interpolated cross-correlation. Although very time-consuming, this procedure is not based on a grid-search procedure, thus allowing for slowness estimates which are more precise than those derived from MUSIC. The very first P-wave arrival (from seconds 0.15 to 0.4 in Fig. 7) incides steeply at the array, as shown by the low values of the ray parameters. Consequently, Backazimuth values are markedly unstable, thus making difficult any reliable directional estimate. The subsequent, largest amplitude pulse exhibits a shallower incidence, and it has well defined

directional properties clustered around 220°, thus pointing some 25° southward of the revised RSNC location (Fig. 8).
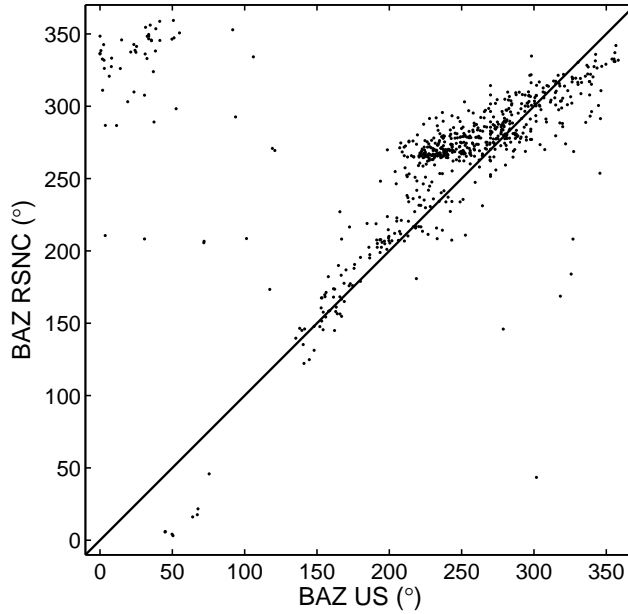

Figure 6: UnderSeis Backazimuths (measured clockwise from N) from multichannel analysis compared to those expected on the base of RSNC catalog.

The P-wave particle motion trajectory for the same time interval (black line in Fig. 8) is polarised along the propagation direction, thus confirming the slowness measurements. RSNC locations have formal errors on the order of $1 - 3km$, which could account for azimuthal discrepancies of at most a few degrees. Such uncertainties, however, do not account for errors associated with the 1-D travel-time predictions routinely adopted by RSNC. A velocity tomographic image obtained from local seismicity and receiver function analysis (Claudio Chiarabba, personal communication), indicates that the shallowest $10km$ of the study region exhibit marked velocity heterogeneities, depicting variations on the order of $15\% - 20\%$ with respect to an average P-wave velocity of $6.5km/s$. Therefore, travel time predictions at RSNC stations may have errors of up to $0.5 - 0.8s$. Once these errors are included in a probabilistic location procedure, epicentral uncertainties may become as large as $\pm 5km$, corresponding to an array-backazimuth difference on the order of 13°. This value is still lower than the observed $\sim 25°$ discrepancy, indicating that RSNC location errors alone are not sufficient to explain the observed azimuthal anomalies. Overall, these observations suggest that the reported azimuthal discrepancies are likely due to a combination of both poor resolution of the array and complex wave propagation. In fact, although the direction-of-arrival of the very first P-wave onset couldn't be retrieved precisely due to its steep incidence angle, it is likely consistent with the region spanned by the RSNC location error bounds. Most of the energy of the P-wave train, however, travels along a different, shallower trajectory: since slowness analysis is selectively sensitive to the largest amplitude oscillations, our backazimuth estimates are biased toward this latter
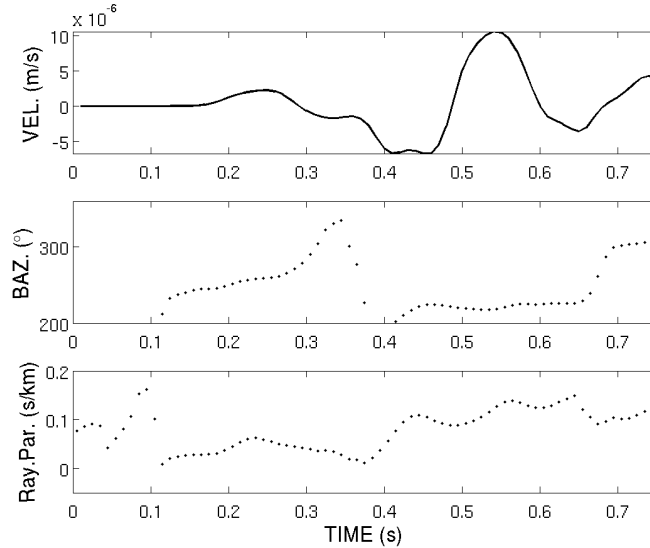
direction of propagation.

Figure 7: Top: vertical-component recording from the $M_d = 2.85$ earthquake occurred on February 19, 2006. Time at the beginning of the record is 03:43:36 UT. Bottom: backazimuths estimated from a plane-wave fitting procedure. We obtained delay times from the maximum of the crosscorrelation function calculated over a 0.2s-long window sliding by 1 sample along the 110 Hz band-pass-filtered array recordings.

This is suggestive of a focusing effect, where wavefronts interact constructively along directions which are different from the source-to-receiver one. Such complicate effect could be attributed to either a strong, near-source scatterer, or channeling of waves along a velocity discontinuity.

4   Conclusions

The UnderSeis three-component seismic array provides a powerful monitoring device for delineating a consistent picture of the seismic activity along the Central Apennines, one of the areas depicting the highest seismogenetic potential of Italy. The underground location allows a good detection threshold, which is better than, or comparable to that of the RSNC up to epicentral distances of $25-30km$. Moreover, the continuous recording of multichannel, low-noise seismograms might help revealing the possible existence of other signals of tectonic origin, as those related to slow earthquakes already reported for the same area by Crescentini *et al.* (1999), or deep tremor episodes as reported in the last years for several seismic active regions in the world (see Obara K., 2002; Rogers and Dragert, 2003; La Rocca *et al.*, 2005; Nadeau and Dolenc, 2005). The observed azimuthal discrepancies between RSNC and array locations may be attributed to a combination of scarce array resolution and velocity heterogeneities affecting both travel-time and ray geometry predictions. In addition, focusing of energy in the late P-wave wavetrain contributes to

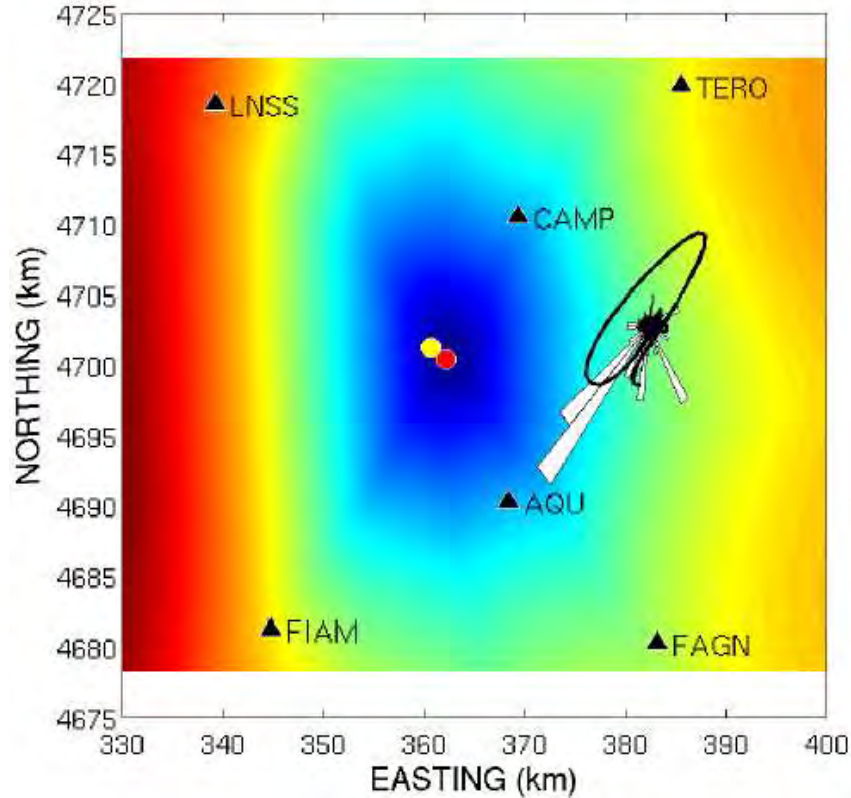significantly bias directional estimates.

Figure 8: RSNC location compared to propagation and polarisation azimuths for the event shown in Figure 7. The white dot is the catalog location. The gray dot is the location recalculated using revised phase pickings from the closest RSNC stations (black labelled triangles). The underlying color map is the marginal probability density function for hypocenter location with respect to the two horizontal coordinates. For the location, we calculated travel times using an homogeneous half-space with $V_P = 5.5km/s$, and a V_P/V_S ratio of 1.8. The rose diagram represents the direction-of-arrival derived from slowness measurements (Fig. 7); the black line is the particle motion trajectory projected over the horizontal plane.

Future efforts will thus be aimed at improving UnderSeis resolving capabilities by increasing its temporal sampling rate, and including S-wave directional data into the location procedure. Hopefully, this will help mitigating the effects of the reduced array aperture once compared to the dominant wavelength of the incoming signals. This study further confirms the importance of local structure in locating earthquakes at local distances using array data, as already evidenced by previous works (e.g., Lin and Roecker, 1996; Xu *et al.*, 1996; Saccorotti *et al.*, 2001). In fact, since the ray trajectory is sensitive to the gradient of the velocity field, lateral discontinuities affect more severely the geometry of the ray than its associated travel time. The enormous number of events recorded by both the RSNC and UnderSeis since the beginning of the 2009 sequence is providing a large travel-time databases, which will hopefully permit detailed tomographic imaging of the subsurface structure. These efforts will improve the precision and reliability of ray

paths and travel time predictions, thus permitting accurate estimates of microseismicity locations from either large-aperture network or array data.

5   Acknowledgements

6   List of Publications

1. R. Scarpa, C. Fischione, L.A. Formisano, M. La Rocca, F. Tronca, 2009. *Low frequency non volcanic tremor along the Apennines, Italy.* Geoph., Res., Abstr., Vol. 11, EGU2009-3726, 2009.

2. Galluzzo D., La Rocca M., Del Pezzo E., Fischione C., Tronca F., Scarpa R., Formisano L.A., 2009. *How local site conditions can bias source spectral parameters estimations: preliminary results on earthquake motions recorded at surface and underground at Gran Sasso.* 28° Convegno Nazionale G.N.G.T.S. (Gruppo Nazionale di Geofisica della Terra Solida); Trieste, Italia, 16-19 Novembre 2009.

3. La Rocca M., Formisano L.A., Scarpa R., Galluzzo D., Fischione C., 2009. *Coerenza del campo d'onda sismico all'array Underseis nel periodo aprile-maggio 2009.* 28° Convegno Nazionale G.N.G.T.S. (Gruppo Nazionale di Geofisica della Terra Solida); Trieste, Italia, 16-19 Novembre 2009.

References

[1] Agnew D. C., 1986. *Strainmeters and tiltmeters.* Rev. Geophys. 24, 579-624.

[2] Crescentini L., Amoruso A., Scarpa R., 1999. *Constraints on slow earthquakes dynamics from a swarm in Central Italy.* Science, 286, 2132-2134.

[3] Benioff H., 1935. *A linear strain seismographs.* Bull. Seism. Soc. Am. 25, 283-309.

[4] Bolt B. A., 1976. *Nuclear explosions and earthquakes. The parted veil.* Freeman, San Francisco.

[5] Capon J., 1969. *High resolution frequency-wavenumber spectrum analysis.* Proc. IEEE 57, 1408-1418.

[6] Chouet B., 1996. *New methods and future trends in seismological volcano monitoring.* In "Monitoring and mitigation of volcano hazards", R. Scarpa and R. Tilling (Eds.), Springer-Verlag, New York.

[7] Chouet B., G. Saccorotti, M. Martini, P. Dawson, G. De Luca, G. Milana and R. Scarpa, 1997. *Source and path effects in the wavefields of tremar and explosions at Stromboli Volcano, Italy.* J. Geophys. Res., 102, 15,129-15,150.

[8] Amoruso A., Crescentini L., Morelli A., Scarpa R., 2002. *Slow rupture of an aseismic fault in a seismogenic region of Central Italy.* Geophys. Res. Lett., 29, 2219, doi: 10.1029/2002GL016027.

[9] De Luca G., Del Pezzo E., Di Luccio F., Margheriti L., Milana G. and Scarpa R., 1998. *Site response study in Abruzzo (centraI Italy): underground array versus surface stations.* J. Seismol., 2, 223-226.

[10] Farrell W. E., 1969. *A gyroscopic seismometer: measurements during the Borrego earthquake.* Bull. Seism. Soc. Am. 59, 1239-1245.

[11] Green Jr., Frosh B. A. and Romney C. F., 1965. *Principles of an experimental large aperture seismic array.* Proc. IEEE 53, 1821-1833.

[12] Kedrov O. K. and V. M. Ovtchinnikov, 1990. *An on-line analysis system for three component seismic data: method and preliminary results.* Bull. Seism. Soc. Am. 80, 2053-2071.

[13] Lee W. H. K. and Stewart S. W., 1981. *Principles and applications of microearthquake networks.* Academic Press, New York, 293 pp.

[14] Lee T. and Wallace T. C., 1995. *Modern Global Seismology.* Academic Press, New York, 517 pp.

[15] Mikkeltveit S., 1985. *A new regional array in Norway: design, work and results from analysis of data from a provisional installation, in The Vela Program.* A twenty- Five Review of Basic Research, edited by U. A. Kerr (Defence Advanced Research Project Agency), 546-553.

[16] La Rocca M., McCausland W., Galluzzo D., Malone S., Saccorotti G., Del Pezzo E., 2005. *Array measurement of deep tremor signals in the Cascadia subduction zone.* Geophys. Res. Lett., 32, doi:10.1029/2005GL023974.

[17] Wielandt E., 1983. *Design principles of electronic inertial seismometers.* In H. Kanamori and E. Boschi (Eds.) "Earthquakes: Observation, Theory and Interpretation". Proc. Int. School of Phys. "E. Fermi", North Holland, Amsterdam.

[18] R. Scarpa, R. Muscente, F. Tronca, C. Fischione, P. Rotella, M. Abril, G. Alguacil, W. De Cesare, M. Martini, 2004. *UNDERSEIS - Underground Seismic Array.* Seis. Res. Lett. Vol. 75, number 4, July/August 2004.

[19] G. Saccorotti, B. Di Lieto, F. Tronca , C. Fischione, R. Scarpa, R. Muscente, 2006. *Performances of the UNDERground SEISmic array for the analysis of seismicity in central Italy.* Annals of Geophysics, Vol. 49, number 4/5, August/October 2006.

[20] Obara K., 2002. *Nonvolcanic deep tremor associated with subduction in Southwest Japan.* Science, 296, 2002; doi: 10.111/science.1070378.

[21] Rogers G., Dragert H., 2003. *Episodic tremor and slip on Cascadia subduction zone: the chatter of silent slip.* Science,300, 1942-1943.

[22] Chiarabba, C. et al., 2009. *The 2009 L'Aquila (central Italy)* M_W = 6.3 *earthquake: Main shock and aftershocks.* Geophys. Res. Lett., 36, L18308, doi:10.1029/2009GL039627.

[23] DAgostino N., J.A. Jackson, F. Dramis and R. Funiciello, 2001. *Interactions between mantle upwelling, drainage evolution and active normal faulting: an example from the Central Apennines (Italy).* Geophys. J. Int., 147, 457497.

[24] De Luca G., R. Scarpa, L. Filippi, A. Gorini, S. Marcucci, P. Marsan, G. Milana and E. Zambonelli, 2000. *A detailed analysis of two seismic sequences in Abruzzo, central Apennines, Italy.* J. Seismology, 4, 121.

[25] Galadini F., P. Messina, B. Giaccio and A. Sposato, 2003. *Early uplift history of the Abruzzi Apennines (central Italy): available geomorphological constraints.* Quat. Geol., 101, 125135.

[26] Lin, CH, S.W. Roecker, 1996. *PWave Backazimuth Anomalies Observed by a Small-Aperture Seismic Array at Pinyon Flat, Southern California: Implications for Structure and Source Location.* Bull. Seism. Soc. Am., 86, 470476.

[27] Nadeau R.M., D. Dolenc, 2005. *Non volcanic tremors deep beneath the San Andreas fault.* Science, 307, 389.

[28] Rost S., Thomas Ch., 2002. *Array Seismology: Methods and Applications.* Rev. of Geophys., 10.1029/2000RG000100, 2002.

[29] Saccorotti G., J. Almendros, E. Carmona, J. Ibanez and E. Del Pezzo, 2001. *Slowness anomalies from two dense seismic arrays at Deception Island Volcano.* Antarctica. Bull. Seism. Soc. Amer., 91, 561571.

[30] Xu, Z., Schwartz, S., and T. Lay, 1996. *Seismic WaveField Observations at a Dense, SmallAperture Array Located on a Landslide in the Santa Cruz Mountains, California.* Bull. Seism. Soc.Am., 86, 655669.

THE PIERRE AUGER EXPERIMENT

for the Collaboration

F. Arneodo[a], A.F. Grillo[a], M.Iarlori[b],
C. Macolino[b], S. Parlati[a], S. Petrera[b], V. Rizi[b], F. Salamida[b]

[a] INFN Laboratori Nazionali del Gran Sasso
[b] INFN and Physics Department, L'Aquila University

Abstract

The Pierre Auger Project is an international Collaboration involving over 400 scientists from 17 countries, with the objective of studying the highest energy cosmic rays. Recent results from the Collaboration as well as further developments in the detector are presented in this report.

1 Introduction

Ultra-high energy cosmic rays are of intrinsic interest as their origin and nature are unknown. It is quite unclear where and how particles as energetic as $\simeq 10^{20}$ eV are accelerated. Over 40 years ago it was pointed out that if the highest energy particles are protons then a fall in the flux above an energy of about $\times 10^{19}$ eV is expected because of energy losses by the protons as they propagate from distant sources through the CMB radiation. At the highest energies the key process is photo-pion production in which the proton loses part of its energy in each creation of a Δ resonance. This is the Greisen-Zatsepin-Kuzmin (GZK) effect. It follows that at 10^{20} eV any proton observed must have come from within about 50 Mpc and on this distance scale the deflections by intervening magnetic fields in the galaxy and intergalactic space are expected to be so small that point sources should be observed. Despite immense efforts in the period since the prediction, the experimental situation remains unclear. The main problem in examining whether or not the spectrum steepens is the low rate of events which, above 10^{20} eV, is less than 1 per km^2 per century so that the particles are only detectable through the giant air showers that they create.

These showers have particle footprints on the ground of $\simeq 20$ km^2 and suitably distributed detectors can be used to observe them. Also the showers excite molecules of atmospheric nitrogen and the resulting faint fluorescence radiation, which is emitted isotropically, can be detected from distances of several tens of kilometers.

The Pierre Auger Observatory has been developed by a team of over 400 scientists from 17 countries. The Southern Observatory is located in Malargüe (Argentina) and

comprises about 1600 10 m$^2 \times$ 1.2 m water-Cherenkov detectors deployed over 3000 km^2 on a 1500 m hexagonal grid. This part of the Observatory (the surface detector, SD) is over-looked by 24 fluorescence telescopes in 4 clusters located on four hills around the SD area which is extremely flat. The surface detectors contain 12 tonnes of clear water viewed by 3×9" hemispherical photomultipliers. The fluorescence detectors (FD) are designed to record the faint ultra-violet light emitted as the shower traverses the atmosphere. Each telescope images a portion of the sky of 30° in azimuth and 1°-30° in elevation using a spherical mirror of 3 m^2 effective area to focus light on to a camera of 440×18 cm^2 hexagonal pixels, made of photomultipliers complemented with light collectors, each with a field of view of 1.5° diameter.

An important feature of the design of the Observatory was the introduction of the hybrid technique as a new tool to study airshowers. It is used here for the first time. The hybrid technique is the term chosen to describe the method of recording fluorescence data coincident with the timing information from at least one surface detector. Employing these two complementary observation methods provides the Auger Observatory with high quality information about angular reconstruction, determination of the core position of the shower and of the types of particles in the primary cosmic rays. Comparing results from the different types of detectors also helps scientists reconcile the two sets of data and produce the most accurate results about the energy of primary cosmic rays.

2 Recent results from the Pierre Auger Cosmic Ray Observatory

An overview of the most recent results from the Auger Observatory can be found in the 37 papers presented at the ICRC 2009 Conference in Lodz (Poland). They have been collected into 5 e-print articles dedicated to the different subjects: the energy spectrum [1], the mass composition [2], the search for astrophysical sources [3], calibration and monitoring [4], the operations and future plans [5]. Hereafter we summarize a few selected results obtained in 2009.
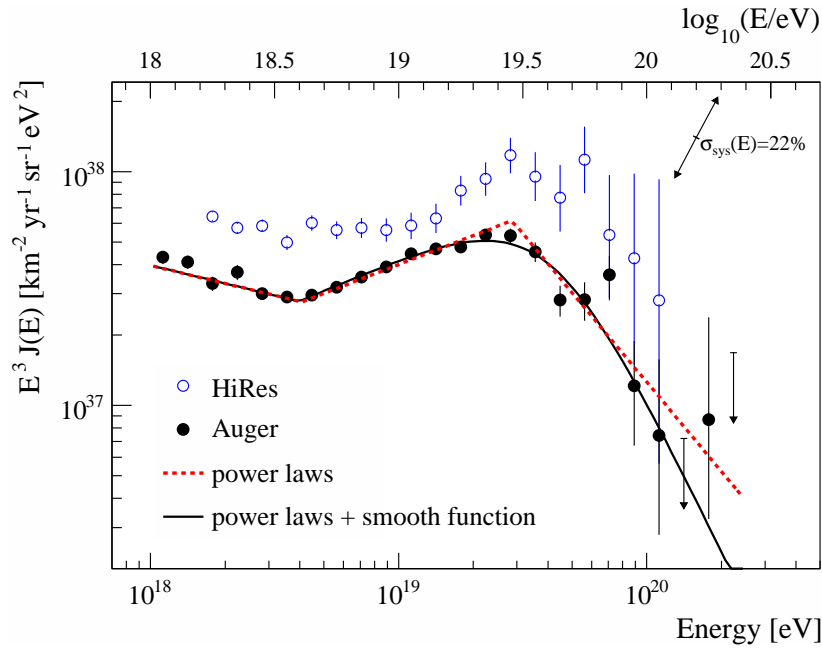
2.1 The Energy Spectrum

The energy spectrum of ultra-high energy cosmic rays at energies greater than 2.5×10^{18} eV has been derived using data from the surface detector array of the Pierre Auger Observatory [6]. This measurement provided evidence for the suppression of the flux above 4×10^{19} eV and is updated here. In 2009 we extended the previous measurements to lower energies by analysing air showers measured with the fluorescence detector that also triggered at least one of the stations of the surface detector array. Despite the limited event statistics due to the fluorescence detector on-time of about 13 %, the lower energy threshold and the good energy resolution of these *hybrid* events allow us to measure the flux of cosmic rays in the region of the ankle.

The energy spectrum of hybrid events is determined from data taken between November 2005 and May 2008, during which the Auger Observatory was still under construction. Using appropriate selection criteria, the exposure accumulated during this period was

computed and the flux of cosmic rays above 10^{18} eV determined. The spectrum obtained with the surface detector array, updated using data until the end of December 2008, is combined with the hybrid one to obtain a spectrum measurement over a wide energy range with the highest statistics available.

The combined energy spectrum scaled with E^3 is shown in Fig. 1 in comparison with the spectrum obtained with stereo measurements of the HiRes instrument [7]. An energy shift within the current systematic uncertainties of the energy scale applied to one or both experiments could account for most of the difference between the spectra. The ankle feature seems to be somewhat more sharply defined in the Auger data. This is possibly due to a systematic energy offset between the experiments. However, for a complete comparison, care must also be taken to account for energy resolution and possible changes in aperture with energy.

Figure 1: The combined energy spectrum is fitted with two functions (see text) and compared to data from the HiRes instrument [7]. The systematic uncertainty of the flux scaled by E^3 due to the uncertainty of the energy scale of 22% is indicated by arrows. A table with the Auger flux values can be found at [8].

The dominant systematic uncertainty of the spectrum stems from that of the overall energy scale, which is estimated to be 22%.

The position of the ankle at $\log_{10}(E_{\text{ankle}}/\text{eV}) = 18.61 \pm 0.01$ has been determined by fitting the flux with a broken power law $E^{-\gamma}$. An index of $\gamma = 3.26 \pm 0.04$ is found below the ankle. Above the ankle the spectrum follows a power law with index 2.55 ± 0.04. In comparison to the power law extrapolation, the spectrum is suppressed by a factor two at $\log_{10}(E_{1/2}/\text{eV}) = 19.61 \pm 0.03$. The significance of the suppression is larger than $20\,\sigma$. The suppression is similar to what is expected from the GZK effect for protons or nuclei as heavy as iron, but could in part also be related to a change of the shape of the average

injection spectrum at the sources.

2.2   The Mass Composition

The atmospheric depth, $X_{\max}$, at which the longitudinal development of a shower reaches its maximum in terms of the number of secondary particles is correlated with the mass of the incident cosmic ray particle. With the generalization of Heitler's model of electron-photon cascades to hadron-induced showers and the superposition assumption for nuclear primaries of mass A, the average depth of the shower maximum, $\langle X_{\max} \rangle$, at a given energy E is expected to follow [9]

$$\langle X_{\max} \rangle = \alpha \left(\ln E - \langle \ln A \rangle \right) + \beta,) \tag{1}$$

where $\langle \ln A \rangle$ is the average of the logarithm of the primary masses. The coefficients α and β depend on the nature of hadronic interactions, most notably on the multiplicity, elasticity and cross-section in ultra-high energy collisions of hadrons with air, see e.g. [10].

At ultra high energies, the shower maximum can be observed directly with fluorescence detectors. Previously published $X_{\max}$ measurements [11, 12] as a function of energy had only limited statistics above 10^{19} eV.
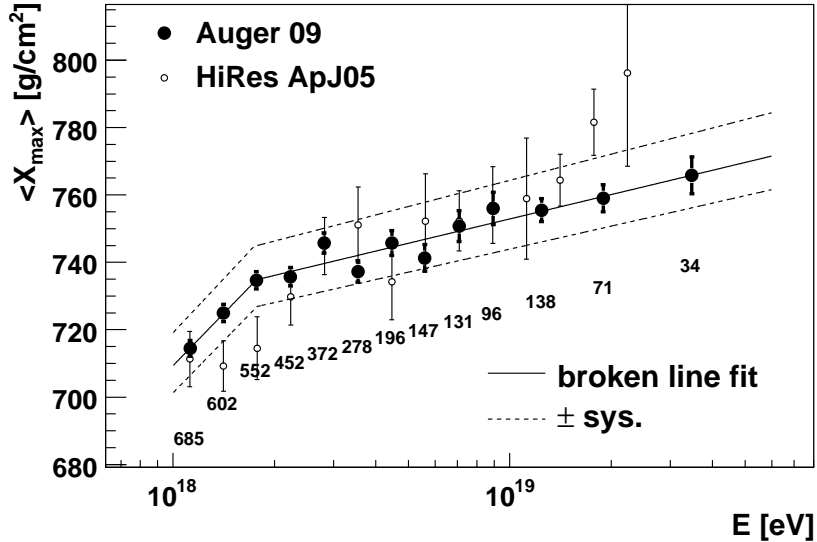
Figure 2: $\langle X_{\max} \rangle$ as a function of energy. Lines denote a fit with a broken line in $\lg E$. The systematic uncertainties of $\langle X_{\max} \rangle$ are indicated by a dashed line. The number of events in each energy bin is displayed below the data points. HiRes data [12] are shown for comparison.

A recent analysis based on high quality and high statistics hybrid data collected with the southern site of the Pierre Auger Observatory has been addressed to the $\langle X_{\max} \rangle$ measurement and its energy dependence. The measured $\langle X_{\max} \rangle$ values are shown in Fig. 2. We use bins of $\Delta \lg E = 0.1$ below 10 EeV and $\Delta \lg E = 0.2$ above that energy. The last bin starts at $10^{19.4}$ eV, integrating up to the highest energy event ($E = (59 \pm$

8) EeV). The systematic uncertainty of the FD energy scale is 22%. Uncertainties of the calibration, atmospheric conditions, reconstruction and event selection give rise to a systematic uncertainty of $\leq 13\,\mathrm{g/cm^2}$ for $\langle X_{\max} \rangle$ and $\leq 6\,\mathrm{g/cm^2}$ for the RMS. The results were found to be independent of zenith angle, time periods and FD stations within the experimental uncertainties.

A fit of the measured $\langle X_{\max} \rangle$ values with a constant elongation rate does not describe our data ($\chi^2/\mathrm{Ndf}{=}34.9/11$), but as can be seen in Fig. 2, using two slopes yields a satisfactory fit ($\chi^2/\mathrm{Ndf}{=}9.7/9$) with an elongation rate of $(106^{+35}_{-21})\,\mathrm{g/cm^2}$/decade below $10^{18.24\pm0.05}\,\mathrm{eV}$ and $(24\pm3)\,\mathrm{g/cm^2}$/decade above this energy. If the properties of hadronic interactions do not change significantly over less than two orders of magnitude in primary energy ($<$ factor 10 in center of mass energy), this change would imply a change in the energy dependence of the composition around the ankle, supporting the hypothesis of a transition from galactic to extragalactic cosmic rays in this region.

2.3   The Cosmic Ray Anisotropy

With data collected by the Pierre Auger Observatory between 1 January, 2004 and 31 March, 2009, we have updated the analysis reported in [13] of correlation between the arrival directions of the highest energy cosmic rays and the positions of nearby objects from the 12th edition of the Veron-Cetty-Veron catalog of quasars and active galactic nuclei. The total number of events above 55 EeV is 58. A subset of 44 events are independent of those used to determine the parameters ($\psi_{max} = 3.1°$, $z_{max} = 0.018$ and $E_{th} = 55$ EeV) with which we monitor the correlation signal. 17 of these 44 events correlate under these parameters. This correlation has a less than 1% probability to occur by chance if the arrival directions are isotropically distributed. The evidence for anisotropy has not strengthened since the analysis reported in [13]. The degree of correlation with objects in the VCV catalog appears to be weaker than suggested by the earliest data. We note that there is an excess of events in the present data set close to the direction of the radio source Cen A, a region dense in potential sources. This excess is based on a posteriori data but suggests that the region of the sky near Cen A warrants further study. Additional data are needed to make further progress in the quest to identify the sites of ultra high energy CR origin.

The time sequence of the correlations between events with energy exceeding 55 EeV and AGN in the VCV catalog is shown in Fig. 3. Period I is the exploratory period [13] from 1 January, 2004 through 26 May, 2006. The data collected during this period was scanned to establish the parameters which maximize the correlation. Period II is from 27 May, 2006 through 31 August, 2007 when the correlation paper [13] was published and period III includes data collected after, from 1 September, 2007 through 31 March, 2009. The time sequence is shown in terms of p_{data}, the degree of correlation with objects in the VCV catalog as a function of the total number of time-ordered events after the exploratory period.
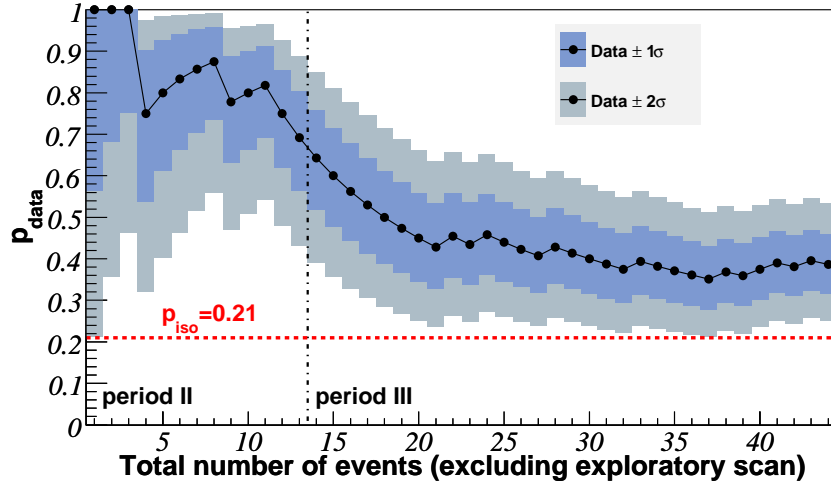
Figure 3: The most likely value of the binomial parameter $p_{data} = \mathrm{k}/\mathrm{N}$ is plotted with black circles as a function of time. The 1σ and 2σ uncertainties in the observed value are shaded. The horizontal dashed line shows the isotropic value $p_{iso} = 0.21$. The current estimate of the signal is 0.38 ± 0.07. In both plots events to the left of the dashed vertical line correspond to period II and those to the right, collected after [13], correspond to period III.

3 Enhancements of the Southern Observatory

After having completed the southern observatory, there are several enhancements under construction to improve the sensitivity of the observatory at low energy. Many of these activities are motivated by the interest in understanding the transition between galactic and extragalactic cosmic rays [14]. Three *High Elevation Auger Telescopes* (HEAT) are being built near the Coihueco fluorescence station. These telescopes will cover an elevation angle from about 30° 60° and improve the sensitivity to and reconstruction of the longitudinal shower profile at low energy [15]. It is expected that shower with energies as low as $10^{17.2}$ eV will be well reconstructed. In front of HEAT, a graded infill array is foreseen to lower the trigger threshold and to allow direct muon detection. The *Auger Muons and Infill for the Ground Array* (AMIGA) will consist of SD stations and buried muon detectors of 30 m^2 effective area [16]. AMIGA will have nearly full acceptance for showers of 10^{17} eV. Layout of the planned enhancements AMIGA and HEAT for the southern observatory. The layout of AMIGA and HEAT is shown in Fig. 4. It is also planned to deploy a radio antenna array to study the feasibility of using this new detection technique for air shower measurements [17]. First measurements with different antennas have been carried out in preparation of the development of a design for such an array.

References

[1] Pierre Auger Collaboration [J. Abraham et al.], The Cosmic Ray Energy Spectrum and Related Measurements with the Pierre Auger Observatory, arXiv:0906.2189 [astro-ph].
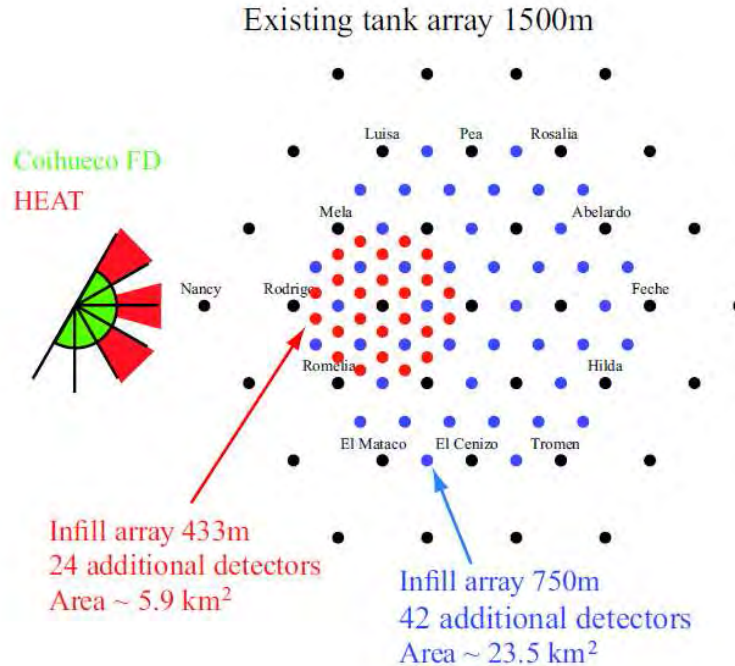
Figure 4: Layout of the planned enhancements AMIGA and HEAT for the southern observatory.

[2] Pierre Auger Collaboration [J. Abraham et al.], Studies of Cosmic Ray Composition and Air Shower Structure with the Pierre Auger Observatory, arXiv:0906.2319 [astro-ph].

[3] Pierre Auger Collaboration [J. Abraham et al.],, Astrophysical Sources of Cosmic Rays and Related Measurements with the Pierre Auger Observatory, arXiv:0906.2347 [astro-ph].

[4] Pierre Auger Collaboration [J. Abraham et al.], Calibration and Monitoring of the Pierre Auger Observatory, arXiv:0906.2358 [astro-ph].

[5] Pierre Auger Collaboration [J. Abraham et al.], Operations of and Future Plans for the Pierre Auger Observatory, arXiv:0906.2354 [astro-ph].

[6] Pierre Auger Collaboration [J. Abraham et al.], Phys. Rev. Lett. **101** (2008) 061101

[7] [HiRes Collab.] R. U. Abbasi *et al.*, Astropart. Phys. **32** (2009) 53–60.

[8] http://www.auger.org/combined_spectrum_icrc09.txt

[9] W. Heitler, Oxford University Press, 1954; J. Matthews, Astropart. Phys. **22** (2005), 387.

[10] T. Wibig, Phys. Rev. D **79** (2009), 094008; R. Ulrich *et al.*, Proc. 31st Int. Cosmic Ray Conf. (Lodz, Poland) (2009) and arXiv:0906.0418.

[11] D.J. Bird *et al.* [Fly's Eye Coll.], Phys. Rev. Lett. **71** (1993), 3401.

[12] R. U. Abbasi *et al.* [HiRes Coll.], Astrophys. J. **622** (2005), 910.

[13] Pierre Auger Collaboration [J. Abraham et al.], Science, 318 (2007) 938 and Astropart. Phys., **29** (2008) 188.

[14] G. Medina-Tanco et al. for the Pierre Auger Collab., Proc. of 30th Int. Cosmic Ray Conf., Merida 5 (2007) 1101.

[15] M. Kleifges et al. for the Pierre Auger Collab., Proc. 31st Int. Cosmic Ray Conf. (Lodz, Poland) (2009) and arXiv:0906.2354 [astro-ph.HE].

[16] M. Platino et al. for the Pierre Auger Collab., Proc. 31st Int. Cosmic Ray Conf. (Lodz, Poland) (2009) and arXiv:0906.2354 [astro-ph.HE].

[17] A. M. van den Berg for the Pierre Auger Collab., Proc. 31st Int. Cosmic Ray Conf. (Lodz, Poland) (2009) and arXiv:0906.2354 [astro-ph.HE].

List of Publications

1. "The Fluorescence Detector of the Pierre Auger Observatory", Pierre Auger Collaboration [J. Abraham et al.], submitted to Nuclear Instruments and Methods in Physics Research (NIM A) (arXiv:0907.4282 [astro-ph]).

2. "Atmospheric effects on extensive air showers observed with the Surface Detector of the Pierre Auger Observatory", Pierre Auger Collaboration [J. Abraham et al.], Astroparticle Physics **32**, 89 (2009).

3. "Limit on the diffuse flux of ultra-high energy tau neutrinos with the surface detector of the Pierre Auger Observatory", Pierre Auger Collaboration [J. Abraham et al.], Physical Review **D79**, 102001 (2009).

4. "Upper limit on the cosmic-ray photon fraction at EeV energies from the Pierre Auger Observatory", Pierre Auger Collaboration [J. Abraham et al.], Astroparticle Physics **31**, 399 (2009).

LIBS-X

L. Reale[a], L. Palladino[a], A. Ritucci[a], P. Tucceri[a], S. Prezioso[a],
P. De Marco[a], L. Ottaviano[a], A. Reale[a], A. Gaudieri[a], S. Santucci[a],
P. Parisse[b], D. Luciani[b], A. D'Angelo[b], A. Poma[c], L. Pace[c],
A. Bruno[c], A. Tucci[c], A. Lai[d], F. Flora[d], L. Mezi[d],
P. Dunne[e], J. Kaiser[f], R. Malina[f], M. Liska[f], L. Juka[g],
V. Haikova[g], J. Chalupsky[g], M. Stormer[g], F. Ruggieri[h],
M. Fanelli[h], L. Mancini[i], G. Tromba[i]

[a] LNGS-INFN and Physics Dept. of Univ. of L'Aquila, Assergi(AQ), Italy
[b] Physics Dept. of Univ. of L'Aquila, Via Vetoio Coppito(AQ), Italy
[c] Biology Dept. of Univ. of L'Aquila, Via Vetoio Coppito (AQ), Italy
[d] Dept. FIM-FIS-ACC, ENEA-Frascati, Via E. Fermi 44 Frascati, Italy
[e] School of Physics, Univ. College Dublin, Belfield, Dublin 4, Ireland
[f] Inst. of Phys. Eng., Brno Univ. of Technology, Brno, Czeck Rep.
[g] Free Electron Laser in Hamburg (FLASH) facility, Hamburg, Germany
[h] Dip. di Chimica, Ing. Chimica e Materiali, Univ. dell'Aquila, Italy
[i] Sincrotrone Trieste SpA, Area Science Park, Basovizza, 34012, Trieste, Italy

1 Introduction

As we reported in the previous reports to LNGS the initial aim of the experiment was an application of the capillary discharge EUV laser at 46.9 nm built in our laboratory (in line with a research initiated by J.J. Rocca at Colorado Univ.) as a tool for elemental analysis mainly of biological samples by the Laser Induced Breakdown Spectroscopy (LIBS) technique. LIBS consists essentially in detecting the fluorescence lines of trace elements emitted by the plasma produced focusing a Laser source on a sample. The high fluence (of the order of 10-100 GW) of our source can generate a plasma such that the critical density is about 1023 cm^{-3}. Thus, the Laser can ionize the atoms of the target by a single photon interaction. This makes the mechanism of deposition of the energy different from the conventional plasmas. Moreover, the use of a short wavelength X ray laser is of great interest due to the high spatial resolution given by the very small diameter at the focal spot (few micron). This can allow to study thin films and micrometric structures with micrometric spatial resolution in the chemical sensitivity.

However, due to a very interesting emerging line of research, Since 2007 we definitively divided the original proposal into two main goals: the first one was the prosecution of the LIBS experimentation with our EUV laser, the second one is the use of the x-ray laser for interference lithography applications. This important byproduct of our experiments takes advantage of the high level the coherence degree of our Laser Source. In spite of its limited energy delivery (150microjoule/pulse, 0.2Hz) the coherence can be used to produce interference patterns, that eventually are lithographed on a photoresistive layer. Due to the short wavelength used, this interference lithography is a technique very promising for creating nanoscale periodic structures.

The earthquake in LAquila seriously damaged our laboratory early in 2009. Nonetheless, achievements along the above two lines will be illustrated hereafter. Along the LIBS-X line, during this year we could succeed in modifying the experimental apparatus in order to improve the fluorescence light collection and find the best focusing conditions of our EUV laser. Before the earthquake in fact, we were using a simple optical fiber for light collection system to an Ocean Optics spectrometer, but no relevant results were achieved in the fluorescence detection. Then we studied a collection system using a high numerical aperture Thorlab collector coupled to the previous optical fiber. To improve also the layout alignment precision and to achieve a greater mechanical stability we arranged also a compact Melles-Griot micro actuator system. While repairing the earthquake effects on the laser, we went on with our research on lead pollution in plants at the SYRMEP X ray line of ELETTRA storage ring in Trieste.

Along the second line of research, using our table top laser we succeeded in obtaining modulation of the interference fringes with very high spatial resolution and depositing metallic or organic strips on silicon, as Bragg gratings or similar devices, which are very important for photonics and optoelectronics applications.

Besides the above two mentioned lines of research, in the framework of a more general scientific collaboration (ref. 4) we have also carried out some satellite interesting characterizations of the spectral content of radiations in the EUV regime.

2   Experimental results in 2009

Concerning the first goal, our study was related to the application of the X-ray dual-energy micro radiography technique combined with atomic absorption spectroscopy (AAS) for the detection of lead on Zea mays stem, ear, root, and leaf samples. To localize the sites where lead is present, i.e. to recognize the biological structures involved in the intake ,many planar or tomo- radiographies were taken by monochromatic X-ray in absorption regime, in a photon energy range below and above the absorption edge of that chemical element .Images were analyzed , processed .and compared to the optical images of the same Zea mays plant. The ear, stem, root, and leaf samples have also been analyzed with the AAS technique to measure the exact amount of the hyper accumulated lead. The measurements revealed that the highest intake occurred in the roots while the lowest in the maize ears and in the leaves. It seems that there is a particular mechanism protecting the seeds and the leaves in the intake process (see ref.1).

Concerning the second goal, i.e. the characterization of our laser for X- ray Interference Lithography (XIL), since 2007 we reported on periodic structures by XIL on photosensitive polymers with half-pitch less than 50 nm. In 2009 the potentiality of the technique has been tremendously improved with regular patterns down to 22.5 nm on PMMA/Si (Fig.2), together with some applications to nano-photonics. The results shown in the following figures have been published in high impact factor journal in nanotechnology (refs 2,5). The excellent XIL potentiality of the source have been acknowledged also by INFN via the grant of funds for new experiments (XILOPHON, X-Ray Interference Lithography for Photonic in Nanotechnology) for the year 2010.
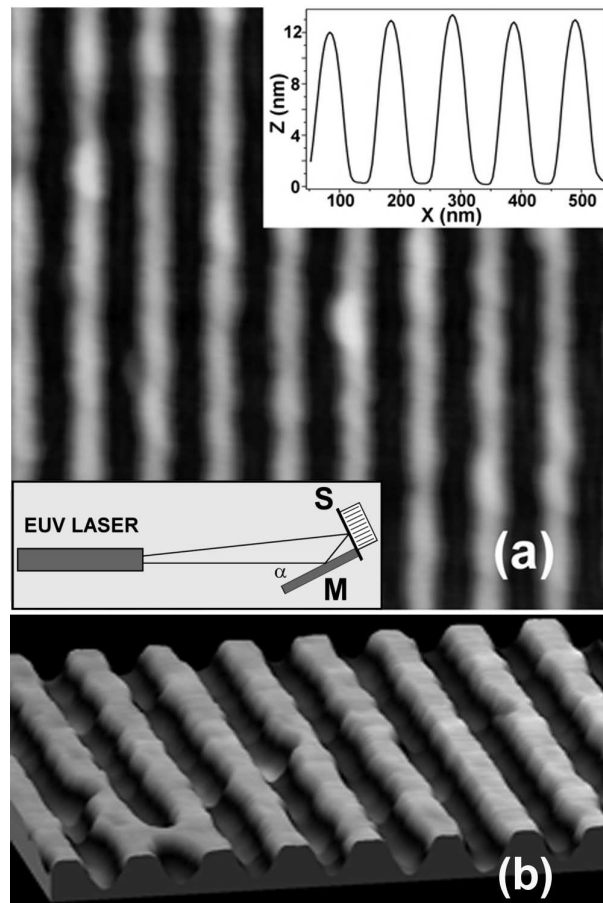
Figure 1: (from ref. 5) AFM (plan view in (a) and three-dimensional plot in (b)) images of patterned PMMA/Si(100) with 50 nm half-pitch. Lower left inset in (a): scheme of the Lloyd interferometer ((S) sample, (M) mirror). Upper inset in (a): average of 256 horizontal height line profiles taken on the corresponding AFM images. The vertical Z scale in (b) is reversed.

More interestingly, our experimental results were also discussed in terms of the coherence of the x-ray laser and of the physical parameters that determine the performance of
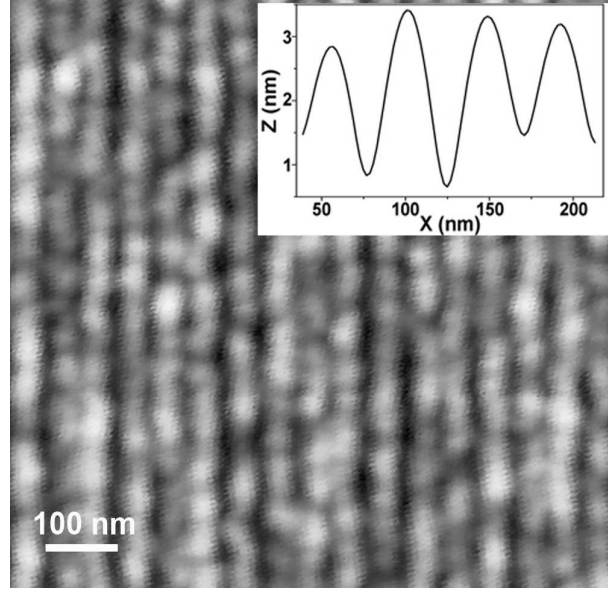
Figure 2: (from ref. 5) X AFM scan of XIL patterned PMMA/Si(100) with 22.5 nm half-pitch. Upper inset: Average of 256 horizontal height line profiles taken on the AFM image.

the interferometer used.

A discussion follows that lead to the conclusion that the coherence degree of the X-Ray LASER source developed is excellent.

Given the low fluence of the primary x-ray beam (150 μJ), in this regime a very first reasonable assumption to make, is the linearity of the response of the photoresist layer to the radiation dose. In this assumption, if d is the thickness of the resist layer engraved by light exposure, then $d = KIN$, where I is the (average) intensity of the laser light at each shot, N is the number of PMMA exposure shots, and K is a parameter accounting for the PMMA sensitivity at the wavelength of radiation under consideration. In interference lithography, the intensity of the light at the sample surface is, indeed, modulated by the interferometer, thus there will be a maximum (I_{max}) and a minimum (I_{min}) intensity. Accordingly there will be (as observed) an height modulation Δd of the PMMA after light exposure and development. This value will be $\Delta d = K(I_{max} - I_{min})N$. The values of I_{max} and I_{min} can be simply related to fundamental physical parameters according to the following formula:

$$I_{max} - I_{min} = 4I\gamma R \tag{1}$$

where I is the intensity of the undeflected beam, γ is the mutual coherence degree of the light waves at the sample and $R = \sqrt{R_p} + \sqrt{R_s}$ is a function of R$_p$ and R$_s$, that are the reflectivities of the p and s beam polarization. Accordingly,

$$\Delta d = 4KI\gamma RN \tag{2}$$

It is worthwhile to note that K, expressing the resist sensitivity, is depending only on the wavelength of the light, while γ and R depend on the period of the pattern to be engraved. A convenient parameter to define is what will be called henceforth the lithographic efficiency of the laser source defined as $E_l = \Delta d/N$. This parameter has been measured for XIL periods of 45 nm, 100 nm (data reported in figures 1 and 2) and also from AFM data of XIL patterned samples at 200, 400 and 800 nm (images not reported for brevity). According to the above formulae, the ratio of the lithographic efficiencies at two given XIL periods, p_1 and p_2 can be derived experimentally as:

$$E_l(p1)/E_l(p2) = \frac{\Delta d(p1)N(p2)}{\Delta d(p2)N(p1)} \tag{3}$$

but can also be written as

$$E_l(p1)/E_l(p2) = (\gamma_{p1}/\gamma_{p2})\frac{R_{p1}}{R_{p2}} \tag{4}$$

where γ_{p1} and γ_{p2} are the mutual coherence degrees at p_1 and p_2 period respectively, and the factor R_{p1} and R_{p2} can be estimated by known values of the reflectivities of the Si mirror. Accordingly, one can derive as a function of the XIL period the ratio γ_{p1}/γ_{p2}. We have reported in figure 3 the values of γ_{p1}/γ_{800} and R_{p1}/R_{800} considering 800 nm as a reference period. The γ/γ_{800} curve in figure 3, nicely fitted by a parabolic function, shows that, while there is a significant loss (by a factor 5.3) of mutual coherence of the XIL setup when passing from 800 to 100 nm, by further reducing the XIL period to 45 nm the subsequent loss of coherence is only by a factor 1.3. No further significant losses of mutual coherence are expected extrapolating the curve to 23 nm corresponding to the $p_{min} = \lambda/2$ physical limit of the XIL system. Indeed, as indicated by the reflectivity graph in figure 3, below 200 nm, the drop of lithographic efficiency is, by far, mostly determined by the drop of reflectivity of the Si mirror. This bottleneck can be easily removed by the use, for example, of a (35 nm period, ratio of 0.52) multilayer SiSc mirror. This mirror would exhibit a reflectivity exceeding by a factor of almost one order of magnitude the one of Si (at light incidence angles close to 45°).

3   Conclusions

In conclusion even for the year 2009 the LIBS-X experiment has lead to notable scientific results which were reported in a significant number of publications in international scientific journals. The specific LIBS-X studies for biological applications lead to improvements of the experimental setup in use at the university of L'Aquila, and after the April 2009 quake were continued successfully at Elettra. As far as the XIL applications are concerned we demonstrated in 2009 with a systematic investigation that the source shows excellent properties of mutual coherence that will allow to scale the lithography down to the $\lambda/4$ physical limit (half pitch). The features of this technique i.e. its low cost, the portability, the capability to engrave large areas, its being mask less, and, last but not least, the simplicity of the optical interferometer scheme used, make it a very promising tool in many potential applications in nanotechnology. In particular, with this technique the low cost nanofabrication of devices becomes more viable.
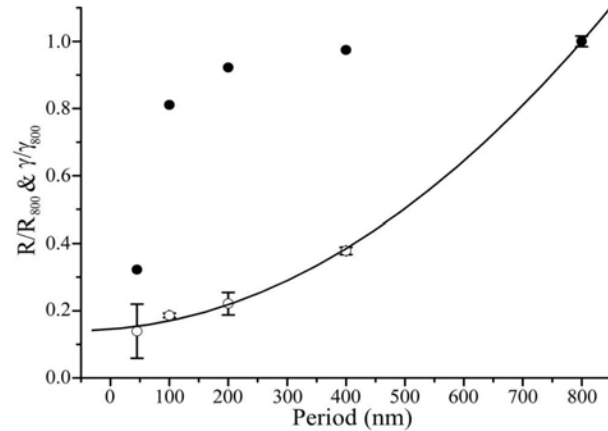
Figure 3: (form ref. 5) Open circles: plot of the measured coherence degree parameter γ of the XIL setup normalized to the γ_{800} value (measured at 800 nm). Full circles: corresponding plot of the overall normalized reflectivity R/R_{800}.

4   Acknowledgments

5   Participation to, and organization of, national or international workshops or conferences

- L. Ottaviano (S. Prezioso and P. De Marco in the Organizing Committed) has Chaired the International conference FNMA09 (Functional and Nanostructured Materials 09 www.fnma09.gda.pl) Held in Sulmona 27-30 sept 2009. 130 attendees from 22 different countries. The event has been sponsored by INFN, ENEA, and MICRON Technology.

- PEARL 2009 Dublin S. Prezioso (POSTER) *Soft X-ray capillary discharge plasma sources for nano-lithography applications.* S. Prezioso, P. Zuppella, A. Ritucci, D. Luciani, P. Tucceri, P. De Marco, F. Bussolotti, S. Piperno, M. Rinaldi, A. Gaudieri, J. Kaiser, F. Flora, L. Mezi, P. Dunne, S. Santucci and L.Ottaviano.

- COST Action MP0601 (Short wavelength laboratory sources) Meeting in Smolenice Czech Republic (November 2009) (POSTER) *Toward the physical resolution limit of table-top X-ray Interference Lithography: a feasibility analysis.* S. Prezioso, D. Luciani, P. Tucceri, P. De Marco, A. Gaudieri, J. Kaiser, S. Santucci, L. Ottaviano, and P. Zuppella.

References

[1] L. Reale, J.Kaiser , L.Pace, A. Lai, F. Flora, B. Angelosante, A. Tucci, P. Zuppella, L. Mancini, G. Tromba, F. Ruggieri, M. Fanelli, R. Malina, M. Liska, and A. Poma. *Detection of Lead in Zea mays by Dual-Energy X-ray Microtomography at the SYRMEP Beamline of ELETTRA Synchrotron and by Atomic Absorption Spectroscopy* - Microscopy Research and Technique (in press 2010).

[2] P. Parisse, D. Luciani, A. DAngelo, S. Santucci, P. Zuppella, P. Tucceri, A. Reale, L. Ottaviano, *Patterning at nanoscale: Atomic force microscopy and extreme ultraviolet interference lithography*, Mat. Sci. Eng. B, **165** (2009) 227.

[3] L. Juha, V. Hajkova, J. Chalupsky, V. Vorlicek, A. Ritucci, A. Reale, P. Zuppella, M. Stormer, *Radiation damage to amorphous carbon thin films irradiated by multiple 46.9 nm laser shots below the single shot damage threshold*, J. Appl. Phys., **105** (2009) 093117.

[4] P. Zuppella, A. Reale, A. Ritucci, P. Tucceri, S. Prezioso, F. Flora, L. Mezi, P. Dunne, *Spectral enhancement of a Xe-based EUV discharge plasma source*, Plasma Sources Sci. Technol., **18** (2009) 025014.

[5] P. Zuppella, D. Luciani, P. Tucceri, P. De Marco, A. Gaudieri, J. Kaiser, L. Ottaviano, S. Santucci, A. Reale, *Large area interference lithography using a table-top extreme ultraviolet laser: a systematic study of the degree of mutual coherence*, Nanotechnology, **20** (2009) 115303.

LASEX Experiment: Design of a Soft X-ray Micro-beam using a Plasma Source

L. Palladino[1,3], R. Gimenez De Lorenzo[1,3], G. Gualtieri[2]

[1]*Physics Department of L'Aquila University*
[2]*Science and Biomedical Technology Department of L'Aquila University*
[3]*INFN, Laboratori Nazionali del Gran Sasso, Assergi (AQ)*

Abstract

In this report, we present the activities of the LASEX experiment in the year 2009. The design of a micro-beam project in the soft X-ray energy region using a plasma source, which operates in the PLASMA-X laboratory of the Physics Department of L'Aquila University. In this work, we discuss the reasons that led to the design of the apparatus. Will describe the main features of the project.

1 Introduction

Many types of sources and X-ray focusing devices have been developed to obtain a micrometric spot [1]. In this contest, top-table soft X-ray for application in radiobiology and biological imaging are very interesting. With this aim we have constructed an X-ray plasma source while the achievement of an optical system based on the zone plates as optical elements, in the soft X-ray region (200 eV - 800 eV), is in progress. The X-rays ranging from $\approx$ 200 eV up to $\approx$ 800 eV are used in several biomedical and X-ray microscopy applications [2, 3]. With this experimental set-up we will want realize a soft X-ray micro-beam and an image system of irradiated biological sample.

2 Experimental Apparatus

The X-ray emission of a plasma-source is based on the production of plasma obtained focalizing a laser beam on a specific target. This source is characterized for an instantaneous spectral high brightness, for a punctiform dimension (some tens microns, focal laser

spot) and for a pulse temporal structure with the same duration of the laser in the whole spectral region. In our case, we use a high power Nd:YAG/Glass laser system whit pulse energy up to 8 J max @ 1064 nm and 6 nsec pulse duration. The laser beam is focalized by an aspherical triplet lens on a target and the plasma and X-ray photons are emitted in 2π sr solid angle [4]. A schematic layout of the interaction chamber is shown in figure 1, where, we note that it is possible to place the target system in different positions respect to the middle of the vacuum chamber (C in figure 1).
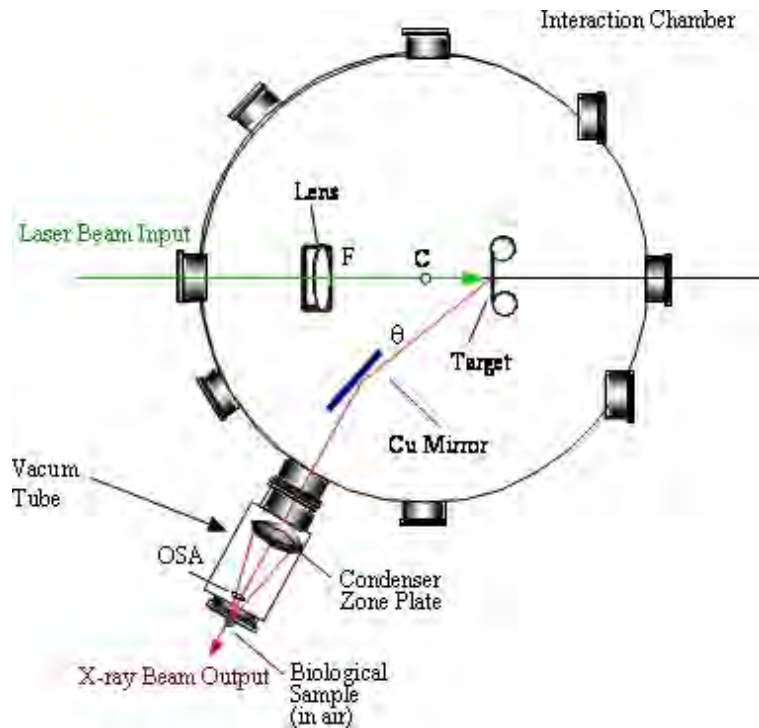
Figure 1: Schematic layout of the interaction chamber. We note that it is possible to place the target system in different positions respect to the middle of the vacuum chamber (C in figure). It is indicated the relative position of the plasma-target and the copper mirror. θ is the grazing angle of the incident X-ray radiation on copper mirror. We show the X-ray optical beam-line layout. The set-up is based on the utilisation a condenser zone plate (CZP). The sample is placed in air at 500 μm from the SiN exit window 100 nm thick.

This configuration makes it possible the employed optical mirror or crystals to select the photon energy in a particular energy interval. In figure 1, it is indicated the relative position of the plasma-target and the copper mirror. It permits that the Cu mirror reflects the incident X-ray radiation with a grazing angle θ. In figure 1, together the interaction chamber, we show the X-ray optical beam layout. The set-up is based on the utilisation a condenser zone plate (CZP) and collimator system (OSA). The biological sample is placed in air at 500 μm from the SiN exit window 100 nm tick. This window separates the vacuum chamber from the outside.

3 X-ray energy interval selection

To select the photons in this energy region a copper mirror at fixed grazing incidence and helium gas at different pressure are used. In fact, in figure 2 and 3 are shown respect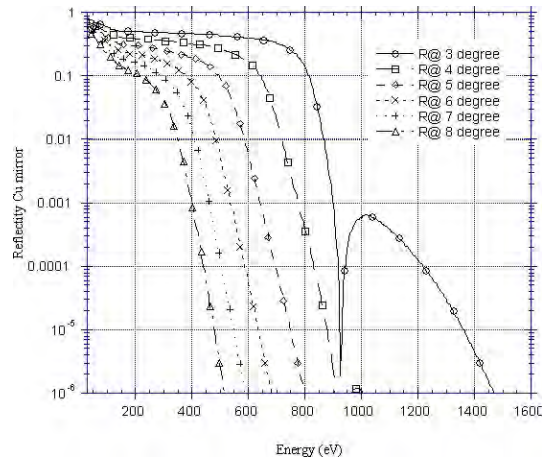ively the copper reflectivity, at different grazing angle θ and He transmission, for different pressure and for 5 cm constant distance [5]. We obtain that optimal grazing angle for stop the X-ray greater than ≈ 900 eV is $\theta = 5 - 4$ degree and the He absorbs at energy lower than $\approx$200 eV, at 1 atm pressure and 5 cm distance.

Figure 2: The copper reflectivity at different grazing angle θ
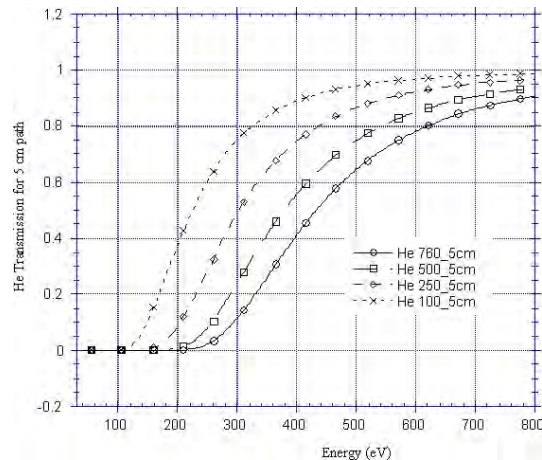
Figure 3: He transmission, for different pressure and for 5 cm constant distance.

The total output transmission of the Cu reflectivity and He transmission, together a SiN 100 nm window, is shown in figure 4. We observe that at a better partial energy resolution of the X-rays corresponds a total transmission lower. To choice the better conditions presented in figure 4, we have designed and built a mirror-holder, in this case

a copper mirror, with accuracy in the rotation angle of 1/10 of degree (see figure 5). It is placed in the interaction chamber (see figure 1) in radial position.
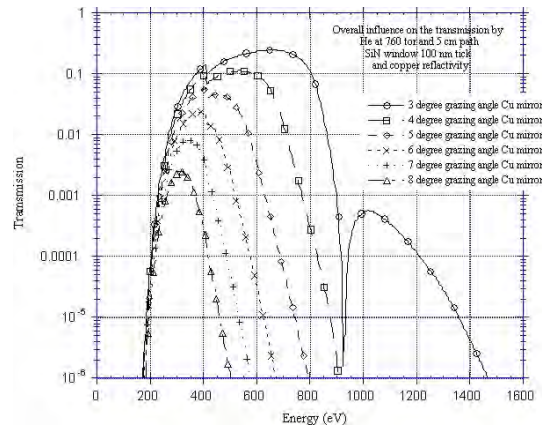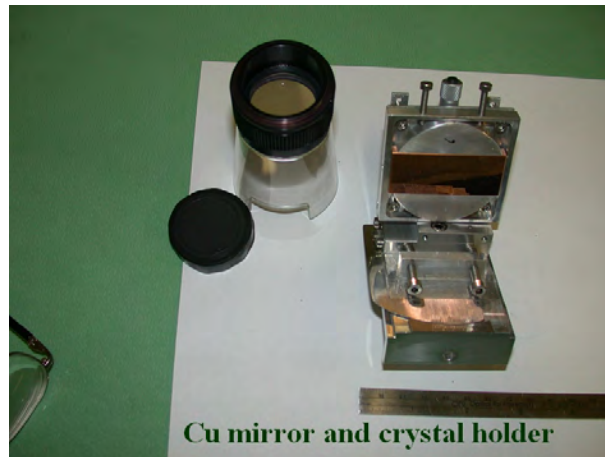

Figure 4: The total output transmission of the Cu reflectivity and He transmission, together a SiN 100 nm window, is shown. We obtain that optimal grazing angle for stop the X-ray greater than ≈ 900 eV is $\theta = 4 \div 5$ degree and the He absorbs at energy lower than ≈ 200 eV, at 1 atm pressure and 5 cm distance.

Figure 5: Photo of the mirror-holder, in this case we see a copper mirror, with accuracy in the rotation angle of 1/10 of degree. For dimensions see the ruler.

4 X-ray optical system

The condenser zone plates are optical elements which selects and focalizes, at different positions on the CZP optical axis, $f_{m,\lambda}$, the wavelength, λ, components through interferential process for the m order. To eliminate the zero order X-ray component (direct

beam), at middle of the CZP is present a central stop, which absorbs the incident radiation completely. This relation

$$f_{m,\lambda} = \frac{(r_{ZP}^2 - r_0^2)}{m \times N \times \lambda} \tag{1}$$

links the CZP focal length, $f_{m,\lambda}$, to the zone plate radius, r_{ZP}^2, the central stop radius, r_0^2, and the zone number, N, fixed the interference order m and the wavelength, λ. In
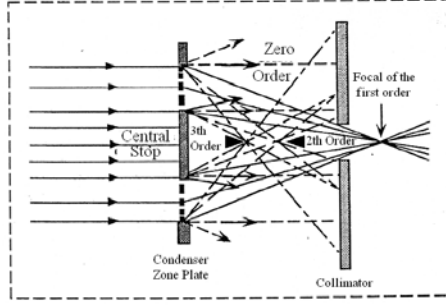

Figure 6: Zone plate - collimator system. It is indicated the position of the zone plate focal for the first, second and third order (indicate by a black triangle) at fixed wavelength.

figure 6, we show the position of the zone plate focal for the first, second and third order at fixed wavelength. To select a wavelength first order (or superior order) or a specific wavelength of our interest, it is necessary to introduce a collimator, which intercept the radiation not useful. Another important optical parameter is the depth of focus. It is defined, for a fixed focal length and wavelength as

$$\Delta z = \pm \frac{1}{2} \frac{\lambda}{(NA)^2} \tag{2}$$

where NA is the numerical aperture of the zone plate lens. The depth of focus limits the region of a tick sample is in the focus and submits at quite constant irradiation and indicates the dimension of the permitted displacement, from the ideal focal plane, for which the beam intensity on optical axis is reduced by only $\pm 20\%$.
In our case, we have the possibility to use a gold CZP, made by Heidenhain, with a diameter 1010 μm, a zone number 506, an outer zone dimension 500 nm and a central spot radius 22.5 μm. The gold wires are freestanding and are 0.5 μm thick. In figure 7, we show a TEM image of our zone plate where are reported the principal CZP features (x100). In figure 8 and 9 we show the focal length and the depth focus of the gold-CZP in relation to the wavelength of X-ray radiation.

The CZP has a average depth focus of ± 150 μm in $2.5 \div 4$ nm wavelength interval. Then the CZP is convenient for tick samples. The dimension of the focal spot depends on Airy distribution in the focal plane and in our case we obtain, by calculations [6], 0.6 μm in diffraction limit conditions and punctiform source. In general, to find the real dimension of the focal spot, it is necessary to add, in quadratic mode, the size of Airy pattern to the dimension of the source, obtained by the geometrical lens law, in the focal spot. In our source the source diameter is 65 μm.

Figure 7: TEM image (x100) of a part of the gold zone plate. 1010 μm diameter and 22.5 μm r_0.
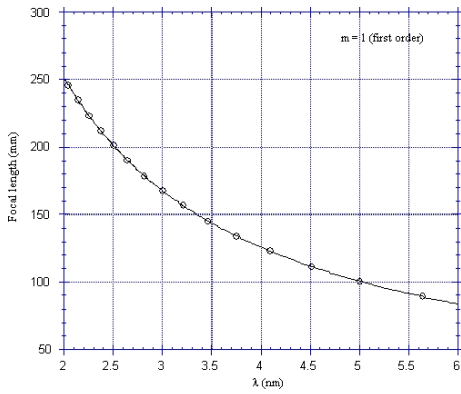

Figure 8: The gold-CZP focal length versus the wavelength of X-ray radiation.
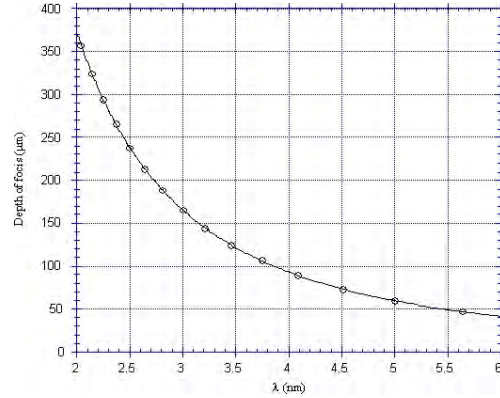

Figure 9: The gold-CZP depth of focus versus the wavelength of X-ray radiation. The CZP has a average depth focus of ± 150 μm.

5   Conclusion

In conclusion, from radiation and optical features of the beam line it is possible to obtain a soft X-ray microbeam for radiobiological applications. The optical features, as the average depth focus of ± 150 μm, are good for the general thickness of the biological samples. In fact for a sample with a thickness greater than of the depth focus, the material outside that region would be not irradiated. The zone plate resolution of 0.5 μm is sufficient to analyze the biological structures. The dimension of the focal spot depends by the geometrical position of the source and the sample respect to the lens and then by the relative demagnification.

6 Acknowledgment

References

[1] G. Schettino et al. - The ultrasoft X-ray microbeam: a sub-cellular probe of radiation response. 4th International Workshop: MicrobeamProbes of Cellular Radiation Resoponse - Dublin 1999

[2] Gerritsen H. C., Van Brug H., Bijkerk F. and Van Der Wiel M. J.: J. Appi. Phys., 59, 2337 (1986)

[3] T.Limongi, L.Palladino, E.Bernieri, G.Tomassetti, L.Reale, F.Flora, P.Cesare, C.Ercole, P.Aimola and A.M.Ragnelli A.M.: J. Phys. IV France 345-348, 104 (2003)

[4] L.Palladino, T.Limongi, G.Gualtieri, R.Gimenez De Lorenzo and P.Zuppella: Radiation Effects and Defects in Solids Vol. 163, N.4-6, April-June 2008, 505-512

[5] Calculated from: X-Ray Data Booklet - Center for X-ray Optics and Advanced Light Source - Lawrence Berkeley National Laboratory

[6] Born and Wolf - Principles of Optics - sixth edition - Pergamon Press